

**NASA TECHNICAL
TRANSLATION**



NASA TT F-782

NASA TT F-782

(NASA-TT-F-782) GENERAL PRINCIPLES OF
DESIGNING CONTROL SYSTEMS (Kanner (Leo)
Associates) 391 p HC \$8.25 CSCL 01C

H74-25594

H1/02 Unclass
40945

**GENERAL PRINCIPLES OF
DESIGNING CONTROL SYSTEMS**

by O. A. Chembrowskiy, Yu. I. Topcheyev,
and G. V. Samoylovich

"Mashinostroyeniye" Press

Moscow, 1972

NATIONAL AERONAUTICS AND SPACE ADMINISTRATION • WASHINGTON, D. C. • MAY 1974

1. Report No. NASA TT F-782		2. Government Accession No.		3. Recipient's Catalog No.	
4. Title and Subtitle GENERAL PRINCIPLES OF DESIGNING CONTROL SYSTEMS				5. Report Date May 1974	
				6. Performing Organization Code	
7. Author(s) O. A. Chembrovskiy, Yu. I. Topcheyev, and G. V. Samoylovich				8. Performing Organization Report No.	
				10. Work Unit No.	
9. Performing Organization Name and Address Leo Kanner Associates Redwood City, CA 94063				11. Contract or Grant No. NASW-2481	
				13. Type of Report and Period Covered Translation	
12. Sponsoring Agency Name and Address National Aeronautics and Space Admini- stration, Washington, D.C. 20546				14. Sponsoring Agency Code	
15. Supplementary Notes Translation of "Obshchiye Printsipy Proyektirovaniya Sistem Upravleniya," Moscow, "Mashinostroyeniye" Press, 1972, 416 pages					
16. Abstract This book presents general methods for the initial stages of designing control systems of aircraft, missile, and space-craft complexes. The methods are based on statistical estimates of the characteristics of flight craft and of ground and onboard control system components. Illustrations are taken from foreign technology. Failure rates and standby status of the control systems of aircraft and missile complexes are discussed. Cost effectiveness criteria in the designing of attack and defense aircraft-missile complexes are described and evaluated with examples. Handbook material presented in the book can be used in the initial stage of designing or in setting up preliminary requirements for systems. The book is written for design engineers and estimator engineers concerned with designing flight craft control systems.					
17. Key Words (Selected by Author(s))			18. Distribution Statement Unclassified - Unlimited Cat. 02		
19. Security Classif. (of this report) Unclassified	20. Security Classif. (of this page) Unclassified	21. No. of Pages 389	22. Price* \$8.25		

Obshchiye Printsipy Proyektirovaniya Sistem Upravleniya
[General Principles of Designing Control Systems], Chembrovskiy,
O. A., Topcheyev, Yu. I., and Samoylovich, G. V., Moscow, "Mashi-
nostroyeniye" Press, 1972, 416 pages.

This book is one of several in the design engineer's hand-
book library, published under the general title Osnovy Proyektiro-
vaniya Sistem Upravleniya Letatel'nykh Apparatami [Essentials of
Designing Flight Craft Control Systems].

The book deals with general methods of designing control sys-
tems of aircraft, missile, and space complexes based on statis-
tical estimates of the characteristics of flight craft, ground,
and onboard control system equipment, and also methods of synthe-
sis for assigned effectiveness criteria. Heavy emphasis is given
to estimates of the technical capabilities of control systems in
various conditions of application. Designing methods are illus-
trated with examples from foreign technology.

Handbook material contained in the book can be used in the
initial stage of designing or for establishing preliminary re-
quirements for systems. The book is intended for design engineers
and for estimator engineers engaged in designing flight craft con-
trol systems. It will also prove useful to instructors, graduate
students, and undergraduates in higher educational institutions.

53 tables, 165 illustrations, and 213 bibliographic entries.

FOREWORD

15

Among the problems confronting design engineers, one of the most important is the synthesis of large nonlinear systems, which include aircraft, missile, and space complexes.

At the present time there are as yet neither mathematical or engineering methods of synthesizing these systems, though several hundred articles dealing with this problem have been published in just the past two years in the periodical press. Therefore in designing these complexes engineers resort to statistical comparative analysis of the parameters of their individual elements. At the same time, methods of optimizing internal loops (damping, stabilization, remote control or homing) based on optimality criteria are widely used. The necessity for simultaneously satisfying several requirements is a complicated mathematical problem. Therefore the design engineer, in selecting the optimal system parameters, is compelled to perform numerous calculations and to plot curve nets, and select desired characteristics directly from these. The large number of loops included in aircraft and missile systems considerably complicates design procedures.

From the foregoing it follows that the synthesis of complexes with optimal or assigned effectiveness can be done only together with the synthesis of all its major systems. Still, the synthesis of a control system taken individually, separate from the entire complex, must inevitably lead to a reduction in its efficiency.

The absence of mathematical, and even more so of engineering methods of optimal designing naturally complicated the work of the authors. Therefore they saw their main problems to lie in demonstrating the complexities arising in the combined designing of control systems and of complexes as a whole; in describing the most interesting design solutions; in clarifying trends in the development of certain kinds of control devices and controlled objects; and, finally, in a general characterization of the routes which the designer must follow, even though these routes do not lend themselves to rigorous algorithmization.

16

The materials on specific complexes, control systems, and individual installations, as well as prospects of their development are presented in accordance with data published in the domestic and foreign press. In several cases they are contradictory in nature, raising difficulties in the statistical estimate of certain characteristics and parameters.

PRECEDING PAGE BLANK NOT FILMED

The functions and graphs presented in the book, along with numerical values of certain parameters are generally approximate and can be used only for rough calculations in the stage of pre-draft designing of control systems. Also, some of the examples given are purely methodological in emphasis, and numerical data obtained therein can in no wise aspire to an estimation of the capabilities of flight complexes.

The authors express their deep gratitude to Candidate of Technical Sciences I. I. Smirnova, who wrote Section Eight of Chapter Four. We would wish to express special gratitude and sincere thanks to Doctor of Technical Sciences, Professor I. V. Ostoslavskiy (deceased), who read the manuscript of the book and made several comments on improving its contents.

All comments and suggestions should be sent to this address: Moscow, B-78, Pervyy Basmannyy Per., d. 3, "Mashinostroyeniye" Press.

EDITORIAL BOARD MEMBERS

Honored Leader in the Science and Technology of the RSFSR, Doctor of Technical Sciences, Professor B. A. Ryabov

Honored Leader in the Science and Technology of the RSFSR, Doctor of Technical Sciences, Professor A. S. Shatalov

Doctor of Technical Sciences, Professor V. A. Bodner; and
Doctor of Technical Sciences, Professor Yu. I. Topcheyev

TABLE OF CONTENTS

Page

Annotation	iii
Foreword	v
Table of Contents	vii
Chapter One -- Flight Craft Control Systems	1
1.1. Function and Typical Structures of Flight Craft Control Systems	1
1.2. Control Systems of Aircraft-Missile Complexes	9
1.3. Control Systems of Antiaircraft Missile Complexes	18
1.4. Ballistic Missile Control Systems	20
Chapter Two -- Flight Craft and Their Main Charac- teristics	37
2.1. Tactical-Flight Characteristics of Fighter- Interceptors	37
2.2. Tactical-Flight Characteristics of Multi- Mission Fighters	49
2.3. Tactical-Flight Characteristics of Bombers	57
2.4. Tactical-Flight Characteristics of Transport Aircraft	65
2.5. Tactical-Flight Characteristics of Air-to-Air Missiles	81
2.6. Tactical-Flight Characteristics of Air-to- Surface Missiles	86
2.7. Tactical-Flight Characteristics of Surface- to-Air Missiles	90
2.8. Tactical-Flight Characteristics of Ballistic Missiles and Missile Launch Vehicles	95
Chapter Three -- Devices of Flight Craft Control Systems	101
3.1. Ground and Onboard Radars of Aircraft Complexes	104
3.2. Ground Radar Stations of Antiaircraft Defense Missile Complexes	118
3.3. Radar and Infrared Homing Heads of Surface- to-Air, Air-to-Air, and Air-to-Surface Missiles	120

Chapter Three -- Devices of Flight Craft Control Systems (Continued)	
3.4. Onboard Equipment of Aircraft Control Systems	131
3.5. Onboard Equipment of Control Systems of Surface-to-Air, Air-to-Air, and Air-to-Surface Missiles	147
3.6. Onboard Devices of Ballistic Missiles and Missile Launch Vehicles	153
Chapter Four -- Combat and Technical Capabilities of Control Systems of Aircraft and Missile Complexes	165
4.1. Interception Lines of Fighter-Interceptors	167
4.2. Operational Radii of Multimission Fighters and Bombers	173
4.3. Operating Economy of Transport Aircraft	175
4.4. Zones of Possible Air-to-Air Missile Launch	182
4.5. Zones of Possible Air-to-Surface Missile Launch	189
4.6. Zones of Possible Interception of Air Targets by Surface-to-Air Missiles	191
4.7. Flight Trajectories of Ballistic Missiles	196
Chapter Five -- Spacecraft and Their Control Systems	210
5.1. Main Characteristics of Spacecraft	210
5.2. Action Zones of Maneuvering Spacecraft	234
5.3. Control Systems of Spacecraft	249
5.4. Ground and Onboard Devices of Spacecraft	272
Chapter Six -- General Principles of Designing Flight Complexes and Their Control Systems	287
6.1. Effectiveness of Complexes	288
6.2. Costs of Complexes	313
6.3. Effect of Natural and Artificial Interference on the Effectiveness of Performing an Assigned Mission	336
6.4. Effect of Active Enemy Countermeasures on the Effectiveness of Performing an Assigned Mission	345
6.5. Groups of Complexes	351
6.6. Synthesis of Control Systems of Flight Craft Complexes	357
References	366

CHAPTER ONE FLIGHT CRAFT CONTROL SYSTEMS

/7

We class flight craft control systems into several independent complexes: aircraft-missile, antiaircraft defense missile¹, and ballistic missile. For military aircraft, the aircraft-missile complex consists of the control system of the aircraft proper and the control systems of its armament (air-to-air and air-to-surface missiles). The antiaircraft defense missile complex includes short-range missiles and tactical and strategic missiles. The ballistic missile complex encompasses not only attack missiles, but also launch vehicles.

This chapter examines the structures and principles of designing both individual control systems executing a number of specific functions, as well as the totality of such systems forming a single integrated system designed to perform a principal mission (for example, interception of air targets or striking of ground targets).

1.1. Function and Typical Structures of Flight Craft Control Systems

The trajectory of the mass center of a flight craft system is described by six functions of time: three coordinates and three velocity components. Sometimes they can be replaced by any six independent parameters uniquely expressed in terms of these functions. The motion of a body relative to its center of mass is also described by six functions, namely: three angles (which form axes of some absolute system and axes of coordinates associated with the body) and their first derivatives.

/8

These functions, as the solution of a system of ordinary differential equations of order twelve, completely represent the trajectory of the craft. The solutions obtained must satisfy the conditions of the technical capability of the given craft to execute the trajectory and guarantee, from the standpoint of the criterion chosen, the optimum solution of the flight mission or the function assigned to the complex as a whole.

Determination of a flight trajectory and its realization are assigned to the control system. The motion of a craft's center of mass and its motion relative to the center of mass can be considered separately in a number of cases.

Everywhere in the book we will mean by the term control only control of the motion of the center of mass.

The trajectory of motion and the control law can be found only given the condition that at some time instant coordinates and velocity components are known, which in turn are determined based on measurements of the parameters of the actual motion. Thus, some subsystem performing functions only of data acquisition and processing belongs to the control system. This subsystem is called the navigation or guidance system. The result of its functioning is a control law or control functions which describe changes in control forces as a function of time. The second part of this system -- the control system proper -- performs the function of implementing the control law developed by the navigation system.

Processes of determining the control law and its implementation need not necessarily follow directly one after the other. They can be separated by long intervals of time, as for example, in the case of the programmed control.

The equipment for data acquisition and processing and the equipment specifically implementing the control law can also be installed on different objects separated by great distances, for example, several missile command--instrumentation complexes. In a number of cases, especially when correcting a trajectory and in the homing process, the acquisition and processing of data and implementation of the control law occur nearly simultaneously. Data acquisition and processing can be implemented directly on board the craft or only on the ground, with subsequent transmission of commands to the control system of the flight craft. Depending on which approach is used, an autonomous or command system type, or some combination thereof are differentiated. An autonomous system presupposes, in addition, the absence of any active sources of radiation outside the flight craft. In these systems the same computer can be used in both data processing and in implementing the control law. /9

Command systems, in addition to data acquisition and processing equipment, include devices for encoding and for transmitting the control law of data reception and decoding. The first two groups of devices are located on the ground, and the second two -- on the flight craft.

Navigation systems are also characterized by the physical nature of the carrier signal conveying information on the actual motion of the object. Depending on this classification, navigation systems can be of the radar, optical, infrared, and inertial types. Moreover, systems can be divided into passive, active, and semi-active. The latter use the energy of active irradiation of external sources.

The advantage of command systems compared with autonomous systems is that in several complexes, for example, in missiles of all types, they permit multiple use of equipment. Their disadvantage is the limitation of the zones within which parameters of

motion and command transmission can be measured, which can deteriorate the effectiveness of mission performance by flight craft, limited carrying capacity of communication (control) channels, their poor antijamming capability, and also the worsening of the precision of measurements at great distances of the flight craft from the instrumentation complex.

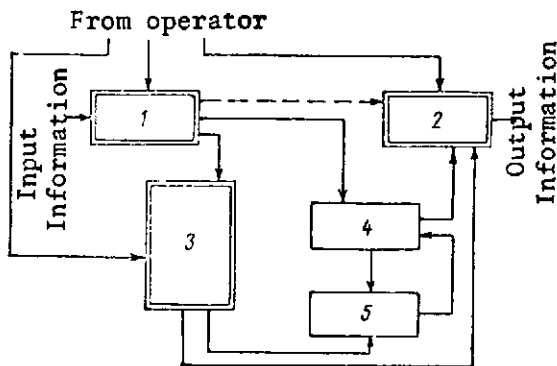


Fig. 1.1. Onboard computer block diagram:

- 1 -- Data input devices
- 2 -- Data output devices
- 3 -- Control devices
- 4 -- Memory
- 5 -- Arithmetic device

Autonomous systems in several cases require complicated onboard equipment with high reliability, which adds to the weight of the flight craft and occasions

special difficulties when the systems are used in long-range craft. /10

Differing degrees of automatization of navigation and control systems are possible, that is, different degrees of participation by man (operator) in data acquisition and processing and implementation of the control law. The current trend of introducing onboard computers does not preclude the duplication of their individual elements by man (Fig. 1.1) and, in particular, assigning him certain hard-to-algorithmize tasks (for example, those associated with image recognition, with decision-making, or with control of data acquisition and processing). In these processes human activity can be rationally combined with the functioning of semi-automatic devices.

To simplify the control of a flight craft, the control law can be found with allowance for certain supplementary conditions imposed on the trajectory. Several guidance methods are differentiated in relation to the kinds of conditions involved (Fig. 1.2) [8, 48, 66]. /11

When guidance by the pursuit method is used, the velocity vector of the flight craft must be continuously aimed at the target. In these cases the relative range r from the flight craft (interceptor) to the target and the angle ϕ_t between the target velocity vector \vec{V}_t and the relative range vector² /12

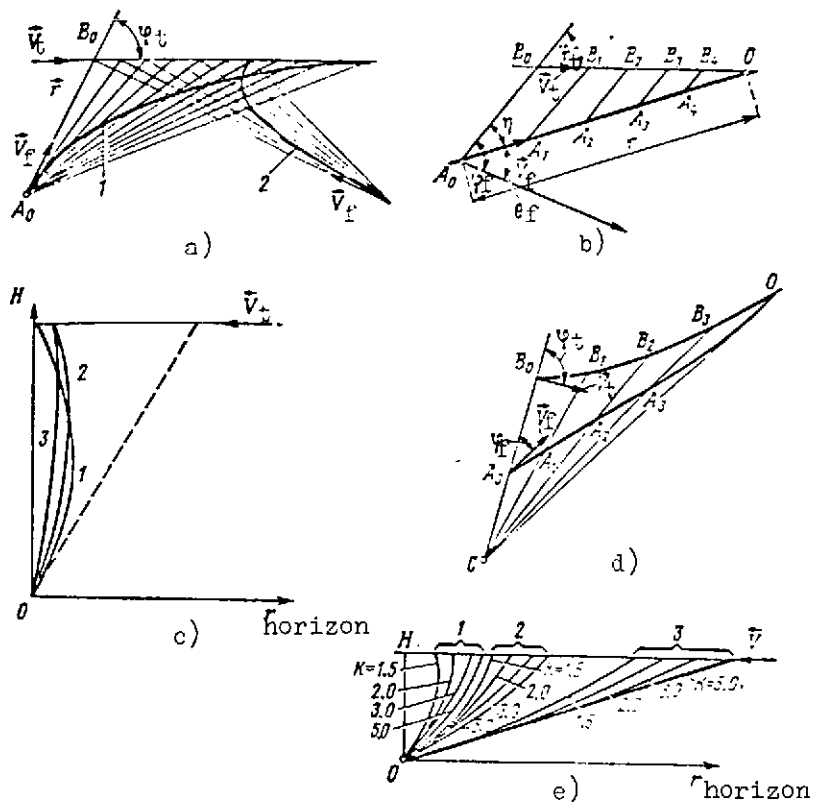


Fig. 1.2. Methods of flight craft guidance:

1 and 2 -- For passing collision and head-on collision courses respectively:

a -- Along pursuit curve
b -- Constant-bearing approach with non-maneuverable target

c -- Proportional approach

d -- Matching-curve approach with fixed guidance point:

A_i, B_i, C = positions of target, interceptor, and guidance point (fixed) at different time instants

e -- Beam-riding:

1 -- $\theta_f = 45^\circ$

2 -- $\theta_f = 30^\circ$

3 -- $\theta_f = 15^\circ$

[66]

are related by the following function:

$$r = c \frac{(1 + \cos \varphi_t)^{\pm k}}{(\sin \varphi_t)^{\pm(k \pm 1)}} \quad (1.1)$$

where

$$c = \frac{r_0 (\sin \varphi_{t0})^{\pm(k+1)}}{(1 + \cos \varphi_{t0})^{\pm k}}.$$

here $k = V_f/V_t$ (V_f is the interceptor velocity, and the index "0" corresponds to values of the function at the initial instant of approach).

The time of approach t is determined from the expression

$$t = \frac{\pm r(\cos \varphi_t \mp k) \mp r_0(\cos \varphi_{t0} \mp k)}{kV_f - V_t}. \quad (1.2)$$

The upper sign in expression (1.2) is taken for head-on collision courses, and the lower -- for passing collision courses.

By the constant-bearing approach method, the vector of the relative position of the interceptor-target (line AB in Fig. 1.2, B) must be shifted parallel to itself, that is, the condition $\dot{\phi}_f = 0$. The condition for the time balance ensuring simultaneous striking of the interceptor and target at the point of impact "0" gives rise to the bearing angle of the interceptor velocity vector \vec{V}_f , calculated in the form

$$\sin \eta = \frac{V_t}{V_f} \sin \varphi_t \quad (1.3)$$

Condition (1.3) is preserved even when the target velocity continuously changes. In this case all the quantities $\eta = \eta(t)$, $V_t = V_t(t)$, $V_f = V_f(t)$, $\phi_f = \phi_f(t)$ are functions of time, and guidance of each instant is exercised at the instantaneous impact point.

The guidance parameters are found from the following ratios: /13

$$\begin{aligned}
\eta &= \arccos \sqrt{1 - \frac{1}{k^2} \sin^2 \varphi_t}; \\
r &= r_0 + (V_t \cos \varphi_t - V_f \sqrt{1 - \frac{1}{k^2} \sin^2 \varphi_t}) t; \\
t_f &= r_0 (V_f \cos \eta - V_t \cos \varphi_t)^{-1}.
\end{aligned}
\tag{1.4}$$

In the proportional approach method (proportional navigation), the following condition must be met:

$$\dot{\theta}_f(t) = c \dot{\varphi}_f(t), \tag{1.5}$$

where ϕ_f is the bearing angle of the flight craft velocity vector; and c is the constant in the proportional approach method.

This method is more general than the two preceding ones. When $c = 1$ and with the appropriate selection of initial value of angle ϕ_{f0} , the condition of the pursuit method will be satisfied, and when $c \rightarrow \infty$, we approach the condition of constant-bearing approach $\dot{\phi}_f = 0$.

The matching-curve approach or the matching method (beam-riding guidance method) presupposes that the flight craft, guidance point, and the target are continuously on the same straight line. This condition is observed if the equality

$$\varphi_t(t) = \varphi_f(t)$$

is satisfied for any laws of motion of target, interceptor, and guidance point.

If the heading ϕ_f of the interceptor velocity vector is determined by the expression where

$$\sin \varphi_f = \frac{V_t}{V_f} \frac{\rho_f}{\rho_t} \sin \varphi_t.$$

ρ_f and ρ_t are the distances from the guidance point to the interceptor and target, respectively, then clearly at the beginning of a guidance when $\rho_f \ll \rho_t$, the trajectory of motion is close to the pursuit curve, and at the end of guidance, when $\rho_f \approx \rho_t$, it is close to the trajectory of the constant-bearing approach.

The so-called angular method, in which the function

/14

$$\Delta\varphi(\pm) = \varphi_t(\pm) - \varphi_f(t) \quad (1.8)$$

varies according to a given law can also be considered; it generalizes guidance by the method of constant-bearing approach and matching-curve technique.

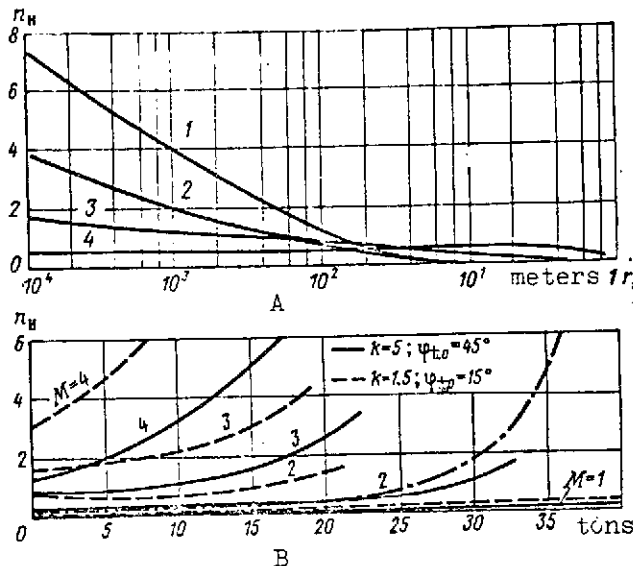


Fig. 1.3. Values of normal g-loads as a function of guidance method, flight time, or range of flight craft [66]:
A -- For guidance by the proportional approach method $\phi_0 = 60^\circ$, $k = 2$;

1 -- For $\eta = 26^\circ$; 2 -- for $\eta = 13^\circ$; 3 -- for $\eta = 3^\circ$; 4 -- for $\eta = 0^\circ$
B -- For beam-riding guidance, $H_t = 9.15$ km, $M = 1-4$ and for two k and ϕ_{t0} values; for comparison, the change in n_H for guidance by the pursuit method is indicated here with a dot-dashed line, $H_t = 9.15$ km, $\phi_{t0} = 14.4^\circ$, and $k = 4$

$$\angle r_h = r_{\text{horizon}}$$

An important parameter characterizing the guidance method is acceleration j_H acting on the flight craft normally to its trajectory (or its required g-load, $n_H = j_H/g$), Fig. 1.3, a-c [6] and determined by the derivative $\dot{\phi}_f$:

$$j_n = |V_T \dot{\phi}_f|. \quad (1.9)$$

The function $\dot{\phi}_f$ is found by using the following expressions: for the pursuit curve

/15

$$\theta_f = \frac{V_{\pm}}{c} \frac{(\sin \varphi_{\pm})^{\pm(k \pm 2)}}{(1 + \cos \varphi_{\pm})^{\pm k}}; \quad (1.10)$$

for constant-bearing approach

$$\theta_f = 0; \quad (1.11)$$

for matching-curve approach

$$\theta_f = \frac{2V_t \sin^2 \varphi_t}{H} \left[1 + r \cot \varphi_t \left(\frac{k^2 H^2}{\sin^4 \varphi_t} - r^2 \right)^{\frac{1}{2}} \right]; \quad (1.12)$$

for proportional approach

$$\begin{aligned} \dot{\theta}_t = & \frac{V_t}{r_0} (k \sin \varphi_0 - \sin \varphi_{f0}) \left(\frac{r}{r_0} \right)^{\frac{2(1+kc'sc_s)}{k^2-1}} \times \\ & \times \exp \frac{2k(r_1 - r_0) \sin \varphi_0}{k^2 - 1}. \end{aligned} \quad (1.13)$$

The upper signs in equation (1.10) are taken when approach is made along head-on collision courses, and the lower for approaches along passing collision courses. Here the appropriate expression for c is substituted according to formula (1.1). The normal acceleration or g -load for motion along the pursuit curve should have increased indefinitely at the instant of impact with the target (cf. Fig. 1.3, e). Actually, being finite, these quantities preserve their maximum possible value until the interceptor again switches to the pursuit method.

As is clear from expression (1.11), the angular velocity $\dot{\theta}_f$ or the g -load j_h for constant-bearing approach are equal to zero for the case of an attack on a nonmaneuvering target, which is an appreciable advantage of the method. When the target does maneuver at constant velocity, the g -load of the interceptor does not exceed the g -load of the target (excluding instrumental errors in the homing equipment and target fluctuations).

Equations describing motion in constant-bearing approaches admit of a solution in a closed form only for the value of the constant $c = 2$ in the method (cf. relationship (1.5)). In fact expression (1.3) is formulated for this case. Though acceleration in this case, as well as for motion along the pursuit curve, can attain high values, the reduction in the g -load during the hop to the target by the constant-bearing approach method renders

this method quite promising for homing systems or for command guidance of aircraft and missiles.

When two flight craft make a constant-bearing approach to an active, maneuvering target, a supplementary force ensuring realization of the approach method must also be imposed, reaching a considerable value for large initial ranges. This renders the use of the above-described guidance methods of flight craft at very large distances irrational.

However, they do find wide use in the guidance of aircraft and missiles of different types.

1.2. Control Systems of Aircraft-Missile Complexes

The aircraft-missile complex combines two flight craft: missile-carrying aircraft and air-to-air or air-to-surface missiles. Systems for guidance and control of aircraft and missile complexes will be divided structurally into two subsystems: long-range guidance bringing the aircraft to a range of up to several tens of kilometers from the flight target; short-range guidance or homing, with which the aircraft autonomously approaches a target, correcting the errors of long-range guidance by information on its relative position obtained by onboard instruments. Aircraft-missile complexes include a third subsystem -- the subsystem of guidance of the rocket to its target.

Long-range guidance systems with varying degrees of automation can be semiautonomous, command, or combination types.

Semiautonomous systems use ground-based localizer beacons, whose signals together with readings of onboard instruments give the pilot the information needed to realize a specific trajectory. /17

Semiautonomous aircraft systems with varying degrees of automation are shown schematically in Fig. 1.4, a and b [30].

In the system of blind or all-weather landing (Fig. 1.4, c), the pilot acts on the control devices guided by information he received from the ground and visually, and also by the readings of director instruments. Control devices also receive signals arriving automatically from the computer. Essentially this system can serve as an example of an automatic system in which control is corrected manually.

Aircraft systems of autonomous navigation are constructed mainly on the basis of inertial sensors (accelerometers). Advantages of the systems include the concealment of their operation (they do not betray themselves by any external radiations), anti-jamming capability, and rapid output of data regardless of meteorological conditions, relief of the terrain over which the aircraft

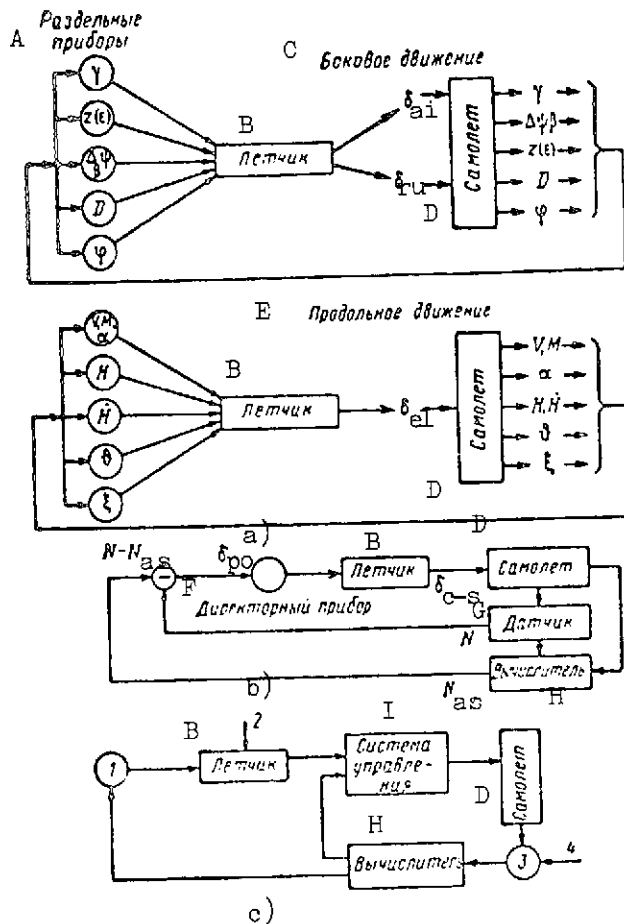


Fig. 1.4. Semiautonomous aircraft control systems:
a -- Manual control by instruments: ψ = radio beacon (radio station) heading angle; L = range to radio beacon; $z(\epsilon)$ is the cross track error from given course; $\Delta\psi$ is the difference between the given and instantaneous course;

α is the angle of attack
 β is the sideslip angle
 γ is the bank angle
 ϕ is the pitch angle
 ξ is the deviation from the given trajectory at height H

δ_{ai} , δ_{el} , and δ_{ru} are the deflection angles of the ailerons, elevators, and rudder

b -- the director heading based on a single channel
 N are the controlling parameters (angles of pitch, bearing, bank, and so on)

N_{as} are the assigned parameters in the computer (the same as those for control)

δ_{po} is the deflection angle of the director instrument pointer

δ_{c-s} is the control surface deflection angle

c -- manual and director controls;

1 -- indicators; 2 -- pilot's visual information; 3 -- ground-data acquisition devices; 4 -- information transmitted from the ground

KEY: A -- Separable instruments
B -- Pilot
C -- Side motion
D -- Aircraft
E -- Longitudinal motion

F -- Director instrument
G -- Sensor
H -- Computer
I -- Control system

is flying, and factors determining the time required to acquire incoming information.

The main drawback of inertial systems is the presence of errors linearly accumulating and varying with the Schuler period, which leads to the necessity of correcting them by feeding information from the Doppler velocity sensors, or correcting the positions of the axes of the accelerometers using radar or star trackers.

Various hyperbolic (Loran, Decca, and Gee) or circular (Shoran) systems are long-range semiautonomous navigation systems. Essentially, the operation of a difference-range finder hyperbolic system (Loran) consists in measurement onboard the aircraft of the difference Δt of the time of arrival of pulsed signals beamed by two ground stations proportional to the difference ΔR of the distances from the aircraft to the two adjoining stations

$$\Delta R = c \Delta t \quad (1.14)$$

(c is the radio wave propagation velocity in a homogeneous atmosphere) and remaining constant for movement along a hyperbola at whose foci these stations are located. To each value of this difference corresponds one of a set of confocal hyperbolas. The intersection of two hyperbolas belonging to different families determines the location of the aircraft relative to the ground stations, whose coordinates must be known well. /19

Two families of hyperbolas are realized by means of three stations, one of which is the master (radiating signals), and the two others are the slave stations, retransmitting the signals of the master station; here each pair of stations beams signals of different duration in the pair's carrier frequency.

When continuous modulated signals are beamed, the hyperbolic system can be constructed on the principle of measuring the phase difference (the Decca system). The quantity ΔR , in this case equal to the difference of the distances from the aircraft to the ground stations, is determined in terms of the phase difference $\Delta \Phi$ in the form

$$\Delta R = \frac{\lambda_0}{2\pi} \Delta \Phi, \quad (1.15)$$

where λ_0 is the working wavelength.

Hyperbolic systems can also be used for automatic navigation of aircraft and missiles.

They are characterized by great range (the Omega system, which differs from the Loran system by the lower working frequency, provides a range of more than 10,000 km) with a precision of aircraft position determination of from 0.9 percent of the distance at the angle $\pm 30^\circ$ (relative to the normal to the base line of the two stations) to 1.8 percent of the distance at the angle $\pm 60^\circ$ and nearly unlimited carrying capacity. However, errors in trajectory determination with increase in range become too great and the system itself is subjected to interference.

To acquire the third coordinate, information of a radio altimeter or other altitude meter is fed into the navigation system.

A global system of ultra long-range navigation can be also constructed in several ways based on artificial earth satellites.

First method. The Doppler frequency of a signal emitted by a satellite is measured on an aircraft or other moving object. The minimum distance between the aircraft and the navigation satellite is determined by the transit time of the Doppler frequency past zero and by the shape of the Doppler curve. Radio signals emitted by the navigation artificial earth satellite /AES/ contain information on its orbit (ephemerides), which is continually updated from transmitting ground stations from instrumentation complexes. Data on the absolute satellite position and on the relative position of the airplane at some instant of time and velocity permit its flight trajectory to be determined.

/20

Advantages of this system of navigation (Fig. 1.5, a and b) are not only its global coverage (with the appropriate number and arrangement of AES), high potential accuracy, and independence of meteorological conditions, but also the absence of communications with the ground.

Navigation using special Transit type satellites can provide an accuracy of aircraft position determination to several hundreds of meters.

The second method /150/ is based on measuring the relative range two or three satellites and can be realized both in a version similar to the Loran system (satellites with specific discretization emit coded signals), as well as in a version in which the satellites are used as active two-way relay stations on the lines: aircraft-AES and AES-ground station. When two AES are used, additional radio altimeter data is required; measurement relative to three satellites gives all the needed information.

/21

The third method is based on measuring the aircraft-AES heading relative to some fixed axis. In this case the satellite has two mutually perpendicular directional antennas, whose

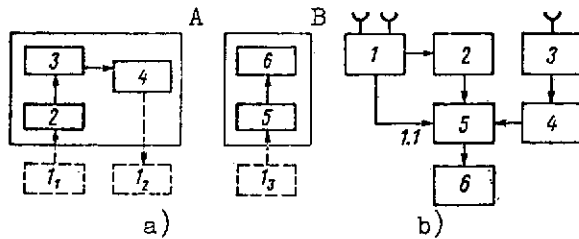


Fig. 1.5. AES-aided navigation block diagram:
a -- entire complex: A -- ground equipment
B -- equipment located on the airplane
 l_1 , l_2 and l_3 -- navigation at time instants t_1 , t_2 , and t_3 ($t_1 < t_2 < t_3$)

- 2 -- AES tracking station
- 3 -- coordination-computer center
- 4 -- station transmitting orbital parameters for the AES
- 5 -- aircraft receiver
- 6 -- computer
- b -- onboard aircraft equipment:
 - 1 -- receiver of AES signals (1.1 -- Doppler frequency)
 - 2 -- orbital data block
 - 3 -- time signal receiver
 - 4 -- time transducer
 - 5 -- computer
 - 6 -- indicators of aircraft position data

position is stabilized in space (the Westinghouse project [1507]), or which on rotating at a certain velocity form a fan-shaped radiation pattern (the Philco-Ford project). In the latter case not only must the time instant and angle at which the aircraft transits the directional radio beam be known, but also the ephemerides of the satellite, its orientation, and its angular velocity.

All these methods presuppose a system including several AES arranged in specific orbits, a ground complex for the determination of their trajectory and the transmission of required data to them, onboard equipment on the aircraft, consisting of receivers acquiring AES data, and sometimes even interrogator-stations and an onboard computer. The onboard aircraft system also needs a high-precision time transducer: time signals, however, can be transmitted to it from the AES.

When building integrated navigation systems (Fig. 1.6, a [307]), various combinations of two or several different data sources are possible. This complexity of the system imposes increased requirements on the computer used not only in solving navigation problems, but also for control. For example, the MH-97 automatic integrated system built by Minneapolis-Honeywell, designed for installation on jet fighters, provides by means of three principal systems the stabilization of the magnetic heading,

altitude, and indicated speed; aircraft control in interception and attack; stabilization of the aircraft with respect to the three axes; and warning of the pilot on ejection in dangerous flight regimes.

In control executed during interception and attack, the pilot must establish one of four operating regimes: maintenance of altitude, maintenance of the M number, turn to the right or left, and automatic piloting (holding to a given flight regime).

/23

/22

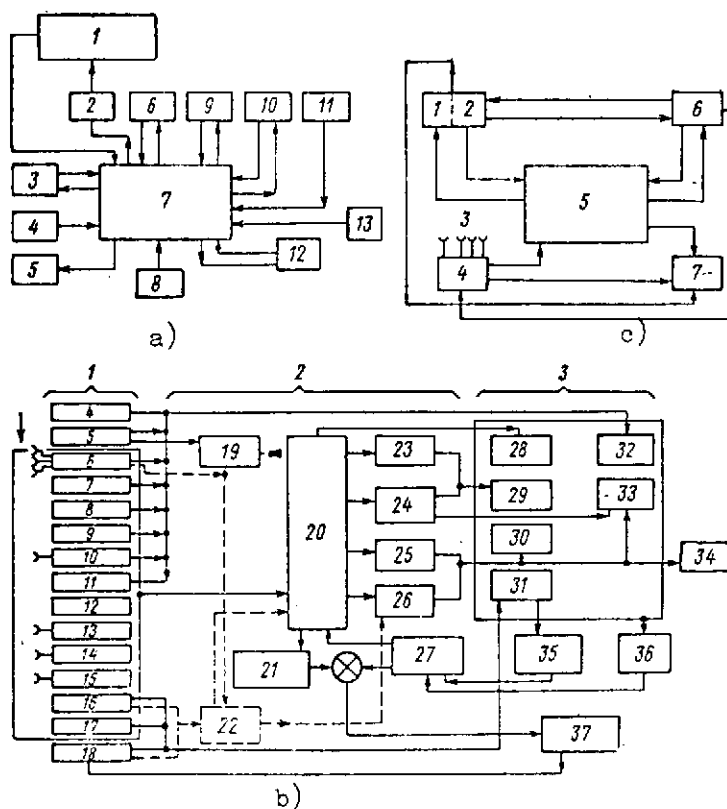


Fig. 1.6. Block diagrams of aircraft navigation and control systems:

- a -- integrated navigation system:
- 1 -- aircraft
- 2 -- autopilot
- 3 -- Doppler sensors
- 4 -- altitude and velocity sensors
- 5 -- data output instruments
- 6 -- compass system
- 7 -- computer
- 8 -- fuel indicators
- 9 -- inertial system

Fig. 1.6. Block diagrams of aircraft navigation and control systems:

/Continuation/

- 10 -- automatic astrosextant
- 11 -- automatic landing system
- 12 -- sight
- 13 -- radio sensors
- b -- AN/ASQ-61 DJANE system:
 - 1 -- sensor
 - 2 -- computer
 - 3 -- indicator
 - 4 -- temperature sensor
 - 5 -- static pressure sensor
 - 6 -- stellar navigator
 - 7 -- compass
 - 8 -- inertial platform
 - 9 -- vertical gyro
 - 10 -- radio altimeter
 - 11 -- angle-of-attack sensor
 - 12 -- slip-angle sensor
 - 13 -- search radar
 - 14 -- tracking radar
 - 15 -- Doppler radar
 - 16 -- fuel consumption meter
 - 17 -- engine sensor
 - 18 -- signaling
 - 19 -- air data system computer
 - 20 -- central computer
 - 21 -- flight control subsystem
 - 22 -- data output device
 - 23 -- analog data scanning generator
 - 24 -- search radar scanning generator
 - 25 -- terrain map scanning generator
 - 26 -- navigator indicator scanning generator
 - 27 -- console
 - 28 -- telescopic sight
 - 29 and 30 -- pilot's vertical and horizontal indicators
 - 31 -- monitoring instruments
 - 32 -- standby instruments
 - 33 -- navigator's indicator
 - 34 -- recorders (for test)
 - 35 -- pilot
 - 36 -- navigator
 - 37 -- aircraft
- c -- MA-1 system:
 - 1 -- fire control system
 - 2 -- radar
 - 3 -- antennas for communication, navigation, data transmission, and blind landing
 - 4 -- communication, navigation, and landing devices
 - 5 -- digiter onboard computer
 - 6 -- control and display devices
 - 7 -- automatic flight control system

In developing aircraft control systems, a trend toward the integration of electronic and instrumental equipment based on the onboard computer has been observed; in this case the computer can function in the aircraft navigation or control system, and in the guidance of guided missiles and fire control.

An example of such a system is AN/ASQ-61 DJANE (Fig. 1.6, b /168/). The pilot's role here amounts mainly to decision-making and executing required corrective actions. The tracking radar (AN/APQ-88) displays an image of the terrain in front of the airplane and may also lock onto moving targets, including guided missiles launched from the ground or from the air, while the search radar AN/APQ-98 detects moving targets, scans the terrain ahead of the aircraft, and operates together with the obstacle-bypassing radar. The central computer not only generates corrective signals for the control system, but also can control the flight of air-to-air or air-to-surface missiles. The automatic control subsystem AN/ASW-16 is capable of realizing all aircraft maneuvers (except for takeoff and landing), including side sighting for bombing. An example of a system functioning in the regime of command or autonomous guidance is the MA-1 system (Fig. 1.6, c), providing for automatic airplane flight from the time of liftoff to leveling at landing. The system has an onboard radar, but can also operate with the ground-based Sage system or the Tacan short-range radio navigation system.

In semiautonomous guidance, the Sage or Tacan system, or just the Tacan system alone are used. Attack on the target is executed automatically or with the pilot's participation by the pursuit or constant-bearing approach method.

The complexity of equipment and the presence of an onboard digital computer make it necessary and possible to assign to the computer the task of monitoring the status of the systems, detection and automatic elimination of malfunctions (as, for example, is done in the JLAAS electronic system of the U.S. Air Force, developed for the A-7A Corsair Ling-Temco-Vought light bomber). These systems, executing self-monitoring during flight, can communicate malfunction data to the pilot and in the event of serious failures take measures for normal functioning. /24

One of the measures used in overcoming antiaircraft defenses equipped with missiles is low-altitude flights toward a target. The navigation system in this case is automatic or semiautomatic and utilizes data coming from sensors and the radar measuring headings and range. Two types of tracking systems for terrain relief are known. In the first of these the azimuthal radar scans in the horizontal plane and feeds information on the distance to the nearest objects at the given altitude in relation to azimuth; the maneuver is executed mainly in the horizontal plane. In this way it is difficult to provide for a very low flight altitude.

In the second case the radar beam is directed in the horizontal plane along the heading and scans the vertical plane. This method makes it possible to guide the aircraft at a lower altitude. A measure of simplification of the system consists in equipping the onboard radar with a nonscanning antenna generating signals about an obstacle in front of the aircraft.

Control of air-to-surface and air-to-air missiles is constructed on one of five guidance schemes: command semiautomatic, command automatic, beam-riding, homing, and combination (for the initial section with inertial or command system, and with homing for the final section).

The simplest semiautomatic system of command guidance, which -- it is true -- has a limited range, is the optical system, providing sighting of ground point targets and missile flare. An increase in the range (for example, to 80 km for the Condor missile) is achieved by using a television system. In the opinion of foreign specialists, the general disadvantage of all these optical and television guidance systems is their dependence on conditions of visibility, and the possibility of camouflaging targets by enemy smokescreens.

When missiles are controlled by radar, the task of using the same radar for actions both against air as well as ground targets is imposed.

/25

Here there arises a difficulty associated with an increase not only in the irradiation frequency, but also in the beam width, which is due to the need to scan the greatest possible portion of the sky for a high probability of air target detection. But a narrow beam must be used in the system for air-to-surface missiles to recognize the target in the midst of local objects producing screen interference. A broad variation in the radar's working frequency with changes in the nature of its operation is used to solve this problem.

In the guidance systems of air-to-air and air-to-surface missiles the same integrating system is used as in navigation systems on aircraft. In particular, when the guidance radar of missiles is used, the Doppler system based on nonattenuated waves, with higher resolving power but not providing rapid information on range, can be combined with a pulsed radar system.

Laser missile control systems are even more precise than Doppler systems (theoretically, by one order of magnitude). The physical nature of the laser beam permits it to be produced without using antennas, which avoids radar blanketing effect, especially for flat angles. Foreign specialists cite as one of the drawbacks of laser systems the impossibility of their functioning in an occluded atmosphere, in rain and fog.

Air-to-air rocket homing systems, as shown by the analysis given in [137], are equipped with semiactive radar or passive heat-seeking heads. The functioning of the former does not depend on meteorological conditions and the time of the day; they are suitable for all-angle and all-weather attacks. The second, in addition to the covertness of operation, exhibit high precision for small mass and are the best for firing from the rear hemisphere.

The sensitivity of radar systems to jamming adversely affects also the effectiveness of radio fuses installed in missiles. Therefore, a remote controlled fuse receiving a command signal from the aircraft radar is used in foreign missiles. Selection of the guidance (or homing) method is reflected in missile design (its strength and mass), and the type and design of its onboard equipment. Since these problems are common to all guided missiles, they are considered in the following section. /26

1.3. Control Systems of Antiaircraft Missile Complexes

Antiaircraft missile complexes are intended to strike the enemy's flight craft (airplanes and missiles) from ground fire positions or ships. The guidance systems are of the automatic or semiautomatic type with very limited operator participation. The most widespread guidance systems for foreign antiaircraft guided missiles (AGM) or surface-to-air missiles (SAM) are the command (beam-riding guidance) or semiautonomous systems.

A feature of command guidance systems is the fact that the miss (the minimum distance in the leg of a missile near a target) is proportional to the range L . A greater miss distance leads to an increase in the size of the warhead. Therefore command guidance systems are used only for antiaircraft missiles of relatively short range; they can be used for guidance of no more than one missile at the same time. The advantage of these systems is the simplicity of the onboard equipment. Of course, this is achieved by increasing complexity of the ground system, which, however, can be used again and again.

In automatic command systems using the lead point guidance method (Fig. 1.7, a), tracking radars provide information on the elevation angle, azimuth angle, and slant range (ϕ, χ, L_H).

Tracking of a missile is made easier if a transponder is installed onboard the missile, sending coded radio pulses to the guidance station.

The data acquisition equipment in the control system using the matching-curve method (Fig. 1.7, b) includes only onboard coordinators [64, 66]. The onboard system of the missile, positioned along the antenna axis, does not develop signals and, thereby, control commands until the antennas located at the ends of the missile fin assembly receive signals of equal intensity. /27

Since the magnitude of the control force must be proportional to the linear deviation from the trajectory, the onboard system must contain elements determining the range to the guidance station.

A version based on this principle of a semiautomatic system is possible in which the operator, by moving the command instrument knob, tries to align the missile marker with the target marker on his indicator. In the layout (Fig. 1.7, b), the computer solves in advance the problem of the proper alignment of the launching installation by aiming the missile along the shortest distance to the radar antenna coverage zone.

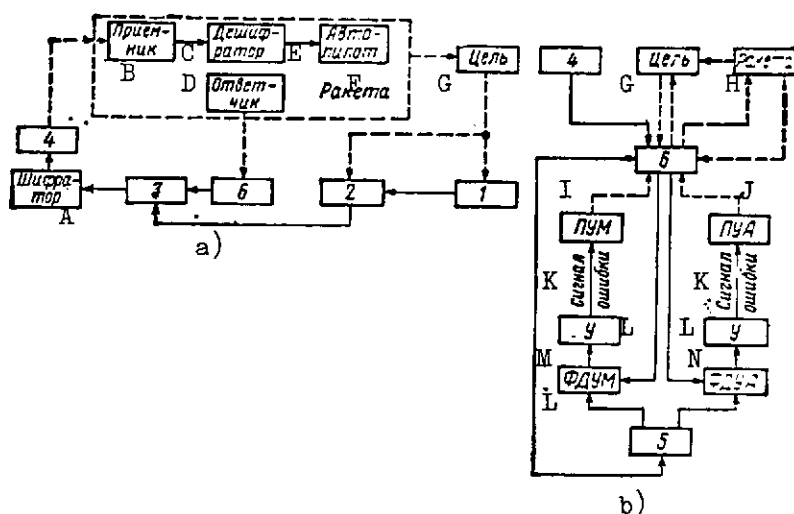


Fig. 1.7. Block diagrams of automatic and semiautomatic surface-to-air missiles using command guidance:

- a -- automatic command guidance system
 - b -- semiautomatic command guidance system
 - 1 -- target detection radar
 - 2 -- target tracking radar
 - 3 -- computer
 - 4 -- master beam radar transmitter
 - 5 -- master beam radar receiver
 - 6 -- antenna
- KEY:
- A -- Encoder
 - B -- Receiver
 - C -- Decoder
 - D -- Transponder
 - E -- Autopilot
 - F -- Missile
 - G -- Target
 - H -- Missile
 - I -- Control drive for elevation angle

Fig. 1.7. Block diagrams of automatic and semi-automatic surface-to-air missiles using command guidance:

[Continuation]

- J -- Control drive for azimuth angle
- K -- Error signal
- L -- Amplifier
- M -- Elevation angle phase discriminator
- N -- Azimuth angle phase discriminator

Analytic functions describing guidance by the matching-curve method show that it is marked by a large trajectory curvature, and, therefore, large g-loads that increase guidance errors. This, in turn, leads to a reduction in the system's effectiveness. The large trajectory curvature leads to the necessity of having large aerodynamic lift surfaces, which adds to the missile's weight.

As can be seen from the functions (1-9) - (1.13) and the curves in Fig. 1.13, other guidance methods are characterized by smaller g-loads. Their implementation, however, requires measurements of range and the solution during the guidance process of fairly complicated equations. All this reduces anti-jamming capability and leads to an increase in the level of noise and fluctuation errors. The time for movement along curved trajectories in the matching-curve method is longer than for guidance by the lead point method. However, as noted by foreign specialists, this advantage of the latter method disappears when guidance toward a nonmaneuvering target is involved. As one of the advantages of the matching-curve method, they note also the possibility of guidance of several SAM with a single master radio beam. /28

Foreign designers, as a rule, use the proportional approach method in the homing systems of antiaircraft guided missiles [AGM], building the systems on the basis of passive or semiactive coordinators ("lighting" of the target is done with ground radar). They believe that semiactive systems with long range capability along with relatively small weight of onboard equipment are best. In large-radius missile complexes they use homing systems in the direct approach to the target after the long-range guidance stage.

1.4. Ballistic Missile Control Systems

Ballistic missiles are designed to strike ground targets at considerable distances from the launch site. Due to the increasing weight of payloads, recently -- according to the data in [138], booster stages of ballistic missiles have begun to be replaced by more powerful launch-vehicle stages (cf. Section 2.8). Carrying out these tasks imposes high requirements on the accuracy of missile motion along a trajectory.

Fig. 1.8 [43] shows the allowable errors of inertial guidance systems of ballistic missiles (BM); also included in this figure for sake of comparison are analogous curves characterizing the control systems of space craft (SC) of various types (SC proper and their control systems are examined in Chapter Five). From the figure it is clear that curve 4 of BM accuracy lies in the region characterizing the accuracy of SC launching for inter-planetary flights (curves 5 and 6).

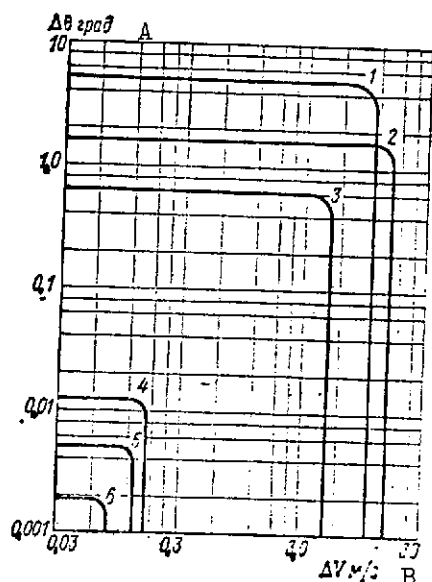


Fig. 1.8. Requirements on the accuracy of determination of velocity vector as a function of mission of ballistic missile or space craft [43]:

- 1 -- V-2 rocket
- 2 -- Artificial earth satellite
- 3 -- Space craft for lunar flight
- 4 -- Present-day long-range ballistic missile
- 5 -- Space craft for Mars flight
- 6 -- Space craft for circumlunar flight

KEY: A -- degrees
B -- m/sec

[In Russian decimal number usage, commas are equivalent to decimal points in American practice.]

Over the long free phase of a SC flight there is the possibility of refining and correcting the trajectory by using data from ground or onboard facilities. This is impossible with the BM [135] in view of the absence of ground stations along routes, the inacceptability of using active onboard devices that would decamouflage the missile, and also due to the complexity of building reliable astronavigational autonomous systems permitting the solution of the navigation problem with high accuracy over a relatively short trajectory phase. All this leads to the use of autonomous and high-precision inertial navigation systems for ballistic missiles. Such is the case, for example, with the inertial navigation system of the Titan II ballistic missile, or -- with the addition of one more stage -- the Titan IIIC launch-vehicle⁵. /30

In the view of its developers, the integrated control system of the Titan missile [62], besides high accuracy of target impact, must provide the following:

- a) short prelaunch preparation period;
- b) reduction in the size of ground equipment (compared with the Atlas missile system);

- c) invulnerability to jamming;
- d) possibility of simultaneous launch of several missiles;
- e) high reliability (automatic detection of malfunctions and their semiautomatic elimination);
- f) minimum [sic] simplicity of replacing and repairing equipment with the minimum number of maintenance personnel; and
- g) the possibility of silo launch of missiles.

The main control stages of a ballistic missile are as follows: flight during the powered phase, stage separation, and stabilization during the transition to the ballistic flight phase. Control of the motion of the mass center and missile orientation are executed during the powered flight phase, and control only by orientation -- during the ballistic flight phase.

A simplified block diagram of the integrated system of the Titan IIIC launch-vehicle is shown in Fig. 1.9 a [62].

Initial orientation of the gyrostabilized platform and its fixation to the absolute terrestrial coordinate system is carried out with platform-mounted pendulums and an optical device for azimuthal orientation.

The onboard integrated control system can operate with automatic self-monitoring and in addition it is linked to the ground station in such a way that the duty operator can monitor it and control it at a distance (Fig. 1.9 b [173]).

Fig. 1.10 a [62] presents as an example the block-diagram of the control system for the pitch channel during the powered flight phase of the Titan IIIC missile, based on ordinary operational amplifiers. The presence of six different flight programs made it necessary to readily adapt the system to changes in the gain factor of the missile itself. To solve this problem, the system is divided into two interchangeable parts. The powered section is standard for all flights, but the passive section depends on the flight program. [31]

A combination of first-order filters is used in the control system for missile stabilization. In all except the zero stage, thrust is controlled by deflection of engines mounted in gimbal suspensions. The engine thrust vector in the zero stage is changed by using injector valve control.

The control system for the powered trajectory section has eight variants for changing the gain factor during flight, which is done by switching in resistors in the amplifier input by command of navigation signals (cf. Fig. 1.10 a). Dynamic compensation is achieved by switching in passive RC-filters in the feedback circuit and in the amplifier input.

Fig. 1.10 b presents one of the control channels for the orientation of the missile warhead during the free flight phase. The control regime is set up in relation to the rate of orientation change. The regime of fixed and variable pulses is used at high velocities; only the fixed-pulse circuit operates at low velocities. The fixed-pulse section stabilizing the head is shaped by two flip-flop pairs, providing two triggering levels in each direction. The variable-pulse circuit includes lead signal-shaping amplifiers, followed by two identical flip-flops. The output of the shaping device depends on the orientation error and on its rate change.

The accuracy of the Titan III missile control system can be characterized, for example, by the results of a December 1964 launch of an AES [artificial earth satellite] into orbit with apogee and perigee of 189 and 182 km, respectively, as against a planned circular orbit altitude of 185 km. The time of revolution (88.2 minutes) differed from the planned value by only 0.04 minutes.

The inertial system of the Saturn IC launch vehicle is another example. It can solve navigation problems autonomously based on information acquired from the gyroinertial block and the rate gyroscope, but also receive correcting radio commands from a ground command-instrumentation complex (Fig. 1.11 a [347]).

/34

/35

The functional diagram of the onboard navigation system of the Saturn V missile, constructed in accordance with an iterative navigation algorithm [70, 130], is shown in Fig. 1.11 a [347]. The ST-124-M three-axes gyro platform, whose stabilization is achieved with two-degree-of-freedom gyros with air suspension, is one of the sources of information for the navigation system and an element in the orientation control system (Fig. 1.11 c [347]). It has unlimited rolling angles relative to the pitch and bank axes and a rolling angle of $\pm 60^\circ$ C about the yawing axis (relative to the launch position). Trends are executed in the sequence of change of the pitch, yaw, and bank angle read off from the stabilized platform.

Readings of the sensors of the gimbal suspension turn angles (measured with two-scale sensors) and the readings of nine (three for each axis) integrating floated gyro accelerometers serve as information sources for the navigation and orientation system, just as for similar systems of the Titan missile.

Information is processed by the onboard computer, converters, and onboard data processing installation.

The onboard computer output consists of control commands for orientation and trajectory change, and also commands for

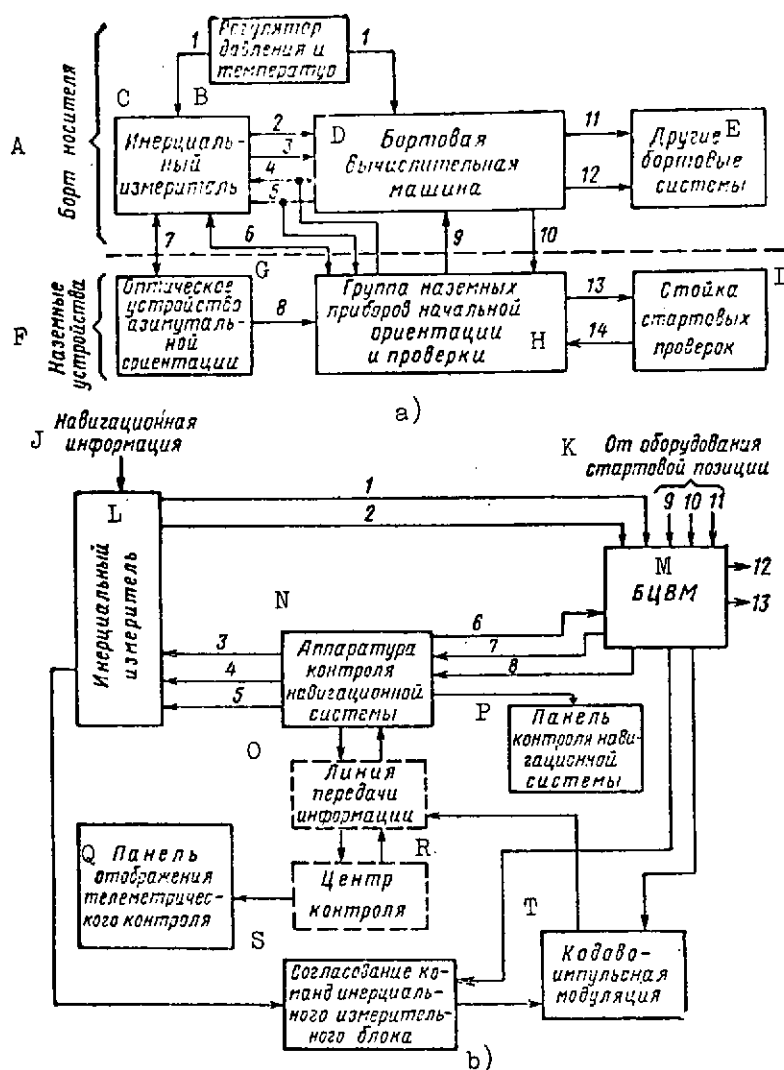


Fig. 1.9. Inertial navigation systems of the Titan IIIC missile:

a -- block diagram:

- | | |
|---|--|
| 1 -- coolant | 8 -- azimuth error signal |
| 2 -- velocity | 9 -- onboard computer data |
| 3 -- angular coordinates | input |
| 4 -- commands | 10 -- readout of onboard computer data |
| 5 -- monitoring signals | 11 -- discrete commands |
| 6 -- initial orientation (erection) signals | 12 -- angular deviations from program |
| 7 -- optical beam | 13 and 14 -- signals from launch check stand |

Fig. 1.9. Inertial navigation systems of the
Titan IIIC missile /continued/:

- b -- data block diagram:
 - 1 -- accelerometer readings
 - 2 -- angles of gimbal-ring deviations
 - 3 -- monitoring signals
 - 4 -- control signals
 - 5 -- gyro-stabilized platform erection signals
 - 6 -- functioning sequence check
 - 7 -- onboard computer monitoring signals
 - 8 -- check of assigned values of controllable parameters
 - 9 -- monitoring variables for accelerometer checks
 - 10 -- monitoring variables for gyroscope checks
 - 11 -- standard target parameters
 - 12 -- control commands
 - 13 -- discrete signals
- KEY:
- A -- onboard the launch vehicle
 - B -- pressure and temperature regulator
 - C -- inertial instrumentation
 - D -- onboard computer
 - E -- other onboard systems
 - F -- ground facilities
 - G -- optical device for azimuthal orientation
 - H -- group of ground instruments for initial orientation and check
 - I -- launch check stand
 - J -- navigation information
 - K -- from launch site equipment
 - L -- inertial instrumentation
 - M -- onboard computer
 - N -- navigation system monitoring equipment
 - O -- data link
 - P -- navigation system monitoring console
 - Q -- telemetric monitoring display console
 - R -- monitoring center
 - S -- matching of inertial instrumentation block commands
 - T -- pulse-code modulation

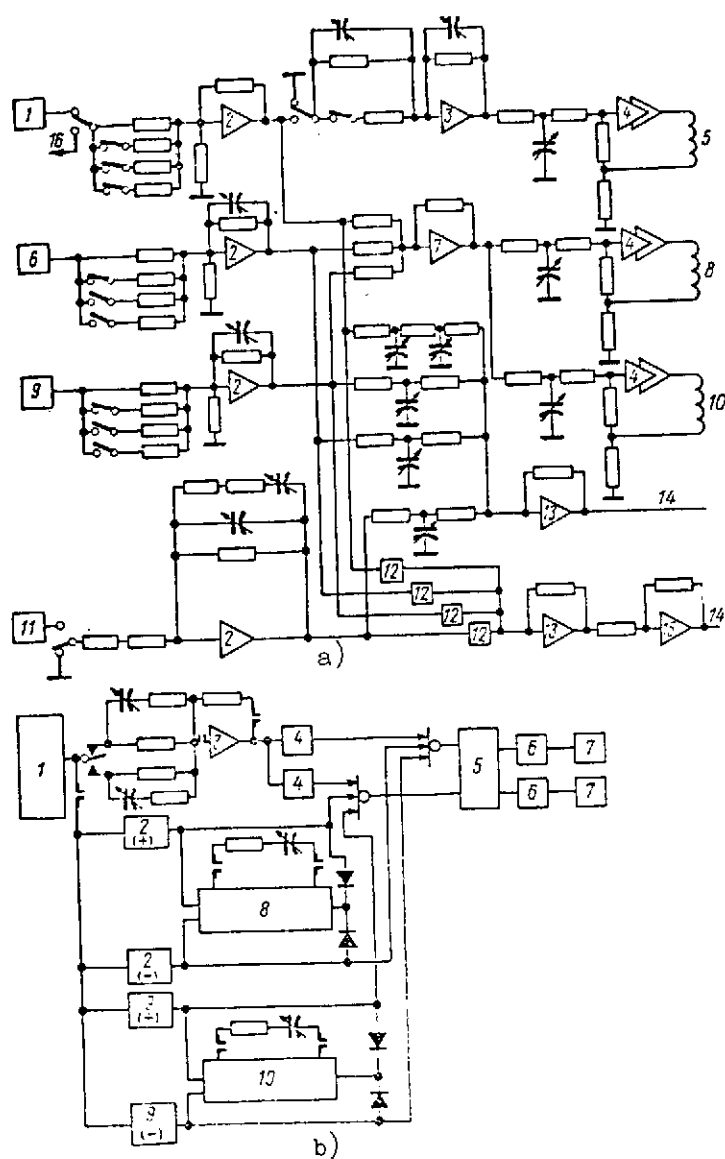


Fig. 1.10. Block diagram of individual flight control systems of the Titan IIIC missile for the powered and free flight phases:

- a -- pitch stabilization system for powered phase:
- 1 -- inertial guidance system
- 2 -- amplifier with variable gain factor
- 3 -- velocity amplifier
- 4 -- servodrive amplifier
- 5 -- third-stage drive
- 6 -- first-stage rate gyro
- 7 -- summator

Fig. 1.10. Block diagram of individual flight control systems of the Titan IIIC missile for the powered and free flight phases

Continued:

- 8 -- second-stage drive
- 9 -- first-stage rate gyro
- 10 -- first-stage drive
- 11 -- accelerometer
- 12 -- filter
- 13 -- thrust vector amplifier
- 14 -- to output of zero-stage solid fuel engine
- 15 -- converter
- 16 -- to ground monitoring system
- b -- control system for orientation during free flight phase:
- 1 -- inertial guiding system
- 2 -- first level discriminator
- 3 -- operation amplifier
- 4 -- level discriminator
- 5 -- multiplexer of engine orientation control system
- 6 -- drive winding
- 7 -- controlling engines
- 8 -- block shaping first single-action (long) pulse
- 9 -- second level discriminator
- 10 -- block shaping second single-action (short) pulse

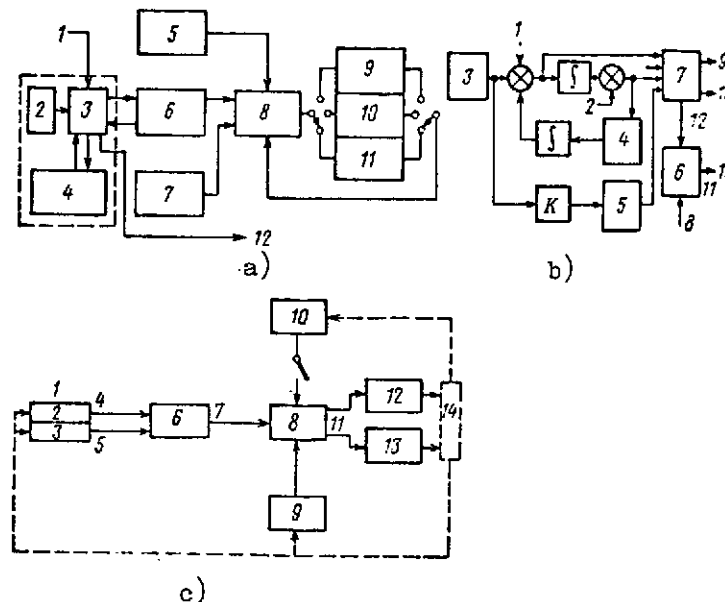


Fig. 1.11. Block diagram and functional diagrams of inertial navigation system of Saturn type missiles

Fig. 1.11. Block diagram and functional diagrams of inertial navigation system of Saturn type missiles

[Continued]:

- a -- block diagram of Saturn IC missile system:
 - 1 -- radio correction commands from ground
 - 2 -- fore-and-aft accelerometer
 - 3 -- data converter
 - 4 -- onboard computer
 - 5 -- accelerometer
 - 6 -- gyrostabilized platform
 - 7 -- rate gyro
 - 8 -- analog computer
 - 9, 10 & 11 -- power drives of first, second, and third stage engines
 - 12 -- commands from various onboard systems
- b -- functional diagram of navigational system of Saturn V missile:
 - 1 -- initial velocity
 - 2 -- initial coordinates
 - 3 -- integrating accelerometer
 - 4 -- computation of gravitational acceleration $g(r)$
 - 5 -- computation of intermediate functions of algorithm for solving navigational problem
 - 6 -- computation of orientation command
 - 7 -- navigational computations
 - 8 -- gyrostabilized platform turn angles
 - 9 -- cutoff of vernier engine and trajectory control
 - 10 -- firing of vernier engine and trajectory control
 - 11 -- orientation commands
 - 12 -- required orientation angles
 - 13 -- other signals arriving at the orientation control system
- c -- control system for Saturn V missile orientation:
 - 1 -- gyrostabilized platform
 - 2 -- articulated platform suspension
 - 3 -- integrating accelerometers
 - 4 -- platform turn angles
 - 5 -- accelerometer readings
 - 6 -- computations of navigation and orientation command
 - 7 -- orientation command
 - 8 -- computation of control command
 - 9 -- rate gyro with fixed axes
 - 10 -- fore-and-aft accelerometer (only in the Saturn IB)
 - 11 -- engine control command
 - 12 -- trajectory-changing engines
 - 13 -- orientation-changing engines
 - 14 -- missile dynamics

stage separation and telemetric data on the functioning of the system and the parameters of the trajectory being executed.

The computer of the control system shapes the commands for the power drives of the swiveling sustainer engines in each of the three stages and controls the firing of six auxiliary engines secured on the third S-4B stage. An operational memory (Fig. 1.12) serves to acquire data which for certain reasons cannot be transmitted at a given instant to the earth. A safety device, with which each missile stage is equipped, provides a command for cutoff of engines in the event of hazard arising during flight (for example, rupture of fuel tanks).

The importance of the Saturn V launch vehicle control system for the life of astronauts and the successive realization of the flight program of the Apollo spacecraft and the complexity of its functioning require several measures to increase reliability. In designing this problem was deemed to be more important than the need to reduce the weight, required power, and even part of the cost. /36

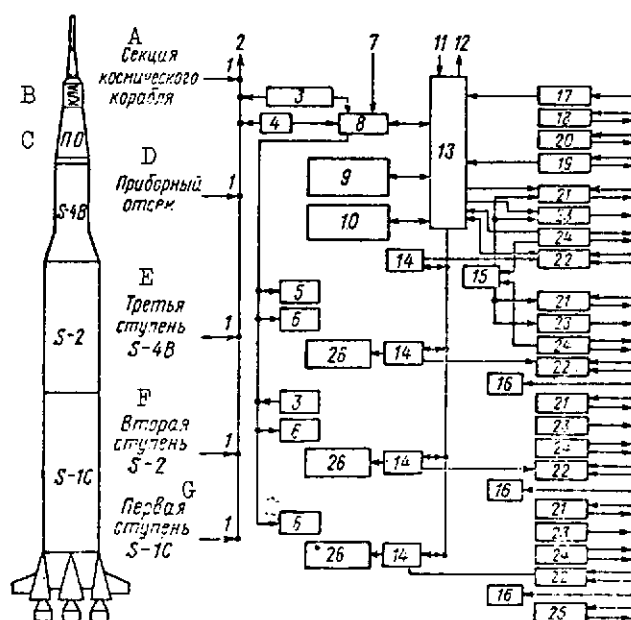


Fig. 1.12. General block diagram of the control system of the Saturn V missile

- 1 -- A system for determining emergency situation
- 2 -- Decisions adopted on emergency return
- 3 -- Control system accelerometer
- 4 -- Rate gyro
- 5 -- Firing of fixed auxiliary engines
- 6 -- Power drive of swiveled sustainer engines
- 7 -- Control commands
- 8 -- Analog computer of control system
- 9 -- Onboard digital computer
- 10 -- Gyrostabilized platform
- 11 -- Orientation of control commands
- 12 -- Signals arriving at the orientation of control system
- 13 -- Converter
- 14 -- Multiplexer
- 15 -- Operational memory
- 16 -- Safety device

Fig. 1.12. General block diagram of the control system of the Saturn V missile

/Continued/

- 17 -- Command link receiver
 - 18 -- Transponder operating in the C-range
 - 19 -- Transponder operating in the S-range
 - 20 -- Radio range beacon transponder
 - 21 -- Digital data acquisition system (DDAS)
 - 22 -- Calibrated telemetric system (RACS /radio acquisition control system/)
 - 23 -- Telemetric data
 - 24 -- Measurement data
 - 25 -- Doppler transponder (ODOP /offset Doppler/)
 - 26 -- Firing and cutoff of power plant
- KEY: A -- Spacecraft section
 B -- Spacecraft
 C -- Instrumentation compartment
 D -- Instrumentation compartment
 E -- S-B third stage
 F -- S-2 second stage
 G -- S-1C first stage

Standby provision of various elements and subsystems in the navigation and control systems of the Saturn V missile was constructed in accordance with the principle of obtaining maximum rational advantage -- use of the simplest elements, absence of appreciable complication of systems, and other significant losses. If u_r is the unreliability factor, the expected number of failures of various elements or subsystems per million flights (with the condition of a successful launch), and u_s is the same index for a wholly nonstandby system (a standby system is absent), the attained reliability characteristics of the control system are specified by the following values /76/:

$$u_r = 10,775, \quad u_s = 56,959, \quad u_s/u_r = 5.3.$$

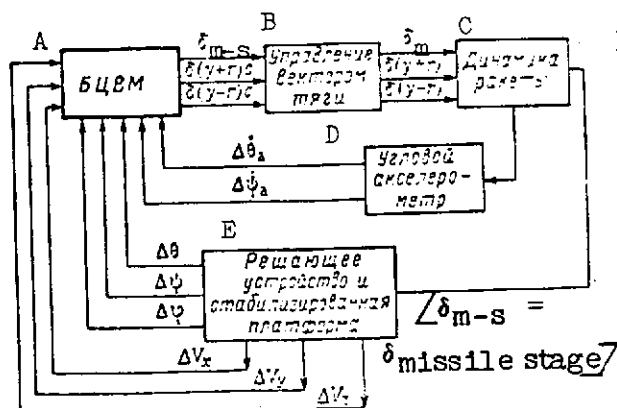


Fig. 1.13. Block diagram of the integrated control system of Minuteman I and Minuteman II

- KEY: A -- Onboard computer
 B -- Control of thrust factor
 C -- Missile dynamics
 D -- Angular accelerometer
 E -- Computer and stabilized platform

Let us examine the integrated control systems of the Minuteman I or Minuteman II missiles; they are identical and differ only by the degree of reliability and by weight of equipment (Fig. 1.13 [102]). The system controls the thrust vector and the third-stage engine cutoff instant, sends commands for stage separation and firing of the next engine, activates missile defense countermeasures at the required time, orients the missile nose cone as to pitch, and fires retro engines for separation of the instrumentation compartment.

The controlling moments in the Minuteman I and Minuteman II are produced in different ways, which can be seen from Table 1.1 [133].

TABLE 1.1

/38

Missile type	Channel	Stage	Method of obtaining angular rate	Method of producing control moment
Minuteman I	θ, ψ	I, II	Acceleration measurement	Rotation of engine nozzles
		III	Attitude signal	
		I, II, III	differentiation	
Minuteman II	θ, ψ	I	Acceleration measurement	Rotation of engine nozzles
		II		Freon injection in posterior nozzle section
		III	Attitude signal	Rotation of engine nozzles
	φ	I, III	differentiation	Nozzle control with hot-gas valves
		II		

The nozzle swiveling rates during control exceed 20 deg/sec, which is due to the demands of stability in the powered flight phase for assigned amplitude and phase stability margins calculated both for a solid and an elastic body, with allowance for the constraints imposed by the design. These rates are also dictated by the requirements of rapid response of stabilization loops in existing perturbations due to gas currents in the silo, wind, and technological errors.

The gyrostabilized platform with displacements with respect to the pitch angle θ , yaw angle ψ , and roll angle ϕ of $+90^\circ$, $+20^\circ$, and $+70^\circ$, respectively, is a source of information; two free spherical gyroscopes on gas-dynamic suspensions (helium) sense one variable -- change of angle ϕ , and another free gyroscope senses the change of the angles θ and ψ . Selection of gyroscopes of this type, without mechanical contact with stator, is dictated by the possibility of long-term use without wear and unbalancing. The mean-square component of drift is hundredths of a degree per hour for gyroscopes of this type. When systematic errors are compensated for, this error value is wholly acceptable. /39

Gyroscopic angular rate sensors require considerable stabilization in the launch position and measure up poorly to the demands of combat readiness and high reliability /102/. Therefore, model 16PJGA integrating floated gyroscopic accelerometers are used on the Minuteman BM. They sense only values of the quantities $\Delta\theta$ and $\Delta\psi$.

A block of six (four in the first models) of two-axis level indicators mounted on the platform serves for its horizontal erection prior to launch and for orientation in the calibration of the accelerometers. A sight window, also on the platform, serves to restrain the platform in the azimuthal plane in the launch position.

A general-purpose onboard computer, processing data, solving navigational problems, the problem of angular stabilization, is used as a second-order filter in the main control loop, determines (in Minuteman II) the amount of consumed freon injected into the second-stage engine, and is used for regulating the gain factor of the angular accelerometer. The onboard computer determines the difference between the measured variables $\Delta\theta$ and $\Delta\psi$ and the derivatives obtained by differentiation of the measured values of the corresponding angles. The calculated difference is used to compensate for attitude errors, which in turn are the differences between attitudes of the missile produced by command and the instantaneous attitudes. This method of compensating systematic errors in accelerometers and gyroscopes permitted a large reduction in the scatter of missile impact points (circular probable error of about 0.8 km for Minuteman II /102/).

Use of a fast-response onboard computer allowed it to be assigned both all logic and computation operations, avoiding auxiliary onboard computation or logic devices, and auxiliary operations performed in the launch position, which lowered the number of cables running from onboard the missile to the launch gantry to 46⁴. The computer performs by way of the auxiliary operations in the launch position the monitoring of the status of various systems and a periodic check of the performance characteristics /40

of various elements and participates in exchanging information between the missile and the launch facility and in control of the missile launch process /170/.

In the prelaunch period, elements of the onboard control systems of the missile function in the same loop with the ground complex elements. To shorten the prelaunch preparation period to 32 seconds (the programmed pitch rotation of the missile begins 3 seconds after the startup of the navigation and control system; prelaunch preparation time is about 2 minutes for the Titan), the principle of the continuous operation of the missile gyrostabilizer is employed, which in turn requires not only the cooling of the operating assemblies, but also measures to increase their reliability. This is achieved by several steps, the chief one of which is a specially developed program for upgrading manufacturing quality and methods of monitoring elements and assemblies. Twenty American companies were chosen to build the elements of these systems by the indicators of the highest reliability of the equipment they produce; nonetheless, the failure rate of the equipment ordered had to be lowered by more than a hundred times /102/.

Aiming of the Minuteman BM is carried out just as described above, using an autocollimator installed in the silo on circular rails, which is oriented with respect to the North Star or to geodetic reference points.

The control and monitoring block (Fig. 1.14) controls the aiming process, as well as all the remaining processes of bringing the missile up to combat readiness and scheduled maintenance and monitoring checks. It also controls the process of storing in the onboard computer memory required information, which is fed at first by means of a special punched metal tape into the block of readout devices.

The operating regimes of the launch position are set by the signal conversion block. The control console supervises the functioning of the launch position equipment and the onboard navigation system while the missile is in the launch position (cf. Fig. 1.14). /41

One of the lightest and most compact BM navigation systems is the autonomous inertial system of the Polaris missile (cf. /186/). It consists of a gyro inertial block and a computer. The former, in turn, is subdivided into a gyro-platform block and an electronic block containing a servoamplifier. The MK-2 gyro-platform incorporating accelerometers is erected at the beginning of the flight in the plane of the local horizon and maintains this orientation throughout the flight. Three 25-JRJG modified beryllium gyroscopes with spherical rotor and magnetic suspension, two 16PJRA integrating accelerometers (these accelerometers and gyroscopes are the same as those in the navigation and control systems of the Apollo space craft), and a 16PJGA gyro-accelerometer are mounted on the platform. /42

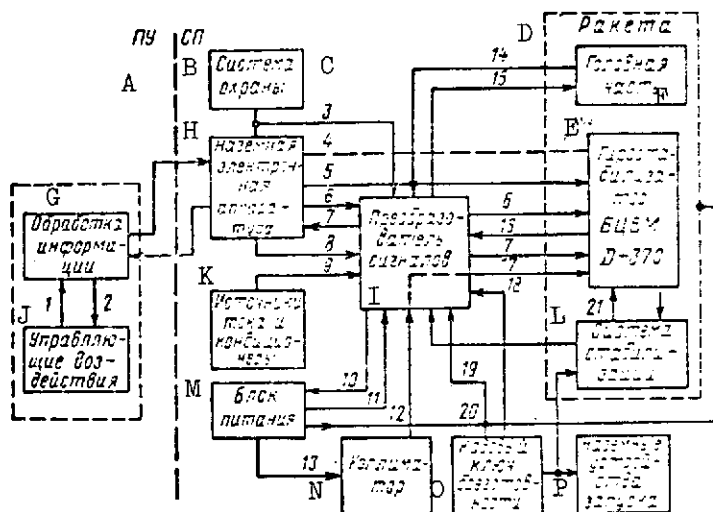


Fig. 1.14. Block diagram of the interaction of the integrated control system of the Minuteman missile with ground facilities

/102/:

- 1 -- Control signals
- 2 -- Indicator signals
- 3 -- Alarm signals
- 4 -- Radio link commands
- 5 -- Cable commands
- 6 -- Radio commands
- 7 -- "Danger" command
- 8 -- Ground monitoring
- 9 -- Monitoring
- 10 -- Power supply block commands
- 11 -- Commands "Alarm", "Malfunction", etc.
- 12 -- Onboard power supply
- 13 -- Collimator power supply
- 14 -- Monitoring of frequency generator
- 15 -- Fuse arming
- 16 -- Memory output
- 17 -- Collimator signal
- 18 -- Combat readiness switch
- 19 -- Monitoring commands
- 20 -- Launch
- 21 -- Commands

- KEY:
- A -- Launch facility
 - B -- Launch position
 - C -- Protection system
 - D -- Missile
 - E -- D-37C onboard computer gyrostabilizer
 - F -- Nose cone
 - G -- Data processing
 - H -- Ground electronic equipment
 - I -- Signal converter
 - J -- Controlling actions
 - K -- Current sources and conditioners
 - L -- Stabilization system

- M -- Power supply block
- N -- Collimator
- O -- Combat readiness switch
- P -- Ground launch installations

The onboard computer of the Polaris A-1 and Polaris A-2 was built with semiconductor multifunctional integrated circuits.

One feature of the Polaris BM's navigational system is its mating and functioning in the prelaunch period together with ship-board equipment.

The navigational system acquires needed information during the prelaunch period from the missile launch control system. In addition, data on the geographical location of the launch, northward bearing, linear and angular ship velocities, and local vertical are fed to it from the ship's navigational system.

The fire control system, equipped with its own computer and data storage devices, performs six tasks:

- a) computes the ballistic trajectory ensuring impact on the given target with given initial conditions;
- b) assigns values of the variable parameters of the integrating accelerometer;
- c) transmits values of the trajectory coefficients and the terminal velocity to the onboard computer;
- d) provides for the erection of the platform with respect to the local horizon by introducing into accelerometer readings a correction allowing for ship motion;
- e) calculates the required values for the erection of the platform with allowance for data of optico-electronic devices and precise northward heading; and
- f) continuously checks the missile onboard systems and its equipment, reflecting the degree of their readiness.

During the powered flight phase the program of pitch change is implemented by the stabilization system in the operation of the first stage, and by the inertial navigation system and the stabilization system in the operation of the second stage. The actuating devices in the latest version of the Polaris A-3 are the main solid-fuel jet engines, which have swivel nozzles in the first stage and a system of freon injection into the postcritical nozzle section -- in the second stage.

FOOTNOTES

¹This complex can also include antimissile defense control systems [114, 116, 214].

FOOTNOTES [Concluded]

²This angle is commonly taken as the target heading. The angle between the target heading and the velocity vector η is called the lead angle.

³The Gemini space craft were launched into orbit with Titan IIIC launch-vehicles.

⁴They number in the several hundreds for the Titan and Atlas missiles. This added to the weight of the Minuteman missile onboard computer by only 10 percent [102].

CHAPTER TWO FLIGHT CRAFT AND THEIR MAIN CHARACTERISTICS

/43

Modern flight craft can be divided into four main classes, depending on their function: aircraft, helicopters, missiles, and spacecraft. Each of these classes in turn is divided into several subclasses.

Each of these flight craft subclasses can be divided into different types by function.

A classification of flight craft by function (without aiming at completeness) is given in Table 2.1.

It must be noted that the same flight craft, depending on the equipment, use of auxiliary fuel tanks, and so on, can be located in different places within the classificatory table not only by the type of flight craft, but also by its subclass.

The F-110 Phantom fighter built by McDonnell since 1960 was produced as an interceptor-fighter for the U.S. Air Force, and then since 1961, after several modifications, this plane began to make an appearance in weapon systems as a deck-launched fighter-interceptor of the U.S. Navy (F-4B). With the replacement of equipment on the F-110 and the mounting of auxiliary fuel tanks, this same airplane is used in the United States as a reconnaissance craft (RF-4C for the Air Force or RF-4B for the Navy). With guided and ordinary bombs, and napalm cannisters, the F-110 is used as an attack craft (F-4E).

The Atlas missile in its three-stage version was adopted in the U.S. arsenal as a long-range ballistic missile, and after addition of a fourth stage was used as a launch vehicle for spacecraft.

These examples show the difficulty of an exact classification of current flight craft.

2.1. Tactical-Flight Characteristics of Fighter-Interceptors

Fighter-interceptors are one of the main elements in anti-aircraft defense and are intended for the interception and striking of air targets in the defense of objects or a country's territory. Fighter-interceptors are used to accompany bombers or in performing air patrol. Still other cases of their combat use are possible, which are discussed in the works [13, 155, 171, 172].

TABLE 2.1 CLASSIFICATION OF FLIGHT CRAFT

/44

Flight craft	Aircraft	Fighter-interceptors	Antiaircraft
			Frontline
			Deck-launched
		Multimission fighters	
		Bombers	Tactical
			Deck-launched
			Strategic
			Antisubmarine
		Reconnaissance	
		Transport	Passenger
			Cargo
			Landing
	Missiles	Air-to-air	
		Surface-to-air	Antiaircraft defense
			Antimissile defense
			Defense of land forces
		Air-to-surface	Air-to-ground
			Air-to-water
		Launch vehicles	
		Ballistic	Tactical
			Strategic
Flight craft		Space flight craft	Artificial earth satellites
	Communications		
	Geodetic		
	Meteorological		
	Air-space craft		Transport function
			National-economic function
	Space craft		

/45

The significant level of advances in aerodynamics and major successes in building aircraft engines and new high-strength materials make it possible to attain high tactical-flight characteristics of fighter-interceptors. By reducing the relative thickness of wing profile to 3.5-5 percent and using boundary layer control, their drag is reduced. By using adjustable inlet diffusers and ejector engine nozzles, appreciable increase in after-burner thrust is attained, engine and equipment weight is reduced, and specific fuel consumption is lowered. As a result, fighter velocity and flight altitude have been increased; longitudinal g-loads, rate of climb, and flight duration have risen; and the kilometer fuel consumption per ton of aircraft weight has been reduced.

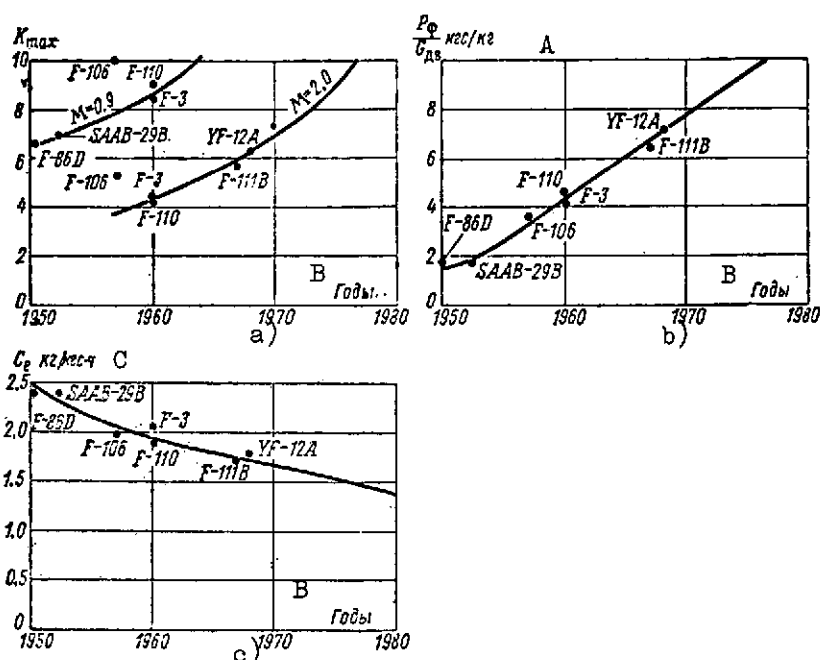


Fig. 2.1. Main performance indicators of fighter-interceptors in relation to the year of initial aircraft manufacture

KEY: A -- P_{af}/G_{en} , kg [force]/kg

B -- years

C -- kg/kg [force] · hr

D -- kg/kg [force] · hr

In order to increase the range of interception, development has begun in building fighters with vertical liftoff, which is provided by special turbojet engines (P-1127 Kestrel in the United Kingdom and Mirage IIIA in France).

The advantage of these fighter-interceptors is the possibility of their takeoff from small landing fields or with a short takeoff run, leading to an increase in the range of high-speed interception. Another technique facilitating aircraft takeoff and landing is the use of variable-geometry wings. /47

Technical data on fighter-interceptors are given in Table 2.2 [13, 28, 128, 130, 131, 135, 137, 155, 157, 160, 167, 171, 172, 174, 193, 203]. Generalized performance indicators -- maximum lift-drag ratio K_{\max} , ratio of afterburner thrust of engines to their dry weight $P_{\text{af}}/G_{\text{en}}$, and specific fuel consumption with afterburner C_e are shown with extrapolation to 1980 in Fig 2.1. These indicators can be calculated using the following formulas [15, 27, 32, 82]:

or

$$\left. \begin{aligned} K_{\max} &= \frac{1}{2} \sqrt{\frac{1}{AC_{x_i}}} \\ K_{\max} &= \frac{1}{2} \sqrt{\frac{\pi \lambda_{\text{eff}}}{C_{x_i}}} \end{aligned} \right\} \quad (2.1)$$

where λ_{eff} is the effective wing aspect ratio (Fig 2.2) [35, 63].

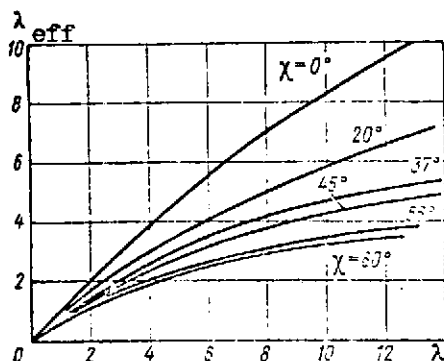


Fig. 2.2. Graph for the determination of effective wing aspect ratio as a function of geometrical aspect ratio and sweep angles

TABLE 2.2 TECHNICAL CHARACTERISTICS OF FIGHTER-INTERCEPTORS

Airplane type		F-86D	SAAB-29B	F-106	F-110	F-3	F-111B	VF-12A
General data	Name	Sabre	—	Delta Dart	Phantom	Lightning	—	A-11
	Country	U.S.	Sweden	U.S.	U.S.	UK	U.S.	U.S.
	Initial production	1949	1950	1957	1960	1960	1967	Experimental
	Number of engines	One J-47-GE-17	One RM-2B	One J-75-R-17	Two J-79-CE-15	Two RB-146	Two TF-30-P-1	Two JT-11D-20B
	Crew	One	One	One	Two	One	Two	Two
	Armament	4 cannons 14 UG	4 cannons 16 UG	4 Falcon missiles	4 Sparrow missiles	2 Red Top missiles	4 Phoenix missiles	8 Falcon missiles
Geometrical dimensions	Wing area, S, in m ²	26.7	24	64.8	49.2	44	64 - 57	147*
	Wingspan, l, m	11.3	11.0	11.7	11.7	11	21.3	16.8
	Aspect ratio λ	4.71	5.05	2.1	2.82	2.74	$\frac{6.80}{2.05}$	1.86
	Sweep angle, χ in deg.	35	25	60	45	56	Variable 15 - 72.5	60

UG = unguided missile

In Russian decimal number usage, commas are equivalent to decimal points in American practice.

TABLE 2.2 TECHNICAL CHARACTERISTICS OF FIGHTER-INTERCEPTORS

Airplane type		F-86D	SAAB-29B	F-106	F-110	F-3	F-111B	YF-12A
Weight data	Relative thickness, %	10.0	10.0	4.0	5.1	5.0	4.0	3.6
	Normal takeoff weight, G_{to} , tons	8.1	6.5	13.6	20.8	16.7	29.5	61.7
	Max. takeoff weight, G_{max} , tons	9.1	7.7	16.0	24.8	19.0	31.0	72.0**
	Wt. of empty plane w/eng's G_{emp} , tons	5.35	4.5	9.0	13.4	12.5	18.0	31.0
	Weight of fuel G_{fu} , tons	2.75	2.0	4.2	6.5	3.8	7.3	23.0
	Weight of fuel in aux. tanks G_{fu} , tons	0.78	1.0	—	2.26	2.20	—	—
	Weight of armament, G_{arm} , tons***	0.90	0.50	0.43	1.02	0.87	2.2	3.2
	Weight of engines, G_{en} , tons	1.5	1.1	2.7	3.3	3.4	3.4	3.5

* In the reconnaissance version (SR-71), the wing area has been increased by 26 percent 130, 137, 171.

** It has been reported that the maximum takeoff weight of the YF-12A airplane is 77 tons 137, 167.

*** The armament weight includes the following: mounted missiles and certain equipment (pylons, connectors, and bundles). Here the weight of the radar station, sites, and onboard computer (required for missile launch and guidance) are not included.

TABLE 2.2 TECHNICAL CHARACTERISTICS OF FIGHTER-INTERCEPTORS

Airplane type		F-86D	SAAB-29B	F-106	F-110	F-3	F-111B	VF-12A
Weight data	G_{fu}/G_{to}	0.34	0.31	0.31	0.31	0.23	0.35	0.37
Main comparative performance indicators	Lift-drag ratio, K_{max} , at $M = 2.0$	6.6 for $M=0.9$	6.9 for $M=0.9$	5.7*	4.13	4.25	5.75	6.25
	Engine performance, P_{af}/G_{en}	1.9	1.8	3.5	4.7	4.25	5.75	6.25
	Specific fuel consumption, C_e , w/o afterburner, $H = 11$ km, $M = 0.9$	1.35	1.35	1.1	1.05	1.25	0.9	0.95
	Specific fuel consumption w/full afterburner, $H=11$ km, $M = 2$	2.4	2.4	1.96	1.92	2.05	1.75	1.85
	Specific wing loading, G/S , kg/m^2	320	270	210	420	380	515	420
	G_{arm}/G_{to}	0.100	0.060	0.032	0.049	0.052	0.075	0.052

* The high value $K_{max} = 5.7$ for the F-106 airplane is due to the internal location (in the wings) of four Falcon missiles.

As we can see, for values of ψ from 35 to 55° and $\lambda > 7.5$, λ_{eff} increases only slightly. Therefore usually $\lambda < 3$ in modern fighters. C_{x_0} is the drag factor of the craft when $C_y = 0$. In modern fighters $0.018 \leq C_{x_0} \leq 0.027$ when $M = 2.0$; C_x values can be calculated by the formula [153]:

$$C_x = (C_x)_{\text{fr}} + \frac{128}{\pi} k_0 r^2 p^2 \left(\frac{l}{L} \right)^2 + \left\{ \frac{1}{\pi} \frac{p}{l/L} \times \right. \\ \left. \times \left[k_{\text{vor}} + k_{\text{wav}} \frac{M^2 - 1}{2} \left(\frac{l}{L} \right)^2 \right] \right\} C_v^2. \quad (2.2)$$

Here $(C_{x_0})_{\text{fr}}$ is the friction drag factor;

k_0 is the Siyers-Hayek constant;

l/L is the relative aspect ratio of the airplane;

$r = V/F^{3/2}$ is the volumetric parameter (V is the aircraft

parameter and F is the wing area);

A is the coefficient that allows for the effect of induced drag:

$$A = \frac{1}{\pi} \frac{p}{l/L} \left[k_{\text{vor}} + k_{\text{wav}} \frac{M^2 - 1}{2} \left(\frac{l}{L} \right)^2 \right], \quad (2.3)$$

where $p = F/lL$ is the relative aircraft parameter (F is the wing area including the underfuselage section; l is the wingspan; and L is the aircraft length); k_{vor} is the vortex drag factor, dependent on the pattern of lift distribution across the wingspan; and k_{wave} is the wave drag factor, dependent on the lift distribution across the wingspan and chord.

From Fig 2.1 it is clear that modern fighter-interceptors have significant potentials for a further increase in technical and tactical-flight characteristics. Fig 2.3 and Table 2.3 give the main tactical-flight characteristics, with their prediction to 1980: maximum level flight velocity V_{max} , static ceiling H_{st} , longitudinal g-load n_x , vertical velocity V_y , climb time t_H , turning radius r_{tu} , and complete turn time t_{tu} , and actual range L_f . All these characteristics are determined, as a rule, for aircraft with the basic version of missile-cannon armament. Therefore in several cases these data may differ somewhat from manufacturing data. /52

In determining maximum level flight velocities, published manufacturing data were used [126-130, 137, 155, 157, 160, 167, 171, 172, 174, 176]; they were calculated by the formula

$$V_{\max} = \left(\frac{1}{\Delta}\right)^{0.15} \cdot \sqrt{\frac{P_{af}}{(C_{x_0} + AC_y^2)S}}, \quad (2.4)$$

where Δ is the relative air density;
 P_{af} is the static thrust with complete afterburner;
 C_y is the lift coefficient; and
 S is the wing area.

The C_{x_0} values were calculated with allowance for the effect of the mounting devices and the air-to-air guided missiles.

In the opinion of foreign specialists, in the next ten years one can scarcely anticipate a slowdown in the growth rates of maximum velocity for standard antiaircraft defense fighter-interceptors¹.

The n_x value characterizing aircraft response and its vertical velocity are calculated by the formulas

$$n_x = \frac{P_{af}}{G} \left(\frac{0.7pM^2C_{x_0}S}{G} + \frac{AG}{0.7pM^2S} \right), \quad (2.5)$$

where p is the atmospheric pressure for the given flight altitude; G is the aircraft weight with allowance for fuel consumption, and

$$V_y = n_x V. \quad (2.6)$$

To determine the static ceiling, the atmospheric pressure at the ceiling altitude was found as follows:

$$p_{H_{ce}} = \frac{G}{0.7M_{ce}^2 S} \left[\frac{1}{A} \left(\frac{P_{11}}{0.7p_{11}S M_{ce}^2} - C_{x_0} \right) \right]^{-\frac{1}{2}}, \quad (2.7)$$

where M_{ce} is the M number for the aircraft ceiling;

P_{11} is the thrust of engines at the altitude $H = 11,000$ m; and ¹⁵⁶

p_{11} is the atmospheric pressure at $H = 11,000$ m.

The climb time to the altitude H was determined by graphically calculating the integral

$$t_H = \int_0^H \frac{dH}{V_y}, \quad (2.8)$$

TABLE 2.3 MAIN TACTICAL-FLIGHT CHARACTERISTICS
OF FIGHTER-INTERCEPTORS

/54

Airplane type		F-86D	SAAB-29B	F-106	F-110	F-3	F-111B	YF-12A
Maximum flight velocities, V_{\max} in km	H_{\max}	1100	1050	2460	2400	2400	2650	3300
	$H=11$ km	1060	1010	2400	2300	2350	2600	3200
	$H=0^*$	960	960	1360	1400	1350	1470	1480
Ceiling	Static	13600	13500	18500	18000	19100	20000	22500
Longitudinal g-load	$H=11$ km $M=2$	—	—	0.14	0.24	0.26	0.46	0.55
	$H=17$ km $M=2$	—	—	0.030	0.035	0.06	0.14	0.19
Vertical velocity V_y , m/sec	$H=11$ km $M=2$	—	—	82	140	155	270	360
	$H=17$ km $M=2$	—	—	17	21	35	82	125
Climb to alt., t_H , in minutes	$H=11$ km	10.2	11.0	5.7	5.2	3.6	3.8	3.1
	$H=17$ km	—	—	7.8	6.7	5.0	5.2	4.3
Time of right turn, t_{tu} , in minutes	$H=11$ km	0.43	0.5	1.0	1.1	0.9	1.2	2.1
	$H=17$ km	—	—	3.6	4.35	3.3	4.5	8.7
Radius of full turn, r_{tu} , in minutes	$H=11$ km	4.0	4.5	11	12	10	19	28
	$H=17$ km	—	—	38	50	37	65	100
Actual flight range	$H=11$ km $M=0.9$			2500	3000	1600	4300**	4000

/55

* The maximum flight velocities of the fighter-interceptors near the ground are presented for the versions without external armament mountings.

** Based on other data, 4500 km [137, 171].

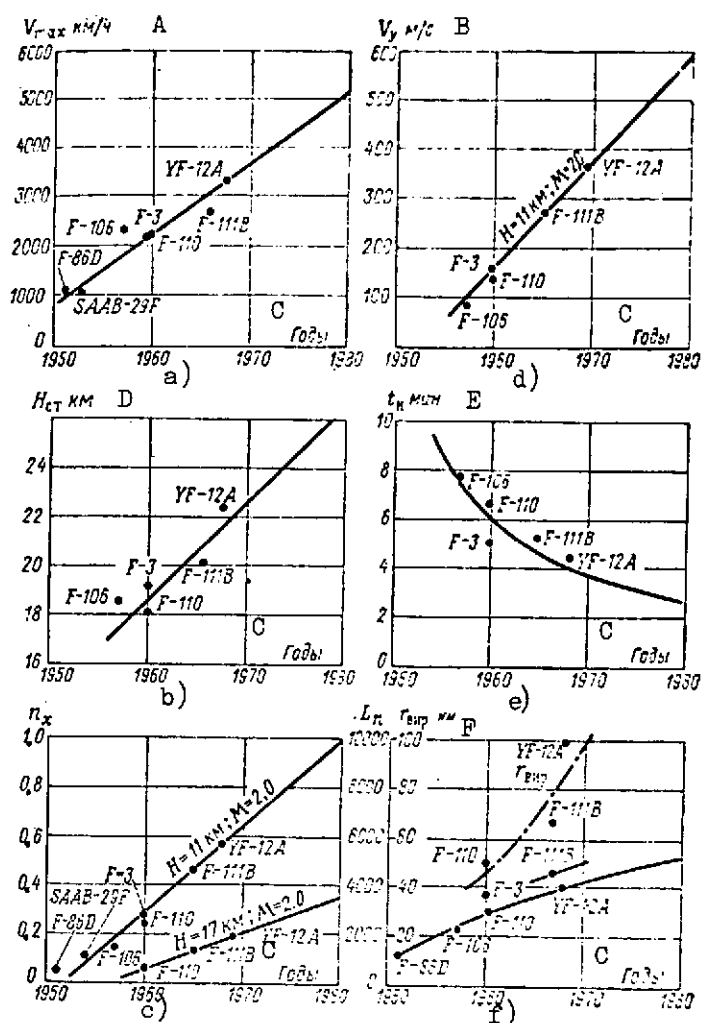


Fig. 2.3. Main tactical-flight characteristics of fighter-interceptors

KEY: A -- km/hr
 B -- m/sec
 C -- years
 D -- H_{st}
 E -- t_H min
 F -- r_{tu}

and r_{tu} and t_{tu} were calculated using the expressions

$$r_{tu} = \frac{V_{tu}^2}{g \sqrt{ny^2 - 1}}, \quad t_{tu} = \frac{\pi V_{tu}}{g \sqrt{ny^2 - 1}}, \quad (2.9)$$

where

$$n_y \approx \frac{\frac{\rho V_{tu}^2 S}{2} + \frac{P}{C_y^a}}{G} C_y,$$

$$C_y^a = \frac{\partial C_y}{\partial a}.$$

The actual range L_F with allowance for a 7 percent remaining fuel reserve is found by the formula

$$L_F = L_{cl} + L_{gl} + L_{la} + \frac{2.3G}{C_q} \lg \frac{G}{G_{fi}}, \quad (2.10)$$

where L_{cl} is the distance flown by the aircraft in making the climb;

L_{gl} is the distance covered in gliding;

L_{la} is the distance covered in landing;

G_a is the weight of the aircraft after climbing to the given altitude;

G_{fi} is the final weight of the aircraft with a 7 percent fuel reserve;

C_q is the kilometer fuel consumption,

$$C_q = \frac{GC_e}{MK}; \quad (2.11)$$

G is the mean weight of aircraft;

a is the speed of sound in km/hr; and

K is the lift-drag ratio of the aircraft.

As we can see from Fig. 2.3 plotted from following data, the long range values for modern fighters, attained in particular by using variable-geometry wings, insures -- with high values for the remaining tactical-flight characteristics -- the interception of high-speed targets at considerable distances from the airfield itself in the frontal and rear hemispheres.

57

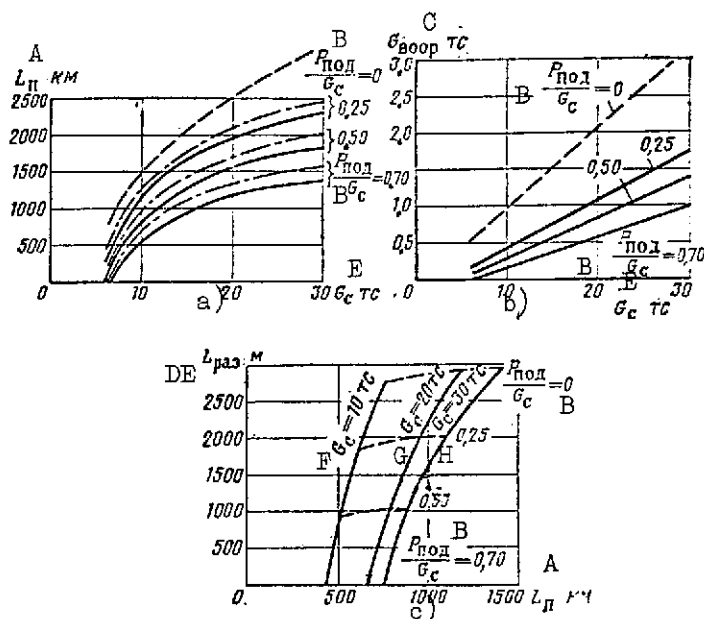


Fig. 2.4. Functions of range, takeoff run, and weight of mounted armament for fighter-interceptors with short take-off run or vertical takeoff:

P_{li}/G_a = ratio of thrust of lift engines to aircraft weight

- KEY: A -- L_f
 B -- P_{li}/G
 C -- G_{arm} , tons
 D -- $L_{to.r}$
 E -- G_a , tons
 F -- $G_a = 10$ tons
 G -- $G_a = 20$ tons
 H -- $G_a = 30$ tons

Fig. 2.4. shows the change in characteristics (actual range, weight of installed armament G_{arm} , and takeoff run) of vertical takeoff aircraft ($P_{li}/G_a \neq 0$) compared with ordinary aircraft ($P_{li}/G_a = 0$) [141, 146, 148, 154, 171].

As we can see, when $P_{li}/G_a = 0.7$ and the aircraft weight $G_a = 20$ tons, the range will be 1200 km for armament weight $G_{arm} = 0.6$ ton and $L_{to} = 0$ m. When the thrust-to-weight ratio of the lift engines is reduced to $P_{li}/G_a = 0.25$, we have $L = 1600$ km, $G_{arm} = 1.2$ tons, and $L_{to} = 2000$ m. As lift engines are improved, their specific thrust will be increased and the tactical-technical characteristics will be upgraded.

/58

2.2. Tactical-Flight Characteristics of Multimission Fighters

Multimission fighters are one of the most widespread types of aircraft in the air forces of foreign countries. The possibility of mounting a large number of ground target armament devices (air-to-surface missiles, guided or ordinary bombs of various sizes, incendiary cannisters, unguided missiles, cannon pods, and so on) has led to the use of the aircraft in penetrating antiaircraft defenses at the front line or for penetration beyond the front line and attacking of ground targets (tanks, armored troop carriers on the move, missile launch positions, infantry subdivisions, and so

/59

TABLE 2.4 TECHNICAL CHARACTERISTICS
OF MULTIMISSIION FIGHTERS

Airplane type		F-100C	Hawker FMk6	F-104G	Mirage IIIa*	SAAB J-35D	F-111A
General charac- teris- tics	Name	Super Sabre	Hawker	Star- fighter	Mirage III	Draken	—
	Country	U.S.	UK	U.S.	France	Sweden	U.S.
	Initial produc- tion	1953	1954	1957	1958	1963	1967
	Number of engines	One J-57-P-21	1 Avon RA-28	One J-79GE-11	One Atar — 9c	One RM-6C	Two TF-30-P3
	Crew	One	One	One	One	One	Two
	Armament	4 cannon 20mm, 45 UG, bombs, incendi- ary tanks	4 cannon 30mm, 74 UG, bombs, incendi- ary tanks	1 cannon 20 mm, 2 Bullpup missiles, bombs	2 cannon 30 mm, 125 UG, Matra, bombs	2 cannon 30 mm, 4 miss- iles, bombs	1 cannon 6 missiles bombs
Geome- trical dimen- sions	Wing area, S, m ²	35.8	32.4	18.2	34	50	64—57
	Wingspan, l, m	11.6	10.26	6.7	8.2	9.4	19.2--9.75

UG = unguided missile

TABLE 2.4 TECHNICAL CHARACTERISTICS
OF MULTIMISSION FIGHTERS
/Continuation/

Airplane type		-100C	FMk6 Hawker	F-104G	Mirage III A	SAAB J-35D	F-111A
Geometrical dimensions	Aspect ratio, λ	3.76	3.26	2.44	2.0	1.77	$\frac{5.7}{1.7}$
	Sweepback angle, χ , in degrees	45	—	0	60	80—57	Variable 16—72.5
	Relative thickness, C , in %	7	—	3.4	3.5—4.5	5	4
Weight data	Normal takeoff weight, G_{to} , in tons	13.1	8.1	9.5	8.7	9.2	32.0
	Maximum takeoff weight, $G_{to \max}$, in tons	16.8	10.75	12.8	11.0	12.6	35.0
	Weight of empty craft w/eng's, G_{emp} , in tons	5.9	6.1	6.5	6.3	7.6	17.5
	Weight of fuel, G_{fu} , tons	3.9	1.9	2.7	2.1	2.1	14.5
	Weight of fuel in aux. tanks, $G_{aux. fu}$, in tons	1.8	1.55	2.1	2.1	1.7	2.5
	Weight of armament, G_{arm} , in tons*	1.5	1.0	1.4	2.0**	1.5	9.0***

* Armament weight includes the following: bombs, air-to-surface missiles, and cannons with normal ammunition reserve.

** There are reports that the weight of the aircraft armament is as high as 3 tons.

*** This figure applies to maximum takeoff weight of bombing armament with external mounting and a 54° wing sweep angle. At maximum wing sweep angle, the weight of the bombing armament is 4.5 tons.

TABLE 2.4 TECHNICAL CHARACTERISTICS
OF MULTIMISSION FIGHTERS
/Conclusion/

Airplane type		F-100C	Hawker FMK6	F-104G	Mirage III A	SAAB J-35 D	F-111A
Weight data	Weight of engines, G_{en} , in tons	1.8	—	3.2	2.6	3.2	3.3
	G_{fu}/G_{to}	0.3	0.24	0.28	0.24	0.23	0.35
Main com- parative perfor- mance indica- tors	Lift-drag ratio, K_{max} , at $M = 0.9$	6.1	5.9	8.0	8.7	9.2	13.5
	Engine performance indi- cator, P_{af}/G_{en}	—	—	5.4	5.5	—	6.4
	Specific fuel consumption C_e w/o afterburner, at $H = 0$, $M = 0.9$	1.48	1.46	1.15	1.15	1.05	0.98
	Specific fuel consumption w/full afterburner, $H = 0$, $M = 0.9$	2.5	2.43	2.2	2.1	2.1	1.73
	Specific wing loading, G/S , in kg/m^2	370	250	520	250	185	550
	G_{arm}/G_{to}	0.11	0.12	0.15	0.23	0.18	0.26

TABLE 2.5 MAIN TACTICAL-FLIGHT CHARACTERISTICS
OF MULTIMISSION FIGHTERS

Airplane type		F-100C	Hawker F-Mk6	F-104G	Mirage IIIA	SAAB J-35D	F-111A
Maximum flight velocity, V , km/hr	$H=0$	1100	1160	1320	1100	1100	1470
	$H=H_{max}^*$	1300	1050	2300	2100	2100	2650
Longitudinal g-load, n_x	$H=0$	0.22	0.21	0.30	0.19	0.25	0.38
	$H=11 \text{ km}$ $M=2$	—	—	0.32	0.15	0.32	0.37
Vertical velo- city, V_y , m/sec	$H=0$	80	75	82	57	80	130
	$H=11 \text{ km}$ $M=2$	—	—	210	100	190	280

* The maximum flight velocities of multimission fighters near the ground are given for aircraft without external armament mountings.

TABLE 2.5 MAIN TACTICAL-FLIGHT CHARACTERISTICS
OF MULTIMISSION FIGHTERS

[Conclusion]

Airplane type		F-100C	Hawker F-Mk6	F-104G	Mirage III A	SAAB J-35D	F-111A
Climb time, t_H , minutes	$H=11$ km	—	—	5.92	6.14	4.40	6.25
	$H=16$ km	—	—	5.85	8.05	5.60	9.00
Time of full turn, t_{tu} , in minutes	$H=0$	—	—	0.42	0.58		1.1
	$H=11$ km	—	—	1.0	1.25		2.6
Radius of full turn, r_{tu} , in km	$H=0$	—	—	2.0	2.2	1.9	
	$H=11$ km	—	—	12.5	13.2	11.8	32
Actual range, km	$H=0$ $M=0.7$	800	750	950	600	750	1500
	$H=11$ km $M=0.9$	1800**	1700*	1600	1400	1450	3200 w/ aux. tanks

** The aircraft range of 1800 km was obviously given for wing-mounted tanks.

on). Abroad, multimission fighters are used also as bombers operating in the near-frontline area or at penetrations of 300-400 km. The possibility of simultaneous mounting of armament to strike air and ground targets allows this kind of airplane to be used also as a frontline fighter. In several cases multimission aircraft can be used as barrage fighters, and so on.

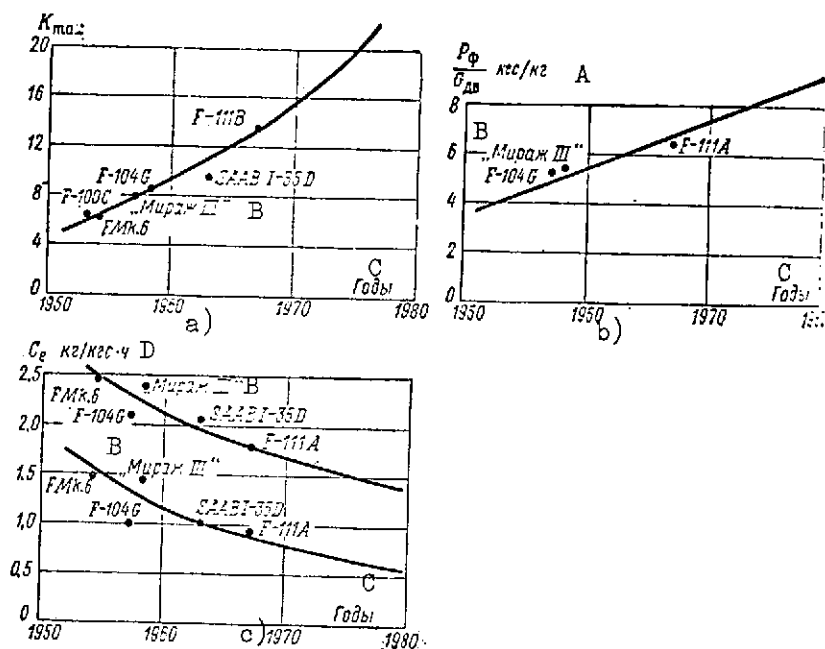


Fig. 2.5. Main performance indicators of multimission fighters (symbols are the same as those in Fig. 2.2)

KEY: A -- P_{af}/G_{en} , kg [force]/kg
 B -- Mirage III
 C -- Years

flow separation at a M number close to 1.0 will permit an improvement in the tactical-flight characteristics of airplanes of this subclass.

The need to fly multimission fighters close to ground at supersonic velocities leads to the selection of armament arrangement schemes by which drag will be reduced to the maximum, even though this is hampered when variable-geometry wings are used. Therefore, in designing multimission fighters with this wing type, compromise solutions must be found, related to the selection of geometrical ratios, location of external suspensions, and so on with which the maximum flight velocity near the ground is not reduced, for it is the most important characteristic of this type of aircraft.

2.3. Tactical-Flight Characteristics of Bombers

By the earlier adopted classification, modern bombers are divided into two types: tactical and strategic. The first type includes aircraft with a flight weight up to 50-70 tons and with a natural range to 4000 km; the second class includes airplanes with a takeoff weight about 50 tons (to 250-300 tons) and with a natural range of as much as 12,000 km and longer. Construction of long-range ballistic missiles armed with nuclear warheads and antiaircraft defense devices led to an appreciable decrease in the size of strategic air forces in a number of foreign countries, especially in the United States. However, the possibility of the flight of strategic bombers over an opponent's territory at low altitudes (about 150 m) does not preclude the possibility of using this type of aircraft under combat conditions. /66

The main technical characteristics of tactical and strategic bombers are given in Table 2.6 and in Fig. 2.7 /128, 130, 131, 135, 136, 137, 155, 160, 171, 172, 174, 167, 200/. These aircraft also reveal a trend for an increase in the lift-drag ratio (Fig. 2.7, a) and in engine performance (Fig. 2.7, b and c) with a simultaneous decrease in specific fuel consumption. Therefore modern aircraft of this subclass can have high tactical-flight characteristics.

A considerable rise in the lift-drag ratio of the B-70A bomber at $M = 2-3$ was achieved by using wings with deflectable wingtips, which increased the lift due to compression. The same increase in flow compression was achieved by the high placement of the wings and by locating supersonic air intakes with adjustable geometry. In addition to these improvements, the B-70A airplane has several other original aerodynamic solutions: a delta wing with curvature and elevons for pitch and bank control, adjustable two-position windshield, two vertical surfaces with tapered hinge lines, and so on. /67

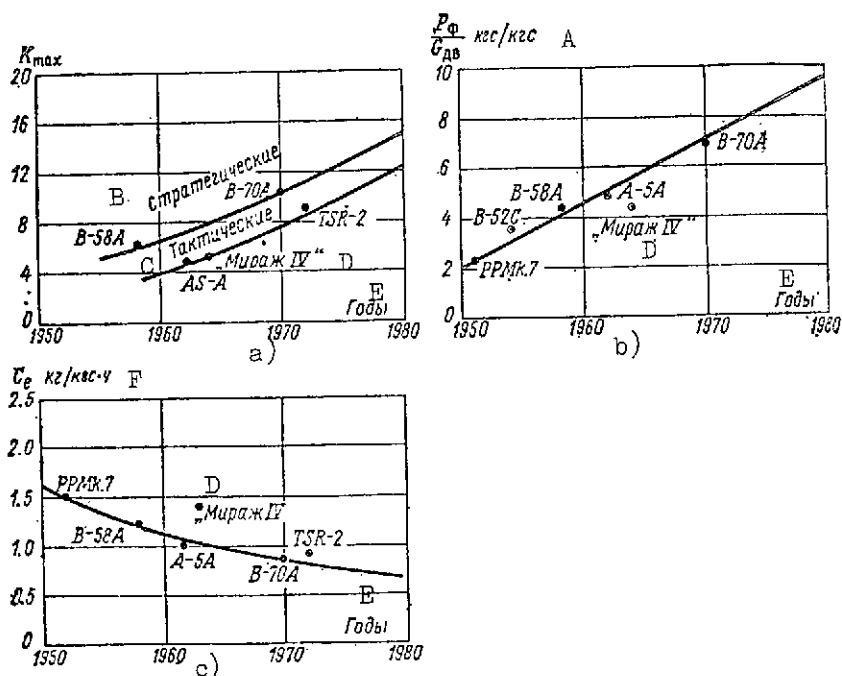


Fig. 2.7. Main performance indicators of tactical and strategic bombers

KEY: A -- $\frac{P_{af}}{G_{en}}$, kg [force]/kg [force]
 B -- Strategic E -- Years
 C -- Tactical F -- kg/kg[Force]·hr
 D -- Mirage IV

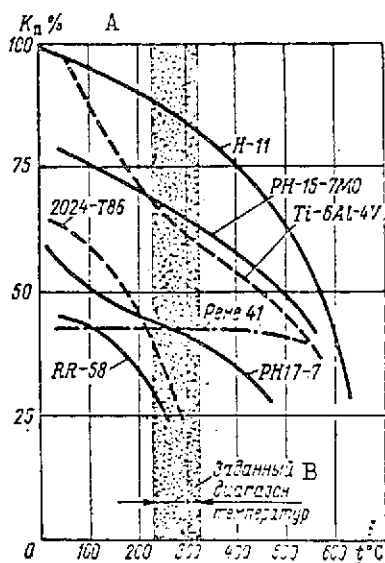


Fig. 2.8. Comparative data of relative strength of aircraft structural materials K_s as a function of heating temperature

KEY: A -- K_s
 B -- Given temperature range

The length of a flight made by the B-70A airplane at cruising speed, close to $M = 3$, led to appreciable heating of its structural elements. Much of the craft's structure must withstand temperature from 230 to 330°C, and certain engine compartments must be able to bear up under temperatures up to 540°C. Prolonged

TABLE 2.6 TECHNICAL PARAMETERS OF BOMBERS

Airplane type		Tactical				Strategic		
		PPMk 7	A-5A	Mirage IVA	TSR-2	B-52C	B-58A	B-70A
General characteristics	Name	Canberra	Vigilant	Mirage	—	Stratofortress	Hustler	Valkyrie
	Country	UK	U.S.	France	UK	U.S.	U.S.	U.S.
	Initial manufacture	1951	1962	1964	Experimental	1954	1958	Experimental
	Engine type	TBP	TBP	TBP	TBP	TBF	TBP	TBP
	Number of engines	One Avon RA-7	Two J-79-GE-15	Two Atar -9k	Two LB-31-22	Eight J-57-P-19W	Four J-79-GE-5B	Six YJ-93-GE-3
	Crew	Three	Two	Two	Two	Six	Three	Two
	Armament [ASM = air-to-surface missiles]	Bombs, 4 20-mm cannon	Bombs, air-to-surface missile	2 DEFA-30 cannon, bombs, Matra 530 missiles	—	Bombs, 2 air-to-surface missiles, movable aft section	Bombs, ASM, movable aft section	Bombs to 32 tons movable aft section

[TBP = turboprop; TBF = turbofan]

TABLE 2.6 TECHNICAL PARAMETERS OF BOMBERS
[Continuation]

Airplane type		Tactical				Strategic		
		PPMk 7	A-5A	Mirage IVA	TSR-2	B-52C	B-58A	B-70A
Geometrical dimensions	Wing area, S, m ²	89.2	65	78	63.6	372	143	585
	Wingspan, l, m	19.5	16.15	12	10.7	56.4	17.4	32
	Aspect ratio λ	4.2	4.0	2.0	1.8	8.5	2.15	1.75
	Sweep angle, γ , deg.	~14	37	60	60	35-37	60	65.5
	Relative thickness, C, %	10.5	3.5	3.6	4.0	11.5	4.0	4.0
	Nominal take-off weight, G _{to} , tons	20.4	22.4	28.6	0.8	0.4	67	250
Weight characteristics	Maximum take-off weight, G _{max} , tons	23.0	27.0	31.6	45.4	225	73	277
	Weight of empty craft w/engines, G _{emp} , in tons	11.8	12.3	14.5	19.5	79	—	73
	Weight of fuel, G _{fu} , in tons	—	6.2	11.0	15.2	114	32	130

TABLE 2.6 TECHNICAL PARAMETERS OF BOMBERS
[Continuation]

Airplane type		Tactical				Strategic		
		PDMk 7	A-5A	Mirage IVA*	TSR-2	B-52C	B-58A	B-70A
Weight charac- teris- tics	Weight of fuel in aux. tanks G_{a-f} , tons	—	—	3.9	—	19	13	136
	Weight of armament*, G_{arm} , tons	3.6	4.1	3.0	—	11.3 34.0	11.3	—
	Weight of engines, G_{en} tons	—	3.3	3.0	—	14.9	6.6	14.2
	G_{fu}/G_{to}	—	0.28	0.35	0.37	0.56	0.48	0.52
Airplane lift-drag ratio, K_{max}		—	4.8	5.3	9.7	—	5.5 $M = 2$	10** $M = 3$

TABLE 2.6 TECHNICAL PARAMETERS OF BOMBERS
Conclusion

Airplane type		Tactical			Strategic			
		PPMK 7	A-5A	Mirage IVA	TSR-2	B-52C	B-58A	B-70A
Main comparative quality data	Engine quality, P_{av}/G_{en}	2.3	4.7	4.3	—	3.6	4.3	6.9
	Specific fuel consumption, C_e , w/afterburner, $H=11$ km $M = 2$	2.4	1.9	2.1	1.7	1.95	2.15	1.85
	Specific fuel consumption, C_e , w/o afterburner, $H=H_{max}$	1.5	1.0	1.2	0.9	0.82	1.2	0.8
	Specific wing loading, G/S , kg/m^2	230	350	400	640	550	470	430—470
	G_{arm}/G_{to}^{***}	0.18	0.19	0.1	—	0.18	0.17	—

* The nominal armament weight is given (cf Chapter Four, Section 3).

** $K_{max} = 11$ is given for the RS-70A 142, 143.

*** The coefficient G_{arm}/G_{to} is given for the nominal armament weight with which the actual range given in Table 2.7 is attainable.

exposure to these temperatures requires the use of materials that preserve specific strength in these conditions, for which Boeing developed new materials exhibiting low specific weight and high specific strength at 230-330°C. Upwards of 78 percent of the aircraft's structural elements, by weight, are made on the basis of laminated material with honeycomb filler of PH15-7MO stainless steel. About 9 percent of the elements are made of the high-strength titanium alloy Ti-6 Al-4V, and 17 percent are made of H-11 tool steel. Fig. 2.8 gives comparative data characterizing the relative strength of the structural materials, K_s , in percent of the heating temperature $\sqrt{130, 143}$. The best materials in this range are as follows: H-11, PH15-7MO, and Ti-6 Al-4V. /72

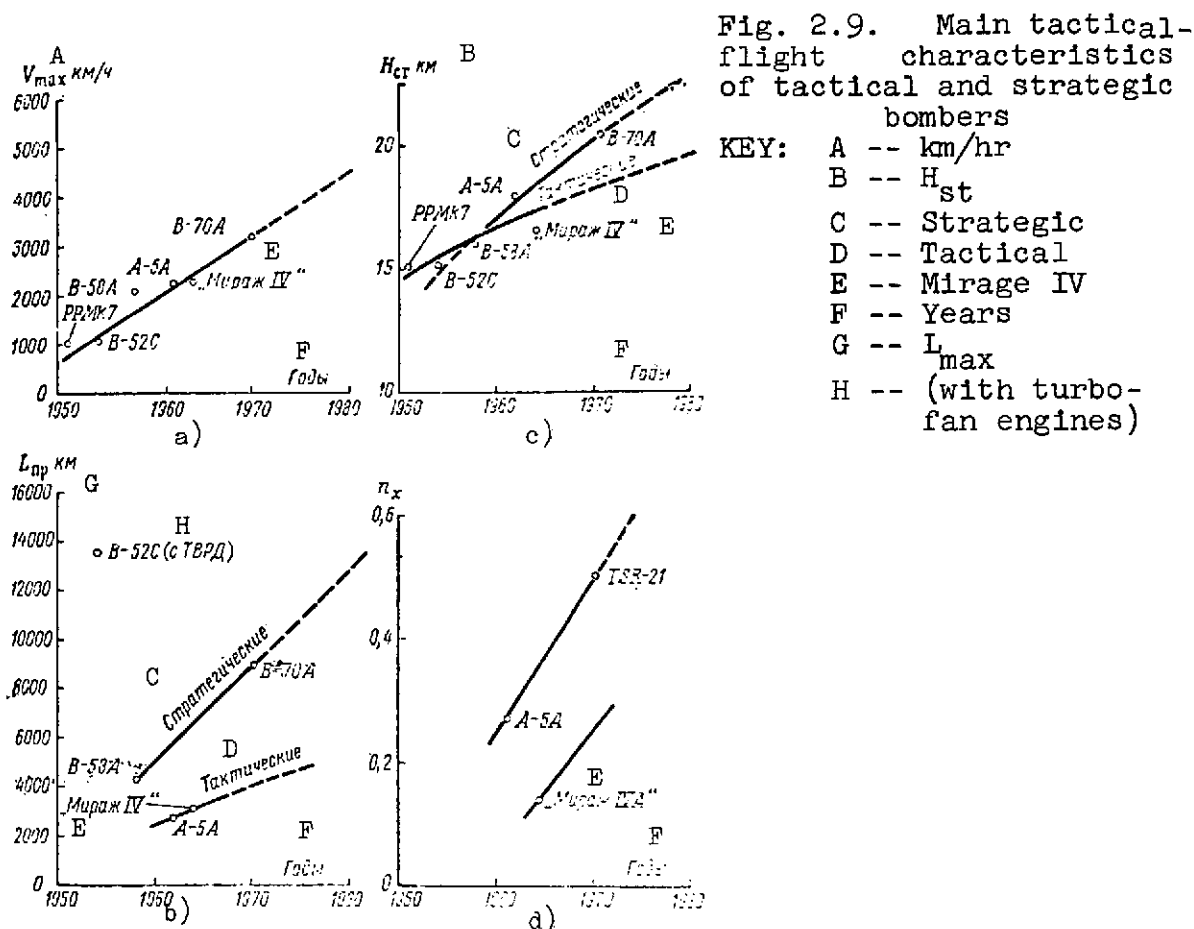
Table 2.7 $\sqrt{128, 130, 137, 155, 157, 160, 167, 171, 174, 176, 177, 200}$ presents the main tactical-flight characteristics of tactical and strategic bombers.

TABLE 2.7 MAIN TACTICAL-FLIGHT CHARACTERISTICS OF BOMBERS

Bomber type	Tactical				Strategic		
	PPMk7	A-5A	Mirage IVA	TSR-21	B-52C	B-58A	B-70A
Maximum flight at altitude, km/hr	1030	2250	2350	2750	1050	2180	3200
Strategic ceiling (w/suspended armament), H_{st} , km	15200	18000	16500	19000	15100	15300	21500
Longitudinal g-load n_x	$H=11$ km $M=2.0$	—	0.25	0.15	0.52	—	—
	$H=17$ km $M=2.0$	—	0.052	0.007	0.11	—	—
Vertical velocity, V_y , m/sec $H=11$ km	—	30.0	15.0	50.0	—	—	—
Actual range $H=11$ km	—	2700	3000	3200	13600	4300	9000

Strategic bombers, just like tactical ones, exhibit high tactical-flight characteristics. The maximum velocity is up to 3200 km/hr for the B-70A (or RS-70A), and the range is up to 9000 km (Fig. 2.9).

In the opinion of U.S. military specialists, the vulnerability of these strategic bombers when flying with a full bomb load is one of the main causes for the halt to developments of this type of aircraft. Thus, the B-70A strategic bomber was modified in 1963-1964 to become the RF-70A strategic reconnaissance craft. Here the flight altitude was increased by 2-2.5 km and powerful radar countermeasures were installed on it. In the opinion of specialists at Northrop developing the RS-70A, these measures considerably reduce the probability of the airplane being hit by anti-aircraft missiles. /73
/74



We must also note the exceptionally high costs of developing and building strategic bombers. The cost of the experimental B-70A was 500 million dollars (i.e., each kg of the aircraft's weight cost 2000 dollars). It was assumed that the costs of 1 kg of weight in a series-produced aircraft will be 800 dollars. At the same time, the cost of 1 kg of the weight of a series-produced U.S. tactical bomber is 120 dollars, which is about 6-7 times less than for the strategic bomber.

2.4. Tactical-Flight Characteristics of Transport Aircraft

Advances in military transport aviation are closely linked with developments in civil transport aviation and occur mainly in two directions. One is characterized by building airplanes with high carrying capacity and high velocity and range, intended for service in high-grade airfields. The other direction is marked by aircraft with relatively low flight velocities and radii, but which operates from small landing fields and field-type airfields.

Technical parameters of transport aircraft are given in Tables 2.8 and 2.9 [35, 36, 128, 130, 161, 166, 172, 174]. The lift-drag ratio of aircraft in the first group with subsonic aerodynamics is $K_{\max} = 15$ for $(C_{x_0})_{\min} = 0.015 - 0.018$. These

K_{\max} values for transonic-speed aircraft can scarcely be increased without using streamlining laminarization; thus, by boundary layer suction, the lift-drag ratio on the X-21 experimental craft was increased by 1.5 times, and $K_{\max} = 20-22.5$ (Fig. 2.10, a) was attained for the Boeing 2707 by boundary layer control and variable geometry.

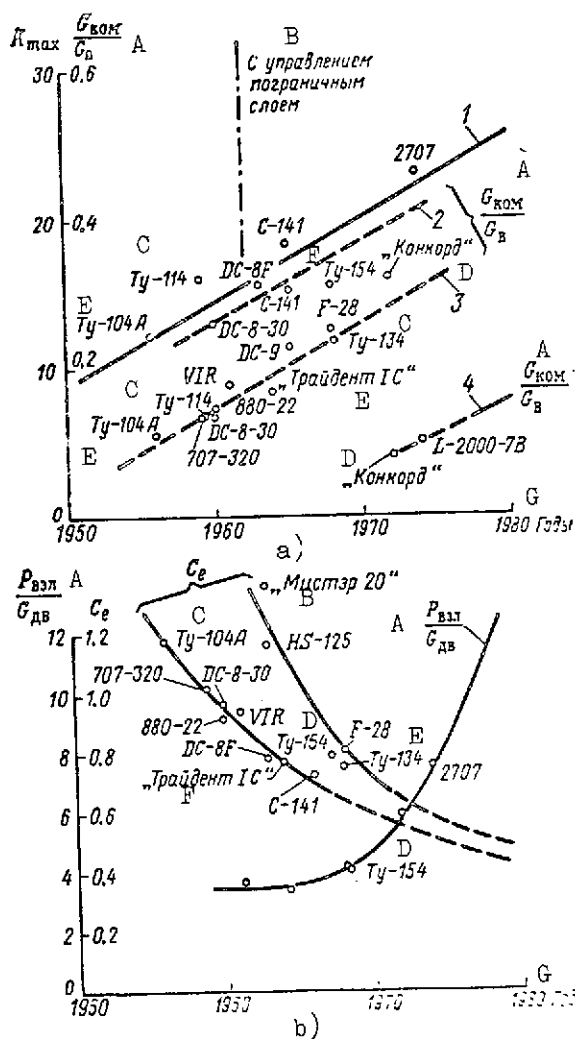


Fig. 2.10. Main performance indicators of transport aircraft:

- 1 -- for K_{max}
 2, 3, 4 -- for aircraft of different weight

KEY for Fig. 2.10 a:

- A -- G_{pay}/G_0
 B -- With boundary layer control
 C -- TU-114
 D -- Concorde
 E -- TU-104A
 F -- TU-154
 G -- Trident IC
 H -- Years

KEY for Fig. 2.10 b:

- A -- P_{to}/G_{en}
 B -- Mystere 20
 C -- TU-104A
 D -- TU-154
 E -- TU-134
 F -- Trident IC
 G -- Years

TABLE 2.8 A. 1. TECHNICAL CHARACTERISTICS OF TRANSPORT
AIRCRAFT OF THE FIRST GROUP WITH TURBOJET ENGINES

176

Airplane type		TU-104A	Boeing 707-320	Convair 440-22	Caravelle VIR	Douglas DC-8-30
General data	Function	Passen- ger	Passen- ger	Passen- ger	Passen- ger	Passen- ger
	Country	USSR	U.S.	U.S.	France	U.S.
	Initial production	1956	1959	1960	1961	1960
	Number of engines	Two RD-3m	Four JT4A-9	Four CJ-805-3	Two JT8D-1	Four JT4A-11
	Maximum seating	100	189	120	89	177
Geome- trical data	Wing area, S, m ²	174.4	268.7	185.8	146.7	257.6
	Wingspan, l, m	34.5	43.4	36.6	34.3	43.4
	Aspect ratio, λ	6.82	7.01	7.2	8.02	7.25
	Sweep angle, χ , deg.	37	35	37	20	30
	Relative thickness, C, %	13	12	11	12	11.5
Weight data	Takeoff weight, G _{to} , tons	76.00	141.52	83.69	52.00	142.88
	Wt. of equipped plane, G _{eq} , tons	42.36	60.16	40.19	30.2	60.37
	Weight of fuel, G _{fu} , tons	26.5	72.38	32.66	15.2	72.15
	Weight of engines, G _{en}	6.39	7.60	—	3.04	—
	Maximum payload, G _{pay} , tons	9.0	18.17	12.15	9.26	18.74
	G _{fu} /G _{to}	0.35	0.51	0.39	0.29	0.5
Main relative perfor- mance in- dicators	Airplane lift-drag ratio, K _{max}	12	17	—	—	13
	Engine perfor- mance P _{to} /G _{en}	—	—	—	—	—
	Specific fuel consumption, C _e , at economical speed	1.18	1.02	0.92	0.94	0.96
	Specific wing loading, G/S, kg/m ²	420	522	450	354	556
	G _{pay} /G _{to}	0.119	0.129	0.145	0.178	0.131

177

TABLE 2.8B. TECHNICAL CHARACTERISTICS OF PASSENGER, CARGO, AND TROOP CARRIER AIRCRAFT OF THE FIRST GROUP WITH TURBOPROP AND TURBOFAN ENGINES

178

Airplane type		TU -114	Douglas DC-8F	Tri-dent1-C	C-141	TU-154	Con-corde	Boeing 2707	L-2000-7B
General data	Function	Passenger	Cargo	Passenger	Milit. cargo & transport	Passenger	Passenger	Passenger	Passenger
	Country	USSR	U.S.	UK	U.S.	USSR	UK & France	U.S.	U.S.
	Initial production	1959	1963	1964	1965	1968	1972	1974	1974
	Number of engines	Four	Four JT6D-5	Three Spey 505-S	Two JT3D-5A	Two	Four 593B	Four GE4-J-85	—
	Engine type	TBP	TBF	TBF	TBF	TBF	TBP	TBP	—
	Maximum seating	170	none	103	154	164	138	313	308
Geometrical data	Wing area, S, m ²	311.1	267.8	126.2	299.9	180.0	358.0	836.0	839.0
	Wingspan, l, m	51.1	43.41	27.38	48.79	37.55	25.6	53.1—32.3	35.4
	Aspect ratio, λ	8.39	7.31	5.95	8.04	7.8	1.82	3.34	—
	Sweep angle, χ , in deg.	33.5	30	35	25.	35	—	20—72	—
	Relative thickness, C, %	12.5	11.5	—	11.5	11.0	—	2.15—2.98	2.3
Weight data	Max. takeoff weight, G _{to} , tons	179.0	142.88	52.16	143.61	84.0	161.9	306.2	—
	Weight of equipped plane, G _{eq} , tons	95.0	58.39	30.57	59.66	43.50	65.2	130.3	98.52
	Weight of fuel, G _{fu} , tons	67.0	71.26	17.56	68.05	33.15	84.0	166.5	—
	Weight of engines, G _{en} , tons	12.02	—	—	8.4	7.05	10.2	18.0	—
	Maximum payload, G _{pay} , tons	22.5	43.22	8.6	43.06	20.0	12.7	34.0	33.6
	G _{fu} /G _{to}	0.376	0.500	0.380	0.475	0.394	0.522	0.545	

179

[TBP = Turboprop engine; TBF = Turbofan engine]

TABLE 2.8 B TECHNICAL CHARACTERISTICS OF PASSENGER, CARGO, AND
TROOP-CARRIER AIRCRAFT OF THE FIRST GROUP WITH TURBOPROP AND
TURBOFAN ENGINES

/80

[Conclusion]

Airplane type		TU-114	Douglas DC-8-30	Tri- dent-C	C-141	TU -154	Con- corde	Boeing 2707	L-2000- 7B
Main compara- tive perform- ance indica- tors	Lift-drag ratio K_{\max}	15,8	—	—	18,0	15,5	13,5	—	—
	Engine perfor- mance, N_{to}/G_{en} ; P_{to}/G_{en} , in kg/kg	4,95*	—	—	—	4,1 (w/re- verser)	6,3	7,6	—
	Specific fuel consumption, C_e , at econo- mical speed, kg/kg.hr	0,207**	0,785	0,77	0,72	0,76	0,70	0,70	—
	Specific wing loading G/S, in kg/m	575	534	413	479	467	445	368	264
	G_{pay}/G_{to}	0,125	0,31	0,165	0,3	0,238	0,078	0,111	—

* hp/kg

** kg/hp.hr

TABLE 2.9 TECHNICAL CHARACTERISTICS OF TRANSPORT
AIRCRAFT IN THE SECOND GROUP

/81

Airplane type		Mystere20	HS-125	DC-9	TU -134	F-28
General data	Function	Passenger	Passenger	Passenger	Passenger	Passenger
	Country	France	UK	U.S.	USSR	Netherlands
	Initial production	1963	1963	1965	1967	1968
	Number of engines	Two ST-12A-8	Two ASV-20	Two D-30	Two D-20m-125	Two Sney- Jukker
	Engine type	Turbojet	Turbojet	Bypass	Turbofan	Turbofan
	Maximum seating	8-12	8-10	60	72	65
Geometrical dimensions	Wing area, S, in m ²	37,0	33	85,9	127,3	86,0
	Wingspan, l, in m	14,5	14,3	26,64	29,0	23,52
	Aspect ratio, λ	5,65	6,17	—	6,56	—
	Sweepback angle, χ deg.	30	20	24	35	16
	Mean relative thickness, C, in %	9,25	12,5	11,6	—	12
Weight data	Maximum takeoff weight, G _{to} , in tons	9,25	8,6	34,9	44,0	24,5
	Weight of equipped plane, G _{eq} , in tons	5,2	4,4	20,9	27,0	13,8
	Weight of fuel, G _{fu} , tons	3,0	4,0	8,5	12,2	7,8
	Wt. of engines, G _{en} , tons	0,66	0,72	2,8	3,1	2,1
	Maximum payload, G _{pay} , tons	0,75	0,65	8,1	7,7	6,1
	G _{fu} /G _{to}	0,324	0,465	0,243	0,278	0,314
Main comparative quality indicators	Airplane lift-drag ratio, K _{max}	—	—	—	14,8	—
	Engine quality, P _{to} /G _{en} , kg/kg	5,75	4,9	4,6	4,4	4,3
	Specific consumption, C _e , at economical speed	1,36	1,16	0,79	0,78	0,8
	Specific wing loading, G/S, in kg/m ²	286	298	405	383	336
	G _{pay} /G _{to}	0,081	0,076	0,232	0,175	0,25

/82

Fig. 2.11 gives the numerical values of the maximum lift-drag ratios of passenger aircraft. As we can see, at subsonic flight velocities the Boeing 2707 with variable-geometry wings ($K_{\max} = 20-22.5$) has the maximum lift-drag ratio. The K_{\max} is much smaller, about 12-14 for aircraft with delta wings (the Concorde and the L-2000). In the supersonic range from $M = 2.0$ to $M = 3.0$, the lift-drag ratio falls off to 7.5-8.5 for these craft, regardless of the wing type [183].

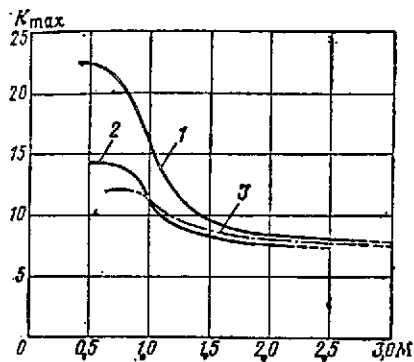


Fig. 2.11. M number dependence of maximum aircraft lift-drag ratio:

- 1 -- Boeing 2707
- 2 -- Concorde
- 3 -- Lockheed L-2000-7B

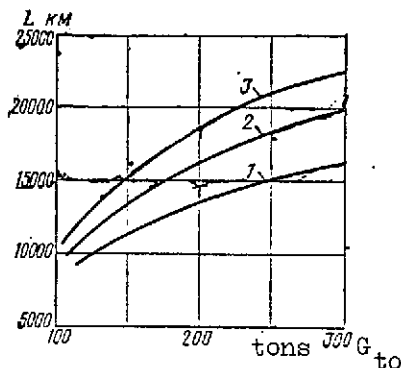


Fig. 2.12. Dependence of passenger airplane range on takeoff weight and wing type:
1 & 2 -- turbulent and laminarized wing streamlining
3 -- laminarized streamlining of wing and tail unit assembly

Further work on the laminarization of streamlining in the United States and the United Kingdom with wing profiles with $C \cong 1.5$ percent with boundary layer suction point of the possibility of a marked reduction in C_{x_0} [135], and thus an increasing K_{max} .

Boundary layer control for streamlining laminarization also has an appreciable effect on the specific fuel consumption and range of aircraft. When using the boundary layer control system, the increase in the mass of the empty craft due to the added weight of wing structures and the installation of air suction devices must be taken into account. Therefore an increase in the range of an airplane with boundary layer control is determined by the formula

/84

$$\frac{L'_f}{L_f} = \frac{\frac{V'K'}{C_e} \cdot \ln \frac{1}{1 - \frac{G_{fu}}{G_0} \Delta \frac{G_{fu}}{G_0}}}{\frac{VK}{C_e} \cdot \ln \frac{1}{1 - G_{fu}/G_0}}, \quad (2.12)$$

where L'_f is the actual range (all values with the prime correspond to flight with laminar streamlining, and those without the prime -- to turbulent streamlining); and G_{fu}/G_0 is the increase in the aircraft's weight due to using the boundary layer control system.

Fig. 2.12 presents the range increases as a function of aircraft takeoff weight for different wing types and optimal aircraft parameters.

Engine quality is also increased by lowering its structural weight and increasing the takeoff thrust (Fig. 2.10 b). A slight reduction in engine weight during the period from 1958 to 1968 is associated with replacement in transport aircraft of TBF (turbofan) engines, which have a lower specific thrust, with turbojet engines [TBJ]; this led to a 15 percent production in the specific fuel consumption; a 15 decibel lowering of the noise level; and increase in the ratio of takeoff thrust to cruising thrust.

In aircraft of the second group whose wings have a smaller aspect ratio with a lift-drag ratio not exceeding 11-12, boundary layer control devices have also begun to be used in recent years.

Small transport aircraft represent the third generation of jet aircraft of this subclass, receiving developmental advances only after 1963. Therefore, only turbofan engines have been installed on them, which given the small fuel margin made it possible to obtain long range values and good takeoff-landing characteristics [35].

The basic tactical-flight characteristics of these two groups of aircraft are given in Tables 2.10 and 2.11 and in Fig. 2.13.

/85

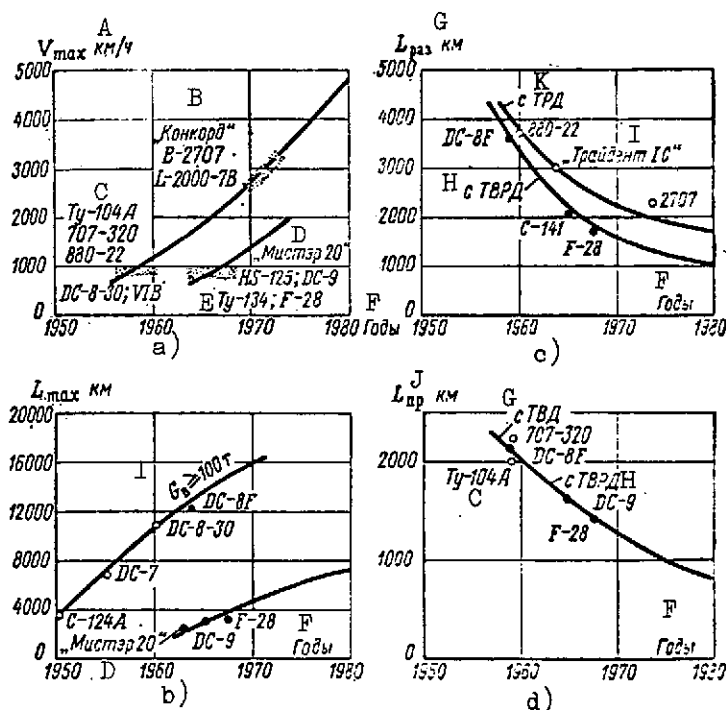


Fig. 2.13. Basic tactical-flight characteristics of transport aircraft in the first and second groups

KEY: A -- km/hr I -- $G_{\geq 100}$ tons
 B -- Concorde J -- $L_{ac} \leq L_{actual}$
 C -- TU-104A K -- With turbojet engines
 D -- Mystere 20
 E -- TU-134
 F -- Years
 G -- With turboprop engines
 H -- With turbofan engines

When the manufacturers did not give range in the tactical-flight characteristics, it was calculated by the formula

$$L = 2440 \frac{KVK_{fu} G_{to}}{C_e G_{fi}} \quad (2.13)$$

where K_{fu} is the coefficient allowing for fuel consumption in takeoff, acceleration, gliding, and landing;
 G_{to} is the takeoff weight; and
 G_{fi} is the weight of the aircraft at the end of a flight for range.

TABLE 2.10 A. TACTICAL-FLIGHT CHARACTERISTICS OF PASSENGER AIRCRAFT IN THE FIRST GROUP WITH TURBOJET ENGINES

/86

Airplane type		TU-104A	Boeing 707-320	Convair 880-22	Douglas DC-8-30	Caravelle VIR
Flight velocity V, km/hr	Maximum	990 H=7 KM	965 H=7.6 KM	988 H=6.9 KM	960 H=8.4 KM	852 H=7.7 KM
	Cruising	800 H=10 KM	850 H=12.2 KM	833 H=10.7 KM	861 H=10.7 KM	725 H=10.7 KM
	Economical	800 H=10 KM	860 H=12 KM	897 H=10.7 KM	876 H=10.7 KM	800 H=10.7 KM
Range, km	With maximum fuel reserve	4300 H=10 KM	10900 H=11.7 KM	6430 H=10.7 KM	10900 H=10.7 KM	4550 H=10.7 KM
	With maximum payload	4000 H=10 KM	7400 H=11.7 KM	6130 H=10.7 KM	9125 H=11 KM	3700 H=10.7 KM
Takeoff-landing characteristics in meters	Takeoff run for G_{to-max} MCA+15°C; H=0	2650	3650	3700	3600	3000
	Landing run at maximum landing weight	2000	2200	1900	2070	1700

TABLE 2.8 B TECHNICAL CHARACTERISTICS OF PASSENGER, CARGO,
AND TROOP-CARRIER AIRCRAFT OF THE FIRST GROUP WITH TURBOPROP
AND TURBOFAN ENGINES

/87

Airplane type		TU--114	Douglas Tri- DC-8P	ident 1-C	C-141	TU--154	Com- corde	Boeing 2707	L-2000- 7B
Flight velocity, V, km/hr	Maximum	820 $H=8$ KM	955 $H=8$ KM	975 $H=7,6$ KM	900 $H=7,6$ KM	975 $H=9,7$ KM	2300 $H=19$ KM	2850 $H=19,5$ KM	—
	Cruising	740 $H=10$ KM	855 $H=10,7$ KM	855 $H=10,7$ KM	815 $H=10$ KM	900	—	—	—
	Economical cruising	750	875 $H=10,7$ KM	930 $H=9,7$ KM	815 $H=11$ KM	850	—	—	—
Range, in km	W/maximum fuel reserve	9900	12200 $H=10,7$ KM	5300 $H=10,7$ KM	10500 $H=11$ KM	7000	7800	8000	—
	At maximum pay- load	9700	6050 $H=9,9$ KM	3250 $H=10,7$ KM	6500 $H=9,1$ KM	4000	6700 $H=16$ KM	6430	—
Landing- takeoff charac- teris- tics	Takeoff run at G_{to} max, MCA + 15° C, $H=0$	2550	3600	3100	2050	1215	2900	2320	—
	Landing run w/max landing weight	1850	2130	1815	2000	710	2400	1950	—

[MCA = minimum crossing altitude]

TABLE 2.11 TACTICAL-FLIGHT CHARACTERISTICS OF TRANS-
PORT AIRCRAFT OF THE SECOND GROUP

/88

Airplane type		Mystere 20	HS-125	DC-9	TU--134	F-28
Flight velocity V, km/hr	Maximum			908 $H=7,6$ KM	870 $H=11,0$ KM	886 $H=7,6$ KM
	Cruising	860 $H=7,6$ KM	805 $H=9,15$ KM	778 $H=9,15$ KM	850 $H=8,6$ KM	815 $H=7,6$ KM
	Economical	740 $H=12,6$ KM	690 $H=12$ KM	850 $H=7,6$ KM	750 $H=8,6$ KM	805 $H=7,6$ KM
Range, km	With maximum fuel reserve	—	—	3000 $H=9,15$ KM	4360 $H=8,6$ KM	3100 $H=7,6$ KM
	With maximum payload	—	—	1720 $H=9,15$ KM	2945 $H=8,6$ KM	1725 $H=7,6$ KM
Landing- takeoff charac- teristics	Takeoff length w/ G_{to} max MCA + 15° C; $H=0$	1300	800	2120	1050	2165
	Landing run with maximum landing weight	700	420	1615	850	1400

In spite of the strong development of transport aviation, the total time spent by the passenger in long flights amounts to several hours. For a range $L = 16,000$ km at a cruising speed of $V_{cru} = 2600$ km/hr, the duration of just flight alone is somewhat more than six hours. In addition, the passenger has to spend time on the road to the airport, wait in the airplane till lift-off, and in the drive from the airport after the plane comes in. Setting this time at two hours, the total time expended by the passenger in a flight is 8.5 hours. The total time outlays of a passenger can be characterized by Fig. 2.14 by the following relationship:

$$t_{tot} = t_{to} + t_f + t_{d.w.} \quad (2.14)$$

Here t_{to} is the time spent in takeoff, landing, accelerating to required speed, and deceleration (it is assumed that the g-load is 0.2 in acceleration and deceleration); t_f is the time spent in the flight at V_{cru} ; $t_{d.w.}$ is the time spent in trips from the airport and in waiting for the flight ($t_{d.w.} = 2$ hours).

The large total passenger time outlays require a significant increase in flight characteristics of transport aircraft. Two fundamentally different solutions are possible in this area.

For aircraft in the first group designed to make long flights, a reduction in the total time can be achieved only by an appreciable increase in cruising speed to $M_{cru} = 8.0-12.0$. This means that hypersonic transport aircraft must appear to replace supersonic transport planes [161, 164, 184, 199, 206]. The additional time outlays must be reduced for aircraft in the second group making short-range flights by bringing the takeoff point closer to cities, i.e., by using vertical takeoff airplanes.

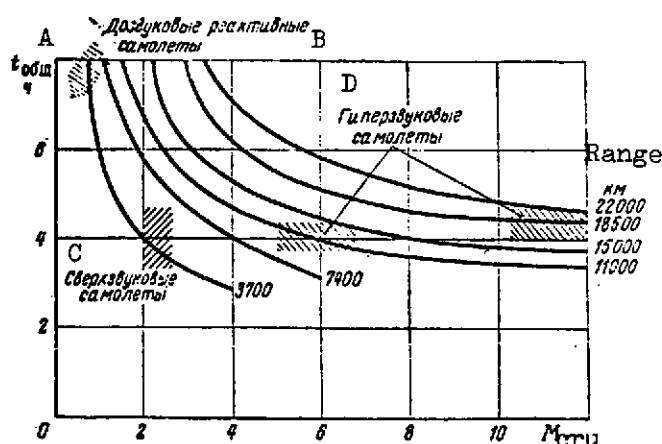


Fig. 2.14. Total passenger time outlays t_{tot} for flights on different types of transport aircraft (subsonic, supersonic, and hypersonic) as a function of M_{cru}

KEY: A -- t_{tot}
 B -- Subsonic jets
 C -- Supersonic airplanes
 D -- Hypersonic airplanes

Fig. 2.14. Continuation

E -- Range
F -- M_{cru}

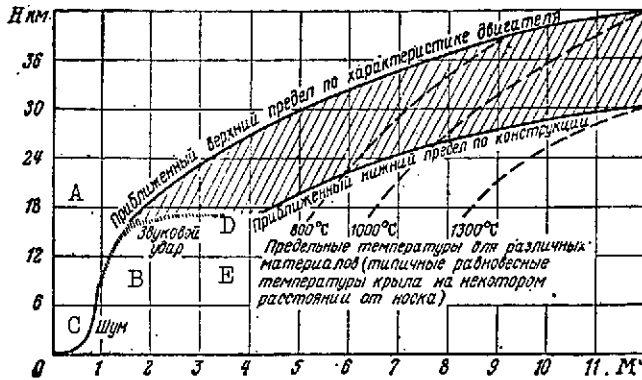


Fig. 2.15. Constraints by hypersonic airplane flight regimes

KEY: A -- Approximate upper limit by engine characteristics
B -- Shock wave
C -- Noise
D -- Approximate lower limit by design
E -- Maximum temperature for various materials (typical equilibrium wing temperatures at some distance from the leading edge)

The flight regime of a hypersonic craft is marked by several constraints (Fig. 2.15 [135]) affecting the characteristics of its use. The upper boundary is determined by the allowable pressure in the air intake ducts, and the lower boundary is set by the structural strength limit. This constraint increases fuel consumption in hypersonic airplane flight. To reduce its value, acceleration to hypersonic velocity will have to be executed at a low altitude, followed by a climb to cruising flight. As can be seen from the constraints (cf Fig. 2.15), this maneuver must be done with simultaneous climbing. Therefore the flight profile of a hypersonic craft with a cruising speed corresponding to $M = 12$ is of the form shown in Fig. 2.16. Since in this regime 91 the turning radius is very large (about 800 km at a 30° bank), the flight trajectory must lie in a great-circle plane.

Let us turn to an analysis of transport aircraft with vertical takeoff for short takeoff run. For lines of several hundreds of kilometers, they must have a fairly high cruising velocity, as we can see from Fig. 2.17 a. In this case the total flight duration is two hours for a range $L = 1000$ km.

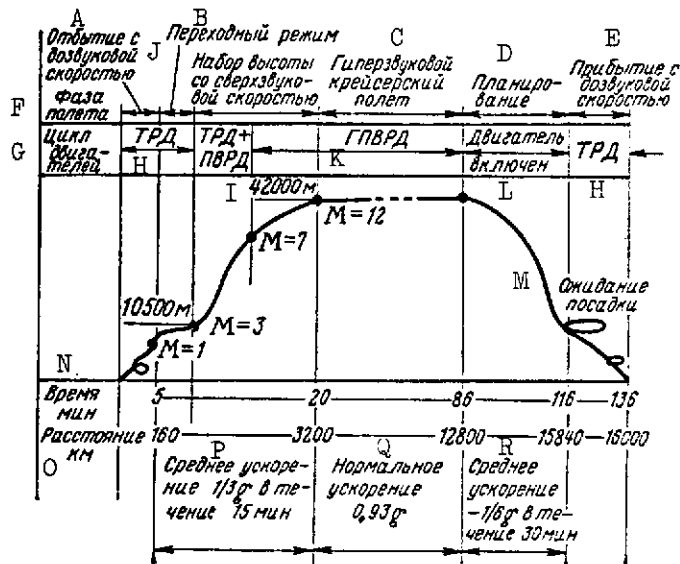


Fig. 2.16. Flight trajectory of a hypersonic transport with allowance for constraints (cf Fig. 2.15)

- KEY:
- A -- Departure at subsonic speed
 - B -- Transitional regime
 - C -- Hypersonic cruising flight
 - D -- Gliding
 - E -- Arrival at subsonic speed
 - F -- Flight phase
 - G -- Engine cycle
 - H -- Turbojet engine
 - I -- Turbojet engine + ramjet engine
 - J -- Climb at supersonic speed
 - K -- Hypersonic ramjet engine
 - L -- Engine fired
 - M -- Awaiting landing
 - N -- Time, minutes
 - O -- Distance
 - P -- Mean acceleration $1/3 g$ for 15 minutes
 - Q -- Normal acceleration $0.93 g$
 - R -- Mean acceleration $1/6 g$ for 30 minutes

Selection of V_{cru} for vertical takeoff craft is based on the effectiveness criterion used in evaluating transport aircraft (Fig. 2.17 b):

$$E_1 = \frac{G_{\text{nom}}}{G_{\text{emp}}} V_{\text{ro-av}} \quad (2.15)$$

where $V_{\text{ro-av}}$ is the mean route speed.

For $L = 1200 - 1400$ km, V_{cru} is 830 km/hr for vertical takeoff 92 airplanes, but 920 km/hr for ordinary aircraft, and thus E_1 is practically identical.

Another indicator of economic effectiveness characterizing the operational flexibility of vertical takeoff aircraft (owing to the possibility of takeoff and landing in required airports regardless of the class of the airport) is the quantity E_2 (Fig. 2.18):

$$E_2 = \frac{G_{\text{nom}} + G_{\text{u}}}{G_{\text{emp}}} \frac{N_{\text{sub}}}{N_{\text{tot}}} \quad (2.16)$$

where N_{su} is the number of suburban airports; and N_{tot} is the total number of airports.

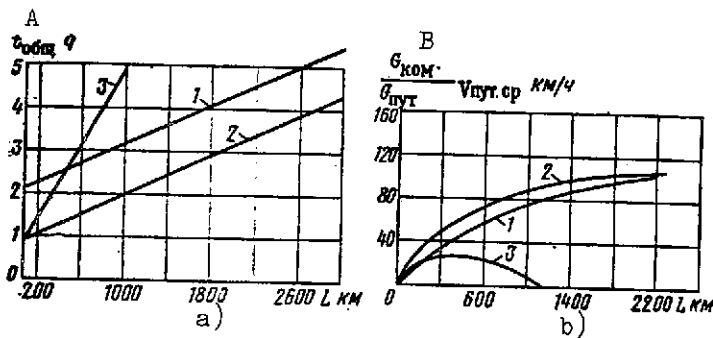


Fig. 2.17. Main indicators of short-haul aviation:

KEY: a -- Total time spent by passengers in flights as a function of range:
1 -- Ordinary aircraft with $V_{\text{cru}} = 920$ km/hr
2 & 3 -- Vertical takeoff aircraft with $V_{\text{cru}} = 830$ and 280 km/hr

b -- Effectiveness indicator as a function of range:
1 -- Ordinary aircraft with $V_{\text{cru}} = 920$ km/hr

2 & 3 -- Vertical takeoff aircraft with $V_{\text{cru}} = 830$ and 280 km/hr

KEY: A -- t_{tot} , hours

B -- $(G_{\text{pay}}/G_{\text{ro}}) (V_{\text{ro-av}})$, km/hr $[G_{\text{ro}} = G_{\text{route}}]$

Fig. 2.18 presents functions of a second indicator of economic effectiveness of aircraft (ordinary aircraft and those with vertical takeoff). As we can see, by this indicator vertical takeoff aircraft not only surpass ordinary aircraft at the present time, but even retain the trend of an increase in the indicator in the immediate future [137]. Additionally, improvements in transport aircraft will lead to fewer airports from which these aircraft can operate, which also favors a rise in E_2 .

The high effectiveness of vertical takeoff aircraft (cf. [137]) can be obtained, in particular, by means of power plants with a wide range of thrust change, from 1.3-1.5 times the weight of an aircraft in the takeoff regime, to 0.1-0.3 times aircraft weight in the cruising flight regime. Producing this thrust range [137] is one of the principal and complex problems in developing effective aircraft of this type. From Fig. 2.19 [154] it is clear that the main requirements imposed on the power plants of vertical takeoff aircraft must be satisfied by 1975. /93

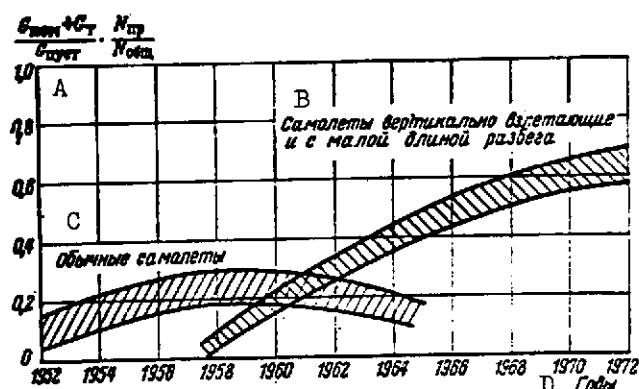


Fig. 2.18. Trends in change of economic effectiveness of short-haul aviation aircraft
KEY: A -- $(G_{\text{pay}} + G_{\text{fu}}) / G_{\text{emp}} \cdot (N_{\text{sub}} / N_{\text{tot}})$
B -- Vertical takeoff and short take-off run aircraft
C -- Ordinary aircraft
D -- Years.

Simultaneously with development of hypersonic transport aircraft, research is underway in the U.S. to build a bomber and fighter-interceptor with $M_{\text{cru}} = 12$ and a flight altitude of 42-43 km [135, 143]. The high velocity of the hypersonic bomber will permit using air-to-surface missiles on it without power plants, but with a considerable range (due to the kinetic energy reserve).

The variation of the lift-drag ratio of hypersonic aircraft (at the 1968 level of theoretical studies) is shown in Fig. 2.20. As this figure makes clear, K_{max} of hypersonic aircraft will vary from 6 to 8. Power plants of hypersonic aircraft will operate on liquid hydrogen and consist of two engines: a turboramjet engine and a ramjet engine with subsonic and supersonic combustion [81]. /94

Comparative characteristics of fighter-interceptor (ordinary types) with hypersonic fighter-interceptors (a U.S. project) are shown in Fig. 2.21, from which it is clear that at the transition to hypersonic flight velocity $M > 8$, the static flight altitude and the takeoff weight of the fighter-interceptors rise appreciably.

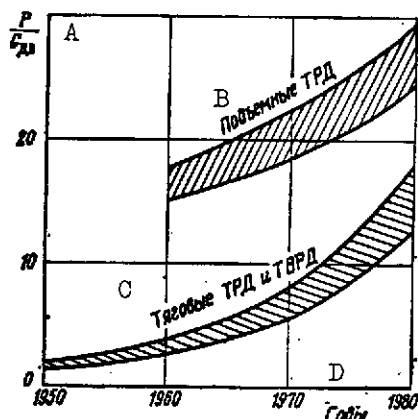


Fig. 2.19. Developmental trends in lift and thrust engines of aircraft

KEY: A -- P/G_{en}
 B -- Lift turbojet engines
 C -- Thrust turbojet engines and turbofan engines
 D -- Years

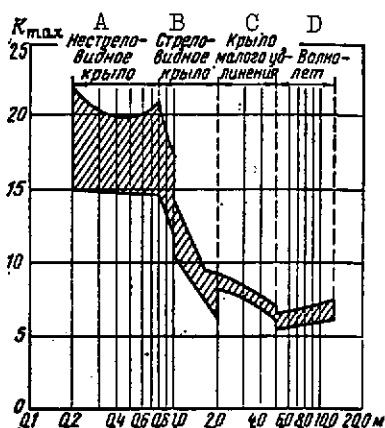


Fig. 2.20. Change in lift-drag ratio of modern aircraft as a function of M number

KEY: A -- Nonsweptback wing
 B -- Sweptback wing
 C -- Small-aspect-ratio wing
 D -- Variable-incidence wing

2.5. Tactical-Flight Characteristics of Air-to-Air Missiles

Air-to-air missiles are one of the most powerful elements in the armament of fighter-interceptors, multimission fighters, and are designed to strike enemy air targets (fighters, reconnaissance craft, bombers, certain types of air-to-surface missiles, balloons, and so on). The considerable range of altitudes and velocities of air targets imposes high requirements on these missiles. Air-to-air missiles must have high power capabilities to strike high-speed targets in the rear hemisphere or air targets flying at considerable speeds above the fighter-interceptor. Large errors in the recovery of a fighter-interceptor at the moment of missile launch owing to its limited maneuvering capabilities as

to altitude, the action of active and passive jamming, and also the rapidity of air combat demand considerable g-loads from a missile in all conditions of its combat use.

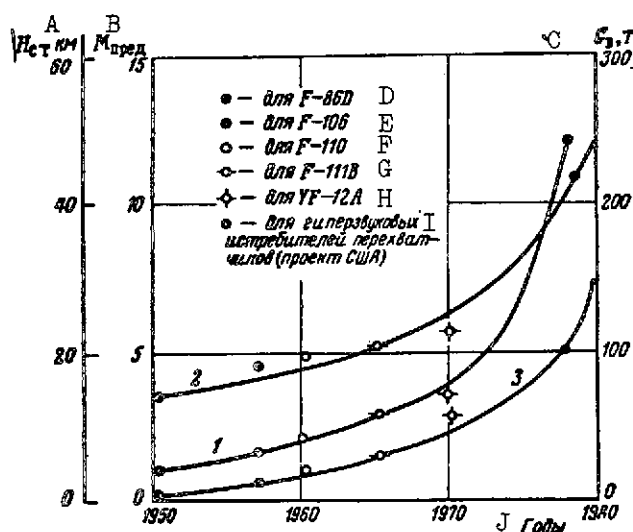


Fig. 2.21. Comparative characteristics of fighter-interceptors (ordinary and hypersonic):

1 -- For maximum M_{\max}
 2 -- For static flight altitude H_{st}
 3 -- For takeoff weight G_{to}

KEY: A -- H_{st}
 B -- M_{\max}
 C -- G_{to} , tons
 D -- For F-86D
 E -- For F-106
 F -- For F-110
 G -- For F-111B
 H -- For YF-12A
 I -- For hypersonic fighter-interceptors (U.S. project)
 J -- Years

It must have small weight and dimensions in order not to reduce the static ceiling, longitudinal g-load, and rate of climb of the fighter-interceptor. At the same time, the missile warhead must be sufficient to strike enemy aircraft with skin thickness to 10-12 mm.

The missile engine and control system must ensure high accuracy of guidance to the target (during its maneuvering and when jamming is present) and must also have high reliability of action under combat conditions and after long storage; the missile design must be intended for mass production. In the opinion of foreign specialists, it is practically impossible to satisfy all these requirements in a single missile type. Therefore modern fighter-interceptors can, depending on the combat tasks assigned them, carry various air-to-air missiles [4, 17, 60, 61, 66].

/96

Table 2.12 gives the main technical and tactical-flight characteristics of certain air-to-air missiles [69, 72, 78, 89, 96, 128, 137, 160, 171].

The main performance indicators of the missiles are the longitudinal n_x and lateral n_y g-loads, thrust-weight ratio and power-to-weight ratio (K_{t-w} and K_{p-w}), and maximum flight velocity V_{\max} . Their rate change graphs have been plotted based on the following functions:

$$n_x = \frac{P_{en}}{G_m} - \left(\frac{\rho V^2 S C_{x_0}}{2G_m} + \frac{2AG_m}{\rho V^2 S} \right); \quad (2.17)$$

$$n_{y-ave} = \rho \frac{V^2 S}{2G} \left(C_v^{\delta_{c-s}} - \frac{m_z^{\delta_{c-s}}}{m_z^a} C_v^a - \right. \\ \left. - \frac{2P}{\rho V^2 S m_z^a} \right) \delta_{c-s \max}; \quad (2.18)$$

$$K_{t-w} = \frac{P_{en}}{G_m}, \quad K_{p-w} = \frac{h_u G_m}{G_m}. \quad (2.19)$$

Here P_{en} is engine thrust;

G_m is missile weight;

I_1 is the specific impulse of engine in kg/kg;

$$C_v^a = \frac{\partial C_v}{\partial \alpha}; \quad C_v^{\delta_{c-s}} = \frac{\partial C_v}{\partial \delta}; \quad m_z^a = \frac{\partial m_z}{\partial \alpha}; \quad m_z^{\delta_{c-s}} = \frac{\partial m_z}{\partial \delta}$$

are the partial derivatives of the lift coefficient and the coefficient of the angle-of-attack moment α and the control surface deflection angle δ_{c-s} .

TABLE 2.12 MAIN TECHNICAL AND TACTICAL FLIGHT CHARACTER-
ICS OF AIR-TO-AIR MISSILES

197

Missile type		Fairey	GAR-1D	GAR-8	GAR-3A	AAM-N-6A	—	R-530	AJM-54A	
General data	Name of missile	Fairey Flesh	Falcon	Side- winder IA	Super Falcon	Sparrow IIIA	Red Top	Matra	Phoenix	
	Country	UK	U.S.	U.S.	U.S.	U.S.	UK	France	U.S.	
	Initial produc- tion	1950	1956	1954	1959	1960	1964	1963	Exper. 1969	
	Guidance system	Radio beam	Semi- active radar homing	Pass- ive infra- red homing	Semi- active radar homing	Semi- active radar homing	Infra- red homing	Radar or infra- red homing	Radio command w/homing in final leg	
Geome- trical dimen- sions	Diameter, D, m	0,147	0,162	0,127	0,168	0,210	0,220	0,260	0,380	
	Length, d, m	2,84	1,98	2,87	2,18	3,66	3,05	3,3	3,96	
	Wingspan, l, m	0,7	0,5	0,53	0,61	1,02	0,9	1,1	0,91	
	Area of two* wings S in m ²		0,165	0,18	0,25	0,236	0,31			
Weight data	Launch weight, G _a in kg	135	55	70	68	172	170	195	450	
	Weight of payload G _{pay} , in kg	60	30	36	35	80	63	92	140	
	Weight of warhead G _{wh} , in kg	10	9,0	11,3	18,0	29,0	26,0	30,0	25,0	
/SFJ = solid- fuel jet/ Engine	Engine type		SFJ	SFJ	SFJ	SFJ	SFJ	SFJ	SFJ	
	Engine oper. period, sec	1st stage								
		2nd stage	2,0	$\frac{1,5}{10}$	2—3	$\frac{1,5}{10}$	1,8	2—3	$\frac{3}{13,5}$	
	Engine thrust, P _{en} , kg	1st stage								
2nd stage		2100	$\frac{2700}{45}$	1600	$\frac{2700}{45}$	3500	3800	$\frac{2900}{200}$		
Condi- tions of com- bat use	Maximum flight al- titude of attacked target, H _t , km		15	18	18	21	20	23	21	26
	Maximum velocity of at- tacked target, V _t , km/hr	frontal hemi- sphere	1500	$\frac{2500}{2000}$	2200	$\frac{2800}{2200}$	$\frac{3000}{2300}$	$\frac{3200}{2500}$	$\frac{3000}{2300}$	$\frac{4200}{3000}$
		rear hemi- sphere								

198

* The area S_{cru} was obtained by calculation from drawings of
general views of the missile for the GAR-3A, Red Top, and
AJM-54A.

TABLE 2.12 MAIN TECHNICAL AND TACTICAL FLIGHT CHARACTERISTICS OF AIR-TO-AIR MISSILES

/99

[Conclusion]

Missile type		Fairey	GAR-1D	GAR-8	GAR-3A	AAM-N-6A	—	R-530	AJM-54A
Main missile performance indicators	Thrust-to-weight ratio, $K_{t-w} = \frac{P}{G_l}$, kg/kg	13,5	49	23	40	20	22	18	
	Power-to-weight ratio $K_{p-w} = \frac{I_{fu} G_{fu}}{G_a}$					35	41	43	70
	Available g-load, n_{y-ava}	$H=5$ km	8,5		11,0		25,0		
		$H=15$ km	4,0	6,0	5,0	9,0	9,0		16
		$H=20$ km				4,0			
	Available g-load, n_{x-ava}	$H=5$ km	12,5		17,5				
		$H=15$ km	15		19,5		38		45
		$H=20$ km							
	Velocity V_p , m/sec	$H=15$ km	600	620	490	950	670	950	1050
		$H=20$ km			520	900		900	

Numerical values of the ratio $m_z^a / m_z^{\delta c-s}$ used in an approximate calculation for layouts of missiles with tilting wings with control surfaces located forward (canard) and aft of the wings can be taken as follows [63]: 5-6, 1.4-1.2. Linearized equations of missile motion [63, 64] we used in deriving the relation (2.18).

/100

The maximum flight velocity V_{max} was determined as the solution obtained for the end of the powered phase

$$V_{max} = V_B - V_j \ln \left(\frac{m_1 - m_{fu}}{m_1} \right) - \int_0^{t_{en}} \frac{(C_{x_0} + AC_v^2) S p V^2}{2 \left(m_1 - \frac{m_{fu}}{t_{en}} t \right)} dt \quad (2.20)$$

of the motion of the mass center described by the equations

$$\left. \begin{aligned} \frac{dV}{dt} &= \frac{P}{m_m} \cos \alpha - \frac{X}{m_m}; \\ P &= sm_{fu} V_j; \\ m_m &= m_1 - sm_{fu} t; \\ X &= \frac{(\overline{C_x} + A\overline{C_y^2})}{2} S \rho V^2. \end{aligned} \right\} \quad (2.21)$$

Here V is the instantaneous missile velocity;
 sm_{fu} is the fuel consumption per unit of time
 ($s = 1/t_{en}$, t_{en} is the engine operating period);
 $(\overline{C_x} + A\overline{C_y^2})$ is the constant mean value of the aerodynamic coefficients;
 m_1 is the missile launch weight; and
 V_j is the nozzle gas exhaust velocity;
 $\cos \alpha = 1$.

From the data in Table 2.12, we can see the increase in the maximum flight velocity (an enlargement of the zone of possible attacks -- cf Chapter Four, Section 4), which allows us to assume that the lateral g-load n_{y-ava} rises to 25, and V_{max} -- to 1300-1500 m/sec at an altitude of 15-20 km.

2.6. Tactical-Flight Characteristics of Air-to-Surface Missiles /101

Multimission fighters and tactical and strategic bombers are armed with air-to-surface missiles. Depending on the type of mother craft, these missiles perform the most varied combat tasks. Missiles of multimission fighters, as a rule, are designed to destroy small ground targets (tanks, armored troop carriers, radar and missile ground complexes, infantry subdivisions, and so on). Missiles of tactical bombers are used to strike bridges, railway junctions, military warehouses, missile launch sites, small and medium-tonnage naval vessels, transports, and barges. Missiles of strategic bombers serve to strike large military targets (military ports, large tonnage naval vessels, and other targets of strategic value). Therefore air-to-surface missiles differ widely in their technical parameters and tactics of combat use [13, 17, 54, 69, 78, 137, 155, 171].

The first group of air-to-surface missiles for multimission fighters are marked by their low weight (down to 600 kg) and limited range of action (to 15-20 km). If missiles of this

group are intended to destroy nonradar-contrastive targets, recognition and tracking of targets is carried out by the pilot or operator visually. Therefore the guidance system is of the semiautomatic type with optical or television sighting devices. The range of these missiles cannot exceed the range of visual target of observation, i.e., 8-12 km. If the targets to be hit are radar-contrastive (bridges, railway junctions, military-transport barges, and so on), guidance toward them is executed semiautomatically or automatically using radio-command methods (Bullpup and Nord missiles). And, finally, if targets are included in operating ground radar stations, guidance toward them is executed automatically by means of a passive radar homing head (Shrike missile [171]).

The second group of missiles for tactical bombers differs by high weight (to 2.5 tons) and range of action (to 50 km). Their guidance systems are automatic with homing from the launch point to the strike instant or with command guidance over the initial section and subsequent transition to homing.

/105

TABLE 2.13 MAIN TECHNICAL AND TACTICAL-FLIGHT CHARACTERISTICS OF AIR-TO-SURFACE MISSILES

/102

Missile type		GAM-78A	GAM-77A	MK-1	GAM-83B	AS-30	AGM-45A	A-4E	AGM-69A
General data	Name of missile	Skybolt	Hound Dog	Blue Steel	Bullpup	Nord	Shrike	Wall-eye	SRAM
	Missile type	Ballistic	Winged (Airplane scheme)	Winged	Winged	Winged	With tilt wing	Glide bomb	—
	Country	U.S.	U.S.	UK	U.S.	France	U.S.	U.S.	U.S.
	Year built		1962	1962	1964	1962	1964	1967	Exper.
	Guidance system	Astro-inertial	Inertial	Inertial	Radio command	Radio command	Passive homing with radar	Television	Inertial with transition to homing
Geometrical dimensions	Diameter, D, m	0.9	0.7	1.27	0.3	0.35	0.21	0.33	—
	Length, d, m	11.6	13.0	10.7	3.2	3.85	2.74	3.44	—
	Wingspan, l, m	—	3.7	3.96	0.94	1.05	—	1.16	—

[SFJ = solid-fuel jet; LFJ = liquid-fuel jet]

TABLE 2.13 MAIN TECHNICAL AND TACTICAL-FLIGHT CHARACTERISTICS OF AIR-TO-SURFACE MISSILES

/103

[Conclusion]

Missile type		OAM-78A	OAM-77A	MK-1	OAM-83B	AS-30	AGM-45A	A-4E	AGM-69A
	Wing area, S , in m^2	—	—	—	—	—	—	—	—
Weight data	Launch weight, G_l , kg	—	4500	6800	260	665	230	450	—
	Payload weight, G_{pay} , in kg	—	—	—	—	—	—	—	—
	Warhead weight, G_{wh} , in kg	Nuclear	Nuclear	Nuclear	118	230	18	340	Nuclear
Engine	1st stage	Engine type	SFJ	Turbo-jet	LFJ	SFJ	SFJ	Not avail.	—
		Engine oper. period, t_{enI} , sec	—	—	—	2	1.8	—	—
		Engine thrust, P_{enI} , kg	17000	3400	7260	5400	3500	—	—
	2nd stage	Engine type	—	—	—	—	—	—	—
		Engine oper. period, t_{enII} , sec	—	—	—	20	—	—	—
		Engine thrust, P_{enII} , kg	9000	—	1800	—	—	—	—
		Altitude range of mother aircraft, $H_{m.a.}$, in km	—	16	20	—	—	21	—
Conditions of combat use	Range of aircraft launch vehicle Mach number, $M_{l.a.}$	—	0.6—1.5	—	—	0.6—2.2	—	—	—
Main performance indicators	Thrust-to-weight ratio of 1st stage $K_{t-wI} = P_{enI}/G_{aI}$	3.85	—	1.07	—	—	—	—	—
	Thrust-to-weight ratio of 2nd stage $K_{t-wII} = P_{enII}/G_{aII}$	—	—	—	—	—	—	—	—
	Available g-load	$H=15$ km	—	—	—	—	—	—	—
		$H=0.5$ km	—	—	—	—	—	—	—
	Maximum range, L_m , in km	—	800	320	9.5	12	20	10	160—180
	Maximum velocity, M	9.0	1.6—2.0	1.6	2.4	2.0	3.0	—	—
	$K_{c.c} = (G_{wh} L_{x_{max}})/G_l$	—	—	40	9.4	4.6	1.6	9.0	—

/104

The third group of the missiles for strategic bombers differs by its high weight (to 10 tons) and considerable range (up to several thousands of kilometers). As a rule, guidance systems in these rockets are purely inertial or inertial with different types of correction: radiocorrection, astrocorrection, etc. The structural arrangements of missiles in this group are quite varied: ballistic missile (Skybolt), winged missile of the aircraft type (Hound Dog, Blue Steel); and cross-wing missiles.

Some technical and tactical-flight characteristics of air-to-surface missiles are given in Table 2.13 [9, 11, 15, 54, 60, 78, 89, 96, 128, 137, 155, 171, 174]. Some of these characteristics were determined by formulas (2.17) - (2.19). In the determination of V_{\max} , the system of equations (2.21) was written separately for the first and second missile stages; moreover, in the right side of the differential equation there appears the term $g \sin \theta_1$, where θ_1 is the angle of inclination of the velocity vector in the flight of the 1-th stage.

Solving the two systems of equations, we get

$$\begin{aligned}
 V_{\max} = & V_{\text{II}} - V_{\text{II}} \ln \left(\frac{m_1 - m_{\text{fuI}}}{m_1} \right) + g t_{\text{enI}} \sin \bar{\theta}_1 - \\
 & - \int_0^{t_{\text{enI}}} \frac{(C_x + AC_y)_{\text{I}} S \rho V_{\text{st}} dt}{2 \left(m_1 - \frac{m_{\text{fuI}}}{t_{\text{enI}}} t \right)} - \\
 & - V_{\text{II}} \cos \bar{\alpha}_{\text{II}} \ln \left(\frac{m' - m_{\text{fuII}}}{m'} \right) + g t_{\text{enII}} \sin \bar{\theta}_{\text{II}} - \\
 & - \int_{t_{\text{enI}}}^{t_{\text{enII}}} \frac{(C_x + AC_y)_{\text{II}} S \rho V^2 dt}{2 \left(m' - \frac{m_{\text{fuII}}}{t_{\text{enII}}} t \right)}.
 \end{aligned} \tag{2.22}$$

Here indexes I and II relate, respectively, to the first and second stages: /106

t_{enI} and t_{enII} are the operating periods of the launch and sustainer engines;

m_1 and m_r are the missile velocities in the launch and the route legs; and

V_1 and V_r are the missile velocities in the launch and the route legs; the overlined functions represent mean quantities.

The values $\theta_I = \theta_I(t)$, $\theta_{II} = \theta_{II}(t)$ and $a_{II} = a_{II}(t)$ can be determined from the kinematics of air-to-surface missile guidance to the target (cf Chapter Four). The maximum level range is determined by the formula

$$L_{x \max} = \int_0^{t_{enI}} V_{cr} \cos \theta_{cr} dt + \int_{t_{enI}}^{t_{enII}} V_m \cos \theta_m dt + \int_{t_{enII}}^{t_{pa}} V_{pa} \cos \theta_{pa} dt, \quad (2.23)$$

where V_f and t_f are the missile velocity and flight time in the free phase. Knowing the level range, we can determine the generalized indicator of missile performance (or the coefficient of its "combat capabilities")

$$K_{wh} = \frac{G_{wh} L_{x \max}}{G_l}, \quad (2.24)$$

where G_{wh} is the weight of the missile warhead in kg [force]; and G_l is the launch weight of the missile in kg [force].

The higher the K_{wh} value, the greater the mass of the warhead² which will be delivered at a greater distance from the missile launch site.

As we can see, for rockets designed to strike small ground targets, lateral g-loads n_{y-ava} at lower altitudes have the largest values, which is due to the appreciable errors in the determination of the coordinates of the target which the missile must select for a short range.

The least lateral g-load is exhibited by the Walleye missile, /107 which is actually a guided glide bomb.

2.7. Tactical-Flight Characteristics of Surface-to-Air Missiles

Surface-to-air missiles gain wide use in antiaircraft defense systems, along with fighter-interceptors and small caliber multiple-barrel cannons.

Antiaircraft guided missiles, depending on the location of the launch site are divided into two types: ground-to-air and water-to-air. The former are used for the defense of ground

objects or a country's territory against air (AAD [antiaircraft defense]) and missile (AMD [antimissile defense]) attack [4, 17, 66, 69, 88, 96, 116, 214]. The latter are used in defending against air or missile attack on naval vessels.

The Bomarc missiles (strategic AAD forces) are used in striking air targets at considerable distances from the location of the launch site in the U.S. Armed Forces. Interception of targets at short distances, but still flying at medium and high altitudes can be achieved by the Nike-Hercules missiles. Interception of low-flying targets is achieved by Hawk missiles. Both types of missiles are classed as tactical AAD weapons.

Defense of infantry groupings against air attack is provided by the Chaparral and Red Eye missiles.

Nike-Zeus³ missiles serve to defend objects and territory against ballistic missiles and spacecraft.

The main technical and tactical-flight characteristics of surface-to-air missiles are given in Table 2.14 [78, 88, 96, 128, 137, 155, 172, 174].

Maximum vertical velocities at the end of the powered phase are determined for two-stage missiles with the following formula: /112

$$\begin{aligned}
 V_{\max} = & -V_{JI} \ln \left(\frac{m_I - m_{fuI}}{m_I} \right) - g t_{enI} - \\
 & - \int_{t_{enI}}^{t_{enII}} \frac{(C_x + AC_y^2)_{IS} \rho V_{st}^2}{2 \left(m_I - \frac{m_{fuI} t}{t_{enI}} \right)} dt - \\
 & - V_{JII} \ln \left(\frac{m_{II}' - m_{fuII}}{m_{II}'} \right) - g t_{enII} - \\
 & - \int_{t_{enI}}^{t_{enII}} \frac{(C_x + AC_y^2)_{II} \rho V_{st}^2}{2 \left(m_{II}' - \frac{m_{fuII} t}{t_{enII}} \right)} dt + V_0.
 \end{aligned} \tag{2.25}$$

where V_0 is the velocity at which the missile leaves the launch pad. For three-stage missiles, three more terms must be added to formula (2.25). The maximum altitude of a one-stage missile is determined by the following formula (similar expressions can be written for two and three-stage missiles):

TABLE 2.14 MAIN TECHNICAL AND TACTICAL-FLIGHT CHARACTERISTICS OF SURFACE-TO-AIR MISSILES

/108

	Missile type	1M-99A	M1M-14A	M1M-23A		M1M-43A	R1M-2E	R1M-24A	DM-15C	
General data	Name of missile	Bomarc	Nike-Hercules	Hawk	Chaparral	Red Eye	Terrier	Tartar	Nike-Zeus	
	Country	U.S.	U.S.	U.S.	U.S.	U.S.	U.S.	U.S.	U.S.	
	Initial production	1955	1958	1958	1967	1966	1956	1958	Exper.	
	Missile function	Plane interception from ground	Plane interception from ground	Plane interception from ground	Plane interception from ground	Plane interception from ground	Plane & submarine interception	Plane & submarine interception	Missile interception from ground	
	Guidance system	Radio command	Radio command	Semi-active radar homing	Infrared homing	Infrared homing	Beam-riding	Semi-active radar homing	Radio command	
Geometrical data	Diameter D , m	0.89	0.79	0.36	0.13	0.076	0.305	0.305	1.17	
	Length, d , m	14.3	12.5	5.1	2.9	1.24	8.2	4.7	14.7	
	Wingspan, l , m	5.54	2.3	1.25	0.76	None	1.17	0.51	2.5	
	Area of both wings, S , in m ²	11.6	4.4	1.3	—	Wingless	—	—	—	
Weight data	Launch weight, G_l , in kg	6800	4600	580	84	8.5	1360	700	10300	
	Weight & type of warhead, G_{wh} , kg	Nuclear	500	50	4.5	0.6	60	60	Nuclear	
Engine	Engine type		Liquid fuel jet	Solid fuel jet	Solid fuel jet	Solid fuel jet	Solid jet w/4 thrust levels	Solid fuel jet	Solid-fuel jet w/2 thrust levels	Solid-fuel jet
	First stage	Engine oper. time, t_{enI} , sec	45	3.3	5	—	0.06	4—5	4—5	5
		Engine thrust P_{enI} , kg	16000	80000	6800	—	320	5600	5600	204000

/109

TABLE 2.14 MAIN TECHNICAL AND TACTICAL-FLIGHT CHARACTER-
ISTICS OF SURFACE-TO-AIR MISSILES
[Conclusion]

/110

Missile type		1M-99A	M1M-14A	M1M-23A		M1M-43A	R1M-2E	R1M-24A	DM-13C
Engine	Second stage	Engine type	Ramjet	Solid-fuel jet	Solid-fuel jet	—	Solid-fuel jet	Solid-fuel jet	Solid-fuel jet
		Engine oper. time, t_{enI} , sec	108		27	—	60	33	33
		Engine thrust P_{enI} , kg	2×4500	6000	850	—	110	850	850
Conditions of combat use	Range of altitude of intercepted targets, H_t , km	6—20	0.5—30	0.2—15	0.1—1.5	0.05—1.5	0.6—18	0.3—12	to 120
	Max. velocity of intercepted targets, V_t , km/hr	—	3000	1600	1100	650	2200	2200	—
Main missile performance indicators	Thrust-to-weight ratio of first stage, $K_{t-wI} = P_{enI}/G_{aI}$	15.0	17.5	11.7	19	37.5	4.1	8.0	—
	Thrust-to-weight ratio of second stage, $K_{t-wII} = P_{enII}/G_{aII}$		25.0	1.17	—	20	1.7	1.55	—
	1st stage power-to-weight ratio, $K_{p-wI} = (P_{fuI}/G_{aI})_{I_{fuI}}$	—	70	57.5	46	86.5	24	47	—
	2nd stage power-to-weight ratio, $K_{p-wII} = (P_{fuII}/G_{aII})_{I_{fuII}}$	—	—	98	—	—	—	78	—
	Available longitudinal $n_{x_{ava}}$	—	—	—	25	—	16	22	—
	lateral $n_{y_{ava}}$	—	$\frac{7.5}{H=15 \text{ km}}$	$\frac{12}{H=8 \text{ km}}$	10	—	$\frac{5.5}{H=10 \text{ km}}$	$\frac{10}{H=10 \text{ km}}$	—
Maximum range, L_{max} , in km		370	185	35	8.0	4.5	24	17	370
Maximum velocity, V_{max} , in m/sec		740	1150	780	450	600	700	880	1480

/111

$$\begin{aligned}
H_{\max} = & \frac{V_j^2}{2g} \left(\ln \frac{m_1 - m_{fu}}{m_1} \right)^2 + V_{jen} \times \\
& \times \left[1 + \frac{m_1}{m_{fu}} \ln \left(\frac{m_1 - m_{fu}}{m_1} \right) \right] + \frac{V_0^2}{2g} - \\
& - \frac{V_0 V_j}{g} \ln \left(\frac{m_1 - m_{fu}}{m_1} \right) - \frac{(C_{x_0} + AC_y^2) S}{2m_1} \times \\
& \times \left\{ \int_0^{t_{en}} \int_0^{t_{en}} \frac{\rho V^2}{1 - \frac{m_{fu}}{m_1 t}} dt dt - \frac{V_0 - V_j}{g} \ln \left(\frac{m_1 - m_{fu}}{m_1} \right) \times \right. \\
& \times \int_0^{t_{en}} \frac{\rho V^2}{1 - \frac{m_{fu}}{m_1 t}} dt - t_{en} \int_0^{t_{en}} \frac{\rho V^2}{1 - \frac{m_{fu}}{m_1 t}} dt - \\
& \left. - \frac{(C_{x_0} - AC_y^2) S}{2m_1} \left(\int_0^{t_{en}} \frac{\rho V^2}{1 - \frac{m_{fu}}{m_1 t}} dt \right)^2 \right\} \quad (2.26)
\end{aligned}$$

In formula (2.26), the first term is the determining term, and its highest value will occur as $m_{fu} \rightarrow m_1$. The second term is always negative, therefore engine operating time t_{en} must be reduced to attain highest missile velocity. Terms including the factor V_0 affect H_{\max} only at high missile launch velocities, while the terms in braces affect H_{\max} at low altitudes where the air density is very high.

As we can see from Fig. 2.14, the velocities and altitudes of missiles of subsequent generations will increase appreciably. As to be expected, a gain in target velocities and altitudes led to an abrupt increase in the thrust-and-power-to-weight ratios of antiaircraft missiles. A still steeper increase in the coefficients K_{t-w} and K_{p-w} is observed for AMD missiles. Owing to the increase in V_{\max} and H_{\max} , antiaircraft defense missiles can by their tactical-flight data ensure the interception of long-range ballistic missile warheads.

2.8. Tactical-Flight Characteristics of Ballistic Missiles and Missile Launch Vehicles

By their mission, ballistic missiles are divided into three groups: short-range missiles and tactical and strategic (long-range ballistic missiles) [39, 78, 107, 111]. Under this classification, they differ appreciably in their technical and tactical-flight characteristics. If the maximum range is taken as the main parameter by which we will differentiate ballistic missiles into groups, Honest John with a maximum range of 20 km and Little John with a range of 10 km can be classified as short-range missiles. The Pershing (maximum range of 560 km) and the Sergeant (range of 160 km) missiles are classified as tactical missiles. The Atlas E (14,500 km), Titan II (16,000 km), and the Minuteman (10,000 km) are classed as strategic missiles (cf Tables 2.15 and 2.16 [15, 124, 125, 137, 155, 157, 160, 171, 185]. Ballistic missile performance is characterized by the coefficients of thrust-and-power-to-weight ratios, maximum g-loads of stages, maximum range and velocity, launch weight G_0 , and weight factor of the warhead $K' = G_{wh}/G_0$ (Fig. 2.22). We can see, the average K' value is 0.3 for unguided tactical missiles, and 0.18 for guided missiles. With improvements in the control equipment of ballistic missiles, the warhead factor can climb to 0.25. Performance indicators of missile launch vehicles are given in Figs. 2.22 and 2.23. By 1967, the weight yield factors of second and third stages of missiles will become equal to the weight return factor of the first stage (0.9-0.92), indicating marked progress in control systems of missile launch vehicles and their structures. An increase in the launch weight of missile launch vehicles and improvements in their structures led to a rise in the payload carried by missiles into earth orbits (Fig. 2.24). In 1968 the Saturn missile launch vehicle lifted a 103-ton spacecraft into an earth orbit.

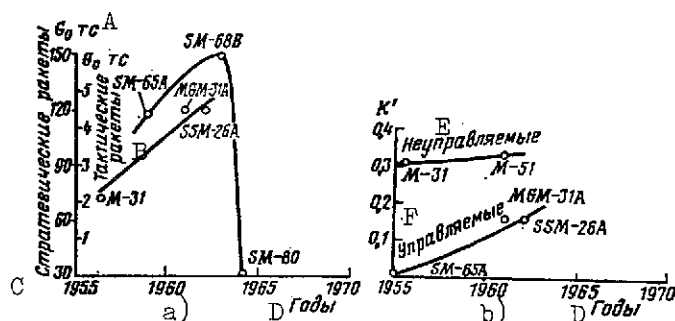


Fig. 2.22. Performance indicators of strategic and tactical ballistic missiles:

- a -- Launch weights
- b -- Warhead weight factors K'

KEY: A -- Tons
B -- Tactical missiles
C -- Strategic missiles
D -- Years
E -- Uncontrolled
F -- Controlled

TABLE 2.15 MAIN TACTICAL AND FLIGHT-TACTICAL CHARACTERISTICS OF BALLISTIC MISSILES

/114

	Missile type	SM-65A	SM-68B	SM-80	A-2	MOM-31A	SSM-A-26	M-31	M-51
General data	Name of missile	Atlas E	Titan II	Minuteman	Polaris	Pershing	Sergeant	Honest John	Little John
	Country	U.S.	U.S.	U.S.	U.S.	U.S.	U.S.	U.S.	U.S.
	Initial production	1959	1963	1964	1962	1961	1962	1956	1961
	Missile type	Strategic	Strategic	Strategic	Naval	Tactical	Tactical	Short-range	Long-range
	Guidance system	Inertial	Inertial	Inertial	Inertial	Inertial	Inertial	None	None
Geometrical data	Diameter, D, m	3.04	3.04	1.88	1.37	1.0	0.79	0.76	0.3
	Length, d, m	25.0	31.0	16.4	9.6	10.5	11.0	8.3	4.4
Weight data	Launch weight, G_1 , in kg	118000	150000	31000	14500	4540	4500	2200	365
	Control system weight, G_{c-s} , in kg	160	140	124	100	45	57	—	—
	Weight & type of warhead, G_{wh} , in kg	Nuclear 1360	Nuclear	Nuclear	Nuclear 460	Nuclear 725	Nuclear 750	Nuclear or expl. 680	Expl. 115
Engines	1st stage	Engine type	Liquid-fuel jet	Liquid-fuel jet	Solid-fuel jet	Solid-fuel jet	Solid-fuel jet	Solid-fuel jet	Solid-fuel jet
		Engine oper. period, sec.	120	150	60	54	33	30	—
		Engine thrust in kg	2×74600	2×97500	77000	36000	20400	22000	—
	2nd stage	Engine type	Liquid-fuel jet	Liquid-fuel jet	Solid-fuel jet	Solid-fuel jet	Solid-fuel jet	—	—
		Engine oper. period, in sec	300	180	60	770	20	—	—
		Engine thrust in kg	27200	45400	29600	9000	—	—	—

/115

TABLE 2.15 MAIN TACTICAL AND FLIGHT-TACTICAL CHARACTERISTICS OF BALLISTIC MISSILES

/116

Conclusion

Engines	Missile type		SM-65A	SM-68B	SM-80	A-2	MGM-31A	SSM-A-26	M-31	M-51
	3rd stage	Engine type	—	—	Solid-fuel jet	—	—	—	—	—
		Engine oper. time, in sec	—	—	60	—	—	—	—	—
		Engine thrust in kg	—	—	16000	—	—	—	—	—
Main missile performance indicators	1st stage thrust-to-weight ratio, $K_{p-wI} = \frac{P_{enI}}{G_{stI}}$		1.27	1.43	2.5	2.6	—	4.9	—	—
	1st stage power-to-weight ratio, $K_{p-wI} = \frac{(P_{enI}/G_{stI})_{I-1}}{I-1}$		245	—	238	—	—	—	—	—
	2nd stage thrust-to-weight ratio, $K_{t-wII} = \frac{P_{enII}}{G_{stII}}$		0.85	—	4.7	—	—	—	—	—
	2nd stage power-to-weight ratio, $K_{p-wII} = \frac{(P_{enII}/G_{stII})_{II-1}}{II-1}$		255	—	—	—	—	—	—	—
	3rd stage thrust-to-weight ratio, $K_{t-wIII} = \frac{P_{enIII}}{G_{stIII}}$		—	—	8.4	—	—	—	—	—
	3rd stage power-to-weight ratio, $K_{p-wIII} = \frac{(P_{enIII}/G_{stIII})_{III-1}}{III-1}$		—	—	94	—	—	—	—	—
	Maximum g-load, n	1st stage	7.5	—	8.5	—	—	—	—	—
		2nd stage	12.0	—	15.0	—	—	—	—	—
3rd stage		—	—	—	—	—	—	—	—	
Maximum range, in km			14500	16000	9300	2800	560	140	20	10
Maximum velocity, M			27	28	22	12	4.5	3.5	—	1.5

/117

TABLE 2.16 MAIN TECHNICAL AND TACTICAL-FLIGHT CHARACTERISTICS OF U.S. MISSILE LAUNCH VEHICLES

/118

Type of missile launch vehicle		Vanguard	Thor Able	Thor Agena D	Atlas SLV-3x Centaur	Saturn IB	Saturn V
General characteristics	Initial production	1957	1958	1962	1963	1966	1967
	Number of stage	3	3	2	2	2	3
	Control system	Inertial	Inertial	Radio-inertial	Inertial	Inertial	Inertial
Geometrical dimensions	Maximum diameter, D, in m	1,14	2,44	2,44	3,05	6,6	10,3
	Length, d, in m	21,9	27,2	27,1	36,2	68	107
Weight data	Launch weight, G_L , in tons	10,25	51,6	56,9	136	582	2820
	G_I , in tons	8,1	49,4	49,3	129	454	2126
	G_{II} , in tons	1,95	1,95	7,0	17,3	110	462
	G_{III} , in tons	0,23	10,31	0,5	2,79	15,7	117
	G_{IV} , in tons	0,25	0,16	—	—	—	101
	Payload weight in kg	25	160	500	2790	15700	101000
Engines	1st stage	Engine type	Liquid-fuel jet	Liquid-fuel jet	Liquid-fuel jet launch	Liquid-fuel jet	Liquid-fuel jet
		Fuel weight, G_{fuel} , in tons	6,8	46,2	46,2	121	415
		Operating period, sec	145	163	165	120	135
		Engine thrust in tons	12,25	68,0	76,5	140	820
	2nd stage	Engine type	Liquid-fuel jet	Solid-fuel jet	Liquid-fuel jet	Liquid-fuel jet	Liquid-fuel jet
		Fuel weight, G_{fuel} , tons	1,63	1,63	6,15	14,6	101
	3rd stage	Engine type	Liquid-fuel jet	Solid-fuel jet	Liquid-fuel jet	Liquid-fuel jet	Liquid-fuel jet
		Fuel weight, G_{fuel} , tons	1,63	1,63	6,15	14,6	101

/119

TABLE 2.16 MAIN TECHNICAL AND TACTICAL-FLIGHT CHARACTERISTICS OF U.S. MISSILE LAUNCH VEHICLES
/Conclusion/

/120

Missile launch-vehicle			Van-guard	Thor Able	Thor Agena D	Atlas SLV-3x Centaur	Saturn IB	Saturn V
Engines	2nd stage	Engine oper. period, sec	115	6.5	240	420	470	390
		Engine thrust in tons	3.45	8.0	7.25	13.6	90.8	454
	3rd stage	Engine type	Solid-fuel jet	Solid-fuel jet	—	—	—	Liquid-fuel jet
		Fuel weight G_{fuIII} , tons	0.13	0.15	—	—	—	104.3
		Engine oper. time, sec	35	40	—	—	—	480
		Engine thrust in tons	1.2	1.2	—	—	—	90.8
Main missile performance indicators	1st stage	$K_{t-wI} = \frac{P_{enI}}{G_{stI}}$	1.2	1.31	1.35	1.03	1.41	1.37
		$K_{GI} = \frac{G_{fuI}}{G_I}$	0.84	0.94	0.94	0.95	0.915	0.935
		$K_{p-wI} = \frac{(G_{fuI}/G_I)^{I_{I-1}}}{(G_I)^{I_{I-1}}}$	208	235	236	248	248	252
	2nd stage	$K_{t-wII} = \frac{P_{enII}}{G_{II}}$	1.77	4.10	1.03	0.79	0.825	0.983
		$K_{GII} = \frac{G_{fuII}}{G_{II}}$	0.84	0.84	0.87	0.845	0.92	0.913
		$K_{p-wII} = \frac{(G_{fuII})^{I_{II-1}}}{(G_{II})^{I_{II-1}}}$	227	227	252	354	388	386
	3rd stage	$K_{p-wIII} = \frac{P_{enIII}}{G_{III}}$	5.2	3.9	—	—	—	0.79
		$K_{GIII} = \frac{G_{fuIII}}{G_{III}}$	0.6	0.48	—	—	—	0.894
		$K_{p-wIII} = \frac{(G_{fuIII})^{I_{III-1}}}{(G_{III})^{I_{III-1}}}$	146	116	—	—	—	375

/121

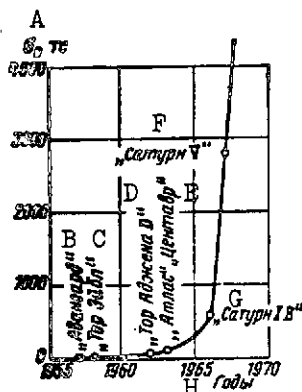


Fig. 2.23. Launch weights of missile launch vehicles

KEY: A -- Tons
B -- Vanguard
C -- Thor Able
D -- Thor Agena D
E -- Atlas Centaur
F -- Saturn V
G -- Saturn IB
H -- Years

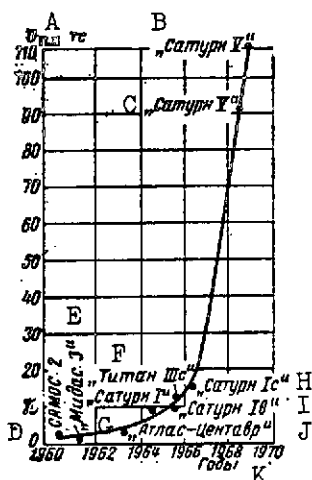


Fig. 2.24. Change of payload weight carried by missile launch vehicle to earth orbit as a function of year of missile production

KEY: A -- G pay, tons
B -- Saturn V
C -- Saturn V
D -- SAMOS 2
E -- Midas 3
F -- Titan 3C
G -- Saturn I
H -- Saturn IC
I -- Saturn IB
J -- Atlas Centaur
K -- Years

FOOTNOTES

¹Foreign specialists have also another viewpoint about the development of fighter aircraft [145] that denies the dominant factor of high speed. In their opinion, one can scarcely anticipate a rise in AAD [antiaircraft defense] fighter speed above $M = 3.0$.

²The weight of the missile warhead depends on the accuracy of its guidance and the type of targets struck.

³Work on developing the Nike-Zeus missile with a radar complex for interception was halted due to its low effectiveness of action with respect to the nose cones of ballistic missiles. This fact does not mean that there is little promise of developing AMD [anti-missile defense] weaponry. In the immediate future 40 billion dollars will be spent on this problem in the United States [137, 171].

CHAPTER THREE DEVICES OF FLIGHT CRAFT CONTROL SYSTEMS

The most important technical requirements imposed on flight craft control systems and which determine their arrangement and characteristics are operating reliability and the weight and overall dimensions of the systems. In particular, the determining requirements for piloted (multiple use) aircraft complexes are as follows: very high operating reliability and long service of control system equipment (up to several thousand hours), where the replacement of components and assemblies is allowed under scheduled maintenance plans during operation of the systems. Monitoring devices of the aircraft complex must check a large number of system parameters both before the aircraft takes off, as well as during its operation. The requirements on weight and overall dimensions of equipment are moderate.

Determining conditions for onboard equipment of antiaircraft missile and ballistic missile complexes are as follows: operating reliability, and low weight and overall dimensions. Naturally, replacement of individual installations during use is most undesirable. The readiness of a control system must be checked only as to the main parameters in the shortest possible time. The total equipment operating time can be regulated in the hundreds of hours.

Onboard computers, continuously monitoring the maximum number of parameters, are used to keep track of the operation of systems.

One of the typical features of the development of modern aircraft and missile complexes is the considerable expansion in the makeup of electronic equipment. Fig. 3.1 shows the variation in the number of electronic elements of the equipment of American bombers (curve 1) and ballistic missiles (curve 2). While in 1943 the American B-29 bomber had 2000 electronic parts, the B-70A bomber, built 25 years later, now has about 200,000 parts. The first American ballistic missile had about 1000 parts, but ten years later their number rose by 500 times. /125

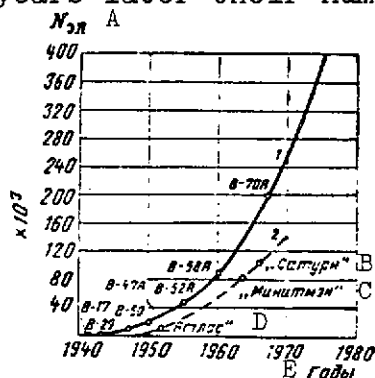


Fig. 3.1. Variation in the number of elements in electronic equipment of American bombers (1) and ballistic missiles (2)

KEY: A -- N_{el}
B -- Saturn
C -- Minuteman
D -- Atlas
E -- Years

The weight of the electronic equipment rose significantly, as a consequence. We will assume that the weight of just the electronic equipment onboard aircraft of early manufacture (1940) was 30 kg, while the weight of electronic equipment of a 1964 aircraft, at the level of technology in 1940, will be 2.5 tons, and 12.5 tons for a 1970 airplane. It does not appear possible to locate this amount of equipment on an airplane. Therefore, recently much attention in aircraft and missile technology has been given to developing new microminiaturized elements (cf 152).

Microminiaturization of control system elements and the use of microelectronic circuitry afforded a marked reduction in the weight and size of devices and an increase in their operating reliability. Microminiaturized elements used in control system are manufactured either as hybrid (thin-film) circuits, or as integrated monolithic (solid) circuits 7, 139. Thin films permit the relatively simple building of passive elements (resistors and capacitors), but active elements (diodes and triodes) are quite complicated to build. Therefore active elements in microelectronic circuits with thin films are incorporated in the form of individual mounted parts, which lowers the operating reliability of such circuit. From this point of view, building microelectronic circuits with solid elements is more preferable, though their dimensions and weight proved to be somewhat higher than for thin-film elements (cf 74).

126

In U.S. aircraft and missile complexes, microelectronic devices of radars, onboard and ground digital computers, navigation equipment, and so on have gained wide application.

For example, the AN/ARN-78 radio receiver of the Loran-C navigation system, built in 1964, consists of 1000 integrated silicon circuits and provides a mean error-free running time of $4 \cdot 10^5$ hours. The Autonetics Company developed a digital computer for the Minuteman ballistic missile using 4000 integrated silicon circuits. The onboard aircraft system Phoenix, installed on the F-111B, consists of 5000 integrated silicon circuits. Complex microelectronic circuits providing 8500 hours of system operation per failure were used in the control system of the Saturn V missile 70, 74, 139).

Let us consider the general trend of development of electronic equipment for control systems of several complexes (based on foreign data 151, 152). Let us use as the equipment's performance indicators its volume V_{eq} in m^3 , element density per decimeter³ -- γ_{eq} , weight -- G_{eq} in kg, and mean time between failures -- T_{av} in hours. Fig. 3.2 presents these indicators for aircraft, missile, and space complexes of the United States as a function of the year in which the equipment was first built 151, 152, 156.

From Fig. 3.2 a it is clear that the greatest progress in reducing the size of electronic elements was made in the digital computer, where solid and thin-film integrated circuits are used. Improvements in the technology of manufacturing integrated solid and thin-film elements with low power consumption for ground and onboard digital computers led to a reduction in their volume during the period from 1958 to 1968 by about 40 times. During the same span the volume of electronic elements in systems of armament and radars (with powerful amplifiers) was reduced only by a factor of 7-8, and the volume of power supply blocks -- by a factor of 5. The reduction of element volume led to a reduction in element weight (Fig. 3.2 b). The density of elements rose (Fig. 3.2 c). In a period of 10 years γ_{eq} increased by 10^4 and by 1968 attained an astounding figure of 10^7 elements/decimeter³ for onboard digital computer elements, and $(3-8) \cdot 10^4$ elements/decimeter³ for radio circuit elements. If it is assumed that advances in electronic circuits will continue at the same rates, by 1975 the density of microcircuits of digital computers will reach the density of nerve cells (i.e., $4 \cdot 10^{10}$ elements/decimeter³). The change in the density of radio circuit elements will occur, evidently, also quite strongly.

/127

/128

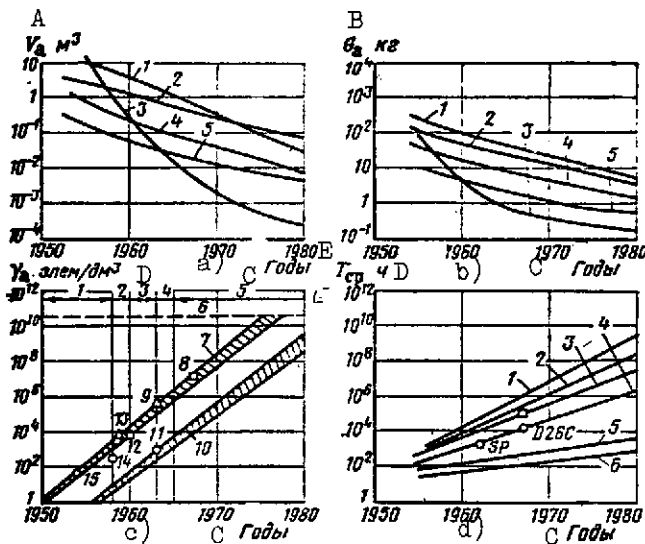


Fig. 3.2. Main performance indicators of radio-electronic equipment of control systems of aircraft, missiles, and spacecraft:

a, b -- Change in equipment volume and weight:

- 1 -- Aircraft armament systems
- 2 -- Radars
- 3 -- Digital computer
- 4 -- Navigation equipment
- 5 -- Power supply blocks
- c -- Change in density of elements per decimeter³:
- 1 -- Limit of vacuum tube use

- 2 -- Limit of printed-assembly element use
- 3 -- Limit of microminiature element use
- 4 -- Limit of integrated element use
- 5 -- Limit of thin-film element use
- 6 -- Density of nerve cells
- 7 -- Density of elements of onboard computer and radio command links
- 8 -- Density of elements of the Apollo onboard digital computer

- 9 -- Density of elements of the Minuteman digital computer
- 10 -- Density of radar circuit elements
- 11 -- Density of Minuteman radio command link
- 12 -- Onboard digital computer density
- 13 -- Density of elements of the Gemini command transmission system
- 14 -- Density of Shrike computer elements
- 15 -- Onboard computer density
- d -- Mean time between two failures:
 - 1 -- For onboard computer subsystems containing 1000 elements
 - 2 -- For radio circuits of Minuteman missile with 1000 elements
 - 3 -- For onboard computer of Minuteman with 10,000 elements
 - 4 -- For radio circuits of Minuteman missile (10,000 elements)
 - 5 -- For aircraft radars
 - 6 -- For radio circuits of civil aircraft

KEY: A -- V_{eq}
 B -- G_{eq}
 C -- Years
 D -- γ_{eq} , elements/decimeter³
 E -- T_{av}

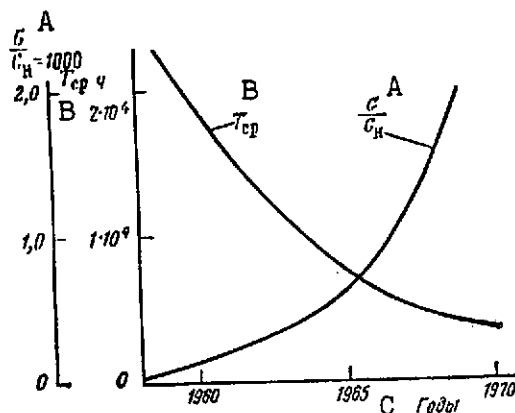


Fig. 3.3. Weight of gyroscopic instruments and their operating reliability as functions of year in which the first series was manufactured

KEY: A -- G/G_{rel} [rel = reliability]
 B -- T_{av} [av = average], hours
 C -- Years

Use of integrated circuits markedly increases the operating reliability of digital computers and the electronic devices of control systems (Fig. 3.2 d). In the 10 years from 1958 to 1968, the mean operating time between two failures for an onboard computer with 10,000 elements rose by 50 times and was 10^7 hours. $T_{av} = 10^4$ hours for electronic circuits of radio command links of spacecraft, and $T_{av} = 600$ hours for radars. Electronic circuits of passenger aircraft have even lower indicators. In these craft $T_{av} = 120$ hours¹. The trend of decreasing weight and increasing reliability also applies to other elements of control systems: electromechanical and mechanical. For example, gyroscopic devices of missiles during this period have reduced their weight per 1000 units of kinetic momentum by a factor of 6 (Fig. 3.3). Here the operating reliability of gyroscopic devices was increased by a factor of 20 (Fig. 3.3). /122

3.1. Ground and Onboard Radars of Aircraft Complexes

Radar devices of aircraft complexes are subdivided into ground and onboard types. Ground radars (RD) serve in searching for, identifying, and transmitting the coordinates of air objects. Coordinates of objects are transmitted to the command station of the AAD /antiaircraft defense/ and to the interceptor. It is guided to the target by ground facilities, and its onboard radar, after target lockon, provides aircraft homing and missile release.

Ground radars must provide for the search, identification, and transmission of the coordinates of an object with high accuracy and with the presence of active and passive jamming. In addition, ground stations must be connected with each other, forming a radar field of antiaircraft defense. The necessity of performing these missions increases the makeup of ground RD equipment. Therefore, they consist of tens, and sometimes even hundreds, of thousands of electronic elements.

Onboard radars of aircraft fulfill the most various kinds of functions. They include search, identification, and tracking of air or ground objects, as well as the transmission of commands to air-to-air and air-to-surface missiles. In launching missiles with active radar homing heads, radars provide coverage of the targets.

Onboard radars measure the range to air and ground objects and produce a radar image of the location. When the onboard radar tracks a moving object against an earth background, the set provides for its selection and automatic indication. When passive jamming is encountered, onboard stations must preclude the reflection of signals from foil dipole reflectors and local objects by means of special data processing. Radars must also operate normally in the presence of active jamming and radar traps. All this means that onboard aircraft radars also are quite complicated radio facilities, consisting of several tens of thousands of electronic elements. It stands to reason that high operating reliability is required both for ground and onboard radars. /130

Ground radars

Ground radars of aircraft complexes include the following stages [29]: long-range detection and identification of objects and command guidance; low-altitude for filling in the gaps in "dead zones." All these radio facilities are united by means of a digital computer into the AAD unit [60].

The computer estimates the importance of targets and their distribution, performs the necessary data processing, and generates the command for guiding interceptors to the selected target. If the air situation changes, the computer redistributes the targets and corrects the interceptor guidance commands.

Ground radars are characterized by the following main parameters: maximum range of target detection R_{det} and capture R_{cap} ; angular scanning zones (with respect to target azimuth $\phi_{sc\ hor}$ and with respect to target elevation angle $\phi_{sc\ h}$ [the subscript hor and h stand for horizon and height, respectively]); tracking angles ($\phi_{tr\ hor}$ and $\phi_{tr\ h}$); carrying capacity; resolving powers with respect to range ΔR_{min} and angles of azimuth

$\Delta\phi_{\text{hor min}}$ and elevation $\Delta\phi_{\text{h min}}$; scan time T_{sc} ; periodicity of control command transmission T_{co} ; antijamming capability and operating reliability; and by the accuracy of determination of the coordinates of the target and of the aircraft itself.

The range of a radar in the modes of object detection or lock-on is determined by means of the fundamental radar equation:

$$R = \alpha \sqrt{\frac{P_{\text{rad}} G_{\text{a}}^2 S_{\text{eff}} \lambda^2 \eta}{(4\pi)^3 P_{\text{re min}}}}, \quad (3.1)$$

where P_{rad} is the radiation power in kw;

/131

G_{a} is the antenna directivity factor;

S_{eff} is the effective reflecting area of the target in m^2 ;

η is the parameter allowing for losses in radio channels, quality of signal reproduction on the indicator, and so on;

λ is the wavelength;

$P_{\text{re min}}$ is the receiver sensitivity; and

α is the normalized range, allowing for the stochastic nature of target detection or capture.

Calculation of the values of the variables appearing in equation (3.1) is carried out as follows.

When determining the coverage of pulse radars, we have

$$P_{\text{rad}} = P_{\text{pu max}},$$

where $P_{\text{pu max}}$ is the maximum pulse power.

In continuous-wave radars, a relationship relating the mean power with the pulse power must be used, i.e.,

$$P_{\text{av}} = P_{\text{pu max}} \tau_0 f_{\text{rp}} \quad (3.2)$$

where P_{av} is the mean power in kw;

τ_0 is pulse duration; and

f_{rp} is the pulse repetition frequency in pulses/sec.

The antenna directivity factor depends on antenna design and the wavelength:

$$G_{\text{an}} = \frac{4\pi S_{\text{eff}}}{\lambda^2}. \quad (3.3)$$

where S_{eff} is the effective antenna area.

The effective area of antennas which are planar radiating surfaces with apertures is determined by the relationship

$$S_{\text{eff}} = K_1 S_g \quad (3.4)$$

where S_g is the geometrical area of the antenna, and

K_1 is the antenna use factor (K_1 is usually taken as 0.6-0.7).

For antennas with a parabolic reflector, we have

$$G_{\text{an}} = (0.6 - 0.7) \frac{\pi^2 D^2}{\lambda^2}, \quad \text{/133} \quad (3.5)$$

where D is the antenna diameter.

The effective reflecting surface is some standard value, different quite widely from the true surface of the ground or air target. Commonly, values of the effective reflecting surface are determined experimentally (by modeling with mockups or full-scale testing). Experimental averaged values of effective reflecting surfaces of targets of different types are given in Table 3.1.

As we see from this table, the wavelength in this range does not appreciably affect the mean effective reflecting surface of the targets.

The sensitivity of a receiver is determined by the formula

$$P_{\text{re min}} = k_{\text{no}} k T \frac{P_{\text{si}}}{P_{\text{no}}} \Delta F, \quad (3.6)$$

where

- k_{no} is the receiver noise coefficient² (noise factor);
- $k = 1.37 \cdot 10^{-23} \text{ W} \cdot \text{sec}$ is Boltzmann's constant;
- T is the absolute temperature of the equivalent resistance at the receiver input (often T is taken as 290° in calculations);
- $\frac{P_{\text{si}}}{P_{\text{no}}}$ is the ratio of useful signal power to noise intensity; and
- ΔF is the frequency passband of the amplifier of the receiver intermediate frequency.

TABLE 3.1 EFFECTIVE MEAN REFLECTING SURFACES OF TARGETS
OF DIFFERENT TYPES*

/132

Types of targets	$S_{\text{eff}}, \text{m}^2$		
	$\lambda=1-6 \text{ cm}$	$\lambda=10-16 \text{ cm}$	$\lambda=16-40 \text{ cm}$
400-600 kg air-to-surface missiles	0.5-1.5	0.4-1.2	0.3-1.0
8-16 ton fighter-interceptors	5-15	4-12	3-10
40-60 ton tactical bombers	40-70	30-50	25-45
Strategic bombers weighing up to 200 tons	100-150	70-120	60-100
1000-3000 ton-water displacement surface vessels	2000-8000	1800-7000	1500-6000
10,000-20,000 ton-water displacement submarines	20000-40000	18000-30000	15000-25000
Submarines surfaced	30-150	20-110	18-100

* The data in column 2 are given on the basis of the materials in [38], and column 3 and 4 were obtained by recalculating column 2 with allowance for change in the wavelength most often used in foreign radars.

The range of a radar is also affected by the wavelength of the transmitter. At wavelength below 40 cm, attenuation of radio waves in the lower atmospheric layers due to rain and fog is increased. Fig. 3.4 a shows the dependence of radio wave attenuation in the atmosphere as a function of the effect of water vapor and oxygen molecules, and Fig. 3.4 b presents the function of the attenuation of transmitted radio waves in rain (curves 1 and 2) and fog (curves 3 and 4). The range of a radar in the modes of

/134

detection, lock-on, or tracking of an object when there is fluctuation in the signal, receiver noise, atmospheric effects, and so on is random in nature. Therefore in the calculated determination of radar range, integral functions of the distribution of the probability of detection, lock-on, or tracking must be used. To do this, let us introduce into formula (3.1) the coefficient of normalized range α , calculated by the probability of a false alarm (i.e., the probability of the appearance of a noise signal at a given level) $F = 10^{-P}$:

$$P(z, \alpha) = \frac{1}{\sqrt{2\pi}} \int_{\alpha}^{\infty} e^{-\frac{n^2}{2}} dn \quad (3.7)$$

where

$$y = z - 0,707 \left(\frac{1}{\alpha^2} + \alpha^2 \right);$$

$$n^2 = \frac{(u_{si} + u_{no})^2}{\sigma_{no}^2}; \quad z^2 = \frac{P_{remin}}{P_{re0}}.$$

Here u_{si} and u_{no} are the intensity of the signal and noise, respectively; σ_{no} is noise dispersion; and P_{remin} is the threshold power of the receiver's input signal (in detection, lock-on, or tracking). The functions $P(z, \alpha)$ or $P(F, \alpha)$ can be calculated by formula (3.7). Ten P values from 1 to 10 are normalized at this false alarm level $\sqrt[4]{47}^3$.

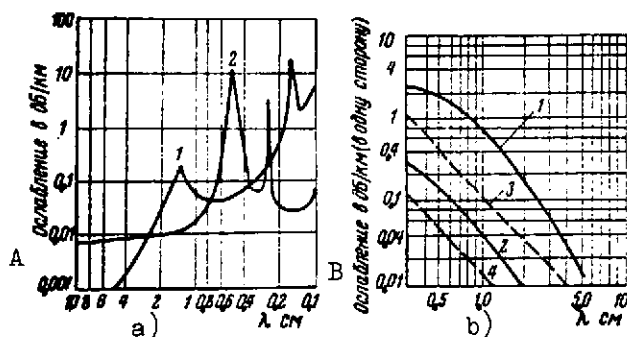


Fig. 3.4. Radio wave attenuation in the atmosphere:

- a -- As a function of the effect of water vapor (curve 1) and oxygen molecules (curve 2)
- b -- As a function of the effect of rain and fog:
 - 1 -- Moderate rain, 4 mm/hr
 - 2 -- Drizzle, 0.25 mm/hr
 - 3 -- Fog, 100-m visibility
 - 4 -- Fog, 600-m visibility

KEY: A -- Attenuation in db/km
B -- Attenuation in db/km (toward one side)

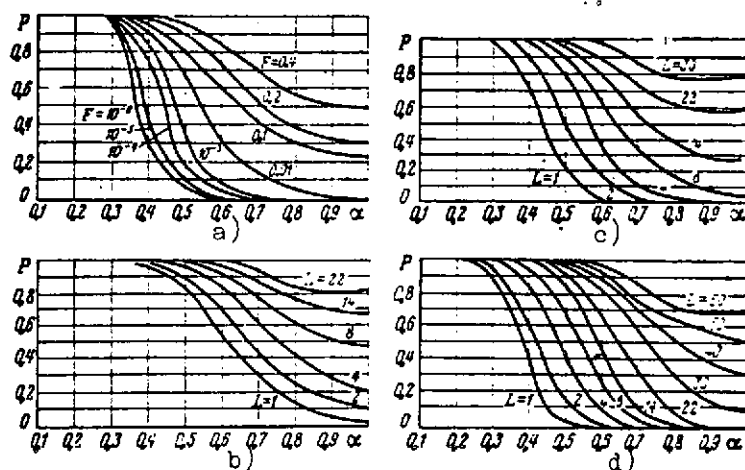


Fig. 3.5. Normalized-range dependence of the probability of actual target detection by radar
 a -- Based on single signal against a background of uncorrelated interference
 b - d -- Based on signal burst
 b -- At $F = 10^{-2}$
 c -- At $F = 10^{-4}$
 d -- At $F = 10^{-8}$

In Fig. 3.5 a, the probabilities of actual detection are plotted as functions of normalized range (for the detection of a single signal against the background of uncorrelated interference), and Fig. 3.5 b, c, d gives these functions for detection based on a signal burst (here L is the number of pulses in the burst) ^[47]. By using these graphs, we can construct the characteristics of the ^[136] variation in probabilities of detection 1 (Fig. 3.6) and lock-on 2 of a bomber with $S_{\text{eff}} = 100 \text{ m}^2$ by a ground radar as a function of range.

The following formula can be used to determine errors in the measurement of radar range:

$$\Delta R = \frac{cv}{4S_r K_{t-v}} \left(1 + \sqrt{1 + \frac{S_r^2 K_{t-v}^2}{V^2}} \right) \quad (3.8)$$

where $c = 3 \cdot 10^8 \text{ m/sec}$;

v is the diameter of the luminous spot on the screen;

S_r is the steepness of the edge of the pulse at the receiver output ($S_r = u_{s1}/t_{fr}$; here u_{s1} is the amplitude of the pulse at the receiver output);

$K_{t.v}$ is the tube sensitivity as to vertical deflection; and
 V_{sp} is the speed of the spots along the scanning trace.

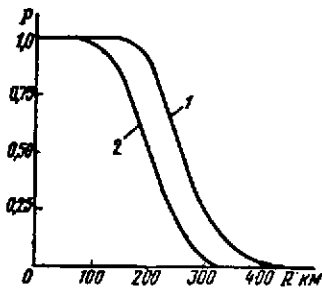


Fig. 3.6. Probabilities of detecting and locking onto a bomber with $S_{eff} = 100 \text{ m}^2$ by a ground radar

The range resolving power ΔR_{min} (or the minimum distance between two targets with identical angular coordinates at which separate measurement of range to each of them is provided) is

$$\Delta R_{min} = \frac{c}{2} \left(\tau + \frac{0.8 - 1.2}{\Delta F} \right) + \frac{D_{scr}}{A_{sc}} \Delta R, \quad (3.9)$$

where τ is the duration of the probing pulse;

D_{scr} is the diameter of the indicator screen;

/137

l_{sc} is the geometrical length of the scanning trace; and

A is the resolving power of the screen tube.

We have

$$\Delta R = \frac{t_{f.t} \cdot c}{2}, \quad (3.10)$$

for the scan trace, where $t_{f.t}$ is the duration of the forward trace of the beam.

The accuracy of angular coordinate determination and the resolving power as to angular coordinates can be found by the formulas: for a type-P display

$$\left. \begin{aligned} \Delta \beta_{max} &= \frac{\gamma_{ap}}{2} + 57.5 \frac{R_{max}}{\Lambda} \frac{1}{R}; \\ \Delta \beta_{min} &= \gamma_{ap} + 115 \frac{R_{max}}{\Lambda} \frac{1}{R}, \end{aligned} \right\} \quad (3.11)$$

where γ_{ap} is the aperture angle of the antenna radiation pattern, and
 R is the instantaneous range; and for a type-B display

$$\left. \begin{aligned} \Delta\varphi_{\max} &= \frac{\gamma_{ap}}{2} + \frac{D_{sc}}{2\lambda_{sc}} \tilde{\varphi}; \\ \Delta\varphi_{\min} &= \gamma_{ap} + \frac{D_{sc}}{\lambda_{sc}} \tilde{\varphi}. \end{aligned} \right\} \quad (3.12)$$

where ϕ is the sector of the spatial scan.

The spatial scan period T_{sc} or the scanning period is determined by the speed of the target V_t , the diameter of the luminous spot on the display ν , and its speed V_{sp} :

$$T_{sc} \leq \frac{\nu c}{2V_{in} V_t}. \quad (3.13)$$

If this condition is not met (i.e., if the scan period is large), discontinuous displacement of the object blip is observed downward the display, which is altogether unacceptable. When this happens the accuracy of the determination of object coordinates is reduced, and sometime the operator altogether loses its blip. The scanning rate can be found by the formula /138

$$\omega_{sc} = \frac{\tilde{\varphi}}{T_{sc}}. \quad (3.14)$$

The range of a radar with active response, for a pulse power of the reply signal P_{re} , can be determined by the formula

$$R = \alpha \sqrt{\frac{P_{rep} G_B^2 S_{EB}^2 \lambda^2}{(4\pi)^3 P_{re \min}}}, \quad (3.15)$$

where G_B is the directivity factor of the interrogator antenna in a heading toward the transponder; and S_{eb} is the effective antenna area of the interrogator aimed at the transponder.

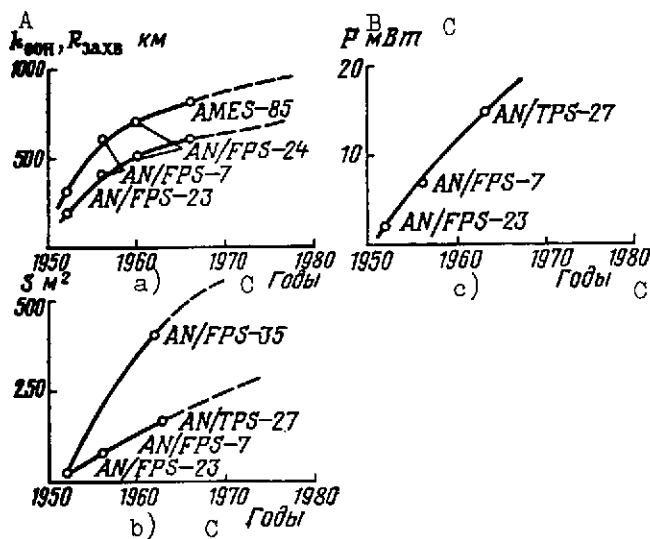


Fig. 3.7. Main characteristics of ground radar stations of airplane complexes:

a -- Target range, detection, and lock-on, reduced to a basis of $S_{eff} = 20 \text{ m}^2$

b -- Radar antenna area

c -- Pulse power

KEY: A -- K_{det}, R_{cap}

B -- milliwatts

C -- Years

As we can see from formula (3.15), the parameters of a radar operating in the mode of active reply are determined in the same way as for a radar with passive reply (formula 3.1), with the exception of the radical index.

The main characteristics of ground radars of aircraft complexes are given in Table 3.2 [151, 152, 170, 171]. These data were used to plot in Fig. 3.7 a the curve of R_{det} and the curve of R_{cap} as a function of the year the radar was first built, and in Fig. 3.7 b -- ground radar antenna area also as a function of the year of manufacture. As we can see from Fig. 3.7, the increase in the range of the ground stations is determined first of all by an increase in the antenna areas and in the pulse intensity, and secondly by greater receiver sensitivity.

Onboard radars

The development of onboard radars in foreign multimission airplanes proceeded in two different directions. The first consisted of the use of individual radars connected into a radio complex on aircraft intended for military actions against air or ground targets. The second involved the use of one combination-type radar for actions against air and ground targets and also for tracking of terrain relief.

The AN/APQ-15 and R-14 installed in the nose section of the F-105D can be classified as radars of the first type, and the RARF radar, with one antenna in the form of a three-dimensional array generating a flat wave by control from the onboard computer executed by phase shifters can be placed in the second type. This scheme permits the detection of ground and air targets and the coverage of targets for the simultaneous launch of air-to-

air and air-to-surface missiles. Tracking of terrain relief in the horizontal and vertical planes is provided with the aid of this same antenna.

The AN/APQ-113 and AN/APQ-110 radars of the F-111A aircraft occupy an intermediate ranking. The AN/APQ-113 radar has two antenna systems: one for search, tracking, and coverage of air targets, and the other for measuring the ranges to target and forming a radar image of the terrain. The AN/APQ-110 radar provides tracking of terrain relief in the vertical and horizontal planes to ensure safe flight across mountains.

Radars measuring range (radar rangefinders) use cannon-gun devices in the control systems as means for determining the range to the air target. /141

TABLE 3.2 MAIN CHARACTERISTICS OF GROUND RADARS OF U.S. AIRCRAFT COMPLEXES /140

Type and name of set	Year built	λ , cm	Radiation power, Mw	Pulse repetition, Hz	Pulse duration, microsec	Antenna size, m ²	Target height, km	Coverage	
								D_{det} km	D_{cap} km
AN/FPS-23	1952	10	2	300-500	1.5-3	4.5×4.5	24	300	200
AN/FPS-7	1956	23	5-10	250	6	12×6	40	600	400
AN/FPS-24	1960	135	5	333, 3 & 1000	6 & 18	36×15	70	700	500
AN/FPS-35	1962	70	5	333	24	36×11.4	70	650	450
AN/TRS-27	1963	23	15	150 to 3000	2-4	160	40	300	200
AN/FPS-88	1964	23	2×5	300-400	2	—	30	450	350
AMES-85	1966	5-7	4×5	270	5	19×7	30	800	600

The main characteristics of onboard radars are as follows: maximum range of target detection R_{det} and lock-on R_{cap} ; zones of scanning angles (with respect to azimuth $\phi_{sc\ hor}$ and with respect to elevation angle $\phi_{sc\ h}$), and tracking angles ($\phi_{tr\ hor}$ and $\phi_{tr\ h}$); resolving powers, with respect to range ΔR_{min} , angles of azimuth

$\Delta\phi_{hor \min}$ and elevation $\Delta\phi_{h \min}$; scan time T_{sc} ; antijamming capability; operating reliability; accuracy of determining the coordinates of target or air-to-air or air-to-surface missiles; operating range of signals with respect to bearing and angular velocity of sighting line (in the horizontal ϕ_{hor} and vertical ϕ_h planes); radar blinding range R_o ; and overall dimensions.

Technical characteristics of onboard radars are determined from the same formulas as applied in the case of ground radars, i.e., (3.1) - (3.15). Corresponding data for onboard radars based on foreign press materials [137, 138, 151, 152] are given in Table 3.3. Graphs in Fig. 3.8 a - d were constructed on the basis of the table. From the graphs it is clear that the weight of radars has decreased markedly in the past ten years, while the range and operating reliability of radars have risen appreciably. This is accounted for by the increase in the power of transmitters, higher receiver sensitivity, reduced weight and overall dimensions of the electronic elements of radars, and also the use of more reliable elements.

/144

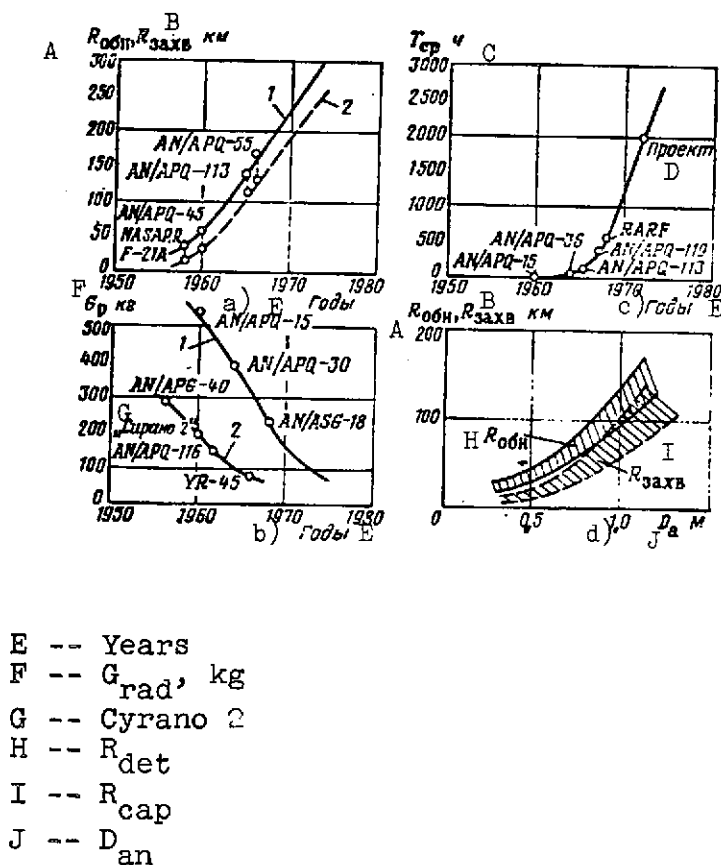


Fig. 3.8. Main characteristics of onboard radars of aircraft complexes:
a -- Detection (1) and lock-on (2) ranges
b -- Weight of radar sets:
1 -- Heavy
2 -- Light
c -- Mean error-free operating time
d -- Dependence of R_{det} and R_{cap} on antenna diameter

TABLE 3.3 MAIN CHARACTERISTICS OF ONBOARD RADARS
(ORAD) OF AIRCRAFT

/142

Name of onboard radar	Country	Year built	Aircraft of installation	λ , cm	Radiation power, kw	Pulse duration, microsec	Pulse repetition, Hz	Antenna size, m	Zone of action		Coverage		Weight, kg
									azimuth, degrees	elevation angle, deg	D_{det} , km	D_{cap} , km	
AN/APQ-40	U.S.	1956	F-86D F-94	3.2— 3.4	200	0.5 or 2.35	415 or 910	0.6	± 70	+35 —15	55	28	270
AN/ASQ-14	U.S.	1958	F-104A, B	3.2	140	1 or 0.5	1000	0.61	± 45	+23 —25	38	18	120
AN/APQ-45	U.S.	1960	F-106	3.2— 3.4	250	2.5 or 0.25	416 or 4000	0.58	± 70	+50 —30	55	30	110
Nassarr F-21A	U.S.		F-104G	3.2	220	1.4 or 0.7	640 or 1280	$0.585 \times$ $\times 0.445$	± 45	+30 —25	38	18	130
A-1MK-23B	UK		Lightning	3.0	175	1	1000		± 50	+26 —25	50	30	150
Cyrano 2	France	1960	Mirage IIIC	3.0	230	1.75 or 0.5	640 or 2000	$0.58 \times$ $\times 0.48$	± 60	± 15	40	25	200
AN/APQ-100	U.S.	1964	F-4G	1.7— 5.7	1000			1.0	± 65	+50 —30	90	50	
AN/APQ-113	U.S.	1965	F-111	1.7— 5.7	1000			0.75			140	115	160
AN/APQ-55	U.S.	1967	F-111	5.5	5 av.		120	1.08	± 50		190		
AN/ASQ-18	U.S.	1968	YP-12A	3.2	2 av.	1	200	1.0	± 45				225

/143

Onboard devices for protection and countermeasures against radar, ground, and aircraft facilities

All devices for the protection and countermeasures to radar, ground, and onboard facilities of aircraft and missiles are commonly subdivided into individualized -- for the protection of the airplane itself, and group -- for the protection of several aircraft [20].

At the present time individualized means of protection and radio countermeasures are used on all combat aircraft [117]. The F-105, F-110 (F-4), B-52, and others can be classified as planes of this type. Group means of protection and radio countermeasures are installed on special aircraft, for example, the RC-47 or the E-6A.

Onboard protection equipment of aircraft does the following: detection and identification of ground or onboard enemy radars; their exact bearing in a 360° scan; and the transmission of commands for switching on active or passive means of countermeasures.

The pilot, receiving information from the protection equipment to the effect that an enemy radar is continuously radiating him, begins to perform various maneuvers trying to bring the aircraft out of the irradiation zone. If he does not succeed in this, then he switches on the radio countermeasures to jam the enemy's radar.

Table 3.4 gives some data on onboard aircraft individual protection facilities. They are light in weight and relatively small in size.

Individualized aircraft countermeasure devices produce radio jamming interfering with the enemy's radar (active interference) or camouflage the aircraft itself by ejecting dipole reflectors (passive jamming). Table 3.5 gives some data on active and passive means of radio countermeasures.

Active interference is either camouflaging noise jamming, or else reply jamming (in the frequency of the enemy's radar), or else jamming modulated with respect to a low frequency and acting on the radar scanning devices, and so on.

Passive jamming in the form of dipole reflectors can be ejected in separate portions with pneumatic devices, fired from cannons, or ejected in canisters from specialized missiles (setting up jamming).

Equipment of specialized jamming-producing aircraft or aircraft affording protection of groups of planes against enemy radar is designed (cf [117]) to detect the locations of radars, study the frequencies they beam, produce different kinds of active and

TABLE 3.4 ONBOARD AIRCRAFT FACILITIES

/145

Set	Country	Aircraft of installation	Working freq. range, MHz	Weight of set, kg
AN/ALR-31	U.S.	F-105		
AN/APS-105	U.S.	B-52	10900—36000	38,5
AN/APS-107	U.S.	F-105, F-110 (F-4)		
AN/APS-109	U.S.	F-111		
AN/APP-25	U.S.	F-100, F-105, RF-4C, F-110, (F-4C)	390—1550	

passive jamming, suppress the enemy's radar facilities, and so on. Digital computers are used to study types of interference and to develop the most effective means of countermeasures. The weight of the equipment of the radio countermeasure facilities of specialized aircraft is as high as 1000-2000 kg /117/.

3.2. Ground Radar Stations of Antiaircraft Defense Missile Complexes

Radar stations of antiaircraft defense missile complexes are used /60/ in search, identification, and tracking of a target or aiming, transmitting guidance command, and also in target coverage. Also these functions cannot be performed by one type of station. Therefore missile complex radars consist of stations of several types.

For example, the radar complex for Terrier missile guidance includes the following: the AN/SPW-2 detection radar and the AN/SPG-49 target coverage radar. The radar navigation control complex of the Hawk missile consists of three sets: the AN/MPQ-35 pulse set used for the interception of high-flying targets, the AN/MPQ-34 continuous-wave set -- for interception of low-flying targets, and the AN/MPQ-33 target coverage set.

Ground radars of each missile complex are connected with each other and form missile zones or belts of antiaircraft defense. To increase their effectiveness, radars are preferably made in the multichannel version /58/. Here one command guidance set provides simultaneous control flight of several missiles launched at a single target.

TABLE 3.5 ACTIVE AND PASSIVE MEANS OF RADIOMEASURES

/146

Kind of interference	Name of set (facility)	Country	Aircraft of installation	Working frequency range	Weight, kg	Function
Active	AN/ALQ-59	U.S.	B-52, F-105		Volume 3 decimeter	Producing noise jamming
Active	AN/QRS-321	U.S.	F-105	3900—6200 1560—5200		Producing jamming of different types
Active	AN/ALQ-78	U.S.	P-3C, S-2		16 0.028	Jamming using on-board computer
Active	AN/ALQ-80	U.S.	F-111A			
Passive	AN/ALE-16	U.S.	B-58			Scattering dipole reflectors
Passive	AN/ALE-28	U.S.	F-111			
Passive	AN/ALE-25	U.S.	B-52			Producing jamming by launching ADK-8A missile

The main characteristics of ground radars of antiaircraft defense of missile complexes are given in Table 3.6. The range of detection, lock-on, and tracking was determined by formulas (3.1) - (3.7) and (3.15), or from the data given in the works [7, 29, 101]. Functions of the lock-on range of antiaircraft complex radars are given in Fig. 3.9. From the comparison of these characteristics it is clear that the modernized radars have a much greater detection range. This evidently is related to the increase in the sensitivity and the reduction of losses in the radar channels. Table 3.6 also gives the coverage zones, the

/150

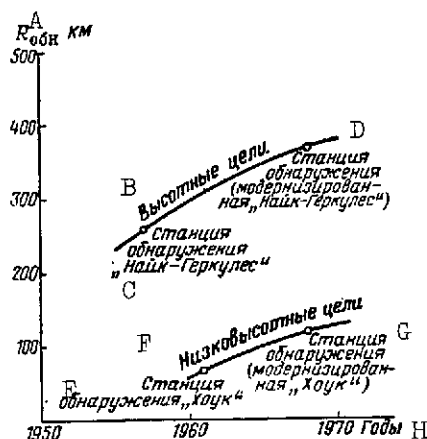


Fig. 3.9. Detection range of missile complex radars

KEY: A -- R_{det}
 B -- High-altitude targets
 C -- Nike-Hercules detection radar
 D -- Detection radar (modernized Nike-Hercules)
 E -- Hawk detection radar
 F -- Low-altitude targets
 G -- Detection radar (modernized Hawk)
 H -- Years

pulse repetition frequency, and the pulse duration for missile complex radars. These characteristics are also close to the corresponding data for aircraft complex radars.

3.3. Radar and Infrared Homing Heads of Surface-to-Air, Air-to-Air, and Air-to-Surface Missiles

Homing heads of surface-to-air, air-to-air, and air-to-surface missiles are commonly subdivided into active, semiactive, and passive, by the principle of application. They can also be classified by the type of energy sensed, i.e., radar, infrared, optical, acoustical, and so on. It must be noted at once that the first two types of homing heads, whose main characteristics we will consider below [8, 61, 64], have gained the greatest acceptance in guided missiles.

Active homing heads at present are made in the radar version and are used for guidance of missiles to air or ground radar-contrastive targets. Semiactive homing heads are also made in the radar version and are used for guidance to air targets. Passive homing heads are built either in the radar (for guidance to operating radars) or in the infrared version for guidance to air targets or surface vessels. Lately passive optical and television and combination (radar-infrared) homing heads have begun to be used [56].

Homing heads of missiles are characterized by the following main tactical-technical parameters: maximum range R_r , minimum range (blinding range) $R_{b.r}$; bearing angles (with respect to azimuth ϕ_{hor} and elevation angle ϕ_h); scatter time of coordinator for target azimuth or elevation angle $T_{\phi_{hor}^m}$ and $T_{\phi_h^m}$; the working range of control signals taken off from the homing head, which

/151

TABLE 3.6 MAIN CHARACTERISTICS OF MISSILE COMPLEX
RADARS

/148

Name of missile complex	Function of set	Name of set	Year built	Kind of radiation	λ, cm	Power, Mw		Rep. freq. Hz	Pulse duration, microsec	Coverage zones		Range	
										azimuth, deg	elevation, deg	$D_{\text{det}}, \text{km}$	D_{tr}, km
Talos	Target detection	AN/SPW-2	1956	Pulse	5.0-5.5	3	450	900	0.3-0.9	360	85	118	—
Talos	Target coverage	AN/SPQ-49	1956	Pulse	5.0-5.5	—	—	—	0.3-0.9	360	85	—	70
Hawk	High-altitude target detection	AN/MPQ-35	1961	Pulse	22-24	0.65	800	—	—	360	88	105	—
	Low-altitude target detection	AN/MPQ-34	1961	Continuous-wave	3	200 w	—	—	—	360	88	65	—
	Target coverage	AN/MPQ-33	1961	Continuous-wave	3	200 w	—	—	—	360	88	—	65
Nike-Hercules	Target detection	AN/MSW-1	1957	Pulse	8.5-1.0	1	500	—	1.3	360	88	260	—
	Target tracking	AN/MPA-4A	1957	Pulse	3.1-3.5	0.25	500	—	0.25	360	88	—	220
	Missile tracking	AN/MPA-4B	1957	Pulse	3.1-3.5	0.12	500	—	0.25	360	88	—	185

/149

provides for a given accuracy of sensing the angular velocity of the sighting line (in the horizontal $\dot{\phi}_{hor}$ and vertical $\dot{\phi}_h$ planes) and the sighting angles ϕ_{hor} and ϕ_h); resolving power as to range and bearing angles; anti-jamming capability; operating reliability; mass; and overall dimensions.

Radar homing heads provide guidance of guided missiles to air targets in the frontal and rear hemispheres; the probability of locking onto an airplane-target or an air-to-surface missile in the frontal and rear hemispheres being about the same at the maximum ranges. Attacks by guided missiles against ground radio radar-contrastive targets are possible here at considerable range at night and day with good and poor visibility. All this leads to the radar homing heads gaining wide acceptance in surface-to-air, air-to-air, and air-to-surface type missiles.

Range is found by means of the functions (3.1) - (3.7) in active radar homing heads (RHH). The blinding range can be calculated by the formula

$$R_{b.r} = \frac{K_{sh} c \tau}{2}, \quad (3.16)$$

where K_{sh} is the pulse shape factor;

c is the speed of light ($3 \cdot 10^8$ m/sec); and
 τ is the pulse duration.

Let us take $K_{sh} = 1.1$ and determine the blinding range of active RHH for different pulse durations. When $\tau = 2$ microseconds, we have $R_{b.r} = 330$ m, and when $\tau = 1$ microsecond, the blinding range drops to $R_{b.r} = 165$ m. Therefore in active radar heads it is best to reduce the pulse duration, i.e., to use radar operating at short wavelength. To determine the range of a semiactive RHH, let us examine Fig. 3.10. Using the symbols given in this figure, we rewrite equation (3.1) in the form

$$R_a = \alpha \sqrt[4]{\frac{P_{rada} G_a^2 S_{eff}^2 \lambda^2 \eta_a}{(4\pi)^3 R_{e min}}}, \quad (3.17) \quad /152$$

where

$$G_a = (0.6 - 0.7) \frac{\pi^2 D_a^2}{\lambda^2}.$$

Here D_a is the diameter of the antenna of the aircraft radar providing coverage of the RHH. For a semiactive system, the range is determined by the formula

$$R_m = \alpha \sqrt{\frac{P_{rad.a} G_m G_a S_{eff} \lambda^2 \eta_a}{(4\pi)^3 P_{remin}}}, \quad (3.18)$$

where G_m is the directivity factor of the homing head antenna

$$[G_m = (0.6 - 0.7) \frac{\pi^2 D_m^2}{\lambda^2}];$$

D_m is the diameter of the antenna of the missile homing head;
and

η_m is the efficiency of the RHH radome.

The range of the coverage set $\sqrt{\text{cf formula (3.17)}}$ and the semi-active homing head (cf formula (3.18)) can be related by the formula

$$R_a R_m = \alpha^2 \sqrt{\frac{P_{rad.a} G_a G_m S_{eff}^2 \lambda^2 \eta_a \eta_m}{(4\pi)^3 P_{remin}}}. \quad (3.19)$$

From (3.19) it is clear that the part of the ranges of the radar set and the RHH within the limits of the coverage range of the radar set is a constant. In addition, from (3.19) it is clear that semiactive homing heads are always energetically more advantageous than active RHH.

To compare the range of the two types of active and semiactive homing heads, we will assume that the active RHH is on a missile. Then

$$R_{m.a} = \alpha \sqrt[4]{\frac{P_{rad.m.a} G_{m.a}^2 S_{eff}^2 \lambda^2 \eta_{m.a}}{(4\pi)^3 P_{remin}}}. \quad (3.20)$$

Assuming that $P_{re\ min} = P_{re\ a\ min}$, we get

$$\frac{R_m}{R_{m.a}} = \sqrt[4]{\frac{P_{rad.a} G_a G_m \eta_m}{P_{rad.m.a} G_m^2 \eta_{m.a}}} \quad (3.21)$$

When $G_m = G_{m.a}$ and $\eta_m = \eta_{m.a}$, we have

$$\frac{R_m}{R_{m.a}} = \sqrt[4]{\frac{P_{rad.a} G_a}{P_{rad.m.a} G_m}} \quad (3.22)$$

or

$$\frac{R_m}{R_{m.a}} = \sqrt[4]{\frac{P_{rad.a} D_a^2}{P_{rad.m.a} D_m^2}} \quad (3.23)$$

Using formula (3.23) it is not difficult to calculate what range advantage is provided by the semiactive head compared with the active head. The corresponding advantages are given in Table 3.7. From the data in this table it is clear that relatively small increase in the power of the coverage radar leads to an increase in the range of semiactive RHH compared to an active head by a factor of 2.414 for different ratios of diameters of radar antennas and homing head antennas.

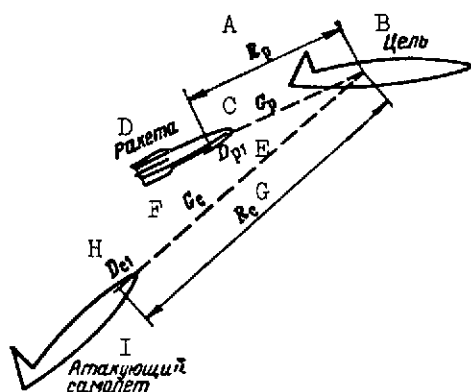


Fig. 3.10. Scheme of semiactive homing

KEY: A -- R_m
 B -- Target
 C -- G_m
 D -- Missile
 E -- D_{ml}
 F -- G_a
 G -- R_a
 H -- D_{al}
 I -- Attacking aircraft

TABLE 3.7 RANGE OF SEMIACTIVE RHH

/154

D_m mm	D_a mm	R_m/R_a			
		$\frac{P_{rad,a=4}}{P_{rad,m,a}}$	$\frac{P_{rad,a=10}}{P_{rad,m,a}}$	$\frac{P_{rad,a=40}}{P_{rad,m,a}}$	$\frac{P_{rad,a=100}}{P_{rad,m,a}}$
250	750	2,4	3,1	4,4	5,5
250	1000	2,8	3,6	5,0	6,3
250	1500	3,4	4,4	6,2	7,8
250	2000	4,0	5,0	7,1	9,0

The range of passive radar homing heads is determined from formula (3.15). Obviously, the range of their coverage for identical values of the remaining parameters (radiation power and transponder power, sensitivity $G_{re min}$, directivity factors, effective surfaces of reflection, and efficiency of radome) is greater than the range of active RHH. Therefore passive radar homing heads are small in size and weight.

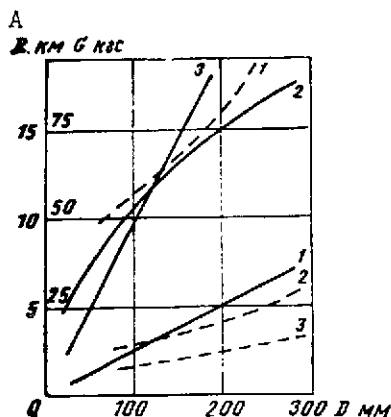


Fig. 3.11. Maximum ranges (solid lines) and weights (dashed lines) of active (1), semiactive (2), and passive (3) homing heads as a function of antenna diameter (for a lock-on probability $P = 0.5$)

KEY: A -- R, km, G, kg [force]

Figure 3.11 gives the maximum ranges of active, semiactive, and passive homing heads as a function of coordinator antenna diameter. Here

/155

also are plotted calculated values of weights of RHH, constructed with printed circuits, shown by dashed lines.

From Figure 3.11 it is clear that for equal antenna diameters passive homing heads have the greatest range, and active RHH -- the greatest weight.

TABLE 3.8 MAIN CHARACTERISTICS OF HOMING HEADS

Name of guided missile	Type of homing head	Country	Year built	Antenna (coordinator) diameter, mm	Coordinator turn angles, deg	Range, km	Weight, kg
Firestreak	IHH	UK	1951	—	—	8	—
Sidewinder 1A	IHH	U.S.	1954	90	± 28	9	5.2
Falcon GAR-2A	IHH	U.S.	1954	—	± 30	8	6.0
Falcon GAR-10	RHH	U.S.	1956	75	± 30	—	9.8
Sparrow-III AAM-N-6A	RHH	U.S.	1960	150	± 45	14	24.8
Matra R-530	RHH	France	1963	150	± 45	10	18.0
Falcon	RHH	U.S.	1969	—	50	—	—
Phoenix AJM-54A	RHH	U.S.	1969	—	50	—	70.0

The main characteristics of radar homing heads (based on foreign materials) are given in Table 3.8.

Infrared homing heads (IHH) are used in guiding targets to heat-emitting targets. These targets include, first of all, aircraft whose jet engine nozzles are heated to 500 - 600°C, surface ships afloat emitting streams of hot gases from stacks, and missiles with operating engines. An increase in aircraft flight velocity led to an increase in the aerodynamic heating of skin to 250 - 300°C. As a result, the intensity of infrared radiation became accessible for the production of signals sensed by infrared receivers of IHH. /156

The integral intensity of radiation of a hot object is determined by the Stefan-Boltzmann law

$$E = \epsilon \sigma T^4, \quad (3.24)$$

where ϵ is the overall saturation capacity (or the black body factor);

σ is the Stefan-Boltzmann constant ($5.7 \cdot 10^{-12} \text{ w/cm}^2 \cdot \text{deg}^4$);
and

T is the absolute temperature (in degrees Kelvin).

Formula (3.24) characterizes the radiation intensity throughout the wavelength range from zero to infinity.

All infrared radiation receivers exhibit a sensitivity dependent on wavelength. Therefore it is important to know the spectral characteristics of the radiation intensity distribution /66/. The spectral distribution of the radiation of a black body according to Plank can be represented as

$$I_\lambda = \frac{C_1}{\lambda^5} \frac{1}{\frac{C_2}{\lambda T} - 1}, \quad (3.25)$$

where $C_1 = 3.732 \cdot 10^{-12} \text{ w} \cdot \text{cm}^2$;

$C_2 = 1.436 \text{ cm} \cdot \text{deg}$; and

λ = wavelength in cm.

The function $I_\lambda = f(\lambda T)$ can be constructed by this formula. From Fig. 3.12 it is clear that the spectral intensity of radiation increases rapidly with temperature, while the wavelength corresponding to the intensity maximum shifts toward the short wave side.

To determine the maximum value $I_{\lambda_{\max}}$, let us differentiate the right side of the expression (3.25) and after equating the derivative to zero, we find

$$\lambda_{\max} T = 2900 \text{ microdegrees} \quad (3.26)$$

Substituting λ_{\max} in formula (3.25) instead of λ , from expression /157/ (3.26) we get

$$I_{\lambda_{\max}} = 21.2 C_1 \left(\frac{T_1}{C_2} \right)^5 \quad (3.27)$$

Thus, the intensity of radiation at the wavelength corresponding to the radiation maximum increases as the fifth power of temperature.

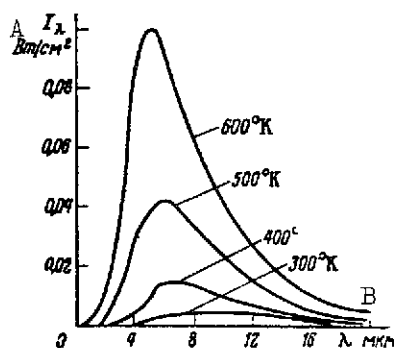


Fig. 3.12. Spectral distribution of radiation intensity according to Planck
KEY: A -- W/cm^2
B -- Microns

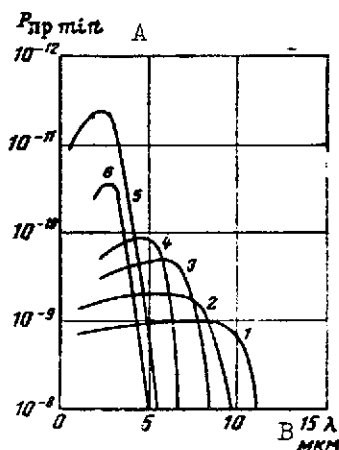


Fig. 3.13. Spectral characteristics of photoresistors:

- 1 -- Cooled, specially treated germanium
- 2 -- Indium antimonide, cooled to 90° K
- 3 -- Lead sulfide, cooled to 90°K
- 4 -- Lead telluride, cooled to 90°K
- 5 -- Lead sulfide, cooled to 193°K
- 6 -- Uncooled lead sulfide

KEY: A -- $P_{re min}$
B -- Microns

The receivers of infrared homing heads sensing the intensity of infrared radiation are photoresistors. The least intensity of infrared radiation that a photoresistor can sense determines its threshold of sensitivity at room temperature

$$P_{re min} = 3 \cdot 10^{-12} \frac{\sqrt{S}}{\tau}, \quad (3.28)$$

where S is the area of the receiver in mm ; and τ is the time constant in seconds.

Using formula (3.28), we can determine the minimum detectable signal. Fig. 3.13 presents the control characteristics of functioning photoresistors that were obtained experimentally. Preliminary cooling to 90 and 193°K was used for several photoresistors. By employing these graphs and knowing the threshold value of the radiation intensity, we can determine the relative spectral sensitivity of the photoresistors

$$S_\lambda = \frac{P_{re min}}{P_{re min}}. \quad (3.29)$$

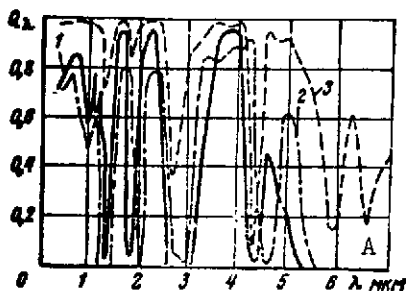


Fig. 3.14 Spectral transmission coefficients of the atmosphere at different altitudes above sea level

- 1 -- H = 0 km
- 2 -- H = 2-4 km
- 3 -- H = 15 km

KEY: A -- Microns

To determine the range of the infrared homing head, we must know the total signal power at the photoresistor output

$$E_{\text{tot}} = \int_0^{\infty} I_{\lambda} S_{\lambda} Q_{\lambda} d\lambda, \quad (3.30)$$

where Q_{λ} is the spectral transmission coefficient of the atmosphere for infrared radiation. The spectral coefficient of the atmospheric transmission depends on the altitudes above sea level. The higher the altitude above sea level, the less oxygen, carbon dioxide, and water vapor strongly absorbing infrared radiation, the atmosphere contains. Fig. 3.14 [66] shows the spectral transmission coefficients of infrared radiation. To determine E_{tot} , in Fig. 3.15 the curve of Q_1 for $H = 2$ km and the curves of S_1 for different photoresistors with a source $I_{\lambda} = 500^{\circ} \text{ K}$ are constructed. Using the graphs (Fig. 3.15), the following integrals (3.30) were calculated for each photoresistor; their values are shown in Fig. 3.16. From the figure it is clear that a photoresistor made of lead telluride exhibits the best yield. Their sensitivity can be compared by taking the ratios of the corresponding areas (cf Fig. 3.15). The values of these ratios are given in Table 3.9.

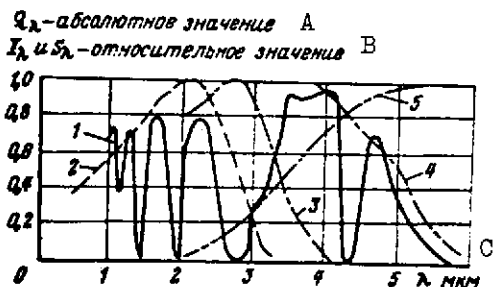


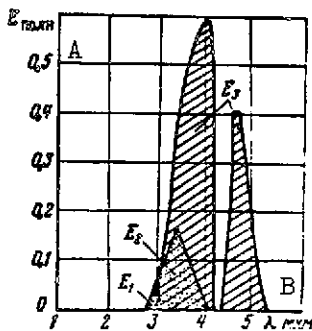
Fig. 3.15 Dependence of Q_{λ} (curve 1):

- 2 -- S_1 , curve 2 for lead sulfide at 193° K
- 3 -- For lead sulfide at 90° K
- 4 -- For lead telluride at 90° K
- 5 -- Absolute value of Q_{λ}

KEY: A -- Absolute value
B -- I_{λ} and S_{λ} are given in relative values
C -- Microns

TABLE 3.9

Ratio of areas	Numerical value of areas
$\bar{E} = \frac{E_2}{E_1}$	4.5
$\bar{E} = \frac{E_3}{E_2}$	5.2
$\bar{E} = \frac{E_3}{E_1}$	24

Fig. 3.16 Graphical calculation of E_{tot} : E_1 -- For lead sulfide at 193° K E_2 -- For lead sulfide at 90° K E_3 -- For lead telluride at 90° KKEY: A -- E_{tot}

B -- Microns

From the table data it follows that a cold lead telluride photoresistor is 24 times more sensitive than a lead sulfide photoresistor at room temperature. The range of infrared homing heads is determined by the formula

/160

$$R = \alpha \sqrt{\frac{E_{tot} S_{ob} S_p \cos \beta \cos \psi}{\pi P_{re \min}}}, \quad (3.31)$$

where α is the normalized range allowing for the stochastic nature of the target capture process;
 S_{ob} is the area of the entrance aperture of the head objective, in cm^2 ;
 S is the target radiation area;
 ρ is the transmission coefficient of the head radome;
 $P_{re \min}$ is the threshold sensitivity of the photoresistor;
 β is the angle between the normal to the target radiation surface and the sighting line; and
 ψ is the angle between the sighting line and the optical axis of the coordinator.

For attacks of aircraft-targets at small heading angles in the rear hemisphere, $\beta = 0$ and $\psi = 0$, then formula (3.31) becomes

$$R = a \sqrt{\frac{E_{\text{tot}} S_{\text{ob}} S_{\rho}}{\pi P_{\text{remin}}}}$$

The dependence of the maximum coverage range of the infrared homing head with respect to a target with I_{λ} (at 500°K) for photoresistors of lead sulfide (1) and lead telluride (2) was constructed in Fig. 3.17 using the formula above. The main characteristics of infrared homing heads are given in Table 3.8 [58, 61, 69, 78, 112].

3.4. Onboard Equipment of Aircraft Control Systems

At the present time two completely different directions are noted in the use of foreign onboard aircraft equipment. The first is when the onboard equipment is included in separate independent subsystems (navigation, landing, armament control, and so on), and the second is when it is included in a single system that is integrated on the basis of the onboard digital computer (ODC). In the control systems of the F-105, F-106, and Mirage III, the equipment is used in separate independent subsystems, but in the form of a single integrated system in the F-111A and F-111B. Naturally, when the equipment is used in an individual system its weight proves to be high. At the same time a single integrated system, in the event the ODC malfunctions, is less reliable than autonomous subsystems. Evidently, it is most correct to consider a rational combination of these two directions, namely to put together a single system on the basis of two or three ODC (for higher operating reliability). In this case when one of the ODC malfunctions, the equipment must be used in the individual most important subsystems. Let us turn to considering the onboard equipment of various systems. /161

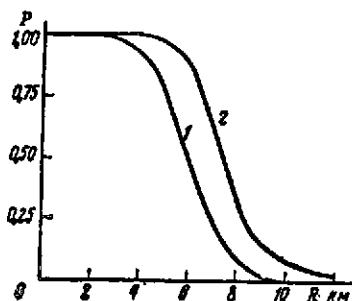


Fig. 3.17 Ranges of IHH [infrared homing head] with two types of photoresistors:
1 -- Lead sulfide
2 -- Lead telluride

Equipment of command (director) semiautomatic systems provides semiautomatic control of the aircraft in complex flight regimes (flying over terrain relief, take-off, landing, flight along a route, and so on) using piloting and navigation instruments, computer, and indicators. Semiautomatic systems as a rule are coupled with autopilots, forming a single system of automatic control (SAC).

The FD-60 semiautomatic system of the Bendix Corporation, installed on F-111 aircraft, consists of the following: a command-piloting instrument (D-300); navigation-heading instrument (7238); computing instruments; vertical gyro; amplifier; and control console. The command-piloting instrument provides a display of the bank and pitch angles in different flight regimes. The angles of heading, bearing, and deviation from assigned route and glide path lines are determined with the navigation-heading instrument. Both these instruments have warning flags which indicate the status of the gyrohorizon, computer, radio altimeter, /162 and heading system. The computing instrument generates the aircraft control laws. The weight of the entire system is 14.2 kg. The precision of the vertical gyro is about 15'.

The SFS-6 semiautomatic system also consists of command-piloting and navigation-heading instruments, a computing device, control console, and comparator. The latter compares the readings of the instruments of the pilot and copilot and signals their failure. The weight of the system is 11.7 kg and the precision of the vertical gyro is 20' /137, 172/.

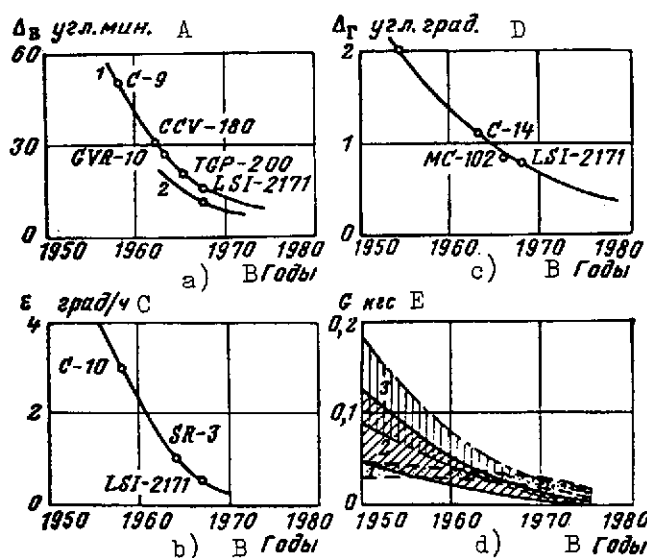


Fig. 3.18. Characteristics of aircraft vertical gyros (autonomous and with corrections from Doppler radars)

KEY: A -- Δ_h , angular minutes
B -- Years
C -- Deg/hr
D -- Δ_{hor} , angular degrees
E -- kg /Force/

Vertical gyro errors Δ_h in different flight regimes (without correction -- curve 1, and with correction from geocentric pendulums -- curve 2) are shown in Fig. 3.18 a as functions

of the year of manufacture. Here also is given the function of gyroscope drift (Fig. 3.18 b). As we can see from Fig. 3.18, gyroscope drift has been reduced by 10 times over a 10-year period; but the accuracy of maintaining a vertical with the gyro instrument has been increased by about three times /13, 137, 172/. /163

Fig. 3.18 b gives the precision of the heading systems as a function of the year of manufacture, and Fig. 3.18 d -- the

weight characteristics of elements of vertical gyros (region 1), computing instruments (region 2) [43, 152], and radar (region 3). As can be seen, the weight of vertical gyros actually changes but little, while the weight of computing instruments was reduced by several times through the use of solid-state elements.

Devices for measuring true airspeed (TAS) and M numbers are used in semiautomatic aircraft control systems. The accuracy of true speed measurements within the velocity range from 290 to 2700 km/hr is 5 km/hr, and the accuracy of M number measurement in the range of 0-2.0 is $\pm(0.002-1)$ [155, 171].

The equipment of automatic systems forms an autonomous control loop (autopilot), providing flight stability and good aircraft controllability in all regimes in the automatic, semiautomatic, and manual control modes. Also, the autonomous loop must provide for the execution of regimes of landing approach coordinated turns, and several other regimes.

The autopilot equipment includes the following: a gyroscopic sensor measuring the angular velocities of the aircraft, sensors of flight altitude H, M number, and velocity head q, accelerometer, amplifier-converters, and control-surface drives. To improve flight stability and controllability, the loop contours are adjusted as to flight altitude H, velocity head, and M number by a programming mechanism.

The programmed variation of autopilot parameters throughout the range of flight altitudes and velocities requires an exact knowledge of aircraft characteristics and imposes quite stringent requirements on tolerances for equipment parameters. All this is difficult to provide for aircraft designed to operate in many regimes. Therefore, self-adjusting autopilots have begun to be used. They include the MH-96 autopilot of the X-15 and the General Electric autopilot of the F-111. A system based on a large gain factor in the system's forward loop is employed in both autopilots. Natural oscillations used to measure the effectiveness of control devices are induced in the MH-96 autopilot. The F-111 autopilot operates near the stability limit. Reference aircraft models are used in these autopilots. /164

The mean parameters of gyroscopic sensors of angular velocities and accelerometers are given in Table 3.10 [77].

Equipment of inertial systems consists of a gyro stabilized platform on which are placed accelerometers measuring accelerations in a three-dimensional reference system; an analog or digital computer, or a digital differential analyzer (DDA) for integrating accelerations; and a Doppler radar for correction of the inertial system. /165

TABLE 3.10 ANGULAR VELOCITY SENSORS

Name [AVS=ang. vel. sensor]	Measure- ment range, deg/sec	Sensiti- vity threshold deg/sec	Natural freq. f_0 , Hz	Degree of at- tenua- tion,	Weight in kg
AVS for AP-28	± 18	0.1	80	$0.7^{+0.1}$	2.6
AVS for AP-6E	± 9	0.05	70	$0.7^{+0.1}$	0.32
Floated AVS	± 30	0.06	150	$0.7^{+0.2}$	0.57
ET-8 floated AVS	± 60	—	400	1.0	0.70

ACCELEROMETERS

Name	Measure- ment range, g unit	Sensiti- vity threshold in g units	Natural freq., f_0 Hz	Precision of meas. %	Weight in kg
Linear accele- rometer LA-800	to 80	$1 \cdot 10^{-4}$	150	—	0.09
Pendulum acce- lerometer F-2401	± 20	$5 \cdot 10^{-5}$	180	—	0.113

The gyrostabilized platform is isolated by means of a system of gimbal suspensions from the aircraft's angular displacements. The gyroscopes sense the angular displacements of the platform and generate signals sent to the turn motors of the gimbal suspension axes, which impart the requisite orientation to the platform. The accelerometers are installed either directly on the gyro-platform, or else by means of a separate suspension.

The inertial system error (or the error of determining the aircraft's position) depends on the inertial errors in determining the aircraft's velocity and position, and also on the flight time, and is generally determined by the gyroscope drift, accelerometer error, and the imprecision of gyro-stabilizer

adjustment. Neglecting the terms that allow for the Earth's rotation, we obtain equations of the gyrostabilizer errors in the form

$$\left. \begin{aligned} \dot{\psi}_x &= \epsilon_x + \tilde{\epsilon}_x \left(\dot{V} + \frac{gVt}{R} \right); \\ \dot{\psi}_y &= \epsilon_y + \tilde{\epsilon}_y \left(\dot{V} + \frac{gVt}{R} \right); \\ \dot{\psi}_z &= \tilde{\epsilon}_z. \end{aligned} \right\} \quad (3.32)$$

where ψ_x , ψ_y , and ψ_z are the angles between the axes determined by computers and the corresponding platform axes;
 ϵ_x , ϵ_y , and ϵ_z are the constant rates of gyroscope drift with respect to the three axes;

$\tilde{\epsilon}_x$ and $\tilde{\epsilon}_y$ are the drift rates of the horizontal gyroscope owing to unbalancing (it is assumed that $\epsilon_z = 0$);

R is the Earth's radius;

V is the level flight velocity of the aircraft;
 and

t is the flight time.

For simplicity of solution, we will assume that in the takeoff of the aircraft, horizontal acceleration is instantaneously communicated and $V = \text{const.}$ Then the solutions of equations (3.30) are written in the form /166

$$\left. \begin{aligned} \psi_x &= \psi_x(0) + \epsilon_x t + \tilde{\epsilon}_x \left(V + \frac{gVt^2}{2R} \right); \\ \psi_y &= \psi_y(0) + \epsilon_y t + \tilde{\epsilon}_y \left(V + \frac{gVt^2}{2R} \right); \\ \psi_z &= \psi_z(0) + \epsilon_z t, \end{aligned} \right\} \quad (3.33)$$

where $\psi_x(0)$, $\psi_y(0)$, and $\psi_z(0)$ are the initial erection errors of the gyrostabilized platform. The errors in the aircraft's position are determined by the following equations:

$$\left. \begin{aligned} \Delta \ddot{x} + \omega_0^2 \Delta x &= -A_x \psi_y + A_y \psi_z + \delta A_x; \\ \Delta \ddot{y} + \omega_0^2 \Delta y &= -A_x \psi_z + A_z \psi_x + \delta A_y, \end{aligned} \right\} \quad (3.34)$$

where Δx and Δy are the aircraft's position error;

A_x , A_y , and A_z are the accelerations acting on the accelerometers;

δA_x and δA_y are the errors at the accelerometer input (zero-drift of the accelerometer, errors in the transmission factor, the linearity error of the accelerometer, and so on); and $\omega_0^2 = g/R$ is the Schuler pendulum frequency.

We will consider two kinds of errors: due to zero-drift B_x and B_y , and due to the transmission factor K_x and K_y . Then

$$\left. \begin{aligned} \delta A_x &= B_x + K_x A_x; \\ \delta A_y &= B_y + K_y A_y. \end{aligned} \right\} \quad (3.35)$$

The acceleration components can be represented as

$$\left. \begin{aligned} A_x &= \ddot{x} + \frac{g V_x t}{R}; \\ A_y &= \ddot{y} + \frac{g V_y t}{R}; \\ A_z &= g. \end{aligned} \right\} \quad (3.36)$$

Using expressions (3.33), (3.35), and (3.36), and equation (3.34), /167 we get

$$\left. \begin{aligned} \Delta \ddot{x} + \omega_0^2 \Delta x &= -\psi_y(0)g + \psi_z(0) \left(\ddot{y} + \frac{g V_x t}{R} \right) + \\ &+ B_x - K_x \frac{g V_x t}{R} - e_x g t + e_z t \left(\ddot{y} + \frac{g}{R} V_y t \right) - \\ &- \tilde{e}_y \left(V + \frac{g}{2} \frac{V t^2}{R} \right) g; \\ \Delta \ddot{y} + \omega_0^2 \Delta y &= -\psi_z(0) \left(\ddot{x} + \frac{g V_x t}{R} \right) + \psi_x(0)g + \\ &+ B_y - K_y \frac{g V_y t}{R} - e_z t \left(\ddot{x} + \frac{g V_x t}{R} \right) + e_x g t + \\ &+ \tilde{e}_x \left(V + \frac{g}{2} \frac{V t^2}{R} \right) g. \end{aligned} \right\} \quad (3.37)$$

Neglecting $\ddot{x}t$ and $\ddot{y}t$ compared with gt , we obtain the following solution of equations (3.37):

$$\begin{aligned}
\Delta x = & \Delta x_0 \cos \omega_0 t + \Delta \dot{x}_0 \frac{\sin \omega_0 t}{\omega_0} - \psi_y(0) R \times \\
& \times (1 - \cos \omega_0 t) + \psi_z(0) \left[V_y \frac{\sin \omega_0 t}{\omega_0} + V_y \times \right. \\
& \times \left(1 - \frac{\sin \omega_0 t}{\omega_0} \right) \left. \right] + \frac{B_x}{\omega_0^2} (1 - \cos \omega_0 t) - (K_x V_x + \\
& + \frac{e_y g}{\omega_0^2}) \left(t - \frac{\sin \omega_0 t}{\omega_0} \right) + e_z V_y \left[t^2 - \frac{2}{\omega_0^2} \times \right. \\
& \times (1 - \cos \omega_0 t) \left. \right] - \tilde{e}_y \left\{ \frac{V_y}{\omega_0^2} (1 - \cos \omega_0 t) + g V \times \right. \\
& \times \left[\frac{t^2}{2} - \frac{1}{\omega_0^2} (1 - \cos \omega_0 t) \right] \left. \right\};
\end{aligned}
\tag{3.38}$$

$$\begin{aligned}
\Delta y = & \Delta y_0 \cos \omega_0 t + \Delta \dot{y}_0 \sin \omega_0 t + \psi_x(0) R \times \\
& \times (1 - \cos \omega_0 t) - \psi_z(0) V_x t + \frac{B_y}{\omega_0^2} (1 - \cos \omega_0 t) - \\
& - \left(K_y V_y - \frac{e_x g}{\omega_0^2} \right) \left(t - \frac{\sin \omega_0 t}{\omega_0} \right) - e_z V_x \times \\
& \times \left[t^2 - \frac{2}{\omega_0^2} (1 - \cos \omega_0 t) \right] + \tilde{e}_x \frac{V g t^2}{2}.
\end{aligned}$$

/168

We introduce the following notation into expression (3.31):

- $\Delta x_1, \Delta y_1$ are errors due to initial errors in measuring aircraft coordinates;
- $\Delta x_2, \Delta y_2$ are errors due to initial errors in measuring aircraft velocities;
- $\Delta x_3, \Delta y_3$ are errors due to gyrostabilizer adjustment in the horizontal plane $\psi_x(0)$ and $\psi_y(0)$;
- $\Delta x_4, \Delta y_4$ are errors due to adjustment as to azimuth $\psi_z(0)$;
- $\Delta x_5, \Delta y_5$ are errors due to the zero-drifts of the accelerometers B_x, B_y ;
- $\Delta x_6, \Delta y_6$ are errors due to the determination of the transmission factor of the accelerometer K_x, K_y ;
- $\Delta x_7, \Delta y_7$ are errors due to gyroscope drift in the horizontal plane ϵ_x, ϵ_y ;

$\Delta x_8, \Delta y_8$ are errors due to the drift of the azimuth gyroscope ϵ_z ;
 and
 $\Delta x_9, \Delta y_9$ are errors due to the drift of gyroscope owing to unbalancing $\tilde{\epsilon}_x, \tilde{\epsilon}_y$.

Then we get

$$\left. \begin{aligned} \Delta x &= \Delta x_1 + \Delta x_2 + \Delta x_3 + \Delta x_4 + \Delta x_5 + \Delta x_6 + \\ &\quad + \Delta x_7 + \Delta x_8 + \Delta x_9; \\ \Delta y &= \Delta y_1 + \Delta y_2 + \Delta y_3 + \Delta y_4 + \Delta y_5 + \Delta y_6 + \\ &\quad + \Delta y_7 + \Delta y_8 + \Delta y_9, \end{aligned} \right\} \quad (3.39)$$

where

$$\Delta x_1 = \Delta x_0 \cos \omega_0 t;$$

$$\Delta y_1 = \Delta y_0 \cos \omega_0 t;$$

$$\Delta x_2 = \Delta x_0 \frac{\sin \omega_0 t}{\omega_0};$$

$$\Delta y_2 = \Delta y_0 \frac{\sin \omega_0 t}{\omega_0};$$

$$\Delta x_3 = -\psi_y(0) R (1 - \cos \omega_0 t);$$

$$\Delta y_3 = \psi_x(0) R (1 - \cos \omega_0 t);$$

$$\Delta x_4 = \psi_z(0) V_y t;$$

$$\Delta y_4 = -\psi_z(0) V_x t;$$

$$\Delta x_5 = \frac{B_x}{\omega_0^2} (1 - \cos \omega_0 t);$$

$$\Delta y_5 = \frac{B_y}{\omega_0^2} (1 - \cos \omega_0 t);$$

$$\Delta x_6 = -K_x V_x \left(t - \frac{\sin \omega_0 t}{\omega_0} \right);$$

$$\Delta y_6 = -K_y V_y \left(t - \frac{\sin \omega_0 t}{\omega_0} \right);$$

$$\Delta x_7 = -\epsilon_y R \left(t - \frac{\sin \omega_0 t}{\omega_0} \right);$$

$$\Delta y_7 = \epsilon_x R \left(t - \frac{\sin \omega_0 t}{\omega_0} \right);$$

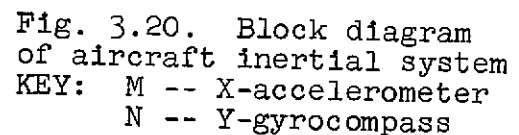
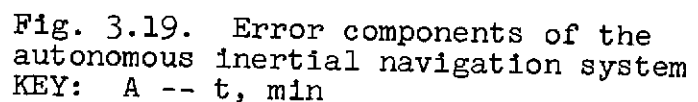
$$\Delta x_8 = \epsilon_z V_y \left[t^2 - \frac{2}{\omega_0^2} (1 - \cos \omega_0 t) \right];$$

$$\Delta y_8 = -\epsilon_z V_x \left[t^2 - \frac{2}{\omega_0^2} (1 - \cos \omega_0 t) \right];$$

/169

$$\Delta y_2 = \frac{\tilde{e}_x g V r^2}{2}$$

/170



171

$$\left. \begin{aligned} \Delta \dot{x}(s) &= \\ &= \frac{sB_x(s) - g e_{yx}(s) + (sK_1 + K_2 \omega_0^2) \delta V_x(s)}{s^2 + K_1 s + (1 + K_2) \omega_0^2}; \\ \Delta \dot{y}(s) &= \\ &= \frac{sB_y(s) + g e_{xz}(s) + (sK_1 + K_2 \omega_0^2) \delta V_y}{s^2 + K_1 s + (1 + K_2) \omega_0^2} \end{aligned} \right\} \quad (3.40)$$

and the steady-state errors of the system will be

$$\left. \begin{aligned} \Delta \dot{x}_{st.s} &= \frac{K_2}{1 + K_2} \delta V_x - \frac{R e_{yx}}{1 + K_2}; \\ \Delta \dot{y}_{st.s} &= \frac{K_2}{1 + K_2} \delta V_y + \frac{R e_{xz}}{1 + K_2}. \end{aligned} \right\} \quad (3.41)$$

For large K_2 , the error of the INS [inertial navigation system] is determined by the inaccuracy of velocity input (i.e., δV_x or δV_y). To refine the aircraft velocity, Doppler radar sets are used. The resulting frequency difference f_D is proportional to the velocity of the moving transmitter and is inversely proportional to the wavelength λ . When a signal reflected from a fixed point is received at the aircraft, we have⁴

$$f_D = \frac{2V}{\lambda} \cos \theta, \quad (3.42)$$

where θ is the angle between the velocity vector and the bearing toward the fixed point. Knowing f_D , θ , and λ , we can determine the aircraft velocity by formula (3.42). An actual antenna beam has some width, therefore the Doppler shift is some frequency band f_D , i.e.,

$$\frac{\Delta f_D}{f_D} = \operatorname{tg} \theta \Delta \theta, \quad (3.43)$$

where $\Delta \theta$ is the width of the antenna beam.

Let us consider the determination of the route velocity V_{ro} and the drift rate $V_{d,r}$ using the Doppler radar. On the aircraft

(Fig. 3.21 a and b)⁵, the Doppler frequencies $f_{D.l}$ (left) and $f_{D.r}$ (right) are determined by the formulas:

$$\left. \begin{aligned} f_{D.l} &= \frac{2}{\lambda} (K_1 V_{d.r} + K_2 V_{ro} - K_3 V_V); \\ f_{D.r} &= \frac{2}{\lambda} (-K_1 V_{d.r} + K_2 V_{ro} - K_3 V_V) \end{aligned} \right\} \quad (3.44)$$

Here V_B is the vertical component of the aircraft velocity; K_1 , K_2 , and K_3 are the antenna placement constants

$$\left. \begin{aligned} K_1 &= \cos \psi_1 \sin \psi_2; \\ K_2 &= \sin \psi_1; \\ K_3 &= \cos \psi_1 \cos \psi_2. \end{aligned} \right\} \quad (3.45)$$

where ψ_1 and ψ_2 are the antenna placement angles (cf Fig. 3.21 a). /173
The sum and difference of Doppler frequencies are determined by the formulas

$$\left. \begin{aligned} f_{D.l} + f_{D.r} &= \frac{4}{\lambda} (K_2 V_{ro} - K_3 V_V); \\ f_{D.l} - f_{D.r} &= \frac{4}{\lambda} K_1 V_{d.r}. \end{aligned} \right\} \quad (3.46)$$

These relations are valid only for a strictly level flight when the pitch θ and bank γ angles are equal to zero. For θ and γ angles distinct from zero, we have

$$\left. \begin{aligned} V_{ro} &= \frac{1}{\cos \gamma \cos \theta - \frac{K_3}{K_1} \sin \theta} \left[\frac{\lambda}{4K_2} \times \right. \\ &\times (f_{D.l} + f_{D.r}) \cos \gamma - \frac{\lambda K_3}{4K_1 K_2} (f_{D.l} - f_{D.r}) \sin \gamma + \\ &\left. + V_V \left(\cos \gamma \sin \theta + \frac{K_3}{K_2} \cos \theta \right) \right]; \\ V_{d.r} &= \frac{1}{\cos \gamma \cos \theta - \frac{K_3}{K_2} \sin \theta} \left[\frac{\lambda}{4K_1} \times \right. \\ &\times (f_{D.l} - f_{D.r}) \left(\cos \theta - \frac{K_3}{K_2} \sin \theta \cos \gamma \right) - \\ &\left. - \frac{\lambda}{4K_2} (f_{D.l} + f_{D.r}) \sin \gamma \sin \theta - V_V \sin \gamma \right]. \end{aligned} \right\} \quad (3.47)$$

Both of these equations are solved with the route velocity analog or digital computer. The main characteristics of a number of Doppler radar sets are given in Table 3.11. Aircraft position errors can be found with the data of the Doppler system using the following formulas:

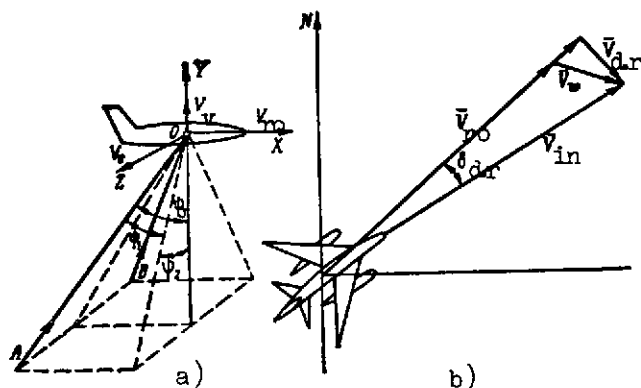


Fig. 3.21. Determination of route speed and drift rate using Doppler radar

$$\left. \begin{aligned} \sigma_{ro} &= \sqrt{\sigma_v^2 + \sigma_{v_f}^2} \\ \sigma_s &= \sqrt{\sigma_v^2 + \sigma_{v_s}^2 + \sigma_{he}^2} \end{aligned} \right\} \quad (3.48) \quad /176$$

where σ_{ro} is the mean-square error of the aircraft's position as to range (along the heading);
 σ_v is the mean-square error of determination (by the Doppler technique) of the route speed;
 σ_{v_r} and σ_{v_s} are the mean-square errors of the computing instrument in determining the range and sight direction;
and
 σ_{he} is the mean-square error of the system of airspeed determination (with respect to heading).

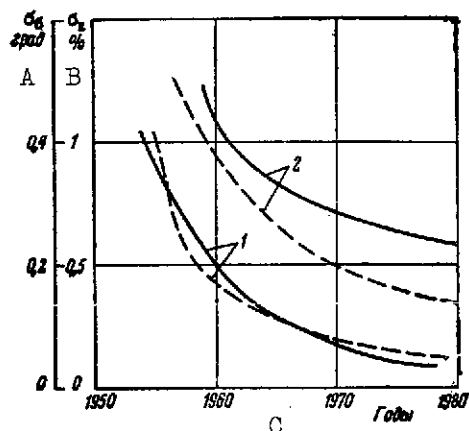


Fig. 3.22. Characteristics of the accuracy of the operation of autonomous (2) and Doppler-corrected (1) inertial systems:

— σ_{ro} ;
--- σ_s
KEY: A -- σ_s , deg
B -- σ_{ro} , percent
C -- Years

TABLE 3.11 MAIN DATA OF DOPPLER RADAR SETS [137, 152]

/174

Set	Radia- tion type	No. of beams	Antenna type	Output data	Conditions of use		Accuracy	Weight, kg
	Freq. MHz				altitude m	speed km/hr		
AN/APN-66	Pulse 8800	4	Line arrays	Latitude, longi- tude, route speed, drift angle, wind speed	150—21000	130—1300	$V_{dr} - 0.2\%$; $\theta_{dr} (\pm 0.2^\circ)$; pos- ition -0.5%	330
AN/APN-81	Pulse 8800	4	Line arrays	Route speed, drift angle, wind velocity and direction	150—21000	130—1300	$V_{dr} - 0.2\%$; $\theta_{dr} (\pm 0.2^\circ)$; $W - (\pm 5, 4)$ km/hr	180
AN/APN-82	Pulse 8800	4	Line arrays	Latitude, longi- tude, route speed, drift angle, wind direction and velocity	150—21000	130—1300	$V_{dr} - 0.2\%$; $\theta_{dr} (\pm 0.2^\circ)$; pos- ition -0.5%	200
AN/APN-89	Pulse 8800	4	Line arrays	Route speed, drift angle, beam angle	150—21000	130—1400	$V_{dr} - 0.2\%$; $\theta_{dr} (\pm 0.2^\circ)$	150
AN/APN-96	Pulse 8800	4	Flat array	Route speed, drift angle, wind direction and velocity	70—21000	180—1800	$V_{dr} - 0.1\%$; $\theta_{dr} (\pm 0.15^\circ)$	50
AN/APN-102	Pulse 8800	4	Flat array	Route speed, drift angle	60—21000	130—1900	$V_{dr} - 1\%$; $\theta_{dr} (\pm 0.5^\circ)$	40
AN/APN-105	Pulse 9800	3	Lens	Latitude, longi- tude, route speed, drift angle, heading	0—25000	90—2800	$V_{dr} - 0.5\%$; $\theta_{dr} (\pm 0.3^\circ)$	100

/175

Characteristics of the operating accuracy of Doppler radar systems (curve 1) are constructed in Fig. 3.22 using the data in Table 3.11. Also given in this figure (curve 2) is the accuracy of an autonomous inertial navigation system. From this figure it is clear that the accuracy of navigation systems that are wholly autonomous (curve 2) and that are Doppler-corrected (curve 1) has continually been increased through improvements both in the gyroscopic equipment and accelerometers, as well as in the Doppler radar sets.

Analog and digital computers (digital differential analyzers /177 or digital computers) are used in autonomous inertial navigation systems and Doppler sets. Analog computers consist of the following elements: amplifiers, potentiometers, sine-cosine converters, tracking systems, tachogenerators, relays, gear transmissions, mechanical plotters, cams, and so on. The operating accuracy of analog computers is determined by the manufacturing accuracy of their elements and varies from 0.2 to 10 percent, depending on the problems solved. An analog computer must have its own computing device in order to perform each mathematical operation. This complicates the computer, reduces the overall operating accuracy, and adds to its weight. Therefore analog computers are not used in modern inertial control systems.

Digital differential analyzers performing only the operations of integration and addition have gained wide acceptance. The sequence of operations performed by the DDA is determined by a program. Only one command is realized at any one time with the DDA.

The DDA has a quite simple arithmetic device, whose capacity is determined by the requirements of problem-solving accuracy. In the increments Δx and Δy , the solution accuracy is determined by the formula

$$\left. \begin{aligned} \Delta x &= \frac{V_{x \max}}{S_x}; \\ \Delta y &= \frac{V_{y \max}}{S_y}, \end{aligned} \right\} \quad (3.49)$$

where $V_{x \max}$ and $V_{y \max}$ are the maximum change rates of the variables x and y . The variables S_x and S_y can be calculated using the following expressions:

$$\left. \begin{aligned} S_x &= \frac{w}{Nk'_{\text{int}}}; \\ S_y &= \frac{w}{Nk''_{\text{int}}} \end{aligned} \right\} \quad (3.50)$$

where w is the access time;

N is the number of digits in the register; and k'_{int} and k''_{int} are the number of operating integrators. /178

Analysis of formulas (3.49) and (3.50) shows that when there are high requirements for accuracy, the operating speed of the DDA (S_x and S_y) is as high as several thousands of calculations per second, which represents certain difficulties. Additionally, the DDA has the following drawbacks:

- a) the impossibility of calculating individual parts of programs at different computational speeds;
- b) the absence of devices for storing large masses of data (tables); and
- c) the impossibility of monitoring the correctness of the problems solved.

These drawbacks of the DDA and the limitations of their logic capabilities in solving a number of combat problems led to the wider use of digital computers on aircraft, including also in navigation systems. Onboard digital computers used in navigation systems have serial or parallel adders.

TABLE 3.12 COMPARISON OF ONBOARD COMPUTER WITH DIGITAL DIFFERENTIAL ANALYZER

Mathematical operations	DDA	ODC	
		with serial adder	with parallel adder
Integration	N	$2N^2$	$2N$
Summation	0	N	1
Multiplication	$2N$	N^2	N

The comparison made in Table 3.12 shows that the DDA and the onboard computer with parallel adder have identical operating speed, while the onboard computer with a serial adder has a slower speed.

Onboard digital computers. The diversity of functions assigned to modern aircraft led to a considerable rise in the variety of their equipment (cf Fig. 3.1). Along with systems for navigation, flight control, and landing, systems controlling sighting devices, armament, monitoring system status, and so on began to be used on combat aircraft. The control of all the systems is possible only when onboard digital computers are used. Basic data on onboard aircraft computers are given in Table 3.13 [74, 91, 137, 152]. The data of Table 3.13 was used to construct in Fig. 3.23 a and b memory capacity and mean speed⁶, per kg of onboard computer weight

(curve 1) and volume occupied per decimeter³ (curve 2) as functions/182 of the year the computer was built. Converting from an onboard computer built with mixed elements (semiconductor devices and vacuum tubes) to onboard computers using solid-state and film elements led to an appreciable increase in the memory capacity and the operating speed, per kg of weight and per decimeter³ of machine volume.

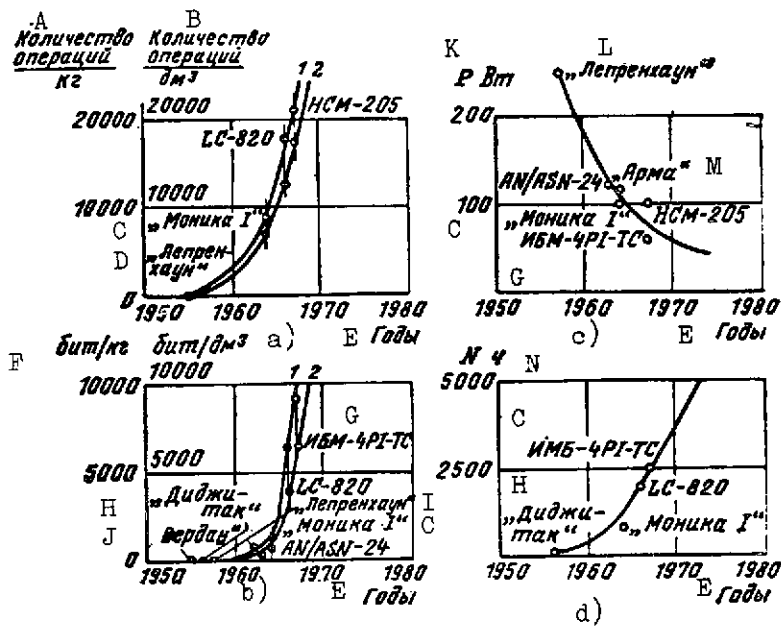


Fig. 3.23. Comparative characteristics of aircraft onboard computers:

- a -- Mean speed per kg of computer weight and per decimeter³ of machine volume
- b -- Memory capacity per kg of weight and per decimeter³ of machine volume
- c -- Required power
- d -- Operating reliability

KEY: A -- Number of operations/kg
 B -- Number of operations/decimeter³
 C -- Monica I
 D -- Leprechaun
 E -- Years
 F -- Bits/kg, Bits/decimeter³
 G -- IBM-4PI-TS
 H -- Digitac
 I -- Leprechaun

Fig. 3.23. Comparative characteristics of aircraft onboard computers /Continued/

J -- Verdan
K -- P, watts
L -- Leprechaun
M -- Arma
N -- M, hours

Fig. 3.23 c presents the change in the required power of ODC as functions of year of manufacture. Here the transition to solid-state and film elements also led to an appreciable reduction in the ODC required power.

Of great interest are the functions characterizing the rise in operating reliability of onboard digital computers. The conversion of onboard computers to solid-state and film elements meant an appreciable gain in their operating reliability.

3.5. Onboard Equipment of the Control Systems of Surface-to-Air, Air-to-Air, and Air-to-Surface Missiles

The makeup of the onboard equipment of the control systems of surface-to-air, air-to-air, and air-to-surface missiles is quite varied. For example, the equipment of the control systems of surface-to-air missiles includes the following: homing heads with gyroscopic drives or tracking systems, amplifier-converters, ODC, free and damping gyroscopes, accelerometers, servo units, power blocks, various kinds of corrective devices, radio receivers, aerial-burst fuses, and antenna-feeder installations. The equipment of air-to-air and air-to-surface missiles is similar in composition to that of surface-to-air missiles, however it differs widely in its characteristics.

In this section we will examine the main characteristics of just the part of the missile's onboard equipment (drives of the homing head and onboard digital computers) that has the main effect on the characteristics of the entire control system. /183

Homing head drives are subdivided into gyro stabilized-power, gyro stabilized with indirect stabilization, and wide-band tracking systems. Gyro stabilized power drives can be constructed with one or two gyroscopes. Fig. 3.24 a shows the gyro stabilized drive /184 of the infrared homing head of the Firestreak missile with one gyroscope.

The optical coordinator of the target consists of a primary 5 and a secondary 1 mirror. It also includes modulating disc 6, infrared energy receiver, and photocurrent amplifier 7. When the coordinator axis is disengaged from the target bearing, the torque sensors 2 and 8 coupled with the axes of rotation of the rings 3 and 4 produce moments serving to precess the gyroscope

TABLE 3.13 ONBOARD AIRCRAFT DIGITAL COMPUTERS

/180

Name of onboard computer	Year built	Country	Aircraft of installation	Characteristics of onboard computer								
				type of elements	number of digits	Time add.	Type of memory	Memory capacity	access time, msec	req. power, w	Weight, kg	volume decimeter ³
						mult. microsec						
Verdan	1955	U.S.	B-52 A-3J	Semiconductor			Magnetic drum	1024		370	37.2	39.6
Digitac		U.S.	F-102	Semiconductor			Semiconductor			50	32	400
Leprechaun	1957	U.S.		Semiconductor		$\frac{40}{375}$	Ferrite cores	1024	8	250		400
AN/ASN-24	1963	U.S.	C-141	Micro-modules			Magnetic drum	2500		120	16.8	8.5
C-900	1963			Solid circuits		$\frac{230}{880}$	Magnetic drum	4096		124	15.8	14.2
Monika I	1964			Solid circuits		$\frac{12-18}{42-284}$	Ferrite cores	4096-16384		50-100	4.5-7	4.25-8.5
Arma	1964	U.S.		Hybrid circuits	22	$\frac{1.5}{-}$	Internal memory Permanent memory	256-11000	2	115	17	17.5
IBM-NAA	1964	U.S.	B-70	—			Ferrite cores Permanent memory	1024-32000				
LC-820	1966	U.S.	F-106	Integrated circuits	16		Ferrite cores	177000		160	28	40
MH-390	1966	U.S.		Solid circuits	36	$\frac{1.25-10}{7.5-60}$	Magnetic film	2048				
HCM-205	1967	U.S.		Solid circuits	18	$\frac{4}{22}$		4096-16384	2	100	6	6
IBM -4PI-IC	1967	U.S.	F-111	Hybrid	16-30	$\frac{9-18}{48-54}$	Thin film	8192-65000	2.5	60	8	11

/181

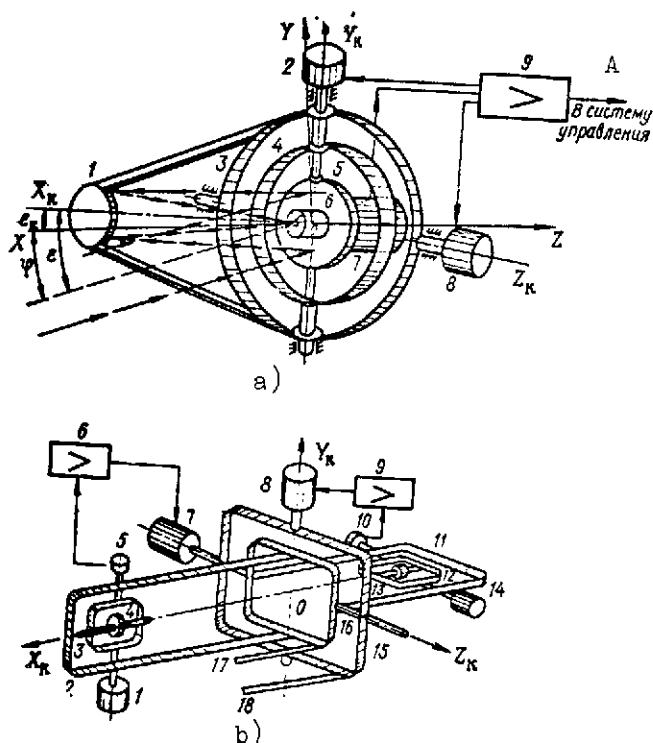


Fig. 3.24. Arrangements of gyro-stabilized drives:

- a -- with one gyroscope:
- 1 -- secondary mirror
- 2 -- torque motor of azimuthal channel
- 3, 4 -- gyroscope rings
- 5 -- primary mirror
- 6 -- modulating disc
- 7 -- photocurrent amplifier
- 8 -- torque motor of angle elevation channel
- 9 -- terminal amplifier
- b -- with two gyroscopes:
- 1, 14 -- torque motors
- 2, 11 -- outer gyroscope rings
- 3, 12 -- inner gyroscope rings
- 4, 13 -- gyroscopes
- 5, 10 -- potentiometric sensors
- 6, 9 -- power amplifiers
- 17, 18 -- thrusts applied to coordinator or antenna

KEY: A -- To control system

in the direction of aligning the line of sighting with the coordinator axis [56]. Precession stops when the coordinator axis coincides with the direction of the sighting line. If the sighting line rotates at some angular velocity $\dot{\phi}$, the optical coordinator will also rotate in the direction of the target, and the currents of the torque sensors are made proportional to the projections of the angular velocity of the sighting line ($\dot{\phi}_y$ -- with respect to the azimuth, and $\dot{\phi}_z$ with respect to the elevation angle). These currents arrive at the input resistor of the power amplifier 9 and further to the missile's control system in the form of the voltages \tilde{u}_{My} and \tilde{u}_{Mz} .

From Fig. 3.24 a it is clear that there are two coordinate systems: fixed XYZ and gyroscope coordinator-associated Ox and $Y_{co}Z_{co}$. The mismatch angle in the gyroscopic system is

$$\varphi = \varepsilon - \varepsilon_{co} \quad (3.51)$$

or

$$\left. \begin{aligned} \varphi_z &= e_z - e_{co.z} \\ \varphi_y &= e_y - e_{co.y} \end{aligned} \right\} \quad (3.52)$$

where $e_{co.z}$ and $e_{co.y}$ are the signal components with respect to the corresponding coordinator axes.

The equation of motion of the gyroscopes will be written as

$$\left. \begin{aligned} J_{co.z} \ddot{\varphi}_z - H_{co.y} \dot{\varphi}_y &= M_{co.y} \\ J_{co.y} \ddot{\varphi}_y - H_{co.z} \dot{\varphi}_z &= M_{co.z} \end{aligned} \right\} \quad (3.53)$$

where J is the moment of inertia of the rotor relative to the axis running through the center of rotation; $M_{co.y}$, $M_{co.z}$ are the moments of the motors causing the gyroscope to precess.

Voltage from the output of the power amplifier is cross-fed to the torque motors, therefore /185

$$\left. \begin{aligned} T_{en} \dot{M}_{co.z} + M_{co.z} &= -K_{en} u_{am.z} \\ T_{en} \dot{M}_{co.y} + M_{co.y} &= -K_{en} u_{am.y} \end{aligned} \right\} \quad (3.54)$$

where T_{en} is the time constant of the torque motor, and

K_{en} is the gain factor of the torque motor.

The voltage at the amplifier output is associated with the voltage of the coordinator by the following two relationships:

$$\left. \begin{aligned} u_{am.z} &= K_{am} u_{co.z} \\ u_{am.y} &= K_{am} u_{co.y} \end{aligned} \right\}$$

where K_{am} is the gain factor of the power amplifier, and

$u_{co.y}$, $u_{co.z}$ are the coordinator voltages with respect to the corresponding axes.

The equation of the coordinator per se will be written as

$$\left. \begin{aligned} u_{co.y} &= K_{ap} u_{co.y} \\ u_{co.z} &= K_{ap} u_{co.z} \end{aligned} \right\} \quad (3.56)$$

where K_{ap} is the gain factor of the photocurrent amplifier.

Equation (3.56) was set up without considering the phase shift introduced by the photocurrent amplifier. Applying a Laplace transform to equations (3.51) - (3.56), we get

$$\begin{aligned}
 \epsilon_{co.z}(s) &= \frac{K_{en}}{sH(T_{en}s + 1)} U_{yz}(s) + \frac{Js}{H} E_{co.y}(s); \\
 \epsilon_{co.y}(s) &= \frac{K_{en}}{sH(T_{en}s + 1)} U_{yz}(s) - \frac{Js}{H} E_{co.z}(s); \\
 U_z(s) &= K_{am} K_{co} \Phi_{co.z}(s); \\
 U_y(s) &= K_{am} K_{co} \Phi_{co.y}(s); \\
 \Phi_z(s) &= E_z(s) - E_{co.z}(s); \\
 \Phi_y(s) &= E_y(s) - E_{co.y}(s).
 \end{aligned}
 \tag{3.57}$$

It is not hard to set up the block diagram (Fig. 3.25 a) based on equations (3.57). The block diagram allows for the effect of the cross-coupling between the channels with allowance for the effect of the equatorial moment of the gyroscope. Neglecting this coupling, let us determine the voltage at the output of the gyroscopic drive

/186

$$\begin{aligned}
 U_{am.z}(s) &= \frac{K_{co} K_{am} H (T_{en}s + 1) s E_z(s)}{s (T_{en}s + 1) H + K_{co} K_{am} K_{en}}; \\
 U_{am.y}(s) &= \frac{K_{co} H (T_{en}s + 1) s E_y(s)}{s (T_{en}s + 1) H + K_{co} K_{am} K_{en}}
 \end{aligned}$$

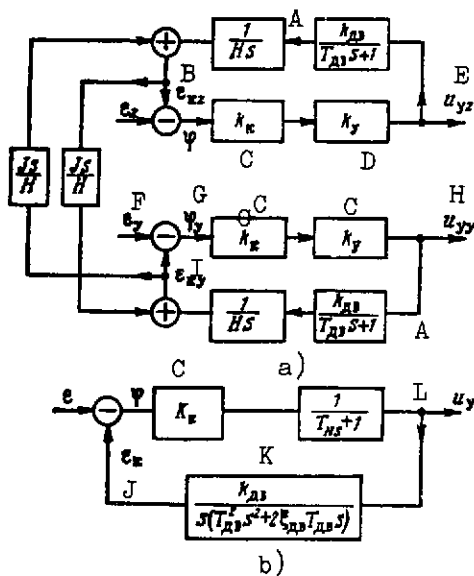


Fig. 3.25. Block diagrams of the control systems of a gyro-stabilized or ordinary (nongyro-stabilized) drive

a -- with one gyroscope
b -- with tracking drive

KEY: A -- $k_{en}/(T_{en}s + 1)$

B -- $\epsilon_{co.z}$ K -- $k_{en}/s(T_{en}s^2 + 2\xi_{en}T_{en}s + 1)$

C -- k_{co} L -- u_{am}

D -- k_{am}

E -- $u_{am.z}$

F -- ϵ_{am}

G -- ϕ_{am}

H -- $u_{am.y}$

I -- $\epsilon_{co.y}$

J -- ϵ_{co}

With steady-state motion, for a constant angular velocity of the sighting line we have $(K_{co} K_{am} K_{en})/H \gg 1.0$. Then

$$\left. \begin{aligned} u_{am.z} &= \frac{H}{K_{en}} \varepsilon_z; \\ u_{am.y} &= \frac{H}{K_{en}} \varepsilon_y. \end{aligned} \right\} \quad (3.58)$$

The presence of cross-coupling and gyroscope drift produces errors in the control signals $\Delta u_{am.z}$ and $\Delta u_{am.y}$, causing an added Δh overflight of the missile past the target (cf. Chapter Four)

/187

$$\left. \begin{aligned} \Delta u_{am.z} &= \frac{H}{K_{en}} \Delta \dot{\varepsilon}_z; \\ \Delta u_{am.y} &= \frac{H}{K_{en}} \Delta \dot{\varepsilon}_y. \end{aligned} \right\} \quad (3.59)$$

where $\Delta \dot{\varepsilon}_z$ and $\Delta \dot{\varepsilon}_y$ are the gyroscope drifts relative to the corresponding axes. It must be noted that an increase in the errors $\Delta \dot{\varepsilon}_z$ and $\Delta \dot{\varepsilon}_y$ occurs due to the sinusoidal signal at the gyro-stabilized drive $f(t) = a_0 \sin \omega_0 t$. This effect is most strongly evidenced for large bearing angles of the homing head. Fig. 3.26 presents the control errors $\Delta u_{am.z}$ as a function of the bearing angle ϕ_{be} for different a_0 and ω_0 .

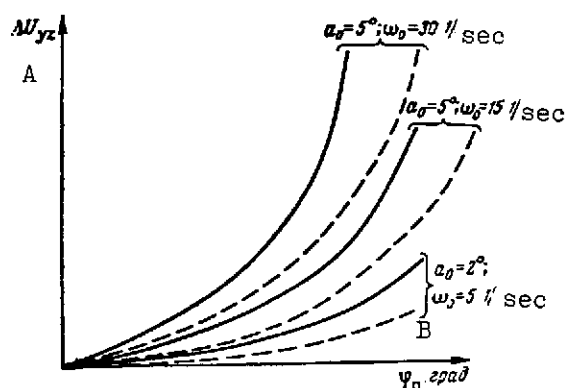


Fig. 3.26. False control signals $U_{am.z}$ in gyro-stabilized heads as a function of gyroscope drift
KEY: A -- $\Delta U_{am.z}$
B -- ϕ_{be} , deg

A gyroscopic drive of homing heads with two gyroscopes is shown in Fig. 3.24 b. Rings 15 and 16 are coupled via thrusts 17 and 18 to the radar antenna or to the optical coordinator of the IHH. The platforms rotate relative to the axes OY and OZ by the torque motors 1 and 14.

The motor windings receive control signals from the coordinator output, as a result of which gyroscopes 4 and 13 begin precessing. To compensate for the external torques, unloading motors

/188

8 and 7 are included in the gyroscopic system. Provision of an unloading channel reduces the gyroscope drifts and makes the gyro-stabilized drive more accurate. Fig. 3.26 shows with a dashed line the errors in the control signals for a two-gyro drive. Obviously, these errors lead to smaller overflights by the missile relative to the target.

With a large mass of the antennas or the optical coordinators, tracking electrical or hydraulic drives are used in the homing heads. A block diagram of one drive channel is shown in Fig. 3.25 b. To reduce the errors in the control signals from the effect of the missile's natural oscillations, the drives must be made in the wide-band version (with cutoff frequencies $\omega_c = 30-70 \text{ sec}^{-1}$), which poses certain technical difficulties.

Onboard digital computers of missiles. An inertial control system with various kinds of correction is used in long-range air-to-surface missiles (Hound Dog, Blue Steel, and others). These missiles use, as the onboard computing block, onboard computers fulfilling the role of second integrator and an installation processing data from astro- or radio-correction systems.

3.6. Onboard Devices of Ballistic Missiles and Missile Launch Vehicles

The makeup of the equipment of a ballistic missile and its arrangement are shown with the example of the three-stage Titan IIIC missile (Fig. 3.27). As Fig. 3.27 shows, the control compartment of the third stage includes the gyroscopic drive 1 for rotating the engine chamber of the third stage, an onboard digital computer 4, and inertial system equipment 5 (gyro-stabilized platform with accelerometers). Hydraulic drive 2 for turning the engine chamber of the second stage, rate gyro 6, and accelerometer 7 are located in the second stage of the missile. In the first stage are housed the system of hydraulic drives 9 for rotating the first-stage engine chambers, along with the hydraulic supply system of the first stage 3 and the rate gyro 8.

Gyro instruments and accelerometers of ballistic missiles. The gyro-stabilized platform of a ballistic missile is a three-ring dynamic system (Fig. 3.28). On the gyro-stabilized platform are mounted three 2FBG-2c floated integrating gyroscopes 2 with intrinsic drift of not more than 0.01 deg/hr, serving as the sensitive elements of the perturbing moments acting on the suspension axes of the gyro-platform. Also installed on the gyro-platform are the local vertical sensor 3, a prism for the azimuthal erection of the platform 4, and three integrating floated 25 PYGA5 gyro-pendulum integrating accelerometers. These gyroscopes, developed at the Massachusetts Institute of Technology for the Polaris BM, are used in many other ballistic missiles as linear velocity sensors for stabilizing the mass center of the

/189

missile on trajectory and for cutting off the sustainer engines. Additionally, they can be employed as local vertical sensors in the erection of the gyro-platform in the horizon at the launch point.

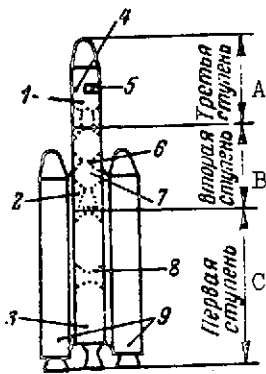


Fig. 3.27. Arrangement scheme of equipment on the three-stage Titan IIIC missile

KEY: A -- Third stage
B -- Second stage
C -- First stage

Their operating principle consists of, as a consequence of the nonalignment of the mass center and the gyroscope suspension center due to acceleration, an inertial moment being induced that causes the gyroscope to precess relative to the input axis. The rate of precession is proportional to the acceleration, and the turning angle of the gyroscope is proportional to the linear velocity.

The turning angle is compensated by the moment required to maintain the rotor in the assigned position (Fig. 3.29). In other words, the mismatch angle between the housing and the rotor of the gyroscope continually tends to zero. The signal is taken off with an electromagnetic device that simultaneously serves the function of a gyro suspension.

The gyro-platform rings are controlled by the potentiometers of gyroscopes 6, amplifiers 8, and torque motors 7 (cf. Fig. 3.28) /190

Temperature constancy is one of the main factors affecting the operating accuracy of a gyro-stabilized platform. To maintain temperature, the navigation and control systems of the Titan missile are provided with a liquid coolant system; its heat-exchanger temperature is monitored with a precision of fractions of a degree. The gyroscopic assembly is combined with the electronics block, containing the power sources and amplifiers controlling the servo-drives of the zero-setting of the position of the gyroscopes and accelerometers. All these assemblies are swept with conditioned air during the period of ground operations. The total weight of the gyro-platform is about 90 kg.

Azimuthal erection of the platform is carried out on the ground. In the silo wall is mounted an electrotheodolite receiving a beam from the main prism located on the ground and a beam reflected from a mirror placed on the gyro-stabilized platform. The mismatch signal generated by comparison of the directions of these beams is used to control the servo mechanisms bringing the gyro-stabilized platform into precise azimuth. /191

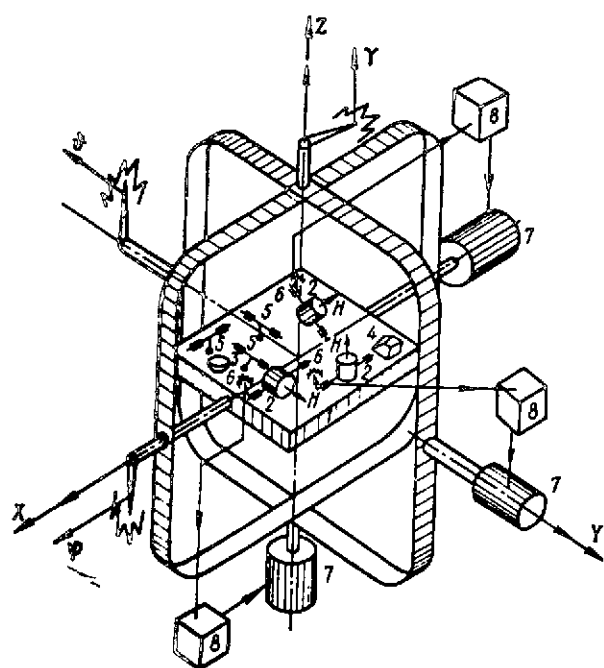


Fig. 3.28. Gyro-stabilized platform

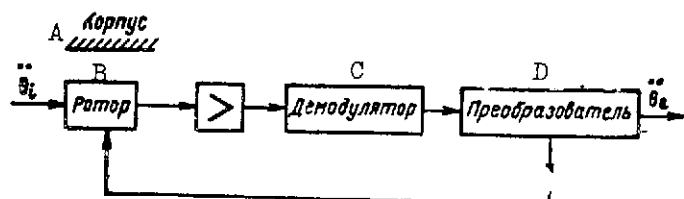


Fig. 3.29. Block diagram of floated integrating gyroscope

KEY: A -- Housing
B -- Rotor
C -- Demodulator
D -- Converter

Let us examine the errors of the gyro-stabilized platform due to gyroscope drift, imprecision of platform erection owing to an error in the tracking system, and deformation.

We will determine the errors of the gyroscopes in the gyro-stabilized platform by using the arrangement scheme of gyroscopes and accelerometers shown in Fig. 3.30. The overall accuracy of a gyroscope is evaluated with respect to the rate of its drift relative to the input axis

$$\varphi_i = e_i + \tilde{k}_n A_m + \tilde{k}_m A_n + q_i A_m A_n, \quad (3.60)$$

$$i = x, y, z,$$

where ϵ_1 is the constant gyroscope drift rate;
 k_n, k_m are the coefficients allowing for the effect of the unbalance of masses;
 q_1 is the coefficient allowing for the effect of the lack of equal ring rigidity; and
 A_n, A_m are the components of acceleration acting along the input axis and the rotor spin axis.

The effect of temperature is allowed for by the coefficients \tilde{k}_n and \tilde{k}_m .

Each term in the expression (3.60) leads to angular errors in the rotation of the gyro-platform. For example, for the placement of the x axis in the xy plane, we have

/192

$$\varphi_{xy} = \int_0^t (\epsilon_z + \tilde{k}_{nz}A_z + \tilde{k}_{mz}A_y + q_1A_yA_z) dt. \quad (3.61)$$

The errors ϕ_{xz} and ϕ_{yz} are determined by formulas similar to expression (3.61).

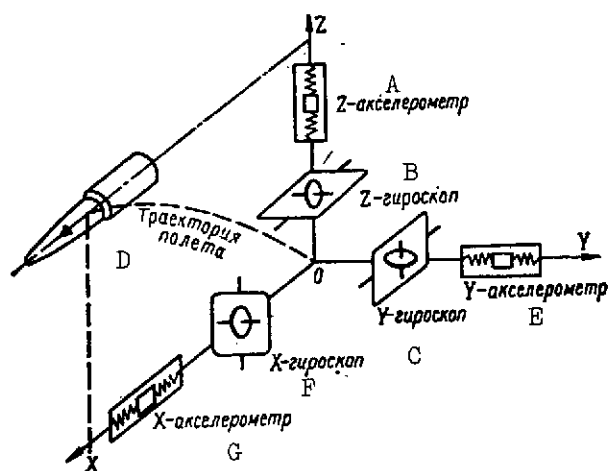


Fig. 3.30. Orientation scheme of gyroscopes and accelerometers on the gyro-stabilized platform

KEY: A -- Z-accelerometer
 B -- B-gyroscope
 C -- Y-gyroscope
 D -- Flight trajectory
 E -- Y-accelerometer
 F -- X-gyroscope
 G -- X-accelerometer

The values of the drift errors of different gyroscopes are given in Table 3.14 as a function of kinetic moment (according to D. Yarosh [43]).

From the table data it is clear that to obtain small drifts it is necessary to have larger rotor moments and small equivalent shifts. The latter requirement poses sizable technical difficulties.

/193

The errors in determining missile velocity due to gyroscope drift are

$$\begin{aligned}
&\text{due to constant speed} \\
&\Delta V_x = \int_0^t \left(\int_0^t \varepsilon_z dt \right) A_y dt; \\
&\text{due to unbalance of mass} \\
&\Delta V_x = \int_0^t \left(\int_0^t \tilde{k}_{xz} A_z dt \right) A_y dt; \\
&\Delta V_x = \int_0^t \left(\int_0^t \tilde{k}_{mz} A_z dt \right) A_y dt; \\
&\text{due to nonequifrigidity of rings} \\
&\Delta V_x = \int_0^t \left(\int_0^t q_z A_y A_z dt \right) A_y dt.
\end{aligned} \tag{3.62}$$

TABLE 3.14

Kinetic moment of gyroscope, g sec m ² /sec	Weight of rotor, g	Angular drift rate, deg/hr	Drift moment, dynes/cm	Equiv. rotor displacement, mm
100 000	35	0.1	0.05	43.2 · 10 ⁻⁶
100 000	35	0.01	0.005	4.32 · 10 ⁻⁶
2 000 000	260	0.01	1.0	100 · 10 ⁻⁶
2 000 000	260	0.001	0.1	1 · 10 ⁻⁶

The platform placement accuracy is evaluated by the formula

$$\varphi_{nm} = \varphi_{nm}(0) + \tilde{\varepsilon}_l + p_{nm} A_n + r_{nm} A_m, \tag{3.63}$$

where ϕ_{nm} is the angular error in the direction of the n axis in the nm plane, and $\phi_{nm}(0)$ is the adjustment error of the gyro-platform during the erection at the launch point.

Using formula (3.63), let us determine the errors in the determination of velocity that are due to the angular errors of the gyro-platform

$$\left. \begin{aligned} \Delta V_{x_1} &= \varphi_{xy}(0) \int_0^{t_{en}} A_y dt; \\ \Delta V_{x_2} &= \tilde{e}_i \int_0^{t_{en}} A_y dt; \\ \Delta V_{x_3} &= \int_0^{t_{en}} p_{xy} A_y dt; \\ \Delta V_{x_4} &= \int_0^{t_{en}} Z_{xy} A_y^2 dt. \end{aligned} \right\} \quad /194 \quad (3.64)$$

All these integrals are computed to the engine cutoff instant t_{en} . Thus, the maximum error in the determination of velocity^{en} due to imprecision in the direction of the input axis of the X-accelerometer is

$$\Delta V_{x_\Sigma} = \Delta V_{x_1} + \Delta V_{x_2} + \Delta V_{x_3} + \Delta V_{x_4} + \Delta V_{x_5} + \Delta V_{x_6} \quad (3.65)$$

The error ΔV_{x_Σ} has a major effect on the impact accuracy of the ballistic missile's warhead on the target.

Gyroscopic sensors of angular velocity (Fig. 3.29) are used in the stabilization loops of ballistic missiles. They take account of the existing deformation of the missile as affecting the stability of the loops. The main characteristics of foreign-built angular velocity sensors are given in Table 3.15 [77].

TABLE 3.15

Instrument model	Meas. range, $\frac{\text{deg}}{\text{sec}}$	Sensitivity thresh. $\frac{\text{deg}}{\text{sec}}$	Natural freq., $\omega_0, \frac{1}{\text{sec}}$	ξ	Weight, kg
T-2008-1A-10	10	—	140	0.4—0.8	750
T-2008-1A-29	30	0.02	120	0.4—1.0	750
T-2008-1A-90	90	0.1	240	0.4—1.2	750

Accelerometers. Errors of accelerometers also strongly affect the impact accuracy of a ballistic missile on its target. /195

$$\Delta \dot{V}_n = B_n + k_{1n}A_n + k_{2n}A_n^2 + k_{3n}A_n^3 + m_n A_m + m_{1n}A_m A_n + n_n A_z + n_{1n}A_z A_n, \quad (3.66)$$

where B_n is the error due to the imprecise placement of the accelerometer zero point;
 k_{1n} is the linear component of the accelerometer transmission factor;
 k_{2n}, k_{3n} are the nonlinear components of the accelerometer transmission factor;
 m_{n1}, n_n is the shift of the accelerometer zero point due to cross-coupling; and
 m_{1n}, n_{2n} are the linear components of the transmission factor due to the cross-coupling effect.

Errors in the determination of missile velocity by one channel (that is, when $\phi_{xy} = 0$ and $\phi_{xz} = 0$) and with the nonlinear components neglected are

$$\left. \begin{aligned} \Delta V_x &= \int_0^t (B_x + k_{1x}A_x) dt; \\ \Delta V_x &= \int_0^t (m_n + m_{1x}A_y A_x) dt; \\ \Delta V_x &= \int_0^t (n_n + n_{1n}A_z A_x) dt. \end{aligned} \right\} \quad (3.67)$$

Thus, the maximum error in the velocity due to accelerometer errors can be determined with the formula

$$\Delta \bar{V}_{x_z} = \Delta V_x + \Delta V_x + \Delta V_x. \quad (3.68)$$

The values of accelerometer errors as a function of pendulosity (according to D. Yarosh [43]) are given in Table 3.16.

Table 3.17 presents the main characteristics of accelerometers [77].

Recently, integrating pendulum gyroscopes have begun to be used in ballistic missiles [43]. The main characteristics of the integrating gyroscopes are given in Table 3.18.

Individual error components in the determination of the missile velocity ΔV_x , ΔV_y , and ΔV_z -- in actual calculations -- can be regarded as independent and subject to the normal

distribution law. Then

$$\sigma_{\Delta V_i} = \sqrt{\frac{\sum_i (\Delta V_i - \Delta V_{av})^2}{n}}, \quad (3.69)$$

where $\sigma_{\Delta V_i}$ is the mean-square error in the missile velocity (X, Y, or Z must be substituted for i), and ΔV_{av} is the mean error.

In using formula (3.69), the maximum error in the determination of the velocity must be determined as

$$\Delta V_{i \max} = 3\sigma_{\Delta V_i} \quad (3.70)$$

TABLE 3.16

/196

Pendulo- sity* of accelero- meter, g·cm	Active mass, g	Overall error in fractions of g	Error moment, dynes·cm	Equivalent mass change, g
1.0	1.0	1·10 ⁻⁴	0.1	1000·10 ⁻⁶
1.0	1.0	2·10 ⁻⁵	0.02	200·10 ⁻⁶
80.0	8.0	2·10 ⁻⁵	0.16	160·10 ⁻⁶
80.0	8.0	1·10 ⁻⁶	0.08	8·10 ⁻⁶

* The pendulosity of an accelerometer refers to the product of its mass by the pendulum length.

TABLE 3.17

/197

Instru- ment model	Type of instru- ment	Sensi- tivity thresh- old, g	Meas. preci- sion, %	Meas. range, g	0, 1 sec	Weight, g
F-2401	Pendulum	5·10 ⁻⁵	0.01	±20	1100	110
LA-800	Linear	1·10 ⁻⁴	—	1-80	—	90
A-141-02	Pendulum	5·10 ⁻⁵	0.01	±15	—	200
A-200, A-300	"	5·10 ⁻⁵	0.01	±20	—	75

For higher accuracy of inertial control systems in ballistic missile flight various methods of compensating for the equipment errors are used. For example, the shifting of the zero point of an accelerometer (this compensation is most often performed

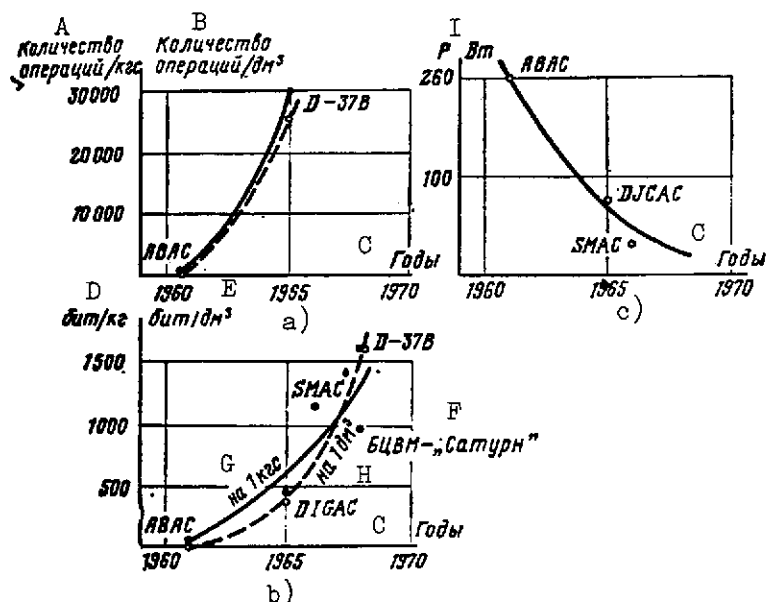


Fig. 3.31. Main characteristics of onboard digital computers of ballistic missiles:

- a -- mean operating speed per kg of weight and per decimeter³ of volume of computer
- b -- volume of memory per kg of computer weight and per decimeter³ of computer volume
- c -- required power

KEY: A -- Number of operations/kg
 B -- Number of operations/decimeter³
 C -- Years
 D -- Bits/kg
 E -- Bits/decimeter³
 F -- Saturn onboard computer
 G -- per kg
 H -- per decimeter³
 I -- P, watts

with jet accelerometers); supplementary turning of the gyrosta-
bilized platform; and control of gyroscope precession.

TABLE 3.18

Instru- ment model	Kinetic moment, $\text{g}\cdot\text{cm}^2/\text{sec}$	Drift, deg/hr			Weight, g	Power, w
		inde- pendent of g	propor- tional to g	propor- tional to g^2		
MIG	100	—	0.5	—	220	2.5
OG-37	1020	—	0.05	—	2040	—
G-1-H5	30	3	3	0.18	2830	3
G-T1-B	1800	—	—	—	1590	6

Onboard digital computers of ballistic missiles provide control of missile flight (implementing the flight program and controlling engine cutoff), monitor onboard and ground system equipment, and so on. The main characteristics of onboard digital computers are given in Table 3.19. As we can see from the data in Table 3.19, computers of this class are light in weight and take up little space. The operating speed of an onboard computer is quite high and amounts to 500,000 operations per second [125]. Fig. 3.31 a - c presents functions characterizing trends in the development of computers. At the present time high reliability indicators of computers have been achieved (the mean error-free operating period of the best onboard computers is 15,000 hours).

[199]

TABLE 3.19 ONBOARD DIGITAL COMPUTERS OF BALLISTIC MISSILES AND MISSILE LAUNCH VEHICLES

Name of onboard computer	Yr. made	Country	Name of missile	Characteristics of onboard computer								
				type of elements	number of digits	time add. multip.	Type of memory	Memory capacity	Access time, μ sec	Req. power, w	Weight, kg	Volume, dm ³
ABAC	1960	U.S.	Atlas	Semiconductors	28	$\frac{125}{1000}$	Quartz delay lines	$\frac{128}{2048}$			80	226,5
DJGAC	1963	U.S.		Semiconductors	16		Ferrite cores	$\frac{64}{2048}$		75	11,8	9,1
D26I-1	1965	U.S.		Integrated circuits	12-16	$\frac{8}{18}$	Ferrite cores	8192		50	5,9	~4,8
D-37B	1965	U.S.	Minute-man	Integrated circ.	24		Magnetic discs	6912		30	16,5	20,2
Titan on-board computer	1964	U.S.	Titan III	Integrated circ.	16-24	$\frac{150}{2000}$	Ferrite cores	9742	4	110	12,6	13,5
SMAC	1965	U.S.		Integrated circ.	26	$\frac{16}{78}$	Thin films	~8000	8	30	7	5,4
Onboard computer of Saturn	1964	U.S.	Saturn V	Hybrid integrated circuits	28	$\frac{80}{328}$	Ferrite cores	8x4096		130	34,9	68

FOOTNOTES

¹ The last figure is quite understandable if it is considered that in a modern civil aircraft there are about 2000 connections; if each of them has $T_{av} = 10^7$ hours, the mean time between two failures of the entire system due only to the connections will be $5 \cdot 10^3$ hours. Converting the electronic circuits of civil aircraft to microelectronic circuits will permit an increase in the T_{av} of all the electronic circuits to $5 \cdot 10^3$ hours (including the improvement gained by reducing the number of connections).

² The noise factor is expressed in decibels, that is, $10 \lg k_{no}$. Noise factors of receivers depend on wavelength.

In actual calculations, the following data can be useful /101/:

λ , cm	2-6	10-40	100 and above
k , db	10-20	7-14	5-10

³ Here $z = \sqrt{-2 \ln F} \approx 2.14 \sqrt{p}$.

⁴ In formula (3.42) it is assumed that the displacement velocity of the transmitter is somewhat larger than the radio signal propagation velocity.

⁵ OA and OB are the right and left beams of the Doppler radar, respectively (cf. Fig. 3.21 a).

⁶ The mean operating speed of the onboard computer was determined in carrying out programs when short operations (addition or equivalent operations) represent 90 percent, while long (multiplication) operations represent 10 percent of the total number of operations.

⁷ ϕ_{xy} is the error of placement of the X-accelerometer in the xy plane due to drift of the Z-gyroscope.

CHAPTER FOUR
COMBAT AND TECHNICAL CAPABILITIES OF CONTROL SYSTEMS OF
AIRCRAFT AND MISSILE COMPLEXES

/200

Combat capabilities of control systems of aircraft and missile complexes are determined by the kind of mission performed, the assigned conditions of combat application, and the tactical-flight characteristics of flight craft. When considering combat flight craft, the means of armament, nature and intensity, and counter-measures of the enemy, and other factors are vital. Therefore an exhaustive evaluation of the capabilities of these complexes represents a very difficult mathematical problem, whose solution often cannot be obtained in a final form.

When designing military systems, combat capabilities of complexes are evaluated based on deterministic requirements, among which we can include the lines of interception, practical operational radius, altitude of combat application, bomb load, time for performance of combat mission, and so on.

Strictly speaking, their values change randomly from aircraft to aircraft (of the same model). However, these differences are so small that they are usually neglected. Foreign military specialists ([134, 170, 171]) use one or two generalized criteria permitting a comparison of the capabilities of control systems in evaluating the capabilities of each of the complexes. For example, the evaluation of complexes of interceptors can be made on the basis of the lines of interception with respect to the flight altitudes of targets. Combat capabilities of multimission fighters and bombers can be evaluated from their operational radii with complete payload for adopted types of flight profiles. Capabilities of transport aircraft ([35, 36]) are evaluated by hauling costs (ton-kilometers in rubles)¹. /201

Capabilities of missile complexes [66] can be evaluated by the target interception zones if the interception is executed by surface-to-air or air-to-surface missiles; an air-to-surface missile complex is evaluated by the zones of possible launch. Capabilities of long-range ballistic missiles [39, 96] are determined by the types of the flight trajectory for both the missile itself, as well as its warhead and, in addition, by the warhead characteristics. The time for executing an assignment -- the interception time -- is vital for aircraft and antiaircraft interception complexes. In determining its value, the requisite condition of the equality of the flight time of the interceptor and the flight time of the target up to the impact (interception) point must be satisfied. It is called the time balance condition and is written in the form

$$T_t = \sum_{i=1}^n t_{in.i} , \quad (4.1)$$

where T_t is the flight time of the target up to the impact point, and
 $t_{in.i}$ is the time required by the interceptor to perform the successive stages of interception.

Summation is extended over all stages from the instant of target detection to the instant firing begins or the missile fuse is activated.

Equation (4.1) allows us to determine several parameters characterizing both the complexes, as well as the interception processes. The sum appearing in the right side of equality (4.1) can be expanded as follows:

$$\sum_i t_i = t_{de} + t_{pre} + t_{ap} + t_{at} , \quad (4.2)$$

where t_{de} is the time required by the commander to make a decision on target interception;
 t_{pre} is the time required to prepare the interceptor from the moment the command is transmitted up to the takeoff; /202
 t_{ap} is the time needed for the interceptor to approach the target; and
 t_{at} is the time required by the interceptor to get into a position suitable for firing and destroying the target.

The two left terms depend both on the initial conditions (takeoff conditions) and the target flight trajectory, as well as on the maneuvering characteristics of the interceptor. In turn, they can be represented as the sum of several terms, each of which depends on the parameters of acceleration and climb in the vertical plane, or on the turn parameters, or else on the parameters and the selected method of guidance in the horizontal plane.

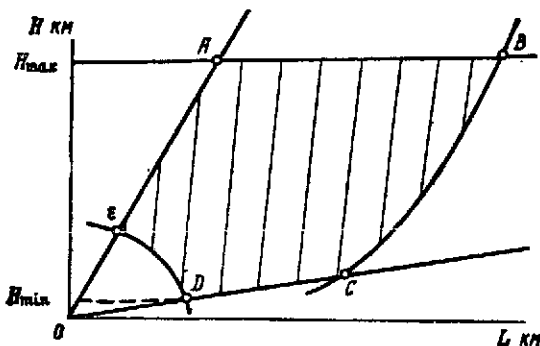


Fig. 4.1. Region of air target interception

The interception complexes are also characterized by the interception region. Fig. 4.1 presents the region of air target interception by aircraft or missile complexes.

It is bounded by the following surface, whose traces are shown in Fig. 4.1 by the following lines: DC bounds the minimum target flight altitude at which it can still be intercepted; AB bounds the maximum altitude at which the given airplane or missile can still perform the interception; the ray AO corresponds to the largest tracking angle of target and interceptor (aircraft or missile) by radar; BC corresponds to the maximum range of the interception missile or aircraft complex; and OE corresponds to the minimum interception range. The larger the interception range for the same initial weight of the flight craft, the greater are the combat capabilities of the complex.

Now let us turn to evaluations of the combat capabilities of various interception and attack complexes based on the main generalized characteristics.

4.1. Interception Lines of Fighter-Interceptors

As already stated, the main characteristic of the combat use of fighter-interceptors is the interception line, i.e., the maximum distances from the takeoff point of the aircraft to the point of air-to-air missile launch or firing of cannon-gun armament. There are several interception schemes, of which two are the most important [72, 215].

The first scheme consists of when the interceptor must attack the target in the shortest time (high-speed interception). In this case the interceptor flight takes place practically entirely at top speed. In Fig. 4.2 a-b is shown the flight profile of a fighter executing a high-speed interception in the frontal and rear hemispheres. When the aircraft returns to the airfield, it must have an unspent fuel reserve equal to 7 percent other than the fuel reserve in the main tanks.

Let us represent the time expended in making the flight for high-speed interception in the rear hemisphere in the form

$$t_{ap} = t_{ac_1} + t_{cl_1} + t_{ac_2} + t_{cl_2} + t_{le_1} + t_{d.at} + t_{gl_1} + t_{le_2} + t_{gl_2} + t_{la}, \quad (4.3)$$

where t_{ac_1} is the time spent in acceleration with afterburner to $V = 1000$ km/hr;
 t_{cl_1} is the time spent in climbing to the altitude $H = 10$ km with afterburner at $V = 1000$ km/hr;
 t_{ac_2} is the time spent in acceleration to $M = 2.0$;
 t_{cl_2} is the time expended in climbing to the altitude $H = 17$ km;

t_{le1} is the time spent in level flight at $M = 2.0$ with afterburner until the moment of target attack;
 $t_{p.a}$ is the time required by the aircraft to disengage from the attack;
 t_{gl1} is the time spent in gliding with deceleration down to $H = 13$ km, $V = 1000$ km/hr;
 t_{le2} is the time spent in level flight at $V = 1000$ km/hr at $H = 13$ km (return to airfield);
 t_{gl2} is the time expended in gliding down to the glide path leg; and
 t_{la} is the time spent in flying along the glide path and landing.

/205

Knowing all these quantities, one can determine the maximum lines of high-speed interception R_{max} when a fighter is sent to the air on a signal from a long-range radar emitted at a distance of R_{fo} from the airfield and with an air target detection range $R_{det} = 600$ km (cf Fig. 4.2 a & b):

$$R_{in\ max} = R_{det} + R_{fo} - V_t(t_{in.cal} + t_{pre} + t_{ac1} + t_{cl1} + t_{ac2} + t_{cl2} + t_{le1}) . \quad (4.4)$$

Here V_t is the target velocity.

Here the following condition must be met:

$$0.07 G_{m.fu} = G_{m.fu} - (G_{tax} + G_{ac1} + G_{cl1} + G_{ac2} + G_{cl2} + G_{le1} + G_{d.at} + G_{le3} + G_{gl2} + G_{la} + G_{gl1}) , \quad (4.5)$$

where $G_{m.fu}$ is the weight of fuel in the main tanks;

G_{tax} is the weight of fuel expended in aircraft taxiing; and G_{ac1}, G_{cl1} , etc. are the amounts of fuel consumed in individual flight phases.

High-speed interception lines as a function of target flight altitude when it is attacked in the frontal hemisphere and for a given R_{fo} value are constructed based on these formulas in Fig. 4.3 a.

The time spent in flying in high-speed interception in the rear hemisphere is increased by the time needed in making a 180° turn (cf formula (2.9)) and by the attack time t_{at} :

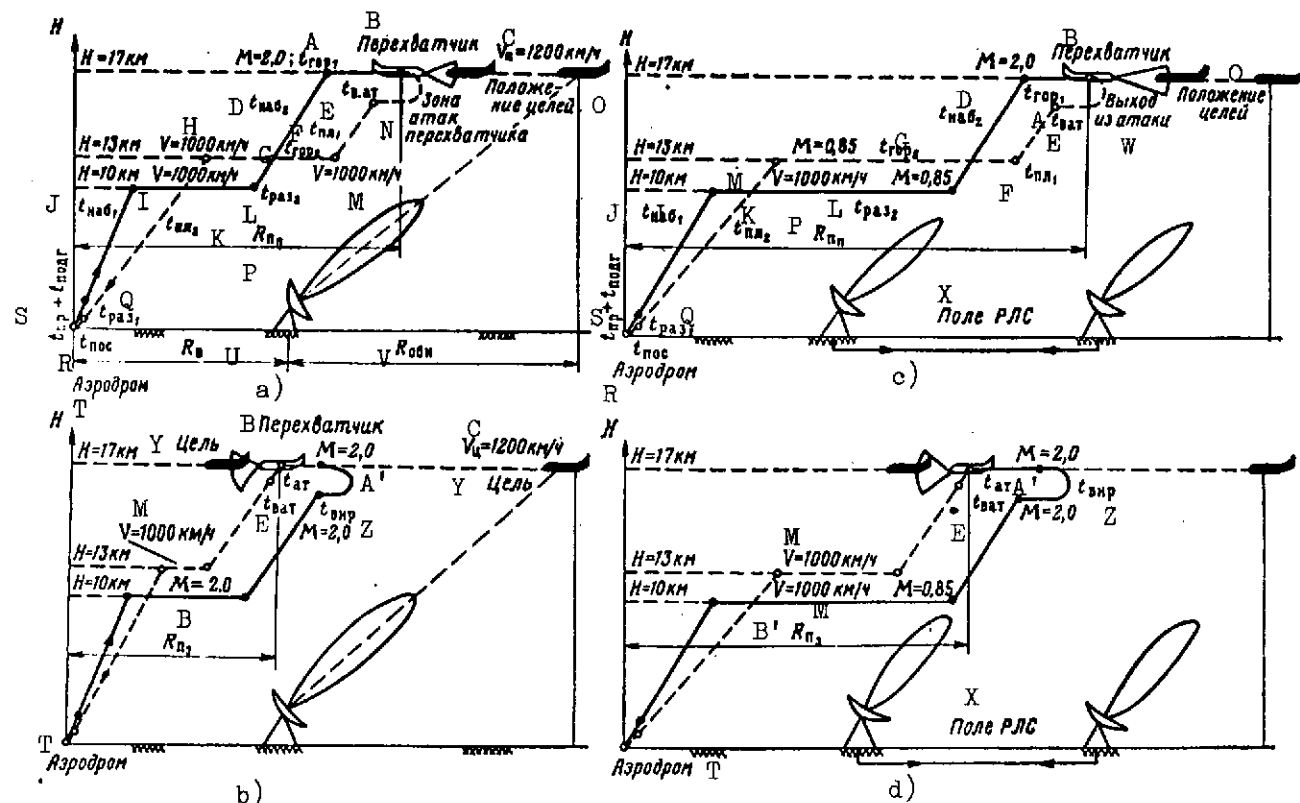


Fig. 4.2. Fighter flight profiles in the interception of an air target [Continued]

L -- t_{ac_2}
M -- $V = 1000 \text{ km/hr}$
N -- Interceptor attack zone
O -- Position of targets
P -- $R_{in_{fr}} \angle \bar{R}_{in_{fr}} = R_{interceptor_{frontal \text{ hemisphere}}}$
Q -- t_{ac_1}
R -- t_{gl_2}
S -- $t_{de} + t_{pre}$
T -- Airfield
U -- R_{fo}
V -- R_{det}
W -- Disengagement from attack
X -- Radar field
Y -- Target
Z -- t_{tu}
A' -- t_{at}
B' -- $R_{in_r} \angle \bar{R}_{in_r} = R_{interceptor_{rear \text{ hemisphere}}}$

$$t_{ap_3} = t_{ap_{in}} + t_{tu} + t_{at} \quad (4.6)$$

The fuel consumption (4.5) is here also increased by G_{tu} and G_{at} .

The high-speed interception lines when a target is being attacked in the rear hemisphere are also plotted in Fig. 4.3 a, [206] in which it is clear that the lines of high-speed interception by modern interceptors extend to several hundreds of kilometers.

The second scheme consists of when the interceptor must strike the target at the greatest distance from the airfield deep within its own territory (long-range interception). In this case the interception is executed in the radar field of stations, and the flight is performed with nonafterburner regimes and only on approach to the target does the fighter use its afterburner (Fig. 4.2, c,d).

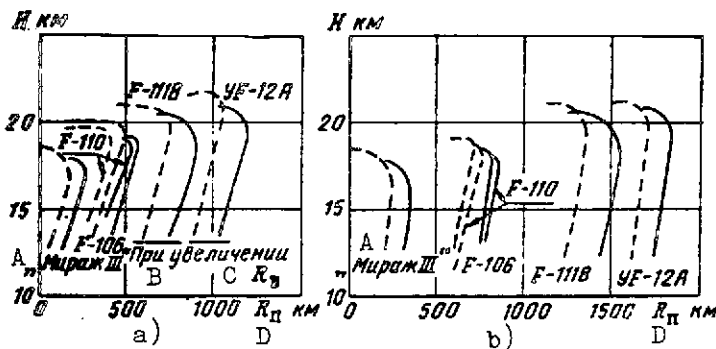


Fig. 4.3. Fighter interception lines:
 a -- In high-speed interception
 b -- In long-range interception
 — frontal hemisphere
 --- rear hemisphere
 KEY: A -- Mirage III
 B -- With increase in R_{fo}
 C -- R_{fo} D -- R_{in}

The long-range interception lines when targets are being attacked in the rear and frontal hemispheres are plotted in Fig. 4.3 b. In the second interception scheme the lines of the given interception are appreciably longer and are 1200 - 1400 km for the best aircraft.

The combat assignment will be successfully executed by the fighter-interceptor if the ORAD [onboard radar] detects the target at R_{det}^{ORAD} and locks onto the target at R_{cap}^{ORAD} . The onboard radar has a scanning sector in which the air target must enter. This is attained by leading the interceptor with ground facilities with given $R_{cap}^{ORAD} < h_{in}$ and velocities V_{in} and V_t into the zone of possible aircraft attacks.

The leading error h_{in} of the interceptor using ground facilities is determined by the following formulas (cf Fig. 4.4): /207

$$\begin{aligned} \eta &= \arcsin \left(\frac{V_t \cos \varphi_t}{V_{in}} \right); \\ R_{in} &= \sqrt{R_t^2 + r^2 - 2R_t r \cos \varphi_{im}}; \\ \psi_1 &= \arcsin \left[\frac{r \sin (\pi - \varphi_{im})}{\sqrt{R_t^2 + r^2 - 2R_t r \cos \varphi_{im}}} \right]; \\ \mu &= \psi_1 + \varepsilon_t \pm \varepsilon_{in} \\ \delta &= \arctan \frac{\left(R_t + \frac{V_t}{V_{in}} r \pm \Delta R_{RAD} \right) \sin \mu}{R_t \pm \Delta R_t - \left(R_t + \frac{V_t}{V_{in}} r \pm \Delta R_{in} \right) \cos \mu}; \\ v &= \mu \pm \varepsilon_t - \frac{\pi}{2} + \delta; \end{aligned} \quad (4.7)$$

$$\begin{aligned}
 \varphi_t &= \pi - \mu - \delta; \\
 \theta_{in} &= \eta - \nu \pm \epsilon_\theta; \\
 h_{in} &= \left(R_{in} \cos \varphi - R_t - \frac{V_t}{V_{in}} r \right) \cos \theta_{in} - \\
 &\quad - r \sin(\pi - \varphi_{in}) \left(\sin \theta_{in} - \frac{V_t}{V_{in}} \right),
 \end{aligned}
 \tag{4.7}$$

where R_{in} is the initial range from the ground radar to the fighter-interceptor; R_t is the distance from the ground radar to point C_1 (impact point); ΔR_t is the error of the radar in determining the range to the target; ΔR_{in} is the error of the radar in determining the range to the fighter-interceptor; ϵ_θ is the error of the radar in determining the target azimuth; ϵ_{in} is the error of the radar in determining the azimuth of the fighter-interceptor; ϵ_θ is the error in determining the fighter-interceptor heading; θ_{in} is the true heading of the fighter-interceptor; $\theta_{in.cal}$ is the calculated heading of the fighter-interceptor; $V_{t.cal}$ is the calculated airspeed of a target; V_t is the true airspeed of the target; and h_{in} is the error in guidance of the fighter-interceptor.

The fighter-interceptor guidance errors h_{in} are determined by formulas (4.7) in relation to the initial conditions, ground radar errors, and the variation of h_{in} as a function of the quantities ϵ_t and ϵ_{in} is plotted in Fig. 4.5 [72]. From this graph it is clear that an increase in radar error leads to an increase in the error in guiding the fighter-interceptor to the target, therefore, to an increase in the required capture range of the ORAD.

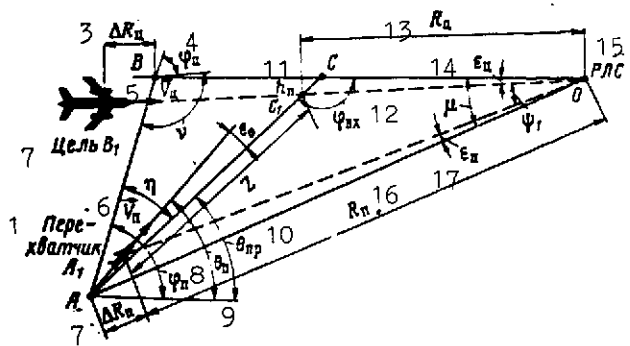


Fig. 4.4. Main symbols in the scheme of guidance of an interceptor to a target

KEY: 1 -- Interceptor

2 -- Target B_1

3 -- ΔR_t

4 -- ϕ_t

5 -- \vec{V}_t

6 -- \vec{V}_{in}

7 -- ΔR_{in}

8 -- ϕ_{in}

9 -- θ_{in}

10 -- $\theta_{in.cal}$

11 -- h_{in}

12 -- ϕ_{im} [$im = impact$]

13 -- R_t

14 -- ϵ_t

15 -- Radar

16 -- R_{in}

17 -- ϵ_{in}

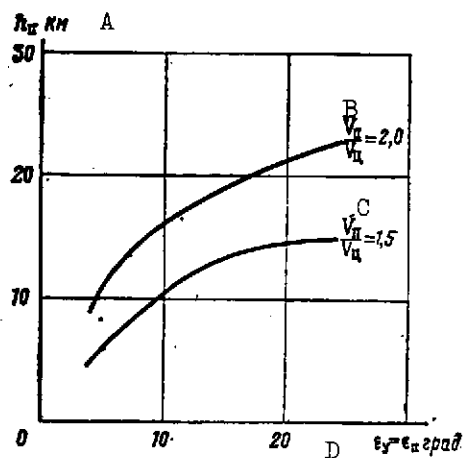


Fig. 4.5. Guidance errors of fighter-interceptor h_{in} as a function of errors

ϵ_t and ϵ_{in} of ground radar. $R_t = 200$ km, $\Delta R_{in} = \Delta R_t = 3.3$ km

KEY: A -- h_{in}

B -- $V_{in}/V_t = 2.0$

C -- $V_{in}/V_t = 1.5$

D -- $\epsilon_t = \epsilon_{in}$, degrees

4.2. Operational Radii of Multimission Fighters and Bombers

The high level of equipment of AAD with missile complexes radically alters the tactics of the combat use of attack aircraft. Aircraft of this type began to deliver means of attacking ground targets either at high flight altitudes (close to the maximum) or

at low flight altitudes (100-200 m), which strongly reduced the probability of their being hit by antiaircraft missiles and fighter-interceptors.

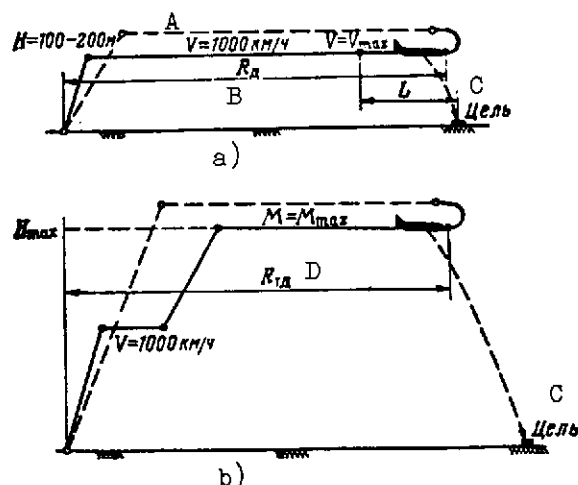


Fig. 4.6. Flight profiles of multimission fighters and bombers

KEY: A -- $V = 1000$ km/hr
B -- R_{str}
C -- Target
D -- $R_{l str}$

Multimission fighters supplied with bombs and air-to-surface missiles, and also bombers can perform flights in three of the most expedient flight profiles.

The first profile is when the flight is performed entirely at a low altitude (so-called low-altitude flight). In this case after climbing to $H = 100-200$ km, the flight is performed at the velocity $V = 1000$ km/hr until the aircraft reaches a distance to the target $L = 80-100$ km, after which the flight velocity is increased to V_{max} (usually this is 1200-1300 km/hr). After dropping the bombs and releasing the air-to-surface guided missiles, a turn is performed and the aircraft returns to its airfield, initially at V_{max} , but then its speed is reduced to $V = 1000$ km/hr (Fig. 4.6 a).

/210

The second profile is when the flight is executed at a high altitude at the speed V ($M = M_{max}$) (so-called high-speed, high-altitude flight). Here the aircraft climbs to $H = 10$ km, then executes level flight at $V = 1000$ km/hr, and again climbs to the assigned altitude. Flight at the assigned altitude can be performed at $M = M_{max}$. After dropping the bombs and releasing the missiles, the aircraft turns around and returns to its airfield also at $M = M_{max}$. In the leg to the airfield, the aircraft glides in and lands (cf Fig. 4.6 b).

The third flight profile does not differ in any manner from the second, however flight at H_{max} toward the target and the return to the airfield is performed at $M = 0.9$ (so-called long-range, high-altitude flight). Fig. 4.7 presents the operational radii of multimission fighters and bombers as a function of flight altitude. An increase in the payload weight reduces the operational radii of attack fighters and bombers and reduces the altitudes of their

/211

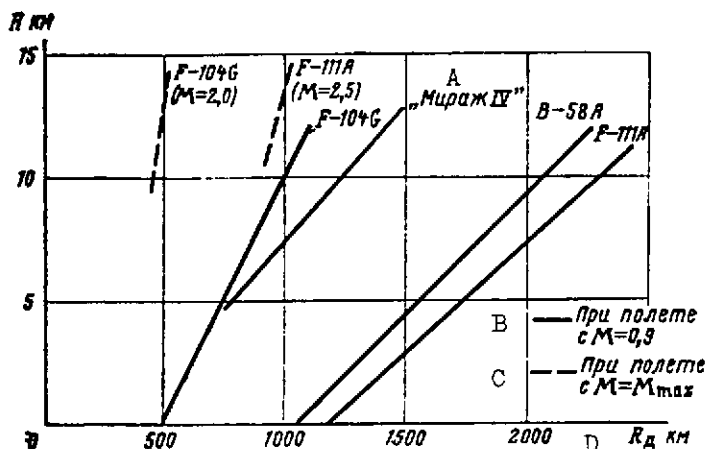


Fig. 4.7. Operational radii of multimission fighters and bombers as a function of flight altitude for normal payload weight (without auxiliary fuel tanks)

KEY: A -- Mirage IV
B -- For flight at $M = 0.9$
C -- For flight at $M = M_{\max}$
D -- R_{str}

combat use. Fig. 4.8 shows the dependence of the bomb load weight on the range of the B-52C bomber, and Fig. 4.9 shows the decrease in the flight altitude of the B-58, Mirage IV, and F-104G as a function of payload weight (bombs and missiles in mountings).

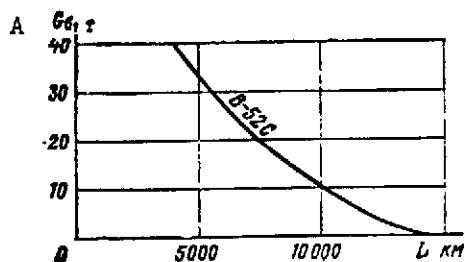


Fig. 4.8. Variation in range of B-52C bomber as a function of bomb load weight
KEY: A -- G_b [G_b = bombs]

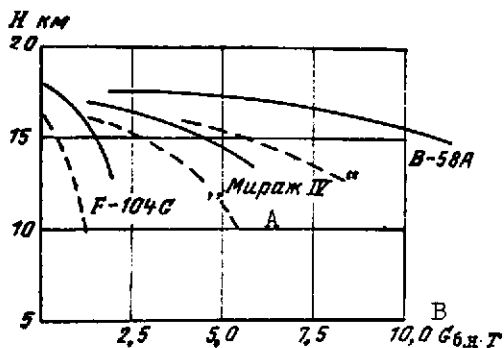


Fig. 4.9. Variation in combat-use altitude of the B-58, Mirage IV, and F-104 as a function of payload weight:

— Afterburner
---- Without afterburner
KEY: A -- Mirage IV
B -- G_{pay} , tons

4.3. Operating Economy of Transport Aircraft

The operating economy of transport aircraft is the mean indicator characterizing the costs of cargo or passenger transportation. The indicator of operating economy, as is usual, refers to the cost of a ton-kilometer in rubles [35], i.e.,

/212

$$C = \frac{P_{op}}{\Pi}, \quad (4.8)$$

where P_{op} are the costs of operating the aircraft for one flight hour, in rubles/hr; and
 Π = planned aircraft capacity in tons·km/hr.

The capability of a transport aircraft is determined by its planned hourly capacity, which depends on the aircraft's payload and flight velocity. Planned capacity is determined by the formula

$$\Pi = K_{pay} G_{pay} V_{gr}, \quad (4.9)$$

where G_{pay} = maximum payload in tons;

V_{gr} is the aircraft's design speed; and

K_{pay} is the payload factor (based on the standards of the Civil Aviation Fleet, $K_{pay} = 0.65$).

The design aircraft speed can be found by using the following function:

$$V = \frac{L}{\left(\frac{L - L_{to.cl}}{V_{cru} + W}\right) + t_{to.cl}} \quad (4.10)$$

where L is the difference between airfields in km;

$L_{to.cl}$ is the horizontal projection of the route covered by the aircraft during the takeoff, climb, descent, and landing, in km;

V_{cru} is the flight cruising speed, in km; [sic]

$t_{to.cl}$ is the time spent in taxiing, takeoff, climbing, acceleration, descent, gliding, and landing ($t_{to.cl} = 15$ minutes for turboprop aircraft, and $t_{to.cl} = 10$ minutes for turbojet aircraft); and

W is the wing velocity, in km/hr (usually W is taken as 50 km/hr).

The maximum payload is usually indicated in the main technical characteristics of aircraft (cf Tables 2.7 and 2.8). The payload can be calculated by the following formula for passenger aircraft:

$$G_{co} = 75N + qN + 290 \left(V_{bag} - \frac{qN}{120} \right) \text{ kg} \quad (4.11)^2 \quad \underline{213}$$

where N is the number of passenger seats;

q is the weight of one passenger's baggage ($q = 30$ kg for main lines of the CAF Civil Aviation Fleet and $q = 15$ kg for local CAF lines); and

V_{bag} is the capacity of the baggage and cargo compartments of the aircraft in m^3 .

Thus, to determine the costs of flights at varying speeds (formula (4.8)), it remains to determine the costs in operating the aircraft for one flight hour. In accordance with the method adopted for the CAF, operating costs per flight hour depend on the amortization of the aircraft ($P_{a.a}$, amortization of the engines $P_{a.en}$, outlays for repair and maintenance P_{ma} , fuel costs P_{fu} , and crew wages $P_{c.w}$:

$$P = 1.35K'(P_{a.a} + P_{a.en} + P_{t.e} + P_{c.w}), \quad (4.12)$$

where K' is the coefficient allowing for other direct costs (overhead costs are allowed for by a coefficient of 1.35).

Individual terms appearing in formula (4.12) are calculated using the following expressions:

$$\left. \begin{aligned} P_{a.a} &= \frac{C_a \left[1 + K_{\text{cap.a}} \left(\frac{T_a}{t_a} - 1 \right) \right]}{T_a}; \\ P_{a.en} &= \frac{C_{en} \left[1 + 0.2 \left(\frac{T_{en}}{t_{en}} - 1 \right) \right] N_{en}}{T_{en}} \end{aligned} \right\} \quad (4.13)$$

where C_a is the price of the new aircraft (without engines), in rubles;

T_a is the amortization, or total service life of the aircraft, in hours;

t_a is the service life of the aircraft between two overhauls, in hours;

$K_{\text{cap.a}}$ is the ratio of the cost of one overhaul to the price of the new aircraft without engines (usually, $K_{\text{cap.a}}$ is taken as 0.1-0.12);

C_{en} is the cost of a new engine in rubles;

T_{en} is the amortization, or total service life of an engine, in hours;

t_{en} is the interrepair service period of an engine service life, in hours; and

N_{en} is the number of engines on the aircraft.

In the second formula (4.13), the coefficient of 0.2 shows that the mean costs of repairing an engine are 20 percent of its initial value.

S. M. Yeger [35] proposes that the costs of an airplane and an engine (in rubles) be determined by the following relationships:

$$\left. \begin{aligned} C_a &= 20(G_{\text{emp}} - G_{\text{en}}); \\ C_{\text{en}} &= 7P_{\text{to}} \text{ for TJE}; \\ C_{\text{en}} &= 11N_{\text{to}} \text{ for TBP} \end{aligned} \right\} \quad (4.14)$$

[TJE = turbojet engine; TBP = turboprop engine]

Outlays for repairs and technical maintenance of aircraft and engines are determined by the formula

$$P_{\text{ma}} = K_{\text{ma}} G_{\text{emp}} + K_{\text{ma.en}} N_{\text{to}} P_{\text{to}}$$

where K_{ma} is the specific cost of maintenance and repair of the airframe of the aircraft with equipment installed, in rubles/hour·ton;

$K_{\text{ma.en}}$ is the specific cost of maintenance and repair of an engine in rubles/kg of thrust·hour; and

P_{to} is the takeoff thrust (for turbojet and turbofan engines, in kg).

If the aircraft is operated with a turboprop engine, then N_{to} must replace P_{to} in formula (4.14), in hp.

The cost of fuel per flight hour is determined by the formula

$$P_{\text{fu}} = \frac{C_{\text{fu}} K_{\text{fu}} (G_{\text{fl.fu}} + G_{\text{fu.r}})}{T_{\text{f}}} \quad (4.15)$$

where C_{fu} is the cost of one ton of fuel³;

K_{fu} is the coefficient allowing for an increase in fuel cost due to the consumption of aviation oil;

$G_{\text{fl.fu}}$ is the total reserve of fuel consumed in the flight, in tons; /215

$G_{\text{fu.r}}$ is the fuel reserve, in tons; and

T_{f} is total flight time, in hours.

The corresponding values of variables appearing in formula (4.15) are determined by the following functions:

$$T_{\text{ap}} = \frac{L - L_{\text{to.cl}}}{V_{\text{in.cal}} \pm W} + t_{\text{to.cl}}; \quad (4.16)$$

$$G_{\text{fl.fu}} = Q_{\text{cru}} \frac{L}{V_{\text{cru}} - 50} + 0.28 P_{\text{to}}$$

where Q_{cru} is the mean hourly fuel consumption at a given altitude and cruising speed, in kg/hr.

Crew wages per hour of aircraft operation are determined by the formula

$$P_{wa} = C_{fl.p} N_{fl.p} + C_{ste} N_{ste}, \quad (4.17)$$

where $C_{fl.p}$ and C_{ste} are the mean hourly wages of one person of the flight personnel and cabin attendants, respectively.

The costs C as functions of flight altitude, velocity, and range (Fig. 4.10 a-d) were calculated based on formulas (4.8), (4.17). From Fig. 4.10 a, b, and d it is clear that with a reduction in flight range it is more advantageous to reduce the flight altitude and to increase the cruising speed, since an increase in fuel consumption in the level flight phase is compensated by a reduction in fuel consumption in climbing and in descent. The operating economy of the aircraft rises with increase in payload (Fig. 4.10 c).

Fuel consumption in transport aircraft calculated for a flight range $L = 3500-8000$ km is 30-55 percent of total outlays. Therefore the use of modern engines with more fuel consumption on transport aircraft will permit a reduction in the costs of passenger and cargo transportation.

With the transition of transport aircraft to supersonic flight speeds, the general trend in improvement of operating economy has been maintained. An increase in range leads to reduction in the costs of passenger transportation. Fig. 4.11 shows the cost of transportation as functions of flight range for supersonic aircraft. As Fig. 4.11 shows, by this indicator aircraft of this type are close to subsonic craft. /216

To determine the optimum cruising speed, let us use plots of the variation of the annual income (in arbitrary units) and the return on capital investments in percent in the operation of a Concorde type aircraft as a function of M_{cru} (Fig. 4.12).

The optimum value for cruising flight speed, as seen in Fig. 4.12, is $M_{cru} = 3.0$. Reducing the variation in annual income and capital investment return at $M_{cru} < 3$ is accounted for by an appreciable rise in the costs of the aircraft and in operating outlays.

The same conclusions about the optimum M_{cru} value can be made on the basis of a determination of the maximum range coefficient (Berget coefficient). The Berget coefficient is calculated by the following formula: /217

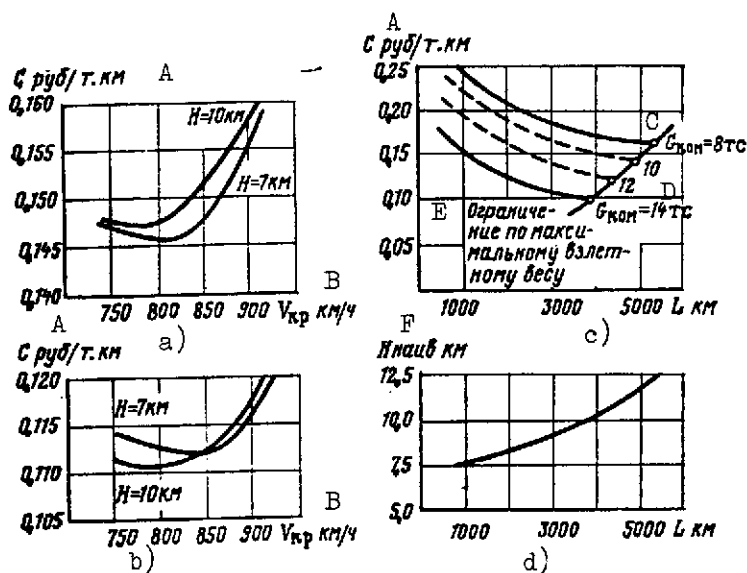


Fig. 4.10. Costs of flights of transport subsonic aircraft as functions of the following variables:
a -- Cruising speed at a flight range $L = 1000$ km
b -- Cruising speed at a flight range $L = 2500$ km
c -- Flight range for payload values $G_{pay} = 8, 10, 12$, and 14 tons
d -- Optimum flight altitudes as a function of range,

from the standpoint of costs
KEY: A -- Rubles/ton-kilometer
B -- V_{cru} , km/hr
C -- $G_{pay} = 8$ tons
D -- $G_{pay} = 14$ tons
E -- Constraint on maximum takeoff weight
F -- $H_{opt} / \text{opt} = \text{optimum}$

$$B = K I_{en} V_{cru}, \quad (4.18)$$

where K is the lift-drag-ratio;
 I_{en} is the specific impulse of engines; and
 V_{cr} is the cruising flight speed.

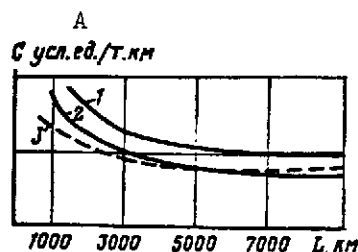


Fig. 4.11. Transportation costs as a function of range or supersonic transport aircraft:
1 -- For the Concorde
2 -- For the Boeing 2707
3 -- For subsonic jet aircraft
KEY: A -- Arbitrary units/ton-kilometer

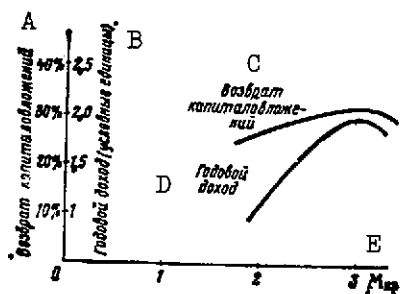


Fig. 4.12. Variation in annual income and return on capital investments in the operation of the Concorde as a function of the number M_{cru}

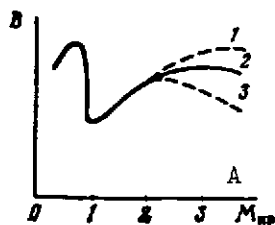
KEY: A -- Return on capital investments
 B -- Annual income (arbitrary units)
 C -- Return on capital investments
 D -- Annual income
 E -- M_{cru}

The dependence of B on cruising flight M is shown in Fig. 4.13: theoretical curve 1, where the B number depends only on velocity; the actual B number curve 2, and curve 3 that allows for the variation in the weight of the empty aircraft -- all these curves have second maxima of M_{cru} when $M_{cru} > 2$. It is clear from Fig. 4.13 that the second maximum of the B number is observed in the range $2 < M_{cru} < 3$. A decrease in the coefficient B for large M_{cru} is

dictated both by an increase in the weight of the empty aircraft, for aerodynamic heating reduces the effectiveness of the design, as well as by increasing the weight of assemblies providing for flight at this speed. The first maximum $M_{cru} = 0.8$ (cf Fig. 4.13) corresponds to the earlier obtained data on the costs of flight in a subsonic transport aircraft (cf Fig. 4.10 a and b).

At the present time, in the development of transport aviation a trend has been noticed abroad of building the same type of aircraft suitable for use in civil and military aviation. The most typical representative of this type of aircraft is the Lockheed C-5A. Characteristics of the Lockheed C-5A are shown in Table 4.1.²¹⁸

Fig. 4.13. Range coefficient B as a function of the M_{cru} number



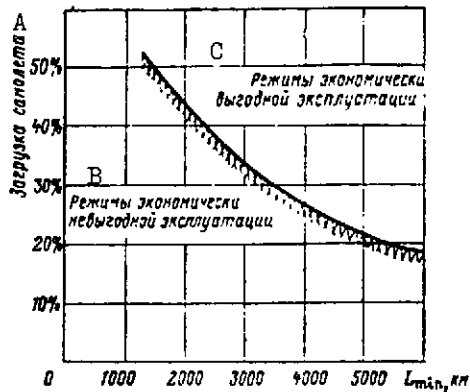


Fig. 4.14. Separation into regions of economically profitable and non-profitable operation of the plane of the following parameters: payload of the Lockheed C-5A and the minimum flight range

KEY: A -- Aircraft loading
B -- Regimes of economically unprofitable operation
C -- Regimes of economically profitable operation

TABLE 4.1

Versions of the C-5A and its loadings	Pay- load, tons	Maxi- mum range, km	Take- off weight, tons
Military transport (600 armed soldiers & truck)	50	10200	330
Passenger (902 seats in economy class or 667 seats in first class)	—	5506	376.4
Cargo-passenger (cabins w/bathrooms, first class, tourist class)	—	9000	—
Cargo with design-thrust engines	110	—	—
Cargo version with instal- lation of bigger engines (with thrust of 22,700 kg, each)	150 136	3700 5500	— —

For the Lockheed C-5A in the cargo version, we can distinguish two regions based on parameters, aircraft loading, and the minimum flight range (Fig. 4.14): economically profitable and economically unprofitable operation. From Fig. 4.14 it is clear that the operation of the cargo version of the C-5A aircraft over long lines is economically profitable even when there is considerable underloading.

4.4. Zones of Possible Air-to-Air Missile Launch

Zones of possible launch are determined by the motion parameters of the fighter-interceptor and the target; by the error in guiding the fighter-interceptor to the instant of missile release; by the missile velocity; by the range of the radar and the RHH [radar homing head]; by the turn angles of the antennas of the radar and the RHH; and by the guidance methods of the fighter-interceptor and the missile.

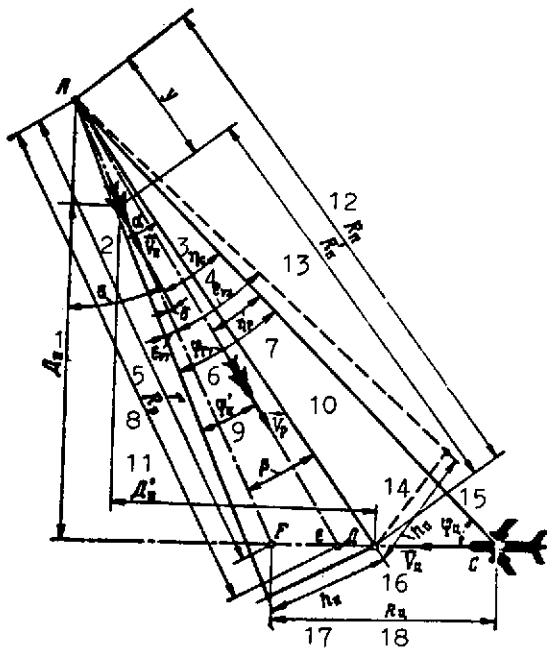


Fig. 4.15. Main symbols in the scheme of target interception in the frontal hemisphere and the release of an air-to-air missile
KEY: 1 -- D_{in} $\angle D_{in}$ = Distance

of interceptor]

2 -- \vec{V}_{in}

3 -- η_a

4 -- ϵ_{V_2}

5 -- ϵ_{V_1}

6 -- $\phi_{hor 1}$

7 -- η_m

8 -- R_m

9 -- ϕ'_{in}

10 -- \vec{V}_m

11 -- D'_{in}

12 -- R_{in}

13 -- R'_{in}

14 -- h_{in}

15 -- ϕ_t

16 -- \vec{V}_t

17 -- h_{in}

18 -- R_t

To construct the missile release zones, we must find, by calculation, the distances from the fighter-interceptor to the target at the instant of missile release as a function of the heading angles, range, and flight time of the missile until it encounters the target. By plotting the calculated values on a polar diagram, we get the zones of possible missile attacks [66]. Fig. 4.15 [72] gives the main symbols used in calculations and in constructing the zones of possible missile launch. Let us set up several mathematical relationships on the basis of the symbols: /220

$$\eta_a = \arcsin \left(\frac{V_t}{V_{in}} \sin \phi_t \right);$$

$$\eta_m = \arcsin \left(\frac{V_t}{V_m} \sin \phi_t \right);$$

$$r = \frac{R_t}{\cos \eta + \sin \eta_a \operatorname{ctg} \phi_a};$$

(4.19)

$$\begin{aligned}
t &= -\frac{R_t V_t \cos \varphi_t}{V_{in}^2 - V_t^2} \pm \frac{1}{V_{in}^2 - V_t^2} \times \\
&\times \sqrt{(R_t - h_{in})^2 (V_{in}^2 - V_t^2) + R_t^2 V_t^2 \cos^2 \varphi_t}; \\
\alpha &= \arctan \frac{h_{in}}{V_{in} t}; \\
B &= \frac{r \sin \eta_a}{\sin \varphi_t} - V_t t; \\
\beta &= \arccos \left(\frac{r^2 + h_{in}^2 + V_{in}^2 t^2 + B^2}{2r \sqrt{h_{in}^2 + V_{in}^2 t^2}} \right); \\
\varepsilon_{v_1} &= \alpha - \beta; \quad \varepsilon_{v_2} = -\alpha - \beta; \\
\varphi_{in} &= \eta_a - \eta_m + \varepsilon_v; \quad T_{in, cal} = \frac{\varphi_{in}}{\dot{\theta}_{in}}; \quad r_{tu} = \frac{V_{in}^2}{ng}; \\
y &= r_{tu} \sqrt{2(1 - \cos \varphi_{in})}; \quad \delta_{in} = \frac{\varphi_{in}}{2}; \\
\sigma &= \frac{\pi}{2} - \varphi_t - \eta_a - \varepsilon_v; \quad D_{in} = R_t \sin \varphi_t - y \cos \sigma; \\
D_{in} &= R_t \cos \varphi_t - y \sin \sigma - V_t T_{in, cal}; \\
\phi_{hor} &= \eta_a + \varepsilon_v; \quad R_{in} = \sqrt{D_{in}^2 + D'^2_{in}}; \\
\phi_{hor} &= \eta_a + \varepsilon_v; \quad R_m = \frac{R_{in}}{\cos \eta_m + \sin \eta_m \operatorname{ctg} \varphi_m}; \\
t_m &= \frac{R_m}{V_m};
\end{aligned} \tag{4.19}$$

where η_m , η_a are the lead angles of the air-to-air missile and the aircraft, respectively;
 t_m is the flight time of the missile to the impact point;
 ε_v is the angular error of guidance;
 t is the time expended in the approach of the fighter-interceptor and the missile given in condition that a minimum miss is attained;
 R'_m is the range between the fighter-interceptor and the target after correction by the aircraft of the error of guidance to the target;
 R_m is the range of the missile flight to the impact point with the target given on condition that the missile launch occurs at the instant of impact;

r_{tu} is the fighter-interceptor turn radius;
 n is the g-load of the fighter-interceptor during the turn;
 and
 ϕ_{hor} is the turn angle of the fighter-interceptor antenna as to azimuth.

The system of equations (4.19) is solved by numerical methods; the functions obtained as a result of the solution are shown in Fig. 4.16. The fighter-interceptor attack zone in the horizontal plane, shown in Fig. 4.17, can be constructed with these graphs. Curve 1 is bounded by the target lighting zone of the ORAD for the launch of an air-to-air missile, and curve 2 is determined by the range of the ORAD. The fighter-interceptor attack zones have been constructed in Fig. 4.17 without the constraints imposed by the conditions of disengagement of the interceptor from the attack [215]. Ordinarily these conditions impose constraints on curve 3. The expansion of the fighter-interceptor attack zones can be obtained by increasing the turn angle of the radar antenna to $\phi_{hor} = 80^\circ$, by changing the aircraft homing method, or by extending the range of the ORAD (the zone is hatched in Fig. 4.17).

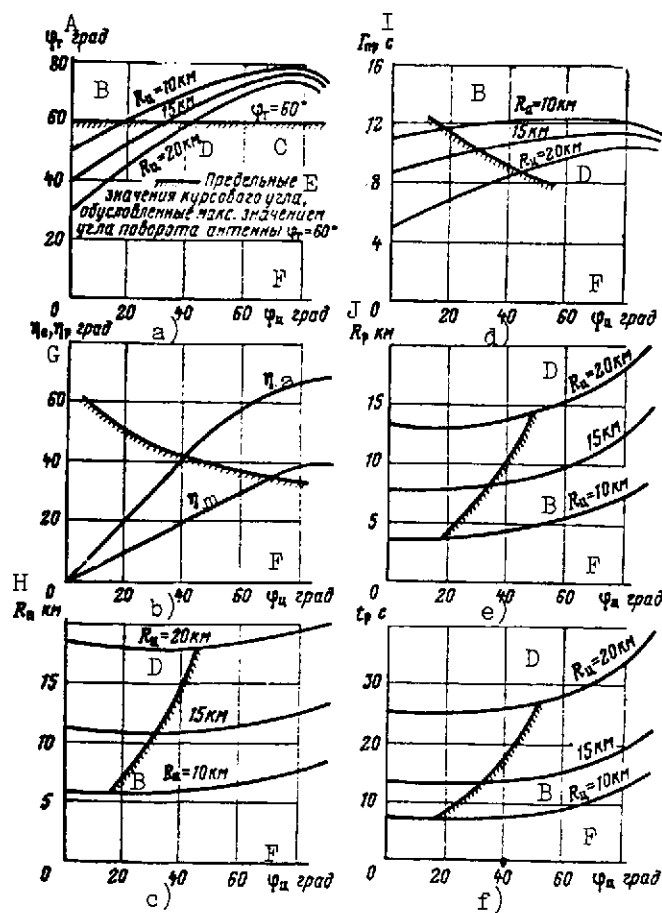


Fig. 4.16. Functions characterizing the homing of fighter-interceptor and air-to-air missile:

- a -- Antenna turn angle as a function of target heading
- b -- Interceptor and missile lead angles as a function of target heading
- c -- Ranges of direct visibility of target after correction of the error in the guidance of the interceptor as a function of target heading
- d -- Time expended in correcting the sighting error as a function of target heading
- e -- Missile flight range to encounter with target as a function of heading
- f -- Missile flight time to encounter with target as a function of heading

- E -- Maximum values of heading dictated by the maximum antenna turn angle $\phi_{hor} = 60^\circ$
- F -- ϕ_t , deg
- G -- η_a , η_m , deg
- H -- R_{in}
- I -- T_{sight} , seconds
- J -- R_m
- K -- t_m , seconds

From this figure is also clear that the homing equipment installed on the interceptor, for $R_{cap} = 20$ km, does not provide a circular zone of aircraft attack (cross-hatched), but this leads to the interceptor being led to this zone at a certain probability W_{cap} (cf Chapter Six).

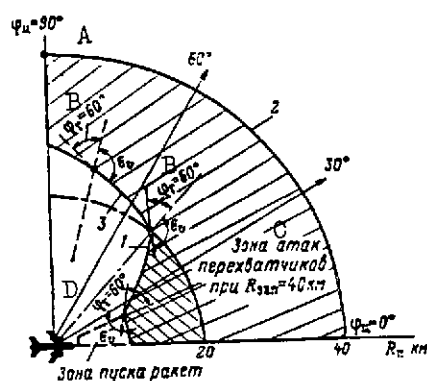


Fig. 4.17. Zones of possible fighter-interceptor attack of target for a limited turn angle of ORAD antenna, $\phi_{hor} = 60^\circ$

- KEY: A -- $\phi_t = 90^\circ$
- B -- $\phi_{hor} = 60^\circ$
- C -- Zone of interceptor attacks at $R_{cap} = 40$ km
- D -- $\phi_{hor} = 60^\circ$
- E -- $\phi_t = 0^\circ$
- F -- Missile launch zone
- G -- R_{in}

The fighter-interceptor possesses a zone of possible attacks also in the vertical plane. The method of constructing the zones is similar to the one examined above. It must be noted that in practical calculations the system designed it determines two zones in the horizontal and vertical planes [66], although actually one three-dimensional attack zone exists. The zones of three-dimensional attacks are determined with refinement of the homing laws of the fighter-interceptors at the stage of preliminary designing of aircraft homing systems. In this case the parameters of the homing systems are selected with allowance for the effective noise (interference) acting on the systems.

Now let us turn to determining the zones of possible air-to-air missile launch. The final section of the zones of possible aircraft attack is the initial section for the missile launch zones (stressed in Fig. 4.17 by cross-hatching).

Knowing the characteristics of the variation in missile flight velocity (or calculating it by formulas (2.20) and (2.21)), let us determine the missile flight trajectory by the formulas

$$\left. \begin{aligned} x &= \int_0^t V_m \cos \left(gn \int_0^t \frac{dt}{V_m} \right) dt; \\ y &= \int_0^t V_m \sin \left(gn \int_0^t \frac{dt}{V_m} \right) dt. \end{aligned} \right\} \quad (4.20) \quad /224$$

In Fig. 4.18 is plotted the corresponding characteristic obtained by the numerical integration of expressions (4.20). The lines of equal values of t_m , $n = V_r^2 / gr_{tu}$, and M are plotted by the last two formulas of the system of equations (4.19). The corresponding construction for n is performed in Fig. 4.19 a. By placing a transparent sheet (with Fig. 4.18 printed on it) on Fig. 4.19, let us find the points of interception equal in time (i.e., $t = t'$) for different initial missile flight directions V_m (coinciding with the target heading). By joining different values of these points with a curved line, we obtain the zone of possible air-to-air missile launches. The boundary of the zone is constructed in Fig. 4.19 a with a solid bold-faced line.

If fighter guidance is executed at the lead point of the encounter of the missile with the target, then we must allow for the lead angle by means of the formula

$$\eta_m = \arcsin \left(\frac{V_t}{V_m} \right) \sin \varphi_t. \quad (4.21)$$

Here the initial bearing to the target must be directed by allowing for the angle η_m (cf Fig. 4.19 c). Under the second guidance method, the missile launch zones are enlarged. /226

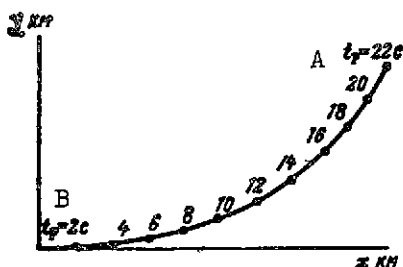


Fig. 4.18. Launch range of air-to-air missiles with different time interval Δt

KEY: A -- $t_m = 22$ seconds
B -- $t_m = 2$ seconds

C-3

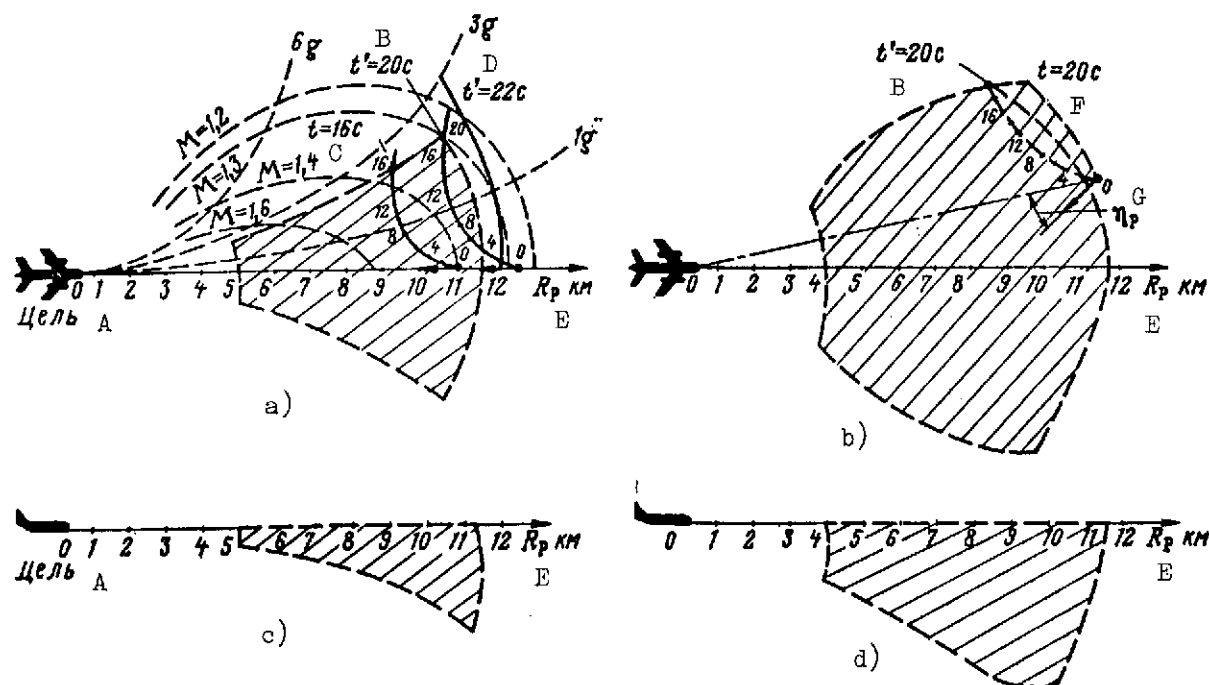


Fig. 4.19. Zones of possible air-to-air missile launches:
 a and b -- For the flight of a fighter-interceptor along a pursuit curve (a -- in the horizontal plane, b -- in the vertical plane)
 c and d -- For the flight of a fighter-interceptor at the lead point of missile-target impact (c -- in the horizontal plane, d -- in the vertical plane)

KEY: A -- Target
 B -- $t' = 20$ seconds
 C -- $t = 16$ seconds
 D -- $t' = 22$ seconds
 E -- R_m
 F -- $t = 20$ seconds
 G -- η_m

The launch zones shown in Fig. 4.19 a and b were constructed in the horizontal plane. Launch zones can be similarly constructed in the vertical plane (cf Fig. 4.19 in c and d). If the missile has good roll stabilization, two types of zones can be used (in the horizontal and vertical planes). In the event of adequate missile roll stabilization, the three-dimensional attack zones must be used.

4.5. Zones of Possible Air-to-Surface Missile Launch

The zones of possible launches of air-to-surface missiles are mainly determined by the missile parameters, flight characteristics of the mother aircraft, and the parameters of the onboard equipment of the aircraft and the missile providing for its guidance to the target. If the air-to-surface missile has a long launch range and its control over the initial flight phase is executed by command from the mother aircraft followed by a transition to homing, the mother aircraft must execute the flight so that the required law of missile guidance is held to in the missile flight over the first stage. After the transition to homing, the aircraft can perform the flight independently of missile motion. To construct zones of possible launches of air-to-surface missiles under this combination guidance method, equations similar to (4.19) can be used. The corresponding zones of possible launches in the vertical plane are constructed in Fig. 4.20 a, and in Fig. 4.20 b -- for the horizontal plane.

When the guidance method is varied (inertial guidance in the initial phase and homing in the latter phase), the navigation control system includes a computer to which data on the location of the missile and the target is computed, and the required parameters of the missile flight trajectory are calculated from these data. The inertial system permits varying the missile motion parameters within wide limits so that it can fly the hop to the target other than at low altitude, or else dive from high altitudes.

A change in the guidance method leads to a change also in the zones of possible missile launch. In Fig. 4.20 c are plotted the zones of possible air-to-surface missile launch under the combined guidance method (in the initial phase missile flight occurs with an inertial system, and in the final phase -- by homing). Launch zones with the missiles sent at high altitudes are constructed in Fig. 4.20 c with solid lines, and the launch zones during flight at low altitudes are indicated by dashed lines.

Semiautomatic control systems control air-to-surface missiles with short ranges in tactical-mission flights. The pilot or the operator tracks the target and the missile and, by shifting a lever, issues commands to the missile and guides it to target. In this case the missile launch zones are appreciably affected by the characteristics of the semiautomatic control system (the sighting devices of the mother aircraft, the frequency on which the commands were sent, and the aircraft piloting techniques).

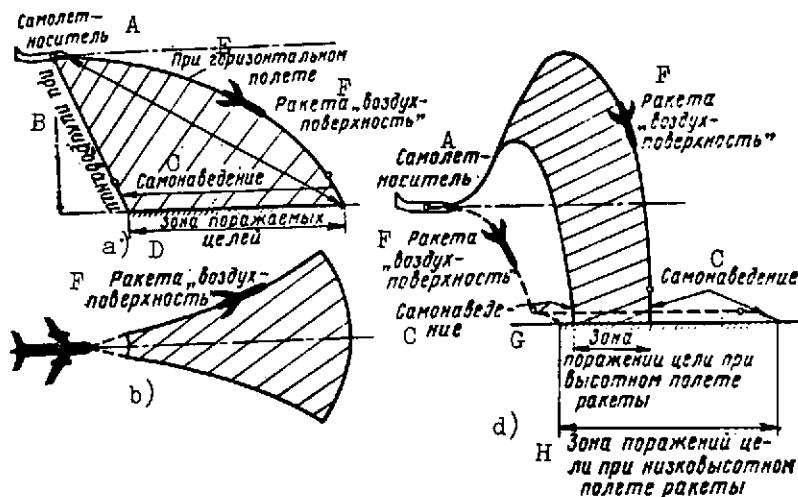


Fig. 4.20. Zone of possible air-to-surface missile launch:

a -- In the vertical plane

b -- In the horizontal plane

c -- Under the combined guidance method

KEY: A -- Mother aircraft

B -- With diving

C -- Homing

D -- Zones of attacked target

E -- In level flight

F -- Air-to-surface missile

G -- Zone of target strike with high-altitude missile flight

H -- Zone of target strike with low-altitude missile flight

Air-to-surface missiles with passive homing head directed toward ground radars have launch zones that depend on the parameters of the missile, homing head, frequency of interruptions in the operation of the ground radar, and the initial error in measuring the radar bearing. When there are sizable errors in the radar bearing angles, the missile homing errors become greater and their launch zones are severely narrowed. To expand the launch zones of missiles with passive homing heads, in the opinion of foreign specialists, it is useful to use inertial guidance systems on the missiles, providing the release of the missiles in the coverage zones of the ground radars. Use of television guidance facilities for glide bombs and missiles also permits enlarging their launch zones, since after the launch of a missile or the dropping of a bomb from an aircraft they become almost independent. The latter application simplifies piloting and reduces the requirements on the leg of the mother aircraft's attack disengagement.

4.6. Zones of Possible Interception of Air Targets by Surface-to-Air Missiles

Zones of possible interception of air targets are determined by the range of the radar facilities of the antiaircraft complex, missile flight speed, the values of its longitudinal and lateral g-loads, the guidance method, and also the target flight velocity and its maneuverability. An increase in the speed of a target for a fixed detection range leads to a narrowing of the zones of possible interception by a missile.

The dimensions of the zone of missile interception of air targets are confined by the following limiting altitudes: maximum $H_{m \max}$ and minimum $H_{m \min}$ (Fig. 4.21); limiting ranges $D_{m \max}$ and $D_{m \min}$; and by the limiting lateral parameter $\pm Z_{m \max}$ (for the interception zone in the lateral plane). The dimensions of these zones are also limited by the tactical-flight characteristics of the missile and the conditions of its impact with the target. These characteristics are usually considered to be the following: minimum missile speed in its encounter with the target $V_{m \min}$; maximum and minimum values of available g-load $n_{m \max}$ and $n_{m \min}$; maximum operating time of onboard equipment and minimum flight time $t_{m \max}$ and $t_{m \min}$; missile launch angles $\theta_{m \max}$ and $\theta_{m \min}$; maximum allowable angles of missile impact with a target $\psi_{im \max}$; and maximum bearing angles ϕ_{\max} .

The maximum range of the interception zone is determined by the values of $V_{m \min}$ and $t_{m \max}$. The minimum speed $V_{m \min}$ is dictated by the requirements of insuring the aerodynamic stability of the missile, and matching the characteristics of the proximity fuse and the warhead. The maximum flight time $t_{m \max}$ is restricted by the reserve of reaction mass on board. The maximum altitude of the zone $H_{m \max}$ is determined by the minimum available g-load $n_{m \min}$ affording the possibility of guidance in the interception of high-altitude targets. /229

The minimum altitude $H_{m \min}$ is often dependent on the capabilities of the operation of the onboard equipment of the missile against an Earth background. The minimum range of the zone is determined by the minimum flight time of the rocket, which in turn is determined by the initial launch errors, the duration of the dynamic processes of selecting these errors, the instant of separation of the launch stages, the range at which the safety system is released, and so on. The minimum range can also be determined by the limited launch angles θ_m and the maximum available g-load $n_{m \max}$.

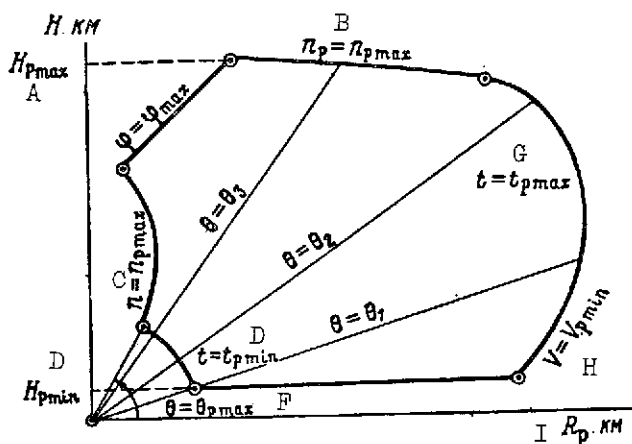


Fig. 4.21. Typical zone of possible interception of air target by anti-aircraft missiles

KEY: A -- $H_m \max$
 B -- $n_m = n_m \max$
 C -- $n = n_m \max$
 D -- $H_m \min$
 E -- $t = t_m \min$
 F -- $\theta = \theta_m \max$
 G -- $t = t_m \max$
 H -- $V = V_m \min$
 I -- R_m

Some boundaries to the strike zone can be dictated by the allowable missile-target impact angles and the target bearing angles. Restricting the target bearing angles can be related to the maximum bearing angles of the missile homing head. There are also other restrictions affecting the geometry of the interception zone, therefore before zones are constructed all limitations intrinsic to the given type of missile must be analyzed. /230

A simplified method of constructing maximum zones of missile interception of air targets amounts to the following. The ballistic-flight characteristics of the missile along reference trajectories corresponding to the method of guidance of the missile to the target are determined. Here it is assumed that the reference interception trajectories of nonmaneuvering targets at the far boundary of the zone are practically independent of the guidance method. Therefore to evaluate the far boundaries arbitrarily linear trajectories characterized by a constant angle of inclination to the horizon θ_{m0} can be used.

The velocity of the missile $V(t)$ or $V(R)$ along the reference trajectory is determined by the value of the so-called g-load trajectory

$$n_{m.tr} = n_m - n_{m.flu} - n_{m.eq},$$

where $n_{m.flu}$ is the g-load caused by fluctuations in the control signal, and $n_{m.eq}$ is the g-load caused by drifts of the missile's onboard equipment (drifts of the homing head gyroscopes). Then the missile flight equation is integrated by numerical methods:

$$m_m(t) \frac{dV_m}{dt} = P_m - X(n_{m.tr}) - G_m, \quad (4.22)$$

where P_m is the projection of the engine thrust on the X axis coinciding with the direction of the velocity vector V_m ;

$X(n_{m.tr})$ is the aerodynamic drag dependent on the lateral g-load along the trajectory; and

G_m is the projection of the weight on the X axis.

Equation (4.22) is integrated from the instant of launch to the instant at which one of the missile indicators constraining the far boundary of the zone and the maximum altitude at the far boundary is attained -- $t_{m \max}$, $V_{m \min}$, and $n_{m \min}$. The last parameter $n_{m \min}$ requires that we calculate the available g-load of the missile along the reference trajectory

$$n_m = \frac{V_m \dot{\theta}_m}{g} = \frac{Y(\delta_{\max})}{m_a(t)g}, \quad (4.23)$$

where $Y(\delta_{\max})$ is the lateral lift of the missile, corresponding to the maximum deflection of the control devices $\delta_{m \max}$ and dependent on the missile flight regime. /231

The near boundaries of the interception zone are strongly related to the missile guidance method and the initial launch conditions. Guidance methods in this case can be conventionally divided into two groups. The first includes guidance methods allowing the motion of the missile along the entire flight trajectory at the limiting maximum g-load $n_{m \max}$ without guidance discontinuity. These methods can include the method of proportional navigation with homing. The second group is characterized by discontinuity of guidance if at some point of the trajectory the required g-load exceeds the available g-load. This principle is characteristic of the matching-curve method of missile guidance.

Constructing the near boundary when the missile travels along a trajectory at maximum g-load $n_{m \max}$ proceeds by the technique of integrating a system of equations including equation (4.22) with $n = n_{m \max}$ (4.23), with reference to the kinematic equations

$$\left. \begin{aligned} H &= V_m \sin \theta_m \\ R_{m.hor} &= V_m \cos \theta_m \end{aligned} \right\} \quad (4.24)$$

The initial conditions with $t = 0$ are taken in the form

$$\left. \begin{aligned} H_0 &= 0; R_{m_0} = 0; V_{m_0} = 0; \\ \theta_{m_0} &= \theta_{m_{\max}} \text{ or } \theta_{m_0} = \theta_{m_{\min}} \end{aligned} \right\} \quad (4.25)$$

If the maximum g-load of the missile $n_{m \max}$ is limited not by the maximum deflection angle of control surfaces $\delta_{m \max}$, but by the strength conditions of missile structure and equipment, i.e., $n_{m \max} = n_{m \max}^*$, then instead of equation (4.23) we have

$$\dot{\theta}_m = \frac{n_{m \max}^* \cdot g}{V_m(t)}. \quad (4.26)$$

When a missile is guided by one of the methods in the second group, the calculations are somewhat more involved. In this case it is necessary to specify a specific target trajectory and integrate equations (4.22) - (4.26) jointly with the equations of target motion /232

$$\dot{R}_{\text{hor.}} = V_t \quad (4.27)$$

and the guidance method relating, for example, the required g-load n_m with the position of the target ρ_t and of the guided missile ρ_m relative to the guidance station:

$$n_m(t) = n_m(\rho_t, \rho_m). \quad (4.28)$$

If the time-variable required g-load of the guidance method at any point on the trajectory exceeds the available g-load, interception at the given initial target position becomes impossible. By calculating several trajectories with the initial target position being varied, we obtain the limiting trajectory for which the method is realized, and the required g-load attains the values of the available g-load only at a single point.

The boundaries of the limiting interception zones in the horizontal plane can also be determined in accordance with the method outlined above, by allowing for the three-dimensional geometry of the trajectory.

The attack zones of maneuvering targets become narrowed, since a target maneuver causes an increase in the required g-load of the missile and the corresponding reduction in its velocity, associated with induced drag. Prolonged maneuvering of the target with a high g-load n_m can lead to the target going beyond the bounds of the zone of missile attainability. In this case the

launch zone becomes narrowed, which ensures the impact of the launched missile with its target.

For an approximate estimate of missile launch zones for a maneuvering target, in several cases an approximate method is used, assuming the target maneuver to be planar and constant and determining the missile trajectory with reference to the g-loads dictated by guidance method. Here the order of determination of the interception zone boundaries remains unchanged.

In the last stages of designing, the attack zones are refined by a technique using the complete system of equations describing the motion of a missile and its target, with reference to the guidance method and the full set of constraints. Integration proceeds, as a rule, with computers, and the algorithm of determining the zones allows for the necessity of sorting through the initial interception conditions to specify the conditions which correspond to the final constraints adopted. In Fig. 4.22 a are constructed the zones of possible interception of Nike-Hercules missiles at $V_p = 1200$ and 2600 km/hr. Also given here, in Fig. 4.22 b, are the interception zones for Hawk missiles, and in Fig. 4.22 c, for Chaparral (curve 2) and Redeye (curve 1) missiles. Fig. 4.23 presents the zones of possible interception at $V_t = 1200$ km/hr for different kinds of missiles (based on the data in Table 2.13).

/233

/234

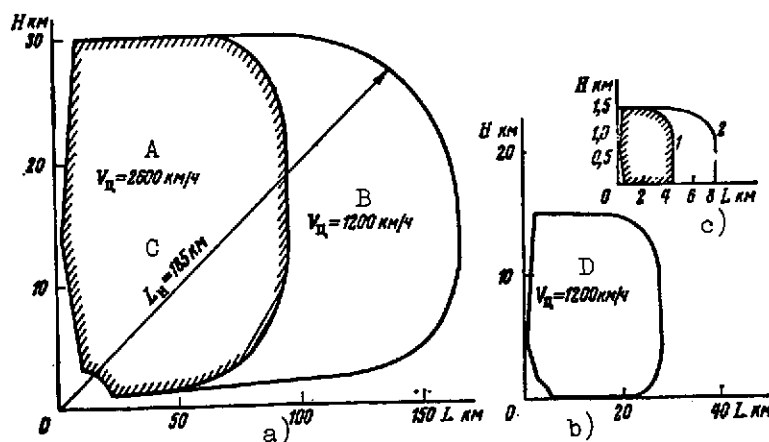


Fig. 4.22. Zones of air target interception by antiaircraft missiles:
a -- For the Nike-Hercules missile
b -- For the Hawk missile
c -- For the Chaparral and Redeye missiles

Fig. 4.22. Zones of air target interception by anti-aircraft missiles [Continued]

KEY: A -- $V_t = 2600$ km/hr

B -- $V_t = 1200$ km/hr

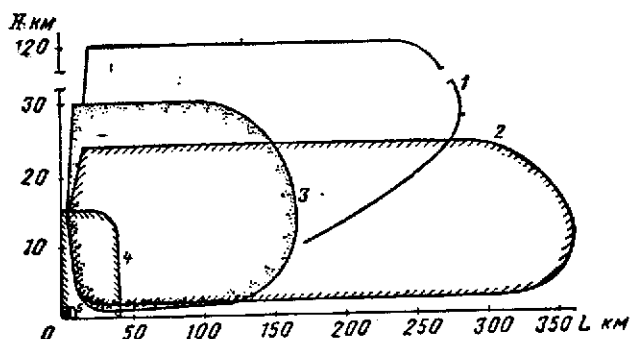


Fig. 4.23. Comparison of interception zones for different anti-aircraft missiles:

- 1 -- For the Nike-Zeus missile
- 2 -- For the Bomarc missile
- 3 -- For the Nike-Hercules missile
- 4, 5, 6 -- For the Hawk, Chaparral, and Redeye missiles (cf Fig. 4.22 b and c)

4.7. Flight Trajectories of Ballistic Missiles

The trajectory of a ballistic missile can be divided into three characteristic phases. The first is the so-called powered phase over which the missile is accelerated to the velocity required in magnitude and direction. It lies in the region of space where the aerodynamic effects of the environment cannot be neglected. The powered phase forms the entire flight trajectory of the missile, and random factors acting on its extent have a predominating effect on the dispersion of the motion parameters and the point of impact. Therefore in part in several cases it is the only phase in which the missile motion is controlled. But if the missile flight is controlled also later on, guidance over the powered phase is still given decisive importance.

Since long-range ballistic missiles have as a rule two powered stages, there can be thus two or more powered phases in the trajectory. Sometimes from the conditions of construction of the optimal control law, these phases of motion with booster engine running are alternated with the segment of the ballistic trajectory along which only passive forces act.

The second trajectory phase -- the ballistic -- lies at considerable distances from the Earth where the atmospheric effects can be neglected. It is the longest and the farthest removed from the Earth; the length of the ballistic trajectory and the time of motion along it are almost equal to the entire length of the trajectory and the flight time of the ballistic missile. As a rule, the missile is not controlled over this phase.

The last (third) flight phase is not long and again passes through the atmosphere. Atmospheric influence, dissipative and aerodynamic, most fully marks this phase of motion. The trajectory here can also be affected by random actions that are considerable in magnitude, whose effect -- just as the effect of the preceding random factors -- must degrade the system of navigation and control. /235

The planar motion of the missile is described in a system of polar coordinates shown in Fig. 4.24.

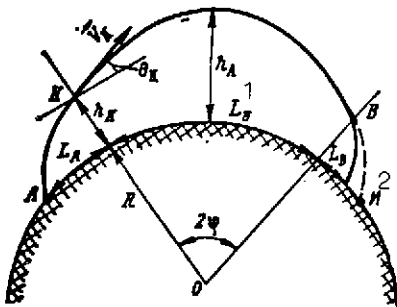


Fig. 4.24. Parameters of the flight trajectory of a ballistic missile:

- A -- Launch point
- K -- End of powered phase
- R -- Mean Earth radius
- h_K -- Altitude of missile at instant of engine cutoff
- h_A -- Altitude of missile at apogee
- L_A -- Flight range over powered phase
- L_C -- Flight range over atmospheric phase
- KEY: 1 -- Point of imaginary landing (neglecting atmospheric effects)

2 -- Range of ballistic flight phase

The projection of the total missile flight range on the Earth's surface is

$$L = L_A + L_B + L_C,$$

where L_A , L_B , and L_C represent the projections onto the Earth's surface of the powered, ballistic, and terminal trajectory phases.

Since $L_B \gg L_A + L_C$, then to the first approximation we can neglect the extent of the projections of the first and last phases.

Thus,

$$L \simeq L_B = 2\psi R, \quad (4.29)$$

where ϕ is the central angle shown in Fig. 4.24 a, and R is the mean Earth radius (the radius of a spherical Earth).

An infinite set of ballistic trajectories can be drawn through the initial and terminal flight points. They will differ by the

magnitude and the direction of the velocity vector at the initial point of the ballistic phase, i.e., by the conditions at point K /236 (Fig. 4.24) of the end of the powered phase.

The relationship between velocity V_K , the angle of its inclination to the horizon θ_K , the altitude of the end of the powered phase h_K , and the angular flight range 2ϕ is expressed by the relationship [3, 6]

$$V_K^2 = \frac{\mu}{r_K} \frac{1 - \cos 2\phi}{\left[\frac{r_K}{R} \cos^2 \theta_K - \cos(2\phi - \theta_K) \right] \cos \theta_K} \quad (4.30)$$

Here $\mu = fM$, where f is the gravitational constant, and M is the mass of the Earth ($\mu = 398,600 \text{ m}^3/\text{sec}^2$);

$$r_K = h_K + R = R \left(1 + \frac{h_K}{R} \right).$$

Referring to equality (4.29), the function $V_K(\theta_K, L_B)$ shown in Fig. 4.25 a can be constructed with the function (4.30). Among these trajectories can be found one characterized by the lowest energy outlays.

Actually, the energy outlays are equal to the sum of the kinetic and potential energy at point K; they are determined by V_K -- the velocity at the end of the powered phase, and by h_K -- the altitude of this point over the Earth's surface. Neglecting the quantity $h_K < h_A$, $h_K \ll R$ (h_A is the altitude of the apogee, the farthest removed point from the Earth), we can to the first approximation assume that the minimum energy is proportional only to the minimum V_K and will depend only on the angle of inclination of the velocity vector to the horizon.

In Fig. 4.25 a points with minimum θ are marked by circles.

From (4.30) we can find the value $\theta_K = \theta_K^*$, yielding $V_K = (V_K)_{\min}$

$$\tan 2\theta_K^* = \frac{\sin 2\phi}{\cos 2\phi - \left(1 + \frac{h_K}{R} \right)} \quad (4.31)$$

The dependence of the optimum angle θ_K^* on range for different values of the parameter h_K/R is shown in Fig. 4.25 b (based on [1],

/237

3, 67). Neglecting the value of h_K/R compared to unity, we get the simple expression

$$\theta_K^* = \frac{\varphi + \pi}{4}.$$

Fig. 4.25 c shows the dependence of the missile flight time over the ballistic phase of the trajectory on the angle θ_K for different L_B values. The circles indicate the flight time for the trajectories optimal in the sense of $(V_K)_{\min}$ for different ranges.

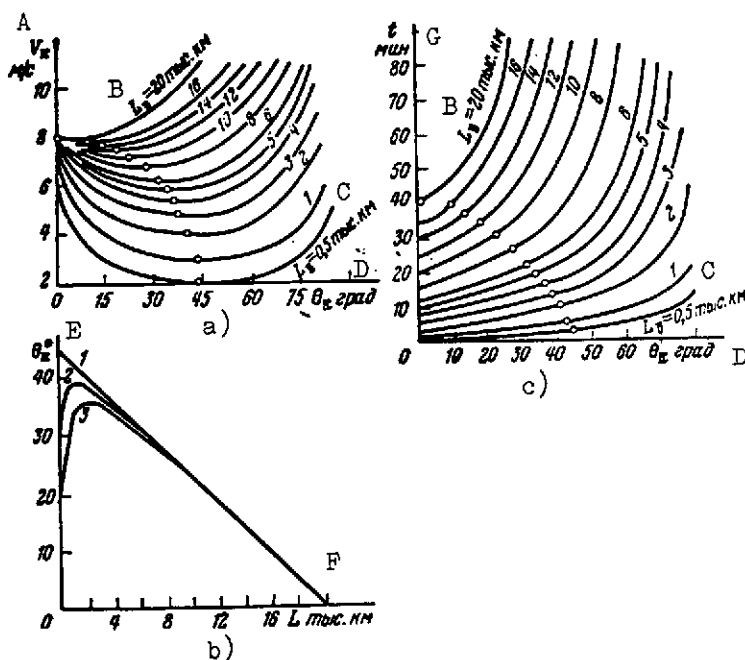


Fig. 4.25. Flight characteristics of a ballistic missile:
a -- Velocity at instant of engine cutoff
b -- Angles of inclination of velocity vector at cutoff instant
c -- Total missile flight time
KEY: A -- V_K , m/sec
B -- $L_B = 20,000$ km
C -- $L_B = 500$ km
D -- Deg
E -- θ_K , deg
F -- L , thousands of km
G -- t , min

If the second point of the trajectory is "liberated", then by varying the vector \vec{V}_K , we can obtain a set of trajectories with different L values. L_B is determined in the general case (on the /238 assumption of the Keplerian motion of the missile, which will be discussed below) from the expression

$$L_B = 2R \arctan \frac{\eta \tan \theta_K}{1 - \eta + \tan^2 \theta_K}; \quad (4.32)$$

$$\eta = \frac{V_K^2}{g_K(R + h_K)}. \quad (4.33)$$

Since $h_K \ll R$, we can set

$$R + h_K \simeq R; \quad g_K = g_0,$$

where g_0 is the acceleration due to gravity at the Earth's surface at point A (Fig. 4.24). By differentiating (4.32), we get a function for the maximum range L_{Bmax} :

$$\left. \begin{aligned} L_{Bmax} &= 2R \arctan \frac{\eta}{2\sqrt{1-\eta}}; \\ \theta_{K/L_{Bmax}} &= \theta_K^{**} = \sqrt{1-\eta}; \\ 2\varphi/L_{Bmax} &= 2\varphi^{**} = 2 \arctan \frac{\eta}{2\sqrt{1+\eta}}. \end{aligned} \right\} \quad (4.34)$$

Several characteristics of the maximum range of a trajectory calculated with these formulas are shown in Fig. 4.26. Due to the symmetry of the ballistic trajectory relative to an axis drawn through the center of the Earth and the apogee point, V_K and θ_K are equal to the values of the corresponding functions of the ideal trajectory at the point of missile impact (the section B-1 in Fig. 4.24 -- the extension of the ballistic trajectory neglecting atmospheric effects).

One of the two conditions considered: the minimum expended energy and the maximum range (in addition to a third condition of minimum dispersion of trajectories, examined below), is the criterion which together with several constraints of a technical design, and sometimes even tactical nature determine the choice of the missile's trajectory and control law.

As we know, only one of the optimality conditions can be satisfied, i.e., the trajectory with maximum range will not be the trajectory with minimum energy, and vice versa. However, the values of their parameters (and correspondingly the values of the /239

parameters at point K) are close to each other. The most important deterministic (cf Chapter Six) criterion for ballistic missiles is maximum range.

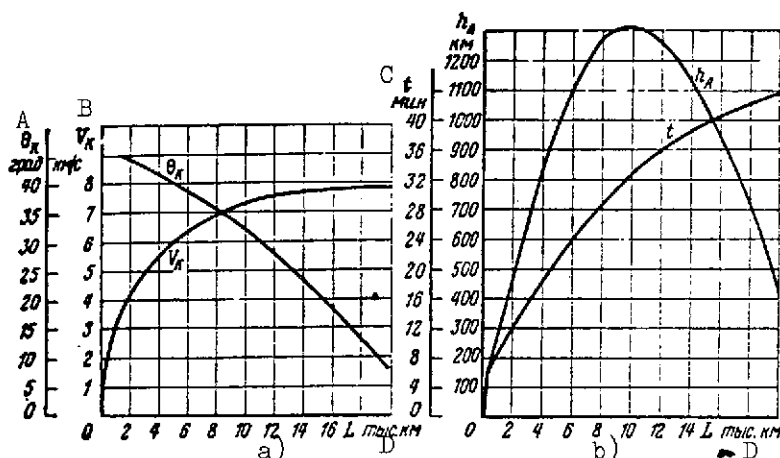


Fig. 4.26. Characteristics of trajectories with maximum flight range:

a -- Dependence of velocity at angle of inclination of velocity vector at the instant of engine cutoff on flight range

b -- Dependence of apogee altitude and flight time on range

KEY: A -- θ_K , deg

B -- km/sec

C -- Minutes

D -- Thousands of km

Thus, the ballistic, and thus almost the entire flight trajectory of the missile is determined at point K by these conditions. Satisfying these conditions is the principal task of guidance and control over the powered phase. Though its extent is very small ($L_A = (0.04-0.1)L$) and the main parameter determining L_{\max} is V_K^* for the angle θ_K^* is associated with it by the function (4.34), still the flight range L_{\max} is a function also of the coordinates of point K, i.e., the altitude and distance of the end of the powered phase from the launch point. In an approximate examination, however, we can neglect this effect, thereupon introducing certain corrections into the results of the calculation.

The velocity of the missile at the end of the powered phase can be determined as follows [6]: /240

$$V = V_{id} - \Delta V_1 - \Delta V_2 - \Delta V_3 =$$

$$= -u_n' \ln \mu^* - T I_1 - \frac{gT}{P_{mi}} I_2 - (u_n' - u_0') I_3. \quad (4.35)$$

Here V_{id} is the ideal velocity, neglecting the effects of gravity and atmosphere;
 ΔV_1 are the velocity losses due to the effect of gravity;
 ΔV_2 are the velocity losses due to the dissipative atmospheric effects;
 ΔV_3 are the velocity losses due to the atmospheric effects on the specific impulse of the engine;
 g is acceleration due to gravity, $g \cong g_A$;
 μ^* is a dimensionless coefficient characterizing the relative missile mass. For an assigned initial mass and mass flow rate of fuel consumption per second

$$\mu^* = 1 - \frac{t}{T} \quad (\text{theoretically } 0 \leq \mu^* \leq 1),$$

where t is the instantaneous time, and T is the total operating time of an ideal missile for which $\mu^* = 0$;
 P_M is the launch load at the midline;
 u'_0 is the imaginary escape velocity of combustion products at the Earth's surface, defined by the ratio of the absolute thrust at the Earth's surface to the per second mass consumption;
 $u'_{c.p}$ is the imaginary escape velocity of the combustion products in airless space, defined by the ratio of the absolute thrust in a vacuum to the per second mass consumption; and
 I_1, I_2, I_3 are several integrals with respect to the argument t or μ^* characterizing losses $\Delta V_1, \Delta V_2$, and ΔV_3 .

For assigned missile parameters, V_K in formula (4.35) is decisively affected by $\theta = \theta(\mu^*)$, the instantaneous angle of inclination of the velocity vector to the local horizon. The shape of this function is approximately identical for all missiles and is shown for several θ_K values in Fig. 4.27 a [6]. In Fig. 4.27 b is shown the variation of $V_{id}(\mu)$ and the variation in absolute /241
 $\Delta V_1(\mu), \Delta V_2(\mu), \Delta V_3(\mu)$, and relative (in terms of true velocity) losses. The function (4.35), as already noted, is only an approximate expression of the flight velocity.

An exact solution of the problem of determining the motion program for a flight at maximum range has thus far not been obtained. Approximate methods lead to a program for the pitch

angle $\phi = \theta + \alpha$ (the angle between the longitudinal axis of the missile and the horizon), with the form shown in Fig. 4.27 c [6]. Also in the figure is shown the variation in the angle of attack α .

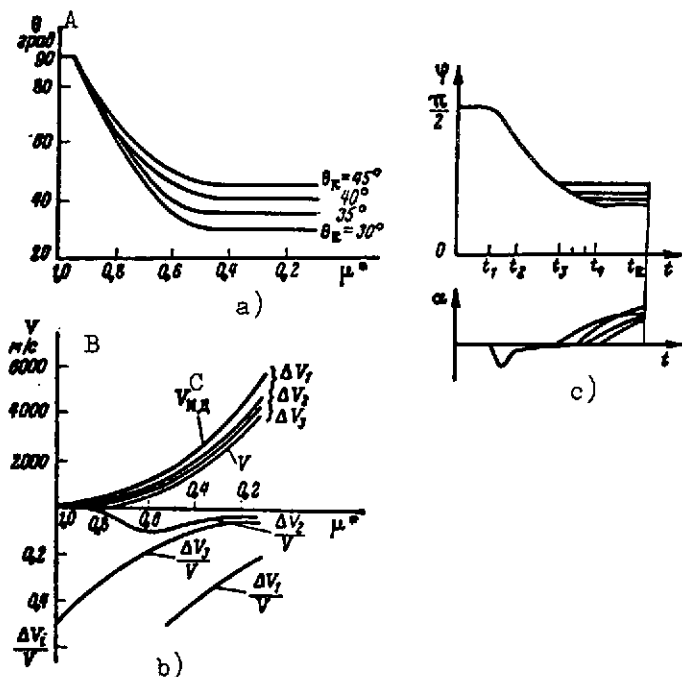


Fig. 4.27. Flight characteristics of a ballistic missile as a function of its relative weight:

- a -- Variation in instantaneous angle of inclination for different θ_K values
- b -- Variation in ideal velocity and in absolute and relative velocity losses
- c -- Program of variation in pitch angle for flight at maximum range

KEY: A -- θ , degrees
B -- V , m/sec
C -- V_{1d}

Takeoff and start of motion are executed with the missile axis in the vertical direction. Over the phase (t_2, t_3) the angle of attack changes according to the law

$$\alpha = \bar{\alpha}k(k-2); \quad k = 2e^{a(t-t_2)},$$

where a is some parameter that is constant for missiles of this class, and

$\bar{\alpha}$ is the maximum angle of attack for the subsonic phase of motion.

When the powered phase is fairly long, beginning from the instant t_3 when the intensity of the atmospheric effects diminishes, motion can occur with increase in angle of attack and constant pitch angle.

Parameters that are varying in the determination of the flight program at maximum range are t_1 , $\bar{\alpha}$, and t_3 . For a multistage missile, the general program of the motion of the powered phase is obtained by combining several programs of the form shown in Fig. 4.27 c, and the number of variable parameters correspondingly becomes greater. Thus, control of the planar motion of the missile over the powered phase is executed by changing the pitch angle

ϕ . The program for flight for maximum range is determined, in particular, in the form of a solution of a variational problem with assigned control law⁴ and assigned constraints.

The main design constraints are as follows [6]:

1. Vertical launch and vertical initial trajectory phase. This requirement is due to the relative simplicity of realizing this launch and the greatest stability of the vertical motion of the rocket over the initial flight phase when the control devices are not yet effective enough.

2. Continuity of the functions $\phi(t)$, $\dot{\phi}(t)$, and $\ddot{\phi}(t)$, and limitation on $\dot{\phi}(t)$. This is due to the technical feasibility of this control law.

3. Constraint on normal g-loads, which is expressed in a constraint of the aerodynamic moment and, ultimately, in a constraint on the angle of attack, especially for high velocity heads.

4. Passage through a region close to the speed of sound ($0.8 \leq M \leq 1.2$) at a zero angle of attack, which is due to the desire to reduce to a minimum the effect of the derivatives $\partial C_y / \partial \alpha$ and $\partial m_z / \partial \alpha$ that are varying strongly for these M numbers.

5. Special requirements related to the technical characteristics of the given control method and the method of engine cutoff. 243

6. The minimum number of control programs for flight at different ranges within the given interval.

Above it has already been stated that the majority of random actions on the motion of a ballistic missile occur for the flight over the powered phase. These include deviations of the geometrical, aerodynamic, and weight characteristics of the missile from calculated values, random deviations of the engine parameters, end of the navigation, orientation, and control systems, departure of atmospheric parameters from calculated values, and so on. Since the range of planar flight is a function of four parameters

$$L = L(V_K, \theta_K, X_K, Y_K);$$

where X_K and Y_K are the coordinates of point K, therefore the effect of random factors on planar flight range is not direct, but via these parametric changes. Therefore the condition of minimum dispersion of the range with reference to the effect of the method of engine cutoff at point K will be written in the form

$$\begin{aligned} \Delta L = & \frac{\partial L}{\partial V} \delta V|_{t=t_K} + \frac{\partial L}{\partial \theta} \delta \theta|_{t=t_K} + \frac{\partial L}{\partial X} \delta X|_{t=t_K} + \\ & + \frac{\partial L}{\partial Y} \delta Y|_{t=t_K} + \frac{\partial L}{\partial t} \delta t|_{t=t_K} = 0. \end{aligned} \quad (4.36)$$

Here δV , $\delta \theta$, δX , δY , and δt_K are variations of the corresponding variables caused by the effect of random factors, $\partial L / \partial t$ is obtained by the differentiation of L as a complex function, and the entire remaining term characterizes the effect of the error in the instant of engine cutoff. The equality $\delta L = 0$ obtained by variation of the program $\phi(t)$ is a necessary condition for the attainment of maximum range. This variation affects the value of the parameters at point K ; here the instant of total burnout is fixed. Therefore the condition of maximum range will be written as

$$\begin{aligned} \delta L = & \frac{\partial L}{\partial V} \delta V|_{t=t_K} + \frac{\partial L}{\partial \theta} \delta \theta|_{t=t_K} + \\ & + \frac{\partial L}{\partial X} \delta X|_{t=t_K} + \frac{\partial L}{\partial Y} \delta Y|_{t=t_K} = 0. \end{aligned} \quad (4.37)$$

Partial derivatives in equations (4.36) and (4.37) characterize the effect of variation in the several parameters on flight range. Fig. 4.28'a, b, and c show the change of some of them as a function of the angle θ_K for different L values [3]. It must be remembered that the axes (X, Y) in a topocentric coordinate system are selected so that Y coincides in direction with the radius drawn from the center of the Earth to this point and, therefore, coincides in direction with pitch. As we can see, conditions (4.36) and (4.37) are not equivalent and therefore cannot be satisfied simultaneously. The condition of minimum dispersion depends on the method of engine cutoff (in terms of the quantity Δt_K). These conditions can be met simultaneously only if the engine is cut off not on the attainment of the given combination of coordinates and velocity, but only based on the engine operating time. This method, however, is by no means the best, since it entails major methodological errors.

Thus, in selecting the control law for the powered phase, only one optimality condition can be satisfied, and then the deviation of the calculation results from the other condition is checked.

In practice some compromise solutions are found, satisfying several requirements to some extent.

The transition from considering planar missile motion to three-dimensional motion does not introduce anything fundamentally new. Missile motion along the ballistic phase occurs according to the same laws and is described by the same functions as the motion of artificial earth satellites above the atmosphere.

The functions presented in this section for the determination of flight range and results of the related calculations reflect Keplerian motion of a missile, i.e., motion occurring under the

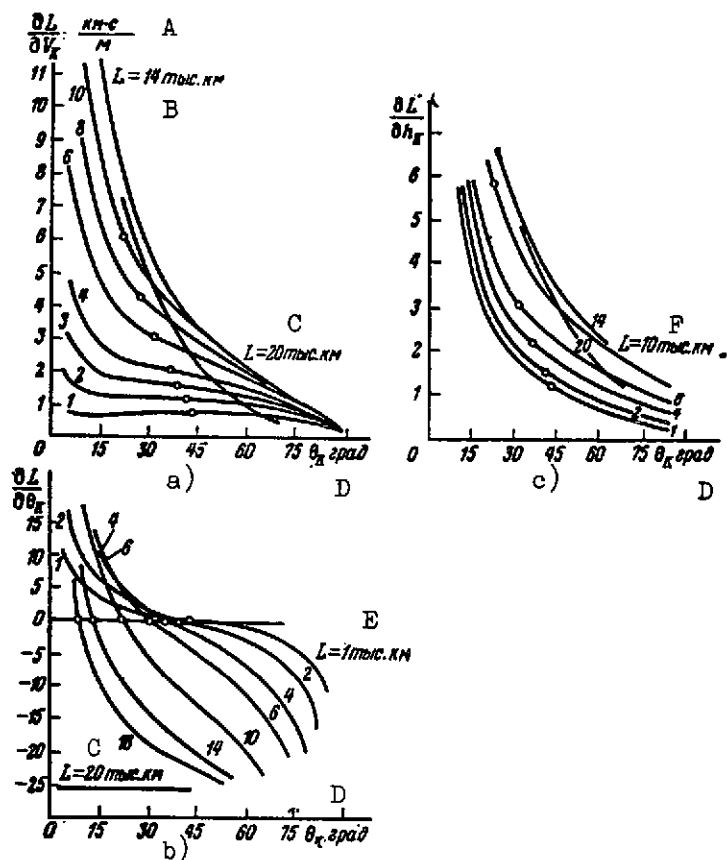


Fig. 4.28. Effect on flight range of ballistic missile:

- a -- Flight velocity
- b -- Angle of inclination of velocity vectors
- c -- Altitude of flight at instant of engine cutoff

KEY: A -- km·sec/m
 B -- $L = 1400$ km
 C -- $L = 20,000$ km
 D -- Degrees
 E -- $L = 1000$ km
 F -- $L = 10,000$ km

effect of just the force of gravity of a material point (a material sphere). This schematization of the physical nature is acceptable only in rough project-planning calculations.

The true figure of the Earth (and thus the true gravity field) is described by an infinite series constructed with Legendre polynomials. Its principal term is proportional to the polar flattening of the Earth. Neglecting the effect of polar

flattening can lead to errors in calculating the altitude of the moving object (for the ballistic missile considered at point 1 in Fig. 4.24, this will be approximately equal to the error at the impact point, i.e., the range of error) from several kilometers to 10 km [34], depending on the parameters of the trajectory at the initial point of the ballistic phase. The effect of the next greatest action, proportional to the square of polar flattening leads to a deviation of the impact point of as much as tens of meters. /246

Thus, referring to the possibility of firing ballistic missiles not only at areal, but also point targets (the launch bases of an enemy and strategic objects), in describing the trajectories of their motion along the ballistic phase, only terrestrial gravity must be considered as among the acting forces, by introducing into the model of the gravity potential terms corresponding to the first and second powers of polar flattening.

This potential sometimes is called the normal potential; the figure of the Earth is represented in this case by an ellipsoid of revolution, with reference to the second power of polar flattening [34].

The trajectory of missile motion calculated in this way is not free of methodological errors caused by the force field model adopted. Random errors acting on the ballistic flight phase are partially also related to an inexact description of the effective forces. This is caused by the fact that the true parameters of the Earth's figure and of the terrestrial gravity field (so-called geophysical constants) are known inexactly. For example, for the Earth's radius the error is +15 km. The values of these parameters express the coefficients in the formula or in the series describing the force function, which therefore are also determined with random errors. Therefore intensified requirements on the accuracy of missile impact give rise to the need for a continuous refinement of geophysical constants.

This effort, combined with the solution of geodetic problems, also pursues the aim of revising the geodetic tie-in of ground objects and the continents per se. Inaccuracy in the tie-in (and it may be as much as several tens of meters) can also markedly affect the missile's target impact errors.

The terminal stage of missile motion takes place again within the atmosphere. It is characterized by large g-loads and by a high surface temperature of the ballistic nosecone. Allowing for these effects and, when necessary, reducing them down to acceptable values is one of the requirements imposed in selecting this trajectory. Two other requirements consist of reducing the motion errors accumulating both in the preceding flight stages as well as arising due to random actions during this present stage, and also in selecting the maneuver or in selecting the trajectory. /247

which would permit a reduction or an exclusion altogether of possible enemy countermeasures. Foreign specialists believe that all this leads to the necessity of guidance of the missile over the terminal flight phase with autonomous guidance or with homing onto the target.

The conditions of nosecone entry into the atmosphere, in particular, entry velocity and angle, determine the g-loads and the nosecone temperature conditions. Depending on their acceptable values, there exists a corridor in which all entry trajectories must lie. In the graphs in Fig. 4.26, the given values of V_K and θ_K are approximately equal to the values of the angle θ and the velocity at the point 1 (Fig. 4.24) and they are also equal, approximately, to the values of these functions at the upper limit of the atmosphere. To obtain acceptable values of the entry and the velocity, correction of the trajectory prior to atmospheric entry can be employed.

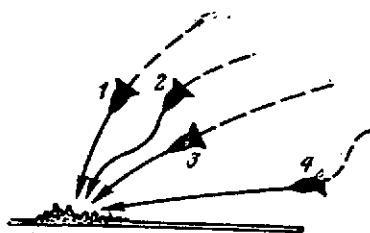


Fig. 4.29. Trajectories of various kinds of ballistic missile nosecones in the atmospheric flight phase:

- 1 -- Nosecone flying along a vertical trajectory: flight time in atmosphere to the target is 8-15 seconds
- 2 -- Maneuvering nosecone of MBRV: flight time 20-30 seconds
- 3 -- Nosecone with powerplant providing great acceleration over the terminal flight phase: flight time 5-10 seconds
- 4 -- Gliding nosecone of BGRV: flight time 2-3 minutes

Temperature stresses can also be reduced by shortening the time the nosecone travels within the atmosphere, which is achieved by applying additional jet thrust over the atmospheric flight phase⁵.

Maneuvering along a trajectory aimed at making difficulties for the enemy's AMD [antimissile defense] is achieved by means of aerodynamic forces. For example⁵, for this purpose the nosecone of an American BGRV has control aerodynamic surfaces in its tail section, while the nosecone of a MBRV has an elongated flare and exhibits a very high lift-drag ratio, 2.8-3.0. The approximate shape of the trajectory of these two nosecones in the atmosphere is shown in Fig. 4.29. Also given there are other trajectories already referred to, and the time the nosecones spend in the atmospheric flight phase is also given.

As we can see, a gliding cone traveling along a trajectory with the smallest g-loads and temperature stresses takes the longest amount of time to reach its target. This facilitates its detection and interception by AMD facilities. Trajectories that are realized in the shortest time do not have the advantages of the gliding trajectory. But maneuvering along a trajectory complicates the guidance and control system [214].

Thus, choice of the flight trajectory of a ballistic missile over the terminal phase is one of the problems that must be solved in each specific case with reference to the requirements specified above.

FOOTNOTES

¹ It must be noted that recently an estimational criterion -- the cost of performing a combat operation [16, 67, 79] -- has also begun to be used in evaluating the capabilities of military complexes. These questions will be dealt with in more detail in Chapter Six.

² The payload depends on the flight range and can vary due to the weight of fuel.

³ The cost of one ton of kerosene is 45 rubles, and the cost of one ton of gasoline is 100 rubles [35, 36].

⁴ The set of allowable control laws comprises a function of the form shown in Fig. 4.27 c. The optimal solution is sought for from this set.

⁵ cf. [131, 137, 171, 200, 202].

5.1. Main Characteristics of Space Craft

The main characteristics of space craft include: function, weight, makeup of installed equipment, presence and number of crew, orbital parameters, and possible range of their use (maneuver). Space craft are divided into artificial earth satellites, manned orbital space craft, unmanned space craft for automatic flight to the planets of the solar system, manned space craft, and so on.

Artificial earth satellites can be used for communications, navigation of ships and aircraft, weather reconnaissance, geological, geodetic, and geographic studies, radio and television communications, fueling of space craft, and crew dispatching and return from orbital space craft (/46,55,57,104,145,148/).

At the present time, USSR and U.S. specialists are examining the feasibility of using space craft as long-term orbital stations. These stations will be used to study the earth's natural resources and conduct studies of installations facilitating the efficiency of crews in extended space flight and the physical properties of outer space.

In addition, orbital station crews will conduct astronomical observations.

In the future, this kind of equipment can be used as way-stations in interplanetary flights.

The motion of space craft -- artificial earth satellites (AES) -- has several characteristics compared with the motion of other flight craft -- airplanes and missiles. AES move at such altitudes, or more exactly, at such separation from the earth that the dissipative effect of the atmosphere is absent. Therefore, their ballistic motion, that is, motion without the application of active forces, occurs mainly under the effect of terrestrial gravity.

/250

To the first approximation, their trajectory can be described by six independent constant quantities -- Keplerian orbital parameters -- uniquely expressed in terms of the first integrals of the equations of motion, and therefore, in terms of the coordinates and velocity at any instant of time. Each of the Keplerian parameters has a geometrical or kinematic sense, and since the parameters themselves remain unchanged, the geometry and kinematics of satellite motion remain constant to the first approximation.

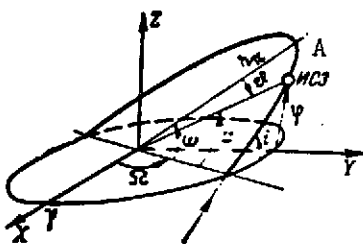


Fig. 5.1. Elements of the orbit of an artificial earth satellite
KEY: A -- AES /artificial earth satellite/

Two Keplerian elements Ω and i characterize the position of the orbital plane. The longitude of the ascending node Ω (Fig. 5.1) is measured by the central angle lying in the plane of the equator and formed by the direction from the orbital focus at the ascending node -- the point of intersection by the satellite of the equatorial plane in its transition from the southern to the northern hemisphere -- and the direction toward any fixed point, for example, the point of the vernal equinox γ . The inclination of the orbital plane to the equator i is the angle between the plane of satellite motion and the equatorial plane.

The parameters p and e -- the focal parameter and the eccentricity -- characterize the size and shape of the orbit. They are related by the function $p = a(1 - e^2)$ with the major semiaxis of the orbit a , which is determined by the total energy of motion of the satellite, therefore in describing the shape and dimensions of the trajectory, any two of these three quantities can be selected. /251

Closed (in the first approximation) elliptical or circular trajectories -- one of the foci of which coincides with the earth's center -- are possible only if the following inequality is satisfied at each instant of the satellite motion

$$V^2 < 2 \frac{\mu}{r},$$

where V is the orbital velocity;

r is the radius-vector extending from a focus to the satellite (focal radius); and

$\mu = fM = 398,600 \text{ m}^3 \cdot \text{s}^{-2}$ is the product of the gravitational constant f by the mass of the earth M .

The eccentricity of these orbits is always smaller than unity ($e < 1$).

The position of the orbit in the plane is given by the angle between the line of the ascending node (the direction from the geocenter to the ascending node) and the direction to the orbital point nearest the earth -- the perigee. This angle ω is called the angular position of the perigee; it is meaningless for circular orbits. When circular and elliptical orbits must be described with a single system of parameters, it is best to replace the

parameters p , e , and ω with the parameters p , q , and k , where q and k are the components of a vector directed from an orbital focus at its perigee (the Laplace vector) [98]. Other independent functions of the first integrals of the equations of motion can also be used.

The parameters a and e are expressed simply in terms of the altitude of the apogee (the farthest removed point) and the perigee of the orbit H_α and H_π :

$$e = \frac{r_\alpha}{a} - 1, \quad (5.1)$$

where

$$a = R + \frac{H_\alpha + H_\pi}{2}.$$

The semimajor axis characterizes the mean dimension of the orbit and is equal to the total energy of motion:

$$\frac{1}{a} = \frac{2}{\mu} \left(\frac{\mu}{r} - \frac{V^2}{2} \right), \quad (5.2) \quad /252$$

which, as a consequence of assuming only conservative effective forces, remains constant throughout the entire motion. The semimajor axis is also associated with the period of revolution of the satellite T by the equation

$$T = \frac{2\pi}{\sqrt{\mu}} a^{3/2} \quad (5.3)$$

Depending on the coordinate system adopted, several periods of revolution are distinguished.

The stellar or sidereal period (T_{st}) is measured in an absolute system of coordinates associated with fixed stars. If the operation of an AES is dictated by objects located on the earth's surface, the synodic period of revolution (T_{syn}) considered with respect to a point rotating together with the earth is more important.

All the five listed parameters describe the orbital geometry. The kinematics of the motion is characterized by a sixth Keplerian element, which can be taken as the instant of transit τ of an AES of the perigee.

The following entities can be the angular quantities specifying the position of the satellite in its orbit:

-- the true anomaly ϑ is the angle formed by the focal radius-vector and the line of apsides connecting the apogee and the perigee of the orbit; and

-- the argument of the latitude u , the angle formed by the focal radius-vector and the nodal line ($u = \vartheta + \omega$), and certain other angular variables.

The relationship between change in the angular position and the time of motion is afforded by the last expression; the inverse function -- the change in angle as a function of time -- is much more complicated and is described by a transcendental function.

All Keplerian elements are constant only when the motion of the satellite is in the field of attraction of a material point (sphere). Since the gravity field of the earth is in reality more complicated and other forces also act on a moving satellite, these parameters vary. This variation, as a rule, is small and therefore methods of perturbation theory are applied to describing this motion, while the parameters themselves are now no longer called Keplerian, but perturbational or osculatory (in accordance with the fundamental concept -- the tangency of the perturbed and the instantaneously unperturbed orbits -- underlying the description of perturbed motion). /253

Of the perturbing forces acting on AES motion, the most important are the noncentrality of the gravity field of the earth and the atmosphere [347]. The remaining forces, such as the gravitational effect of the moon and the sun, solar radiation pressure, and certain other forces, can have a perceptible effect only in individual cases on certain specialized types of satellites. For example, the attraction of the moon and the sun can affect satellites with very elongated orbits, or with orbits very far removed from the earth, and solar radiation pressure can markedly affect Echo type satellites.

The atmosphere has a generally dissipative effect [49,86,106,1207], limiting the lifetime of a satellite in orbit. The gravitational effect of the earth's lack of sphericity can be taken into account with various models of the force field approximating the true field with varying degrees of accuracy. Most of the effect of noncentrality can be taken into account if the earth is approximated with an ellipsoid of revolution [34,99,1207]. An analytic theory of AES motion describing a trajectory with the aid of quadratures can be constructed for this force influence [2,50,517]. The effect of successive approximations to the true gravity field of the earth is more than an order of magnitude less and they need not be taken into consideration when solving several problems in the navigation and control of AES.

The methodological error in the algorithms describing motion is caused to a large extent precisely by the adopted model of the effective forces, and the size of this error is determined by the requirements that are imposed on the accuracy of the

navigation, beginning from the task performed with the given satellite. If the AES motion in navigation and control must be described very precisely, then use of the Keplerian theory in analysis or construction of a system or a complex is wholly acceptable. When necessary, the results of these calculations can be then corrected with reference to the main perturbations.

One of the main features of AES motion stemming from the foregoing and differing essentially in AES use and control is that the shape and position of the trajectory in inertial space are preserved constant (only to the first approximation, as is true of the entire treatment given below). The orbit shifts relative to the earth in such a way that the satellite track point traces a continuous line on its surface. All these tracks will lie in a certain belt bounded by the maximum and minimum geographical latitude. The maximum (moduluswise) latitude of the satellite track point -- the point of intersection of the focal radius-vector with the earth's surface -- depends on the angle of inclination of the orbit, for the spherical latitude φ of the satellite is determined by the function

/254

$$\varphi = \arcsin(\sin i \sin u) \quad (5.4)$$

Since the period of revolution T remains constant (cf. (5.3)), therefore orbits are possible in which a satellite travelling along one of them will periodically pass over the same points on the earth's surface. They are called multiple orbits and can be characterized by the multiplicity factor K :

$$K = \frac{24}{T_{\text{AES}}^K}, \quad (5.5)$$

where T_{AES}^K is the period of the multiple revolution of a satellite satisfying this equation, in hours, and K is any integer.

If $K = 1$, the satellite is called a synchronous satellite and it is roughly 35,680 km from the earth. An equatorial synchronous satellite (its orbital plane and the plane of the equator coincide) moving in the direction of the earth's rotation is called a stationary satellite; it is always over the same point on the earth's surface.

Thus, by varying the semimajor axis one can control the period of revolution of a satellite and the period of its transit over specific points on the earth's surface. Characterizing the total energy of satellite motion, the quantity a determines the energy expenditures in its launch, that is, the ultimate cost of inserting the given satellite into orbit.

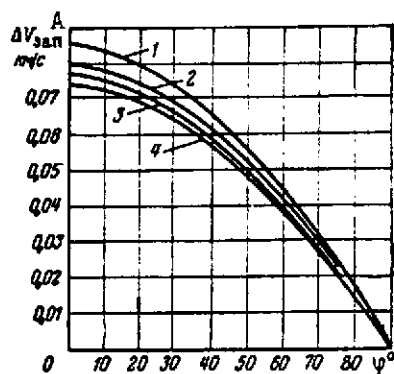


Fig. 5.2. Additional speed of an AES at the end of the insertion phase (ΔV_{ins}) as a function of the geographical latitude of the launch point:

- 1 -- for an orbital elevation $H = 1000$ km
- 2 -- for $H = 500$ km
- 3 -- for $H = 300$ km
- 4 -- for $H = 0$ km

KEY: A -- ΔV_{ins} , km/sec

Use of the earth's rotation in orbiting a satellite (launch in the direction of the earth's rotation -- to the east) yields a further velocity gain ΔV_{ins} , not -- however -- exceeding 460 m/sec at the equator and equal roughly to 200 m/sec for the orbits of most Soviet satellites ($1 \approx 65^\circ$). This additional quantity ΔV_{ins} is determined by the function

(Fig. 5.2):

$$\Delta V_{ins} = \Omega_E r_{ins} \cos \varphi_{ins} \quad (5.6)$$

Here Ω_E is the angular velocity of the earth

r_{ins} is $R + H$, where R is the mean radius of the earth, and H is the altitude of the insertion point.

The possibilities of inserting an AES into orbit at a given altitude and the installation on board of the required research apparatus depends on the power of the launch vehicles placing it in orbit (Fig. 5.3 a) [119], the geographical latitude of the launch point, the direction of the launch, the given insertion altitude, and the type of engine and the fuel-oxidizer [104] (Fig. 5.3 b and c). A greater weight can be inserted into an elliptical orbit than into a circular orbit with the same period of revolution. This becomes understandable if we bear in mind that the period of revolution depends on the major semiaxis and the insertion of a satellite into an elliptical orbit is carried out at the perigee². Since the energy of AES insertion, proportional to the major semiaxis of the orbit, is equal to the total energy at the insertion point, it can be characterized by the value of some energy velocity V_E [112] (Fig. 5.4):

$$m \frac{v_E^2}{2} = E_{\text{tot}} = E_{\text{kin}} + E_{\text{pot}}$$

The orbital altitude is most important for communication satellites, weather satellites, and other AES, for it dictates the extent of the earth's surface S that this satellite "covers" or scans. This surface area is enclosed within a cone with apex angle β and corresponds in the plane to the arc A_1A_2 equal to (Fig. 5.5 a, b) /256

$$L_{A_1A_2} = \alpha \frac{\pi R}{180^\circ}, \quad \alpha = 180^\circ - \beta, \quad \sin \frac{\beta}{2} = \frac{R}{R+H},$$

where R is the mean earth radius.

When the functioning of an AES is associated with its transit into the region of assigned earth stations, the stellar T_{st} is not as important as the synodic period of revolution T_{syn} (Fig. 5.5 c). To perform certain tasks the orbital multiplicities (5.5) must be used, and for other tasks, conversely, it is important that the belt scanned by the satellite be systematically shifted. The daily value of this shift ΔZ_φ can be determined from the equation /257

$$\Delta Z_\varphi = K(T_{\text{mu}} - T_{\text{di}}) \frac{2\pi}{24} R \cos \varphi = 2\pi \frac{T_{\text{mu}} - T}{T} R \cos \varphi.$$

Here T is the period of revolution of the given AES;

T_{mu} is the nearest multiple period corresponding to the multiplicity K ; and

φ is the geographical latitude of the station.

Finally, orbital altitude H , generally the perigee altitude H_π , affects a very important characteristic of the satellite -- its lifetime³. The dissipative effect of the atmosphere, by reducing the total energy of motion, causes a gradually accelerating lowering of the orbit (Fig. 5.6) and leads to the burnup of the AES upon entering the dense atmosphere layers.

We can conventionally define the lifetime of an AES as the time required to reduce its period of revolution to $T = 87$ min, which corresponds to the orbit altitude of about 140 km. The lifetime depends not only on the orbital characteristics, but also on the condition of the atmosphere (on solar activity) and the quantity $(C_x S_M / m) = B$, sometimes called the satellite's ballistic coefficient (C_x is the drag factor of the AES, S_M is the midsection area; and m is the mass of the AES). /258

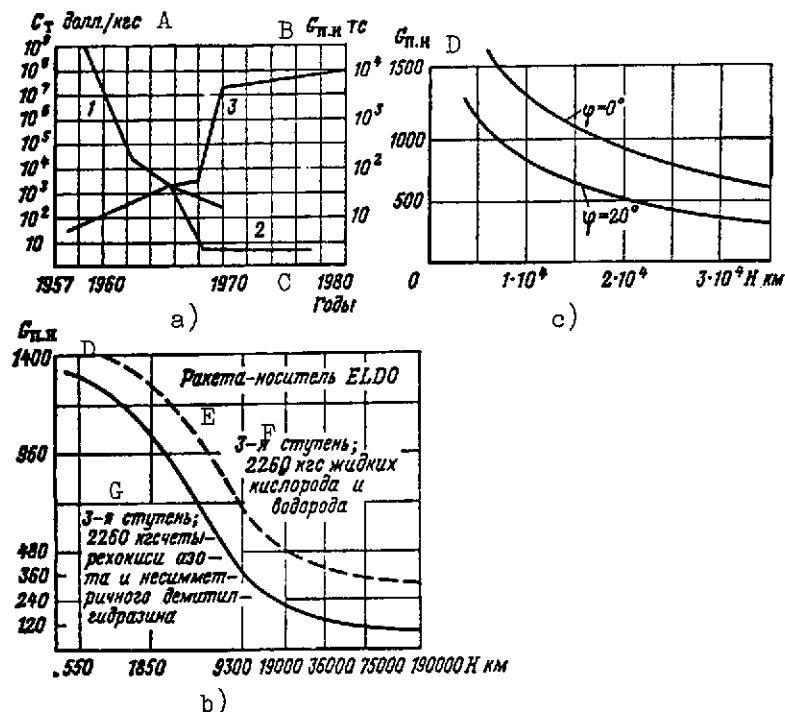


Fig. 5.3. Weight of payload and costs of placing 1 kg of payload into orbit:

- a -- total annual payload inserted into earth orbit (curve 3) and the costs of inserting 1 kg of payload with a ballistic missile (1) and a rocket-plane (2)
- b -- change in the weight of a payload as a function of orbit altitude and fuel and oxidizer used with the example of the ELDO rocket (European Launcher Development Organization)
- c -- payload inserted into circular orbit as a function of its radius and the geographical latitude of the launch point

KEY: A -- C_{tot}, dollars/kg G -- Third stage; 2260 kg of nitrogen tetroxide and asymmetric dimethylhydrazine

B -- G_{pay}, tons

C -- Years

D -- G_{pay}

E -- ELDO launch-vehicle

F -- Third stage; 2260 kg of liquid oxygen and hydrogen

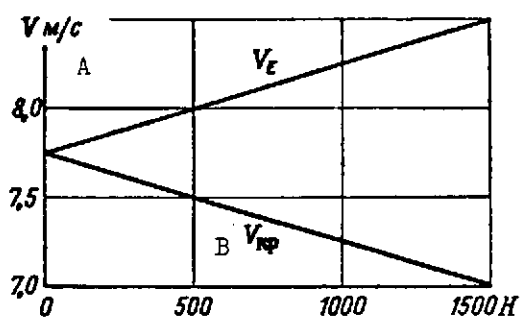


Fig. 5.4. Energy V_E and circular V_{c1} velocities as functions of the flight altitude
KEY: A -- V , m/sec
B -- V_{c1}

Studies of the effect of the atmosphere on the trajectory of a satellite are given in the works [65,86,106,121].

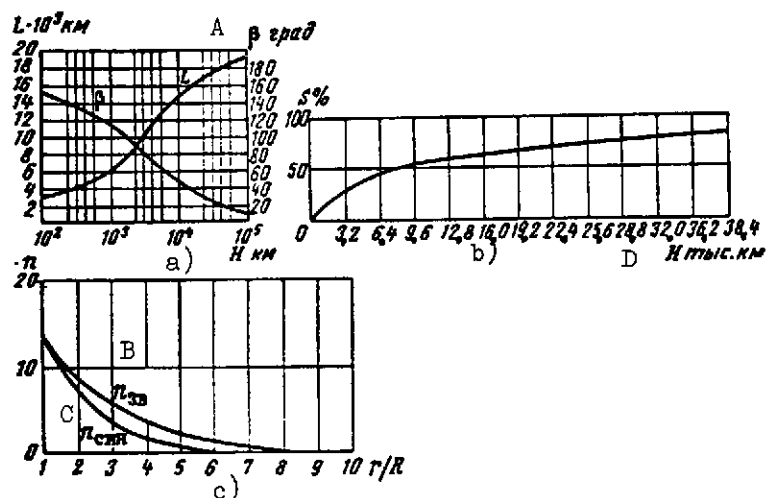


Fig. 5.5. Characteristics of earth-scanning satellites:

- a -- L and β as functions of H
- b -- surface area of the earth S covered by an AES as a function of H
- c -- number of revolutions per day as a function of the relative orbital radius (n_{st} is the number of stellar [sidereal] revolutions and n_{syn} is the number of synodic revolutions)

KEY: A -- β , deg

B -- n_{st}

C -- n_{syn}

D -- H , thousands of km

Studies on the effect of the atmosphere on the trajectory of a satellite are given in the works [65,86,106,121].

These problems are some of the problems of planning orbits, that is, selecting a trajectory most fully carrying out the main mission of the flight with the most economical use of the technical facilities [33]. Maneuvering, that is, the purposeful variation of orbital parameters, must be used to facilitate the flight mission and to modify it. When the actual flight trajectory deviates from the assigned trajectory, correction of motion must be employed. The calculation of the control law in any given case is a task of the navigation system; implementation of this law is a task of the control system. Maneuvering and correction are associated with additional fuel and oxidizer consumption, which is proportional to the velocity change ΔV . Its total value V_Σ is called the characteristic velocity and is an indicator of the operating economy of the selected method of trajectory modification. /259

The brevity of the powered phases during maneuvering and correction permits an idealization, under which the impulse application of the active forces is assumed, i.e., the instantaneous change in the velocity of orbital motion by ΔV . Additionally, in designing and in the preliminary selection of the control law, it is wholly acceptable to limit oneself to the frame of reference of the Keplerian theory.

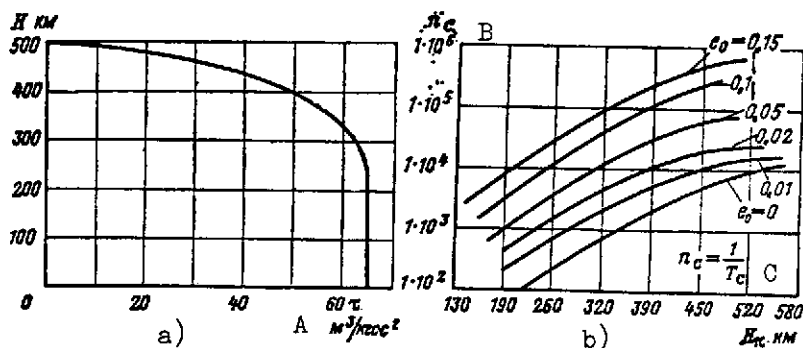


Fig. 5.6. Change in AEC trajectory parameters (according to [120, 42, 105]):

a -- Decrease in altitude of initial circular orbit $H_0 = 500$ km as a function of conventional time

$$\tau = (C_x S_M / 2m)t$$

b -- Number of revolutions of the lifetime of an AES as a function of the perigee altitude for orbit with e_0

KEY: A -- $m^3/kg \cdot sec^2$
 B -- n_{re} [revolution]
 C -- $n_{re} = 1/T_{re}$

In all cases of flight, the application of the velocity impulse at the perigee of the transfer orbit is the most economical.

A noncoplanar transfer or, as it is called, a transfer with a rotation of the orbital plane (Fig. 5.7), requires much greater energy outlays. If the radii of the initial and terminal orbits are equal, this transfer can be made with the application of a single velocity impulse at the point of their intersection.

Its value can be estimated with the example of the rotation of the plane of a circular equatorial orbit by Δi (Fig. 5.7 b). /260
In this case the relative characteristic velocity is

$$\Delta \bar{V} = \frac{\Delta V}{V_1} = 2 \sin \frac{\Delta i}{2}.$$

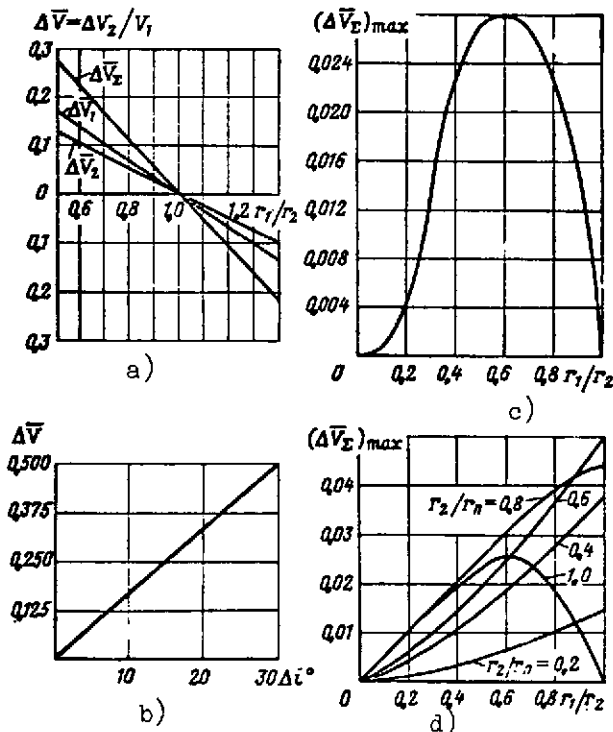


Fig. 5.7. Relative energy expenditures $\Delta \bar{V}$, characteristic velocity $\Delta \bar{V}_\Sigma$ and maximum economy of characteristic velocity $(\Delta \bar{V}_\Sigma)_{\max}$ for two- and three-impulse transfers:

- a -- $\Delta \bar{V}$ for a coplanar transfer between two orbits
- b -- $\Delta \bar{V}$ for the rotation of the plane of the equatorial orbit
- c -- Maximum economy $(\Delta \bar{V}_\Sigma)_{\max}$ when a two-impulse transfer with one rotation of the plane is replaced with a two-impulse transfer with two rotations
- d -- Maximum economy $(\Delta \bar{V}_\Sigma)_{\max}$ when a three-impulse transfer with one rotation of the plane is replaced with a

three-impulse transfer with three rotations of the plane (the plane is rotated by the second impulse; r_{in} is the radius of the intermediate orbit)

Fig. 5.7. Relative energy expenditures $\Delta\bar{V}$, characteristic velocity $\Delta\bar{V}_\Sigma$ and maximum economy of characteristic velocity $(\Delta\bar{V}_\Sigma)_{\max}$ for two- and three-impulse transfers

KEY: A -- $r_2/r_{1n} = 0.8$ [Continued]
 B -- $r_2/r_{1n} = 0.2$

The transfers between two noncoplanar orbits with unequal radii can be executed with different numbers of impulses and with different energy expenditures (cf [189, 192], Fig. 5.7, c - d). /261

The problem of the rendezvous of a spacecraft with another space object does not fundamentally differ from the maneuvers we have been considering. The difference can lie only in the supplementary conditions imposed on the time of motion, for both objects must simultaneously arrive at the point of rendezvous, and on the value of the relative velocity (and possibly also the value of the relative coordinates) at the end of the transfer trajectory dictated by the goal of the rendezvous and the capabilities of the onboard equipment.

If the object of the rendezvous and the transport craft (we will thus conventionally refer to the objects approaching each other) travel along circular coplanar orbits, then for a Hohmann transfer trajectory the rendezvous will occur if the angle between the focal radii at the initial moment of the maneuver is

$$\Delta v = \pi \left[1 - \left(\frac{r_{in} - r_t}{2r_t} \right)^2 \right], \quad (5.7)$$

where r_{in} and r_t are the focal radii-factors of the transport craft and the object of rendezvous, respectively.

To synchronize the time of the transport craft, the maneuver can be begun later (holding in orbit). The transport craft, on executing the maneuver, can specifically transfer from its initial orbit to the holding orbit, which can be elliptical or circular. In the first case, if the orbit of the rendezvous object is circular, it is selected so that it not only lies in the plane of the orbit of the rendezvous object, but also is tangent to it at the apogee or the perigee.

If the holding orbit is circular, then by condition (5.7) the maneuver of approach must be executed along a Hohmann ellipse.

The determination of the control law in landing is also one of the tasks of navigation. It is subdivided into two tasks: determination of the control law for the orbital departure and for motion in the atmosphere.

The first problem is analogous to the ordinary maneuver and consists of applying the retro-velocity impulse, transferring the craft to a descending elliptical trajectory. The difference and /262 complexity lie in satisfying the conditions at the second end-point of the trajectory, located at some arbitrary altitude, which we sometimes will take as the altitude of the effective action of aerodynamic control (80 - 100 km).

The conditions of atmospheric reentry and the retro-impulse $\Delta \vec{V}_{\text{retr}}$ depend, in particular, on the angular range ϕ of the orbital departure trajectory (Fig 5.8).

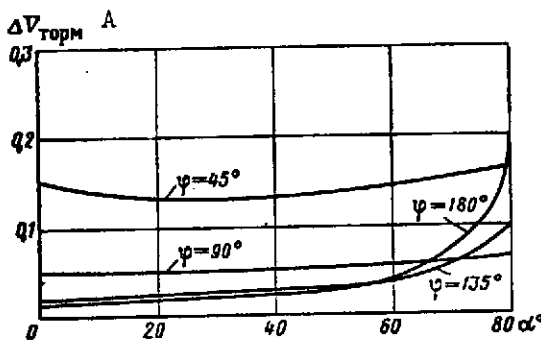


Fig. 5.8. Relative retro-moment values
KEY: A -- $\Delta \vec{V}_{\text{retr}}$

The relative retro-impulse of the circular orbit of departure can be determined from the formula

$$\Delta \vec{V}_{\text{retr}} = \frac{\Delta V_{\text{retr}}}{V_0} = \frac{1}{2} \sec \alpha \{ 2(1 + \bar{H} - \cos \phi) + \tan \alpha \sin \phi - [\tan^2 \alpha \sin^2 \phi + 4(1 - \cos \phi) \times (1 + \bar{H} - \cos \phi + \tan \alpha \sin \phi)]^{1/2} \} \times (1 + \bar{H} - \cos \phi + \tan \alpha \sin \phi)^{-1},$$

where V_0 is the velocity in the circular orbit;

$\bar{H} = H/R$ is the relative orbital altitude; and $\pi - \alpha$ is the angle between the directions \vec{V}_0 and $\Delta \vec{V}_{\text{retr}}$.

The minimum value of $\Delta \vec{V}_{\text{retr}}$ corresponds to the angle $\phi = 180^\circ$, however in this case the trajectory (the value of ϕ) is highly sensitive to errors in the vector $\Delta \vec{V}_{\text{retr}}$ (cf Fig 5.7 b and /263 c). The lateral deviation of the landing point δB can be determined by the function

$$\delta B = R \sin \phi \delta \beta,$$

where $\delta\beta$ is the lateral deviation of the vector $\Delta\vec{V}_{\text{retr}}$ from the assigned direction. The value of $\delta\beta$ [sic] is a maximum for a given $\delta\beta$ with $\phi = \pi/2$. When $\phi = \pi$, the lateral displacement is zero.

In landing from an elliptical orbit for given conditions of atmospheric re-entry and the bounded energetics ΔV_{retr} , formation of the departure trajectories cannot occur at just any instant motion. Forbidden orbital regions, from which transfer to the descent trajectory is impossible, become larger with increase in the eccentricity of this initial orbit.

The trajectory of a craft in the atmosphere can be controlled over the entire extent of motion (cf, for example, [42]). The maneuver is executed by using aerodynamic forces (sometimes the thrust of special jet engines is employed), produced by special surfaces or by the actual body of the craft. The lift-drag ratio in the latter case can be as much as 2.5-3. Maneuvering for a landing in the atmosphere is executed in order to reduce the g-load and the heating of the craft body, modify the trajectory (chiefly its lateral turning for landing at an assigned point), and correct the motion (approximation of the actual trajectory subject to various random perturbations to the nominal trajectory).

The program (or more exactly, the series of programs) of the atmospheric phase is calculated ahead of time. During the flight, depending on the conditions of entry, one of them is selected, for which motion is then realized with the aid of the control system.

When discussing the atmospheric phase of the trajectory, it cannot be forgotten that maneuvering using the action of aerodynamic forces can be used also in the flight itself to alter the plane of motion (cf, for example, [194]). Here the perigee is lowered, by means of a retro-velocity impulse, to the altitude at which the effect of the aerodynamic forces permits the orbital plane to be turned, and then the craft is transferred to the required trajectory using two velocity impulses. For some flight conditions, this combination maneuver can prove more economical than a purely gas-dynamic maneuver. [264]

Let us consider characteristics of certain types of artificial earth satellites.

AES used for communications are subdivided, depending on the equipment layout, into passive and active, and depending on the orbital parameters, into low ($H_\alpha < 5000$ km) and high ($H_\alpha > 5000$ km).

Passive communication satellites, for example, Echo-1 and Echo-2, are reflectors in the form of a metal sphere or an assemblage of angle bars. Their advantage lies in simplicity and operating reliability, due to the absence of any electronic

equipment: their disadvantage is that in intercontinental lines of large extent, the signal-noise ratio is low.

Since energy losses in propagation are in this case involved with reflection, they vary proportionally to the fourth power of the distance (Fig. 5.9 [187]). An increase in the size of the satellites can only slightly reduce the losses (an increase in the diameter of spherical AES by a factor of 2 reduces losses by 6 db and therefore makes necessary the use of ground antenna with large aperture. Additionally, increasing the size of a passive satellite leads to an increase in its weight. A disadvantage of passive AES is also the fact that the deformation of their surface gradually leads to a reduction in the reflection coefficient.

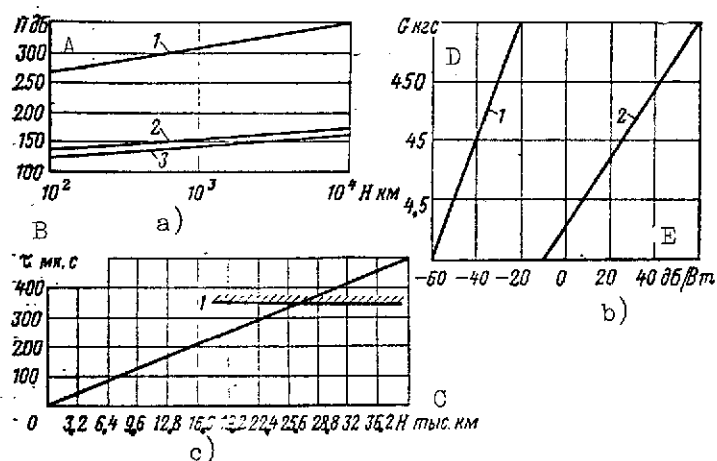


Fig. 5.9. Characteristics of communication systems using AES [104]:

- a -- Energy losses:
 - 1 -- Passive AES
 - 2 -- Active AES with omnidirectional antenna
 - 3 -- Active AES with a 10 db antenna gain factor
- b -- Weight of AES as a function of radiated power, db/w:
 - 1 -- Passive spherical reflector
 - 2 -- Active communication AES

- c -- Radio signal delay time τ as a function of orbital altitude H :
 - 1 -- Boundary of allowable τ values

KEY: A -- Π , decibels
 B -- τ , microseconds
 C -- H , thousands of km
 D -- G , kg
 E -- db/w

Active communication satellites lack these drawbacks. They are equipped with retransmitting equipment amplifying the received signal and sending it to a ground receiving station. The retransmission can be immediate or with delay of data when signals recorded in the onboard memory are transmitted to the region of the ground receiving station according to a previously adopted program or by command from the earth. The satellites can be both oriented, as well as nonoriented with omnidirectional radiation. The latter, naturally, under otherwise equal conditions need retransmitters of greater power, whose disadvantages are lower reliability and lower carrying capacity.

In designing the orbits of communication satellites, certain specific requirements must be taken into account, such as the number and arrangement of ground communication stations, number of channels which must connect different pairs of ground stations, the distribution of the holding time and the signal delay time for duplex telephone lines, problems of coordinating the system, and the effect of outer space conditions on equipment longevity.

One of the important conditions determining the orbit altitude of communications AES is the already referred to quantity of the earth's surface covered by the satellite in which the reception of reflected or retransmitted waves is possible. Angle α is equal to the maximum angular separation at the earth's surface of the transmitting and receiving radio stations. Also associated with the orbital altitude is the time when the satellite is in the earth's shadow; it determines the possibilities for recharging solar cells. The time of the synchronous location of the satellite in the shadow does not exceed one percent.

The time of the mutual visibility of two points on the earth surface also will depend on the orbital altitude, increasing with an increase in this latter quantity. Thus, continuous communications between two given points on the earth surface is dependent on the altitude (circular) of the orbit and the number of satellites (n) traversing it. Therefore, though satellites traveling in low orbit provide communications for a smaller required power and need less energy for orbital insertion, the bounded zone of visibility makes their application difficult. As a rule, only active repeaters with delay feature are used at these altitudes. The disadvantages of low orbits also include the fact that the onboard equipment is subject to radiation effects and the high rate of the angular motion of the satellite makes difficult; the Doppler frequency shift produced also additionally renders the isolation of transmitted data difficult. /266

Also not free of disadvantages is the use of high orbits. The most essential factor in this case is the long signal delay, that causes an echo effect in reception (Fig. 5.9 c). In this case elliptical, severely elongated orbits with apogee lying in the region of the stations in communication are more advantageous than circular orbits. The Molniya AES orbits are constructed in just this manner.

A disadvantage of elliptical orbits is the fact that the antenna gain must be varied in order to sustain a constant signal/noise ratio. Additionally, their perigee can pass through the internal radiation belt of the earth, and also through those layers of the atmosphere which can have a marked dissipative effect on satellite motion.

The number of required AES in a communication system can be markedly reduced if there is a possibility of controlling their relative position by correcting and stabilizing⁴ it (Fig. 5.10 a).

All the system parameters we have been considering: number of AES, orbit altitude, its shape, and the presence of stabilization, as seen in Fig. 5.10 b-c, fundamentally affect the stability of the communications system. /267

With the exception of ECHO type AES, all communication satellites are active repeaters.

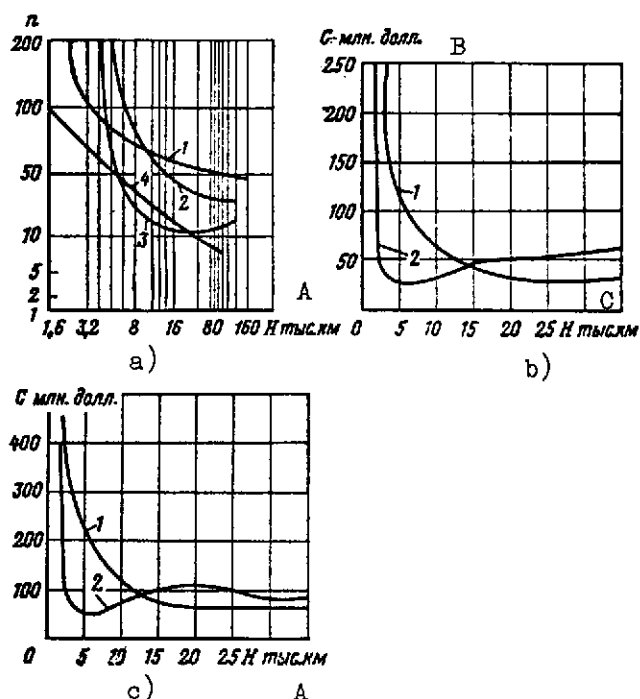


Fig. 5.10. Number of satellites and costs of communication facilities using AES:

- a -- Number of AES for linking New York with Paris:
 - 1 -- For circular polar orbits and 99 percent overlapping
 - 2 -- For circular equatorial orbits and with stabilized AES
 - 3 -- For circular polar orbits and stabilized AES
 - 4 -- For elliptical inclined orbits ($i = 63.5^\circ$) and stabilized AES
- b -- Costs C of building a group of AES for continuous communication between New York and Paris
- c -- Costs of operating this group of AES (in b and c, curve 1 represents AES stabilized in orbit; 2 -- AES are unstabilized)

KEY: A -- H, thousands of km
 B -- C, millions of dollars
 C -- H, thousands of km

Molniya communications AES rotate in strongly elongated orbits with an apogee located in northern hemisphere and with a semidiurnal period of revolution, which permits about an 8-10 hour session of Moscow - Vladivostok communications. The satellite is equipped with a system of high-precision antenna orientation and with an onboard transmitter with a radiation power of 40 w. Telestar satellites

were designed to investigate communication systems using AES and to develop elements of equipment for relaying television programs /268 and two-way conversations in several channels. With a radiation power of the onboard computer of 2-2.5 w, this satellite provides a Europe-United States communications linkup lasting about an hour.

The Relay satellites were designed to determine the optimal operating conditions of equipment and to investigate the capabilities of active space communications systems. They furnished a Europe-United States communications linkup lasting about 70 minutes per period of revolution.

The Syncom satellites are synchronized communications AES. They are designed to develop a worldwide communications system, which can be provided with three such satellites. The Courier AES was an experimental prototype of an active repeater with data delay. Communication with it was ended 17 days after launch.

The Echo satellites are passive repeaters made in the form of an inflated spherical shell of metallized material.

Meteorological AES are used to acquire operational and worldwide information on the condition of the earth's atmosphere, to study the radiation balance of the earth, and to measure the spectral distribution of the radiation of the earth and sun. Problems of setting up a system do not play the role with these satellites as with communications AES. The main conditions that their trajectories must satisfy include providing for the acquisition of necessary data, that is, transiting the required number of times over assigned earth regions with assigned parameters (mainly, altitude) of the orbit and providing for the transmission of the acquired data, that is, transiting of the regions of the ground stations.

In order to conduct studies in all latitudes with meteorological satellites, they are launched into polar orbits. Their altitude is dictated by equipment requirements and can vary from 500 km to several thousands of kilometers. Data from meteorological satellites, as a rule, are transmitted to the earth via television cameras.

The TOS /Tiros Operational Satellite/ system of meteorological satellites includes Tiros satellites, regularly launched in the United States since 1961. By 1967 13 Tiros AES and two Nimbus satellites had been launched. The first meteorological satellites were launched into nearly circular orbits, 700-800 km in altitude. Since /269 the inclination of the orbital plane to the equator is $48^{\circ} - 58^{\circ}$, they can photograph cloud cover in a region of latitudes to $+58^{\circ}$. The later launches of the Tiros AES (beginning with the ninth) were made into orbits that were near-polar ($i \approx 100^{\circ}$), with a mean altitude of about 1400 km ($T \approx 113$ minutes).

TABLE 5.1

Characteristics	AES of the Meteor System: Kosmos-122, -144, -156, -184, -206
Orbit	Circular, near-polar
Orbital altitude, km	625-630
Stabilization system	Triaxial electromechanical with respect to the earth; solar cells are oriented toward the sun with an autonomous sys- tem
Makeup of meteorolo- gical equipment	Two television (TV) cameras; <u>/270</u> infrared (IR) camera of the television type (wavelength range 8-12 microns); actino- metric (AC) camera -- with two narrow-sector scanning and wide-sector scanning radiometers
Width of coverage strip of locale, km:	
TV equipment	1000
IR equipment	1000
AC equipment	2500
Three-dimensional re- solution at the nadir, km:	
Of TV images	1.25 X 1.25
Of IR images	15 X 15
Of AC images	50 X 50
Power sources	Solar and chemical cells

The makeup of the onboard equipment of meteorological satellites includes television cameras with narrow- and wide-angle lenses, infrared detectors, and magnetic tape recorders. These instruments permit transmitting to the earth not only the images of cloud cover and ice field margins, but also observing the buildup of hurricanes, typhoons, storms, and measuring earth temperature.

These data are recorded by onboard memory devices, and then on ground command are beamed to ground stations. This system can transmit to earth up to 400 cloud cover images per day.

TABLE 5.2

Characteristic	Tiros Meteorological Satellite	Experimental Nimbus Meteorological Satellite
Orbit	Circular with different inclinations	Circular, near-polar
Orbital altitude, in km	700	1200
Stabilization system	By rotation, with axis of rotation in the orbital plane for the first models, and with the axis of rotation perpendicular to the orbital plane in later models	Triaxial relative to the earth (accuracy of orientation $\pm 1^\circ$); solar cells are oriented toward the sun
Location of television camera lenses	On the lower base of the body -- in the first models, and on the lateral surface -- in later models. Exposures are triggered by the IR horizon sensor when the camera is pointed toward the earth	On the lower surface of the instrumentation compartment; the cameras are always pointed toward the earth
Resolving power of TV equipment, in km	1.6 (in image center)	0.8 (in image center)
Mean resolving power of IR sensors, in km	48	48
Upper resolving power of IR sensors, in km	—	8
Number of images recorded on magnetic tape per satellite revolution around the earth	32	40

/27:

Meteorological space systems can acquire different kinds of data. In particular, the Soviet Meteor system makes it possible to acquire television, infrared, and actinometric meteorological information both on the day as well as on the night side of the earth (cf Table 5.1⁵). In contrast, the ESSA meteorological system incorporating Tiros satellites has much smaller capabilities, being able to acquire only television images from the day side of the earth (cf Table 5.2⁵).

The system of meteorological AES can also collect data obtained by floating and remote automatic weather stations and transmitted to a single meteorological data processing center (this function can be fulfilled by specialized communication satellites included in the AES meteorological system).

Approximately identical trajectory characteristics of satellites performing different functions permit them to be carried out with the same craft. Thus, in the United States 138 a specialized program has been developed aimed at building a multimission satellite performing functions of meteorological reconnaissance, and in investigation of tectonic activity, volcanic activity, and tidal waves. It is projected that several of them will be launched to orbits 30,000 - 36,000 km in altitude, with the most varied inclinations. 272

Navigation with AES 150 can be carried out in several different ways, considered in Chapter One, Section 2. The method currently realized with Transit satellites is based on measuring the Doppler frequency shift of radio signals beamed from the satellite.

Polar orbits of navigation AES must intersect the equatorial plane at about 45° intervals. This will enable ships and aircraft to determine their position not less frequently than every 110 minutes. The time interval would be shortened with increase in latitude. A more even density of satellite distribution is found for a system of four AES, two of which lie in orbits with inclination $i = 20 - 30^\circ$, and two -- with inclination $i = 65 - 75^\circ$.

A project of the General Electric Company is relative determination of range conducted with an active repeater satellite and a ground radio measuring complex; two AES on a parking equatorial orbit, displaced in longitude by an angle of about 50° , are adequate for navigation in the Atlantic.

The orbits of navigation satellites are always circular, and their altitude is chosen on the condition of the most exact prediction of the trajectory and is about 800 - 1000 km.

Fig. 5.11 schematically presents⁶ the principle of employing AES in the interests of navigation.

The Transit navigation system operates according to this scheme. It includes four Doppler stations for tracking satellites with updating of data twice a day, two stations for data input into the onboard memory devices of the AES, a station for frequency reference standards and common time, a computer center, and a control center.

273

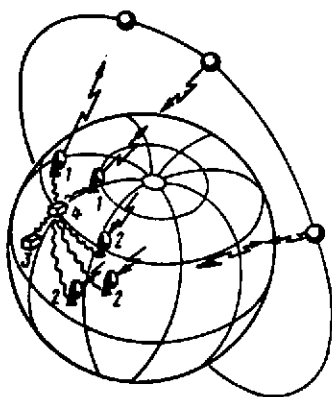


Fig. 5.11. Principle of the use of navigation AES:

- 1 -- station for data input into the onboard memory devices of the AES
- 2 -- AES tracking station
- 3 -- station for reference frequency and common time
- 4 -- computer center and control center
- 5 -- object determining its coordinates with the aid of the navigation AES

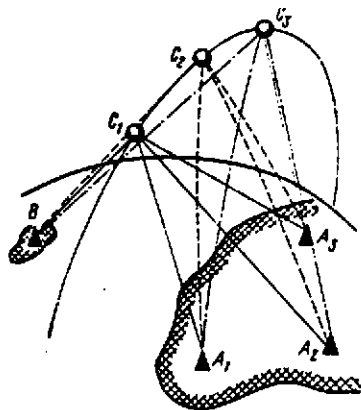


Fig. 5.12 -- Scheme for the geodetic tie-in of ground stations with the aid of AES:

- A_1, A_2, A_3 -- AES observation stations
- B -- station located at the tied-in geographic point
- C_1, C_2, C_3 -- position of satellite in orbit at the successive time instants t_1, t_2, t_3

TABLE 5.2 Continued

Characteristic	Tiros Meteorological Satellite	Experimental Nimbus Meteorological Satellite
Dimensions of earth area covered by a single frame, in km	1120 x 1120 by one camera	With three cameras: in a centralized system with magnetic tape recording 2700 -- as to latitude, and 835 -- as to longitude; in an autonomous system with direct transmission of images from the vidicon. 1600 x 1600
Angle of field of view of TV equipment, in degrees	104 -- first model; 140 -- later models	108 -- in an autonomous system with direct transmission of images from vidicon
Kind of equipment	Vidicon, 12.7 mm in diameter	Vidicon, 25.5 mm in diameter
Power sources	Solar cells and buffer storage battery	Solar cells and buffer storage battery

Compiling exact geographic maps of the earth's surface requires increased accuracy of the geodetic tie-ins of individual geographic objects, continents, and islands. At the present time it is 8 - 16 km for certain islands and up to 1.6 km for the continents [185]. There are two methods of using satellites in the interests of geodesy:

a) the satellite's orbit is known in an absolute geocentric system of coordinates, and coordinates of the assigned stations on the earth's surface are determined with respect to the satellite and thus they are tied in to the absolute system; and

b) the AES orbit is determined from measurements taken by the ground stations; since the AES motion is due to the type of force function, then the kind of function, parameters characterizing the earth's gravitational field, and thus, also parameters

274

describing the figure of the earth can be determined by the calculated trajectory. The ANNA (Army -- NASA -- Navy -- Air Force) and the Starflash geodetic satellites function according to the first method.

The ANNA AES is equipped with four xenon flash tubes designed for 70 days' of operation. The tubes are triggered when the satellite transits the region of the ground observer stations. These flash tubes facilitate spotting of the satellite and permit the determination of the relative position of the ground measuring stations with high accuracy, using optical devices. The Starflash AES, from foreign press data [138], is also equipped with a flash tube beaming coded pulses, designed for 10 months of operation, and permits fixation [tie-in] with an error of 30-50 m.

The SECOR geodetic satellite works according to the second method. To facilitate orbital determination, it is equipped with a radar transponder that operates on interrogation by a ground station.

The Geos is a combination geodetic satellite. It is equipped with flashing light sources, laser reflectors, radar reflectors, and a radio beacon transponder [138].

Fig. 5.12 schematically represents the method of using an AES for mutual fixation of different points on the earth's surface; here the satellite must be simultaneously within the visibility zone of all these stations. The geographic coordinates of the ground stations A_1 , A_2 , and A_3 are assumed to be known precisely. The satellite coordinates (in the figure -- the positions C_1 , C_2 , and C_3) are measured at the instants t_1 , t_2 , and t_3 . If the instantaneous values of the angular coordinates of the satellite are known relative to station B, these data permit the determination or the refinement of the position of station B in the chosen coordinate system. Depending on the method by which the relative position of the AES is measured, particular coordinate surfaces are used to determine its coordinates. For example, if the relative ranges are measured, the rectangular coordinates of the AES at the instants t_1 , t_2 , and t_3 are found as the points of intersection of spherical coordinate surfaces with centers lying at the stations A_1 , A_2 , and A_3 . When determining the coordinates of station B (in the same rectangular system), the centers of the sphere are at the points C_1 , C_2 , and C_3 (cf Fig. 5.12). /275

Much attention in recent years has been given to manned space craft designed to rescue crews in trouble. An existing agreement between the USSR and U.S. on this problem requires the development

of new transport spacecraft. One of the most important tasks in building long-term space transport systems is their multiple use.

5.2. Action Zones of Maneuvering Spacecraft

The action zones of maneuvering spacecraft depend on the reserves of fuel or "reaction mass" onboard, initial and terminal conditions of transfer from orbit to orbit, and also the time spent in this transfer.

We will consider multiple impulse transfers of a maneuvering spacecraft for a given transfer time. Sometimes the determining parameter is the relative velocity at the rendezvous point. We will make the following assumptions: the spacecraft is assumed to be a material point; the parameters of the initial orbit of the maneuvering spacecraft and other space objects are given exactly; instantaneous velocity impulses can be imparted to the maneuvering spacecraft at specific time instants; the Newtonian field of the earth's attraction (the field of a material point) is assumed to be unperturbed.

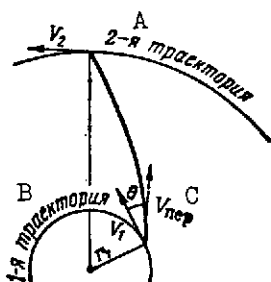


Fig. 5.13. Transfer between circular coplanar orbits

KEY: A -- Second trajectory
B -- First trajectory
C -- V_{tr} [t_r = transfer]

The trajectory of the flight of a maneuvering spacecraft depends on the magnitude of the impulse, on the point of its application, and on the angle between the vector of the initial velocity and the impulse direction. Let us consider the case of circular coplanar orbits. We will denote with θ the angle between the velocity vector of the maneuvering spacecraft at the instant of transfer and the velocity vector at the initial circular orbit (Fig. 5.13). The transfer velocity of the spacecraft is determined by the formula, with reference to angle θ and impulse ΔV : /276

$$V_{tr} = [V_1^2 + \Delta V^2 - 2V_1\Delta V \cos(\pi - \theta)]^{1/2}. \quad (5.8)$$

The transfer orbit parameters are determined as follows:

$$p_{tr} = \frac{r_1^2 V_{tr}^2 \sin^2 \theta}{\mu}; \quad (5.9)$$

$$\left. \begin{aligned}
 e_{tr} &= \left[1 + \left(\frac{r_1^2 V_{tr}^2}{\mu^2} - \frac{2r_1}{\mu} \right) V_{tr}^2 \sin^2 \delta \right]^{1/2}; \\
 r_{max} &= \frac{p_{tr}}{1 - e_{tr}}; \\
 v_{rel} &= \left[\sqrt{\frac{\mu}{p_{tr}}} (1 + e_{tr} \cos \eta_2) - V_2 \right]^2 + \\
 &\quad + \left(\sqrt{\frac{\mu}{p_{tr}}} e_{tr} \sin \eta_2 \right)^2,
 \end{aligned} \right\} \quad (5.9)$$

where

$$\delta = \begin{cases} \frac{\pi}{2} - \arccos \sqrt{\frac{V_1 + \Delta V \cos \theta}{V_{tr}}}, & 0 \leq \theta \leq \pi; \\ \frac{\pi}{2} + \arccos \sqrt{\frac{V_1 + \Delta V \cos \theta}{V_{tr}}}, & \pi < \theta \leq 2\pi; \end{cases} \quad \eta_2 = \begin{cases} \arccos \frac{1}{e_2} \left(\frac{p_{tr}}{r_2} - 1 \right), & 0 \leq \theta \leq \pi; \\ -\pi + \arccos \frac{1}{e_2} \left(\frac{p_{tr}}{r_2} + 1 \right), & \pi < \theta \leq 2\pi; \end{cases}$$

$\mu = fM.$

Here f is the gravitational constant;

M is the mass of the earth;

p is the focal parameter of the orbit; and

e is the eccentricity.

/277

The curves in Fig. 5.14 show the maximum range for a flight with circular orbit $R = 7076$ km for different transfer impulses $\Delta V = 0.1 - 0.5$ km/hr and with a rotation of the angle of impulse application within the range $0 < \theta < \pi$, where for the angles $\pi \leq \theta \leq 2\pi$ the curves lie symmetrical relative to the axis $\theta = \pi$.

As we know, the position of a vehicle in space is wholly determined by the values of four Keplerian elements and the instantaneous time instant or angular argument of the motion. Let us take a system consisting of the following quantities as a set of such parameters:

Ω is the longitude of the ascending node; i is the inclination of the orbit; a is the major semiaxis; e is eccentricity; ω is the angular distance of the pericenter from the ascending node; and u is the angular distance of the object in the orbit from the line of nodes (the argument of the latitude)

Let us set up a problem of determining optimal orbital maneuver of the spacecraft performing the rendezvous mission [121]. /278

The rendezvous point is designated in the orbit of a space object with which the rendezvous must be made by the maneuvering spacecraft, from the condition of matching the time of their motion; the following quantity must satisfy this condition:

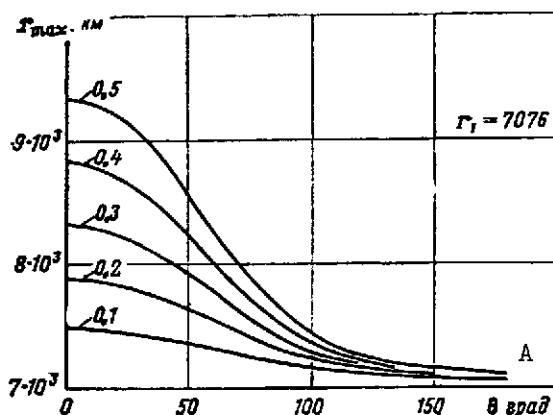


Fig. 5.14. r_{\max} as a function of the angle θ for different values of the impulse for a spacecraft transfer from a circular orbit (orbit altitude is 700 km)
KEY: A -- θ , deg

$$\Delta t_{\text{tr}} = \frac{a^{3/2}}{\gamma \mu} \{E(t_2) - E(t_1) - e[\sin E(t_2) - \sin E(t_1)]\} + lT, \quad (5.10)$$

where Δt_{tr} is the transfer time of the spacecraft;
 $E(t_2), E(t_1)$ are the eccentric anomalies of the rendezvous point and the position of the object at the instant of spacecraft launch;
 l is an integer; and
 T is the total period of revolution of the space object in its orbit.

By varying the position of the rendezvous point in the orbit and thus Δt_{tr} , we obtain different values of the characteristic velocity for an impulse transfer. A one-parametric family of curves, shown in Fig. 5.15, has an envelope determining the minimum values of ΔV . Here the launch point of the spacecraft is fixed. The characteristic velocity of the spacecraft transfer can be calculated by different formulas, whose content -- however -- is the same.

Let us derive formulas for calculating the characteristic spacecraft transfer velocity in the rendezvous mission. To determine the parameters of the transfer orbit, we can use any method of determining a trajectory by two points, for example, the Euler-Lambert or the Gauss method [108].

We will select the Euler-Lambert method [121], which determines the transfer time Δt_{tr} as a function of r_1, r_2 , the angular distance between them $\Delta \vartheta$ in the transfer plane, and the semimajor axis of the transfer orbit a_{tr} .

Different transfer trajectories are obtained for different ratios between these quantities:
elliptical, if

$$a_{tr} > \frac{r_1 + r_2 + s}{4}. \quad (5.11)$$

parabolic, if

$$|r_1 - r_2| < s \quad (5.12)$$

and hyperbolic, if

$$4a_{tr} + r_1 + r_2 > s,$$

where s is the distance between the radii-vectors r_1 and r_2 . The trajectories determine uniquely only for parabolic and hyperbolic orbits. The Euler-Lambert equation for orbits of different types can be written as follows:

for a hyperbolic orbit ($a_{tr} < 0$)

$$\Delta t_{tr} = \frac{[-a_{tr}]^{3/2}}{\sqrt{\mu}} [\operatorname{sh} \tilde{\varepsilon} - \tilde{\varepsilon} \pm (\operatorname{sh} \tilde{\delta} - \tilde{\delta})];$$

for a parabolic orbit ($a_{tr} = \pm \infty$)

$$\Delta t_{tr} = \frac{1}{6\sqrt{\mu}} [(r_1 + r_2 + s)^{3/2} \mp (r_1 + r_2 - s)^{3/2}];$$

for a first-order elliptical orbit ($a_{tr} > \frac{r_1 + r_2 + s}{4}$)

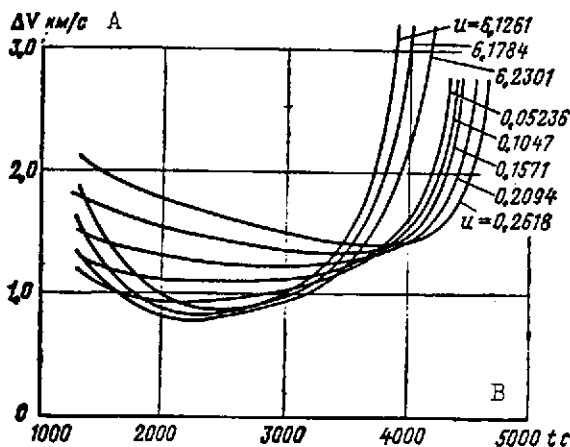


Fig. 5.15. Characteristic transfer velocity as a function of time. The position of the space object in the orbit is determined by the argument of latitude u , in radians. The parameters of the initial orbits are as follows:

$$\begin{aligned} a_1 &= 8000 \text{ km} \\ l_1 &= 0.01 \\ \omega_1 &= 0.78 \\ \Omega_1 &= 0.78 \\ i_1 &= 0 \\ u_1 &= 0 \end{aligned}$$

$$a_2 = 10,000 \text{ km}$$

$$l_2 = 0.015$$

Fig. 5.15. Characteristic transfer velocity as a function of time. The position of the space object in the orbit is determined by the argument of the latitude u , in radians. The parameters of the initial orbits are as follows [Continued]

$$\omega_2 = 1.05$$

$$\Omega_2 = 0.78$$

$$i_2 = 0.08$$

KEY: A -- V, km/sec

B -- Tons

$$\Delta t_{tr} = \frac{a_{tr}^{3/2}}{\sqrt{\mu}} [2\pi n + \epsilon - \sin \epsilon \mp (\delta - \sin \delta)]; \quad (5.13) \quad \underline{/280}$$

for a bounded elliptical orbit ($a_{tr} = \frac{r_1 + r_2 + s}{4}$)

$$\Delta t_{tr} = \frac{a_{tr}^{3/2}}{\sqrt{\mu}} [\pi(2n+1) \mp (\delta - \sin \delta)]; \quad (5.14)$$

for a second-order elliptical orbit ($a_{tr} > \frac{r_1 + r_2 + s}{4}$)

$$\Delta t_{tr} = \frac{a_{tr}^{3/2}}{\sqrt{\mu}} [2\pi(n+1) - (\epsilon - \sin \epsilon) \mp (\delta - \sin \delta)]. \quad (5.15)$$

In formulas (5.13) - (5.15), the sign " - " corresponds to the case when $0 \leq \Delta \vartheta \leq \pi$, and the sign "+" corresponds to the case when $\pi \leq \Delta \vartheta \leq 2\pi$. The quantities s , $\tilde{\epsilon}$, $\tilde{\delta}$, ϵ , and δ are determined from the expressions given below:

$$\begin{aligned} s &= \sqrt{r_1^2 + r_2^2 - 2r_1r_2 \cos \Delta \vartheta}; \\ \operatorname{sh} \frac{\tilde{\epsilon}}{2} &= \sqrt{\frac{r_1 + r_2 + s}{-4a_{tr}}}; \quad \operatorname{sh} \frac{\tilde{\delta}}{2} = \sqrt{\frac{r_1 + r_2 - s}{-4a_{tr}}}; \\ &\quad \tilde{\epsilon} > 0, \quad \tilde{\delta} > 0 \\ \sin \frac{\epsilon}{2} &= \sqrt{\frac{r_1 + r_2 + s}{4a_{tr}}}; \quad \sin \frac{\delta}{2} = \sqrt{\frac{r_1 + r_2 - s}{4a_{tr}}}; \\ &\quad 0 < \frac{\epsilon}{2} < \frac{\pi}{2}; \quad 0 < \frac{\delta}{2} < \frac{\pi}{2}. \end{aligned}$$

After the rendezvous point is selected, the parameters of the transfer trajectory and the impulse value are calculated.

The eccentricity of the transfer orbit is determined from the expression

$$e_{tr} = \left[\left(\frac{r_2 - r_1}{2a_{tr}} \right)^2 \operatorname{cosec}^2 \frac{E(t_2) - E(t_1)}{2} + \left(1 + \frac{r_2 + r_1}{2a_{tr}} \right) \sec^2 \frac{E(t_2) - E(t_1)}{2} \right]^{1/2}, \quad (5.16)$$

where $E(t_2)$, $E(t_1)$ are the eccentric anomalies in the plane of the transfer orbit of the rendezvous point and the launch point of the maneuvering spacecraft. The angular distance of the pericenter from the node of the transfer trajectories is found by the formula

$$\omega_{tr} = -\vartheta_1 + \arctan \frac{y_1}{x_1},$$

in which x_1 , y_1 are the coordinates of the spacecraft launch point /281 in the plane of the transfer orbit (the Ox axis is at the ascending node, Oy is along \bar{V});

ϑ_1 is the true anomaly of the launch point, determined as follows:

$$\left. \begin{aligned} \vartheta_{tr}^* &= 2 \arctan \left| \sqrt{\frac{1+e_{tr}}{1-e_{tr}}} \operatorname{tg} \frac{E_1^*}{2} \right|; \\ E_1^* &= -\vartheta_1 + \arccos \frac{\cosh h_1}{e_{tr}}; \\ \vartheta_1 &= \frac{\varepsilon - \vartheta}{2} + \pi n; \quad h_1 = \frac{\varepsilon + \vartheta}{2} + \pi n \quad \text{for } 0 \leq \Delta \vartheta \leq \pi; \\ \vartheta_1 &= \frac{\varepsilon + \vartheta}{2} + \pi n; \quad h_1 = \frac{\varepsilon - \vartheta}{2} + \pi n \quad \text{for } 0 \leq \Delta \vartheta \leq 2\pi; \\ \vartheta_1 &= \begin{cases} \vartheta_1^* & 0 < E_1^* < \pi, \\ 2\pi - \vartheta_1^* & E_1^* > \pi. \end{cases} \end{aligned} \right\} \quad (5.17)$$

If $E_1^* < 0$, then the supplementary angle \bar{E}_1^* to 2π is considered, and

$$\vartheta_1 = \begin{cases} \vartheta_1^* & 0 < \bar{E}_1^* < \pi \\ 2\pi - \vartheta_1^* & \bar{E}_1^* > \pi. \end{cases}$$

The true anomaly of the rendezvous point ϑ_2 is determined by formulas (5.17), in which the eccentric anomaly

$$E_2 = \vartheta_1 + \arccos \frac{h_1}{e_{1tr}}.$$

is inserted.

The longitude of the ascending node Ω_{tr} and the inclination i_{tr} are calculated in terms of the coordinates of the launch point and the rendezvous point in the geocentric inertial system of

coordinates, as follows. Let C_1 , C_2 , and C_3 be the projections of the doubled area of a triangle taken with the corresponding sign on the coordinate planes in the geocentric inertial system of coordinates; then the longitude of the ascending node of the transfer orbit [108] is

$$\Omega_{tr} = \arctan \frac{[C_2 \operatorname{sign} C_1]}{[C_3 \operatorname{sign} C_1]} \quad 0 \leq \Omega_{tr} < 2\pi.$$

The angle of inclination of the transfer orbit plane is determined by the formula

$$i_{tr} = \arccos \frac{\pm |C_1|}{\sqrt{C_1^2 + C_2^2 + C_3^2}} \quad 0 \leq i_{tr} < \pi.$$

By determining all transfer orbit parameters, we obtain the characteristic velocity; here the following formulas are used: /282

$$\begin{aligned} \dot{x} &= -\sqrt{\frac{\mu}{a(1-e)}} [(\sin u + e \sin \omega) \cos \Omega + \\ &\quad + (\cos u + e \cos \omega) \sin \Omega \cos i]; \\ \dot{y} &= -\sqrt{\frac{\mu}{a(1-e)}} [(\sin u + e \sin \omega) \sin \Omega - \\ &\quad - (\cos u + e \cos \omega) \cos \Omega \cos i]; \\ \dot{z} &= -\sqrt{\frac{\mu}{a(1-e)}} \sin i (\cos u + e \cos \omega). \end{aligned}$$

The relative velocity at the rendezvous point is calculated in similar fashion.

Of greatest interest is the optimization of the characteristic velocity by the angles specifying the position of the starting point u_1 and the position of the rendezvous point u_2 , since for given orbital elements they specify the position and velocity of the satellite.

The characteristic velocity as a function of the transfer time and the angular position of the satellite in the orbit are shown in Fig. 5.16.

The solid lines represent the minimum impulses; the dashed lines represent the relative velocities at the rendezvous point of the spacecraft and the satellite.

The eccentricity, inclination, and relative location of the line of apsides are factors having varying effects on the magnitude and the number of local minima of the quantity ΔV_{\min} and V_{rel} (cf Fig. 5.16). For a complete analysis of the transfer problem, we must note the number, shape, and relative values of all these minima. Since the characteristic velocity is not convex and is not an everywhere-smooth function, it is difficult to employ ordinary numerical methods of optimization, such as the steepest-descent method [73]. Let us therefore use, in investigating the impulse function and in determining the global minimum, its geometric representation in the plane u_1, u_2 . The points of this plane defining all possible transfers of the spacecraft for the rendezvous with the satellite are enclosed in the limits $0 \leq u_1 \leq 2\pi$; $0 \leq u_2 \leq 2\pi$. /283

The geometric position of points with equal impulses ΔV_0 can be obtained in this plane.

These equal-impulse lines are shown in Fig. 5.17 (the space object is in a circular orbit, the spacecraft orbit is circular, and their planes coincide) and in Fig. 5.18 (the inertial orbits are elliptical and noncoplanar). The relative mean distances from the earth and the angle between the planes of motion are the determining parameters in seeking the minimum ΔV . Selection of the optimal solutions in the rendezvous problem depends also on the holding time⁸ and the transfer time.

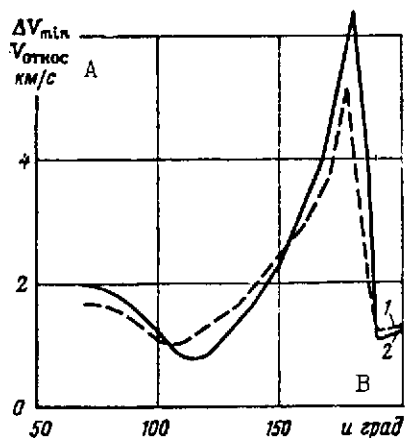


Fig. 5.16. Minimum characteristic velocity 2 and relative velocity 1 at rendezvous point as functions of the angular position of the space object in orbit ($u_1 = 1.92$)
KEY: A -- V_{rel} , km/sec
B -- u , deg

For spacecraft performing a rendezvous with several space objects (their so-called fly-by), not only must individual transfer orbits between two points be determined, but also their optimum sequence.

Since the maneuvering spacecraft can execute more than one revolution in each of the transfer orbits, their distances at the perigee (r_p) must be limited from below, i.e., $r_p \geq r_{\min}$. Orbits satisfying this condition are called real orbits. In searching

for the optimal transfer orbits of a maneuvering spacecraft, we must use the region of values of the initial parameters to obtain real orbits [53].

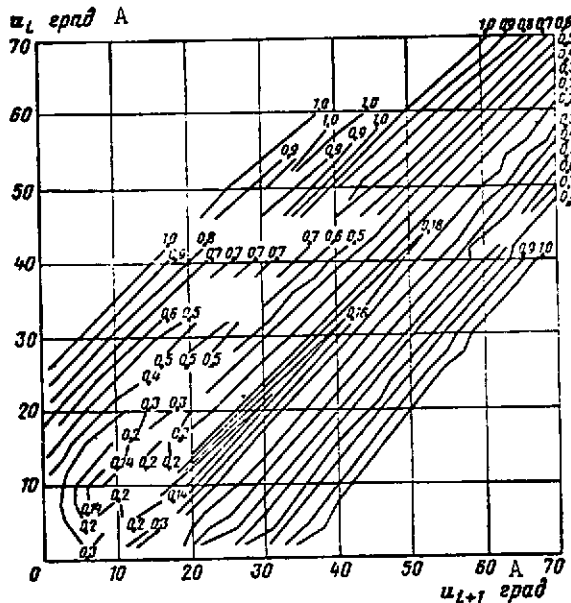


Fig. 5.17. Lines of equal optimal impulses for circular coplanar orbits
KEY: A -- Deg

Suppose the position of the spacecraft launch point and the rendezvous point are determined by the distances from the geocenter r_1 and r_2 and by the angle $2f$ between these radii-factors ($0 \leq 2f \leq 2$). For e close to unity, the limiting values of the true anomaly of the initial transfer point are defined as

$$(\theta_1)_{e \rightarrow 1} = 2 \arctan \left[\cot f \pm \frac{\operatorname{cosec} f}{\sqrt{\alpha}} \right].$$

The perigee values corresponding to the limiting transfer orbits with minimum eccentricity and with eccentricity close to 1 are determined as follows:

$$(\bar{r}_p)_{e \rightarrow \min} = \frac{\alpha(1+\alpha)(\cos 2f - 1)}{(1+\alpha)\sqrt{1+\alpha^2 - 2\alpha \cos 2f} - (1+\alpha^2 - 2\alpha \cos 2f)};$$

$$(\bar{r}_p)_{e \rightarrow 1} = \frac{\alpha(1 - \cos 2f)}{2(1+\alpha \pm 2\sqrt{\alpha \cos f})},$$

where

$$\bar{r}_p = \frac{r_p}{r_1}, \quad \alpha = \frac{r_2}{r_1}.$$

For assigned r_1 and r_{\min} , real orbits obtain only for specific combinations of α and f , where for the same values of α and f the orbit with minimum eccentricity can be imaginary, while with an eccentricity that is very large ($e \approx 1$), this orbit is real, and vice versa.

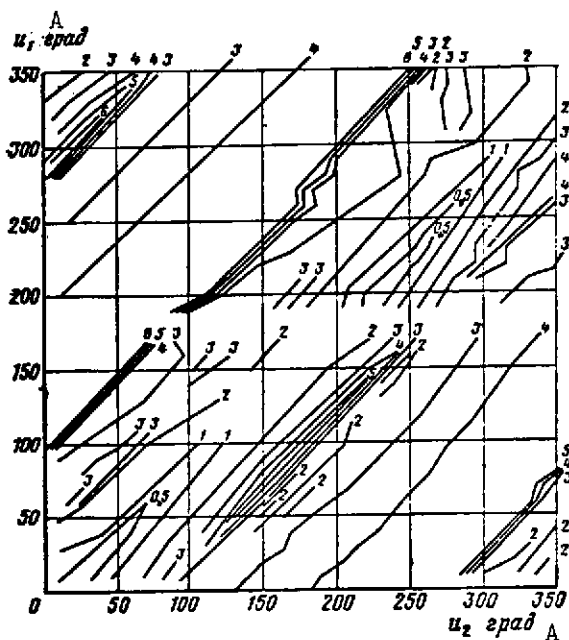


Fig. 5.18. Lines of the equal optimal impulses for elliptical noncoplanar orbits. Initial-orbit parameters:

$$\begin{aligned} a_1 &= 8200 \text{ km} \\ e_1 &= 0.05 \\ \omega_1 &= 0.7854 \\ \Omega_1 &= 0.7854 \\ i_1 &= 0 \\ a_2 &= 10,000 \text{ km} \\ e_2 &= 0.1 \\ \omega_2 &= 1.047 \\ \Omega_2 &= 0.7854 \\ i_2 &= 0.1745 \end{aligned}$$

KEY: A -- Deg

The domain of the existence of real transfer orbits for the case $\alpha \neq 1$ is dictated by the values of the true anomaly $(\vartheta_1)_{bo}$ $\sqrt{bo = \text{boundary}}$ of the spacecraft launch point, specifying two transfer orbits at the bounds of the real domain in which $\bar{r}_p = \bar{r}_{min}$:

$$\begin{aligned} \tan \left(\frac{\vartheta_1}{2} \right)_{bo} &= \\ &= \frac{(\bar{r}_{min} - 1) \sin 2f \pm \sqrt{2 \left(\frac{\bar{r}_{min}}{\alpha} - 1 \right) (\bar{r}_{min} - 1) (1 - \cos 2f)}}{2 \frac{\bar{r}_{min}}{\alpha} - \bar{r}_{min} (1 + \cos 2f) - (1 - \cos 2f)}. \end{aligned}$$

286

The region of angles ϑ_1 for which $r_p > r_{min}$ is defined by the sign of the derivative

$$\text{sign} \left(\frac{dr_p}{d\vartheta_1} \right) = \text{sign} \left[(1 - \alpha) \sin \left(\frac{\vartheta_1}{2} + f \right) \right].$$

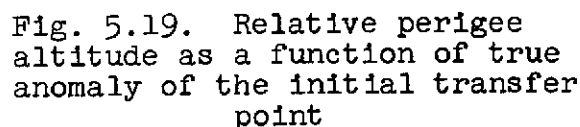
Thus, when $\alpha \neq 1$ for assigned $\alpha_1 f$ and \bar{r}_{min} , the above-written equations wholly specify the regions of the angles ϑ_1 to which real transfer orbits correspond (Fig. 5.19). When $\alpha = 1$ for assigned r_1 , r_{min} , and $2f$, the existence of real orbits is verified by the relationships:

$$\bar{r}_{min} > \frac{1}{2} (1 + |\cos f|), \quad 0 \leq e < (1 - \bar{r}_{min}) / (\bar{r}_{min} - \cos f).$$

where the number n is not given, but $0 < f < \pi$ is assigned.

where the number n is not given, but $0 < f < \pi$ is assigned.

where the number n is not given, but $0 < f < \pi$ is assigned.



In searching for real orbits /287
providing for transfer in a specified time, the integral number of revolutions n corresponding to it is determined. This is done as follows. When $\alpha \neq 1$, for the

$$A = |[n_{I,II}]_i - [n_{I,II}]_{i+1}| \geq 1,$$

If $A \geq 1$, then orbits corresponding to all integral values of $n_{I,II}$ in the range of revolution numbers studied will be real; if $A < 1$, then they are in general no real orbits for the specified n . If an orbit with $\sqrt{1 - A^2}$

orbits with integral values of n within the range from the smaller $n_{I,II}$ to n_{\max} will be real. If the real domain contains an orbit with $e = 1$, then all orbits corresponding to integral numbers of revolutions from $n = 0$ and to the largest in this range will be real. For $\alpha = 1$, all transfer orbits with integral n within the range from smaller $n_{I,II}$ to n_{c1} [$c1$ = circular] will be real. If

244

$$n_{ci} = \frac{\sqrt{\mu} t_2}{2\pi r^{3/2}} - \frac{f}{\pi}.$$

In Fig. 5.20, domains denoted by inside hatching represent the set of initial data α , $2f$, and $\bar{r}_p \min$ corresponding to an unbounded transfer time.

Note that the domain of real transfer orbits of maneuvering spacecraft depends on the parameters of motion as follows:

1) for a specified $\bar{r}_p \min$, with increase in α the domain of real orbits becomes smaller, where for $\alpha < 1$ when $\alpha = \bar{r}_p \min$, the domain degenerates into a straight line $\vartheta_1 = 2\pi - 2f$;

2) for a specified α , an increase in the allowable perigee radius of a transfer orbit leads to a contraction of the domain of real orbits;

3) when $\alpha < 1$, most of the domain contains real orbits with the apogee at the initial transfer point ($\vartheta = \pi$), and when $\alpha > 1$ -- with their perigee at the same point ($\vartheta_1 = 0$); and

4) orbits for which $e = 1$ encompass within the real domain a bounded range of values for the angles f .

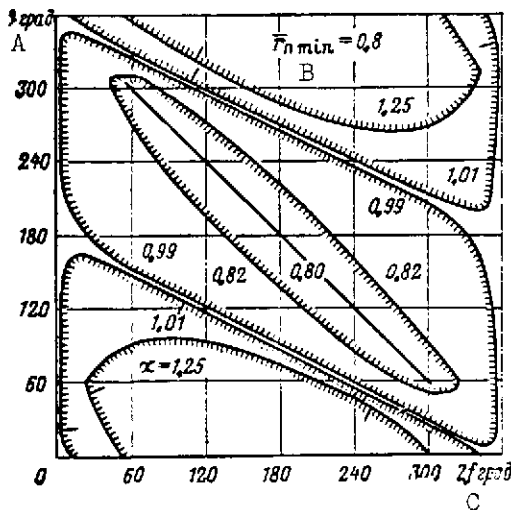


Fig. 5.20. Domains of the function of main initial data α , $2f$, and $\bar{r}_p \min$ for an unbounded transfer time

KEY: A -- Deg
B -- $\bar{r}_p \min$
C -- Deg

Thus, for specified values of the initial data, there is always a wide domain of real orbits such that for an unbounded time a greater opportunity for variation in angles is afforded in selecting the requisite transfer orbit.

In the case of an assigned time, the number of calculations of possible transfer orbits is also reduced.

The domains of real orbits must be determined when seeking the optimal maneuver of a spacecraft in flying past a group of satellites in different orbits. The method of constructing the optimal route for a fly-by past a group of space objects is extremely

cumbersome, for this problem is of the combinatory type, whose specific details consist of the starting points moving according to complex nonlinear laws [12]. The dynamic programming method, allowing the solution of the problem to be subdivided into stages, is a rational method of solving it. In setting up a computational algorithm, special attention must be given to two important points: /289

- 1) selection of the group of parameters characterizing the state of the physical system S ; and
- 2) subdividing the process of controlling the maneuvering spacecraft in the fly-by past n objects into stages. Here the process of transferring from S_0 to S_k must be broken into stages in such a way that they admit of a convenient enumeration and a well-defined sequence of actions.

The principle of dynamic programming presupposes the selection of controls for an individual step with reference to all its consequences in the future, and in accordance with this it is required to find at each step a conditional optimal control for any of the possible outcomes of the preceding step. The proper subdivision of the process of optimizing the trajectory of multiple transfers of a spacecraft is very important, since on it depends not only the accuracy of a solution and the computer time outlays, but in several cases also the possibility of bringing the solution of the problem to a conclusion.

Let us look briefly at the search algorithm for an arbitrary minimum of some specified criterion determining the optimal route of a maneuvering spacecraft in fly-by past a group of satellites in different earth orbits, the dynamic programming method [10, 23] affords minimizing any output parameter characterizing the state. In this case, the optimal route of a spacecraft is defined as the route either with minimum energy outlays for a bounded time, or with minimum time of fly-by past all satellites with a bounded fuel reserve. Different a priori prerequisites relative to the initial data are assumed for these variants, however the solution algorithm used is common.

Let us denote the position of a maneuvering spacecraft by S , the position of the satellites by p_i ($i = 1, 2, \dots, n$), and the entire system of maneuvers with which the state S is changed, by V . The state of system S is described by the seven parameters $a, e, \omega, \Omega, i, u$, and t , which represent a point of seven-dimensional phase space H , and the state change in the course of the control V corresponds to displacement of the point S in the phase space. This trajectory S affords fly-by past all n satellites p_i ($i = 1, 2, \dots, n$) with certain specified conditions at the encounter points maintained. Control of the system is organized so that some criterion I tends to the minimum $I^* = \min I(V, S)$. The criterion I is defined either as the overall characteristic velocity of multiple transfers, or else as the time of fly-by past the n satellites. /290

Let us consider the case when the criterion is the overall fuel reserve of the spacecraft (corresponds to the characteristic velocity). Suppose the initial state S_0 and the domain of terminal states S_k defined by the constraints imposed on the total spacecraft flight time and by the number of satellites past which the fly-by takes place are given.

Then the problem of determining the optimal spacecraft maneuver in the fly-by past the n satellites in a bounded time is formulated as follows: from the set of possible controls $V(\Delta V_1, \Delta V_2, \dots, \Delta V_n)$, we must find the control V^* which transfers the point S in phase space H from the initial state S_0 to the terminal domain of the S_k such that the overall characteristic velocity tends to a minimum.

The variation in the state S is subdivided into n successive stages and optimization of each of them is carried out, beginning with the first. The problem of optimizing the trajectory of the fly-by past the group of satellites will be set up differently, depending on the specification of the boundary values of S_0 and S_k .

If it is required to determine the optimal route for a fly-by past the group of satellites and to arrive at the assigned orbit S_k , the optimization begins with S_k and as a result of the solution of the problem, we obtain the optimal initial orbit.

For assigned initial condition S_k , terminal conditions are not explicitly defined and the fly-by past all satellites is an indicator of the end of the process. The optimization problem is initially solved in this formulation. Each stage represents the selection of possible optimal transfers between orbits of several satellites, where only real orbits are considered. In a particular case, the stage can represent a transfer between only two orbits. Selecting the optimal control V within a stage is subdivided by time into k steps. The number of points k in the transfer orbit dictated by the possible instants of departure of the spacecraft from this orbit defines the scale of controls, for to each point k there corresponds its own value of the characteristic velocity. /291

At each stage of the calculation, we must first seek for the conditional optimal control (for all possible assumptions on the results of the preceding step), and then, after the optimization has been brought to the final stage S_k , we must again carry out the full sequence of steps, but now in the direction from the terminal point to the starting point; here, one of the set of the conditional optimal control is selected at each step.

The operation which brings the control transferring the spacecraft to the encounter point and minimizing the characteristic velocity into correspondence with the starting point of the spacecraft from the transfer orbit and the assigned conditions of encounter with the satellite is called the elementary operation. Any method of determining the optimal transfer trajectory can be used in the elementary operation.

Obviously, wholly specific initial phase positions of the spacecraft and the objects flown past correspond to the optimal route of the maneuvering spacecraft. For any initial phase position an optimal transfer from the holding orbit can be provided. The maximum holding time for which any possible phase position is realized is determined by the periods of the total revolution of the space objects and the maneuvering spacecraft.

The characteristic transfer velocity of a spacecraft between two orbits, with assigned parameters of both orbits, depends on the spacecraft altitudes relative to the line of nodes.

The mutual altitude of two space objects is a periodic function of time, and this period is equal to the maximum possible holding time. For the case of a single transfer with $T^S < T^P$, the period of variation of the phase positions of the maneuvering spacecraft and the space object is determined by the formulas /292

$$\Phi_1 = \begin{cases} \frac{T^S T_1^P}{T_1^P - T^S}, & \left\{ \frac{T_1^P}{T_1^P - T^S} \right\} = 0, \\ p_1, q_1, T^S, & \frac{T_1^P}{T_1^P - T^S} = \frac{p_1}{q_1} \end{cases}$$

where T^S is the period of the complete revolution of the spacecraft in the reference orbit; and

T_1^P is the period of the total revolution of the space object.

For the case of two space objects, the period of the change in their phase disposition and the spacecraft is determined with similar formulas:

$$\Phi_2 = \begin{cases} \Phi_1, & \left\{ \frac{\Phi_1}{T_2^P} \right\} = 0, \\ \frac{\Phi_1 T_2^P}{\Phi_1 - E_{1,2} T_2^P}, & F_{12} = \frac{\Phi_1}{T_2^P}, \left\{ \frac{T_2^P}{\Phi_1 - E_{1,2} T_2^P} \right\} = 0, \\ p_2, q_2, T_2^P, & \frac{T_2^P}{\Phi_1 - E_{1,2} T_2^P} = \frac{p_2}{q_2}, \end{cases}$$

where T_2^D is the period of revolution of the second object and $T_2^D < T_1^D < T_p$. For an arbitrary number of space objects, we obtain the recursive functions:

$$\Phi_k = \begin{cases} \Phi_{k-1}, & \left\{ \frac{\Phi_{k-1}}{T_k^D} \right\} = 0, \\ \frac{\Phi_{k-1} T_k^D}{\Phi_{k-1} - E_{k,k-1} T_k^D}, & \left\{ \frac{T_k^D}{\Phi_{k-1} - E_{k,k-1} T_k^D} \right\} = 0, \\ p_k, q_k, T_k^D, & \frac{T_k^D}{\Phi_{k-1} - E_{k,k-1} T_k^D} = \frac{p_k}{q_k}. \end{cases}$$

If the periods of the total revolution of the maneuvering spacecraft and n objects are similar to each other, the total period Φ_k can be very large. For example, for a pair of orbits with total periods $T^S = 5428$ seconds and $T^D = 5798$ seconds, the total period of change in the mutual space disposition of the spacecraft and the object is $14 T^S$, which is about 21 hours; for two orbits with periods $T^S = 5428$ seconds and $T^D = 6049$ seconds, it is now $\Phi_1 = 1612 T^S$, which is approximately 2430 hours. Knowing the period of the phase disposition of the spacecraft is very important for the elementary operation, since the number of steps in the scale of controls and the time value of the step must be related to the period of phase positions of objects belonging to the same step. The accuracy of the solution determining the proximity of the resulting solution to the absolute or conditional minimum is defined as the value of the step and the number of points in the scale of controls. /293

Owing to the complexity of the problem, any general conclusions and recommendations can hardly be arrived at. Therefore we must speak only of certain partial conclusions, namely that the optimal route, if there is no time limit, lies in the plane of the initial orbit of the spacecraft and provides for the absolute minimum of the overall characteristic velocity. When the time is unlimited, the minimum characteristic velocity does not depend on the initial phase locations of the space objects. A rigorous minimum of the characteristic velocity for an assigned time can be obtained by a numerical method by setting up a system of conditional optimal transfers at each stage, with the holding time calculated from the assigned time of fly-by past n satellites, with reference to preceding transfers and the necessary time reserve for the future.

5.3. Control Systems of Spacecraft

The first and one of the main stages in the operation of the control system of space complexes is the insertion of the spacecraft

into orbit or a flight trajectory. This stage does not differ fundamentally from the insertion of a ballistic missile into its trajectory. The insertion point of the satellite, as a rule, coincides with the orbit's perigee. Obtaining a velocity of given magnitude V_k and a direction perpendicular to the focal radius-vector of the insertion point (i.e., the apsidal line of the orbit being formed) is a necessary condition for this. The position of the orbital plane is determined by the vector product of the velocity \vec{V}_k and the radius-vector \vec{r}_k . The error in the launch angle θ_k (the angle between the velocity vector \vec{V}_k and the local horizon) leads to the velocity vector at point K of the orbital insertion being not perpendicular to the line of apsides, the orbital perigee being displaced, and if the modulus of the velocity V_k is equal to the assigned value, the eccentricity e changes. /294

Thus, if the coordinates of the position point r_k , ϕ_k , and λ_k (ϕ and λ are the geographic latitude and longitude, respectively), and the direction of the velocity vector in the plane of the local horizon is specified by the angle ϕ_k between its projection onto this plane and the local meridian, then the Keplerian elements will be functions of the initial conditions of the orbital motion. By differentiating them, let us determine the errors in the orbital parameters as functions of the insertion errors. According to [3], we will write these variations as

$$\left. \begin{aligned} \frac{\delta a}{a} &= A_a^r \frac{\delta r_k}{r_k} + A_a^v \frac{\delta V_k}{V_k}; \\ \delta e &= A_e^r \frac{\delta r_k}{r_k} + A_e^v \frac{\delta V_k}{V_k}; \\ \delta \omega &= A_\omega^\phi \delta \varphi_k + A_\omega^\psi \delta \psi_k + \delta V_k; \\ \delta \Omega &= \delta \lambda_k - A_\Omega^\phi \delta \varphi_k - A_\Omega^\psi \delta \psi_k; \\ \delta i &= A_i^\phi \delta \varphi_k + A_i^\psi \delta \psi_k. \end{aligned} \right\} \quad (5.18)$$

The expression for δe does not contain the term $\frac{\partial e}{\partial \theta} \delta \theta_k$, since the eccentricity, to the first approximation, does not depend on the angle θ_k . In contrast, the term δV_k does appear in the expression for $\delta \omega$, since in the differentiation the relation $\omega = u - \vartheta$ was used.

The coefficients of equations (5.18) are as follows:

$$\left. \begin{aligned}
 A_a^r &= \frac{r_k}{a} \left(\frac{\partial a}{\partial r} \right)_k; \\
 A_a^v &= \frac{V_k}{a} \left(\frac{\partial a}{\partial V} \right)_k; \quad A_e^r = r_k \left(\frac{\partial e}{\partial r} \right)_k; \\
 A_e^v &= V_k \left(\frac{\partial e}{\partial V} \right)_k = 2A_e^r;
 \end{aligned} \right\} \quad (5.19) \quad \underline{/295}$$

$$\left. \begin{aligned}
 A_\omega^\varphi &= \left(\frac{\partial \omega}{\partial \varphi} \right)_k; \quad A_\omega^\psi = \left(\frac{\partial \omega}{\partial \psi} \right)_k; \\
 A_\Omega^\varphi &= \left(\frac{\partial \Omega}{\partial \varphi} \right)_k; \quad A_\Omega^\psi = \left(\frac{\partial \Omega}{\partial \psi} \right)_k; \\
 A_i^\varphi &= \left(\frac{\partial i}{\partial \varphi} \right)_k; \quad A_i^\psi = \left(\frac{\partial i}{\partial \psi} \right)_k.
 \end{aligned} \right\}$$

By knowing them, we can estimate the extent of the effect that the insertion errors have on errors of the orbital parameters (Fig. 5.21).

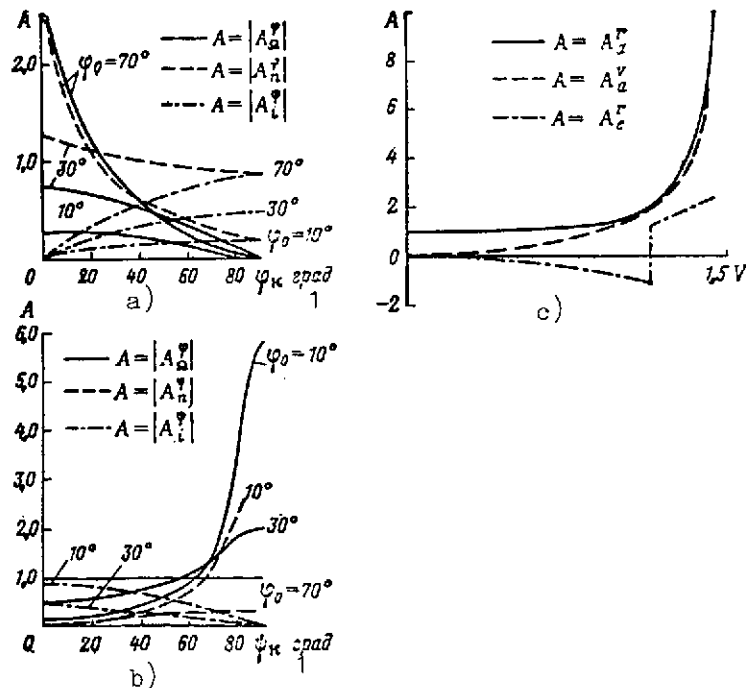


Fig. 5.21. Plots of the coefficients of errors in the insertion of AES or a spacecraft as functions of the parameters ϕ_k (a), ψ_k (b), and $V_k = V_k/V_{c1}$ -- the ratio of the velocity V_k to the local circular orbital velocity (c)

Fig. 5.21. Plots of the coefficients of errors in the insertion of AES or a spacecraft as functions of the parameters $\phi_k(a)$, $\psi_k(b)$, and $V_k = V_k/V_{c1}$ -- the ratio of the velocity V_k to the local circular orbital velocity (c)

[Continued]

KEY: 1 -- Degrees

Navigation and control in the insertion of a satellite into an orbit are executed on the command principle (Fig. 5.22) using the same method and facilities as for the powered phase of ballistic missile motion. A difference here is that as a rule the satellite has a terminal acceleration stage during which the engines of the last stage operate and the exact value of the direction of the velocity required for orbital motion is set.

/296

Since in the initial stage of motion interferences associated with the effect of the earth hamper the use of the tracking radar, missile coordinates can be determined onboard using inertial sensors and then either transmitted to a ground command complex, or directly fed into the onboard computer of the control system. In this case the tracking radar is replaced with a telemetric data receiver.

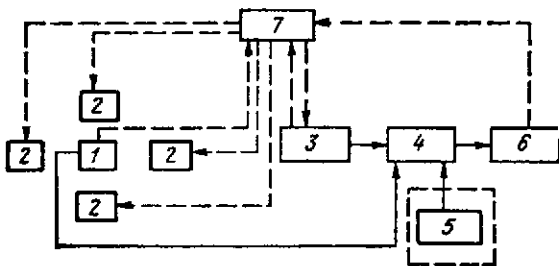


Fig. 5.22. Block diagram of the command control system of an AES in its powered phase:

- 1 -- Doppler transmitter
- 2 -- Doppler receivers
- 3 -- Tracking radar
- 4 -- Computer of ground command complex
- 5 -- Memory
- 6 -- Transmitting radio set
- 7 -- AES with onboard control system

Errors in satellite insertion into orbit can be corrected later on by using navigation and control systems. For flights to other planets, the correction as a rule is realized by subdividing the entire trajectory into three characteristic phases: within the sphere of earth influence, within the sphere of planet influence, and the intermediate phase. As shown in [90], a characteristic feature is the fact that in the sphere of earth influence and in the intermediate trajectory phase there are points such that correcting impulses must be applied near them for multiple optimal correction. Moreover, the application of impulses precisely at these points is difficult for single-action correction.

Since the aim of correction is to eliminate random perturbations of motion, statistical criteria (cf Chapter Six, Section 6.1) can be advantageous criteria of the effectiveness of this process. Accordingly, it is of interest to investigate the problem /84/ in which the correction times and the correcting impulse are found from the results of measuring the parameters of actual motion. The correction strategy is set up here in accordance with the maximization of the probability of the correcting parameters lying within the assigned region, with constraint on the fuel consumed. /297

In addition to the trajectory correction, navigation and control systems must provide for landing and maneuvering of the spacecraft, i.e., variation in its orbital parameters.

Both command, as well as autonomous navigation systems or their various combinations can be used in an orbital flight. The predominant use thus far of command navigation systems in spacecraft is attributed to the greater accuracy (under otherwise equal conditions) of ground instrumentation facilities, and also due to the inadequate advancement of onboard instrumentation and computing facilities. When these systems undergo relative evaluation /104/ (Fig. 5.23), the main advantages which the autonomous navigation system of spacecraft possesses must be borne in mind: the possibility of performing navigation tasks at any time, regardless of the relative position of the craft and the ground command-instrumentation complex, the absence of any radiation into outer space, high anti-jamming capability (which American military specialists value highly), and the independence of the errors in the determination of the actual trajectory, of the distance between the craft and the earth (which is important in long-range space flights).

With the autonomous navigation of a spacecraft, considerably more methods of data acquisition can be used and in the command navigation approach /110/. This means that measurement of a large number of different quantities containing information about the trajectory of motion and with the aid of a large number of varied technical devices is possible (Table 5.3 /52/).

The radio method of data acquisition, being one of the principal approaches in command navigation, can be successfully used also in autonomous systems.

The most common version of an onboard radio-data acquisition device -- the radio altimeter -- measures the distance R to the earth, the angle θ characterizing the direction toward it with respect to any fixed axis, and their derivatives. In determining the distance between moving objects, the quantities ΔR and $\Delta \theta$ can also be measured.

TABLE 5.3

/298

Method of measurement	Measured quantity						
	R	\dot{R}	\ddot{R}	ΔR	$\Delta \dot{R}$	θ	$\dot{\theta}$
Radio	+	+		+	+	+	+
Optical	+	+		+	+	+	+
Inertial			+			+	
Magnetic						+	
Acoustic	+			+		+	
Radiation	+					+	

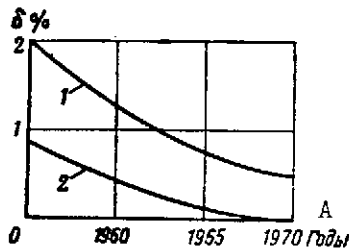


Fig. 5.23. Variation of the errors in autonomous 1 and command 2 control systems of AES
KEY: A -- Years

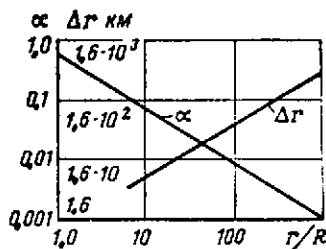


Fig. 5.24. Change of the angular size of the earth's disk (α) and errors in range determination (Δr) as functions of the relative distance (r/R). When $R = 6400$ km, the error in measurement of the angular value $\leq 10^{-4}$

The optical method can be employed in several versions. One of them, traditional generally in navigation and introduced into modern space navigation, is measurement with the aid of a sextant of the angular distance between stellar reference points, in particular, a star and a planet (earth and moon). The requisite number of these measurements (the minimum number is six angles between the planet and different stars), fixated in time, specifies the orbit. By measuring the angular size of a celestial body with known linear dimension (for example, the diameter of disk of a planet or the known distance between reference points on its surface), one can find the distance to it. /299

The possible error in this quantity, if the telescopic measurements of the angles are made with an error not exceeding 10^{-4} [18] is shown in Figure 5.24.

The use of measurements of the angle between bearings to the navigation star and the limb of the earth's disk, in flights into near-earth space, is complicated by the fact that the optical horizon of the earth is blurred owing to atmospheric effects, its altitude is unstable and, in general, is known with large errors. Therefore before requisite statistical data on its altitude and spectral characteristics have been accumulated, it is best to employ different combination methods, for example, measurement of the angle between the bearing to the star and the earth vertically with the addition of measurements of the altitude above the earth's surface (cf, for example, 927).

The theoretical possibility of determining trajectory parameters by using different sets of measurements (the so-called observability problem) is extremely important in the problem of navigation generally, and -- in particular -- in autonomous navigation. Thus, a problem has been posed in work 977, where in particular it is shown that when derivatives of certain functions (not the functions themselves) are measured, observability defects can only become greater.

Performing measurements in the optical range is also possible using laser devices, capable of measuring all quantities indicated in Table 5.3. Here also can be included the method of constructing a vertical in the infrared range (IR vertical).

The inertial data acquisition equipment is at present, 300 one must admit, the most widespread. By integrating acceleration measured with accelerometers in the direction of known axes, at any time one can calculate all six quantities (coordinates and velocity components) required to describe a trajectory. Since an accelerometer responds only to the action of nonconservative forces, to determine the orbit in "free" ballistic flight known equations of motion must be integrated, by solving the Cauchy's problem for initial conditions corresponding to the beginning of the ballistic phase, i.e., the instant of cutoff of the spacecraft engines.

In spite of the high accuracy of measuring accelerations with onboard accelerometers, this method has some drawbacks, for the directions of the axes along which the accelerometers are erected and fixated using gyroscopes contain errors that increase in time and are periodically variable (Schuler fluctuations). They are corrected with telescopes sighting directions to known stars. Other methods of "correcting" data acquired from inertial sensors are also possible.

Most promising from the standpoint of accuracy and reliability are integrated autonomous navigation systems acquiring data from several different sensors and using it with appropriate statistical weights, or combination systems functioning on some trajectory phases in the command, and on others -- in the autonomous mode. In all versions of autonomous and combination systems, the second

fundamentally important onboard assemblage, in addition to the data acquisition equipment, is the onboard computer that serves to process measurements and determine the motion control law.

The three last methods of data acquisition shown in Table 5.3 are completely undeveloped in space navigation and their effectiveness of use is thus far unclear.

Let us consider control systems of several manned and unmanned spacecraft. The Soviet spacecraft Vostok, Voskhod, and Soyuz, and the American craft Mercury and Gemini are manned flight craft for earth flights. They are intended to perform scientific and technical research and also to develop certain systems for future spacecraft.

The rendezvous and docking of the Soyuz 4 and Soyuz 5 spacecraft represent the development of a technology of assembling large orbital stations in space. Experimental studies conducted with the participation of astronauts in the Soviet Union during the flights of the Vostok and Soyuz spacecraft, and in the United States during 301 flights of the Mercury and Gemini spacecraft demonstrated the fundamental possibility of the participation of astronauts in navigating and controlling spacecraft, which can increase the reliability of the systems. Still, the problem of constructing a rational system with human participation has thus far not been completely resolved.

A fundamental task of navigation and control systems in spacecraft designed for encounter with maneuvering and unmaneuvering AES consists in their approach by a specified, quite close distance. Here not only the position vectors, but also the velocity vectors of the spacecraft and the AES, which will subsequently be referred to as the target for sake of convenience, must be matched in a specific way. For example, in the building of spacecraft in orbit, fueling them, replacing crew equipment, and so on, a control craft must not only approach by a close distance, but also executes soft contact with the AES, by reducing its relative velocity nearly to zero.

The nature of the task which a maneuvering spacecraft must perform is dictated by the relative velocity with which it enters the neighborhood of the target, and by the actual extent of this neighborhood.

In all these versions of encounter can be executed by the successive application at different instants of a number of small, modulus-decreasing thrust impulses 18, 437. The realization of this process will be divided into three stages.

During the first stage the craft executes an approximate maneuver. It is launched and accelerated to a fairly high velocity

ensuring flight along a ballistic trajectory which passes in direct proximity to the target. The craft and target velocities are different. /302

The second method consists in performing a number of maneuvers imparting to the orbital craft the velocity close to the target velocity (or to an assigned velocity). These two stages, combined in the common name of "approach" or "long-range guidance", can be recommended without using equipment reporting on the relative motion of the guided craft.

A third stage -- docking -- consists in performing correction and the terminal maneuver affording mating or the condition for performing any other specified tasks.

This requires exact information on relative motion, which can be acquired only by means of onboard sensors.

The vector $\Delta \vec{V}$ of the mismatch of the actual and the required overall velocities can be used as the controlling parameter in all stages. In the docking of the Kosmos 186 and Kosmos 188 craft and the Soyuz 4 and Soyuz 5, the first two approach stages were implemented by selecting the launch time of Kosmos 188 and Soyuz 5, following guidance using terminal inertial correction and trajectory correction.

The parameters of the orbits of the Kosmos 186 before docking and of the Kosmos 188 after insertion are as follows:

Type of AES	Perigee altitude, H_{π} , km	Apogee altitude, H_{α} , km	Period of rev., T , min	Incl. of orbital plane, i , deg
Kosmos-186	180	260	88,64	51,68
Kosmos-188	200	276	88,97	51,68

The relative distance between them at the instant of Kosmos 188 insertion was 24 km, and the relative velocity was 25 m/sec.

In the third stage, beginning approximately at several tens of kilometers, automatic radio search by the active craft (Kosmos 186 and Soyuz 4) of the passive craft was carried out.

To do this, in addition to the mandatory systems of orientation, stabilization, and gas-dynamic control (the engine installation for correction and approach, and the vernier engine for orientation and docking), the active craft is equipped with a homing radio system acquiring data on the relative distance and its derivatives, on the angle between the sighting line and the structural axes of the satellite, and its velocity. /303

Since the search antennas are located at the opposite end of the active satellite, detection can be executed for any mutual position of the two spacecraft. When there is an unfavorable relative position, the active satellite turns around, orients itself as required, and executes firm radio lock-on. Guidance in this mode consists of varying the relative velocity according to a special law with unchanged direction of the sighting line /100/.

Up to the distance when the approach terminates and the docking stage begins, the craft is controlled with a correcting engine installation, and then with vernier engines providing a relative velocity of 0.1-0.5 m/sec at the end of the docking stage.

In contrast to the automatic docking of the Kosmos spacecraft, guidance and control of the Soyuz craft was executed in the last stage manually from a distance of 100 m.

The block diagram of the possible approach control systems of the spacecraft and a block diagram for manual control of the Gemini craft are shown in Figs. 5.25 and 5.26, respectively.

The sequence of maneuvers performed by Gemini VI in approaching a space target, a previously launched Gemini VI craft, is shown in Fig. 5.27. These maneuvers are characterized by data listing in Table 5.4 /137, 151/.

Moving on to an examination of the control systems of spacecraft intended for long-range space flights (to the moon and the planets of the solar system), we note that in addition to the ordinary requirements, they must have a long series of features associated with ensuring safety, life support, and efficiency of astronauts spending long periods of time in the space flights. Characteristics of the control system of a shift of this kind are mainly dictated by the following:

1. Large energy outlays required for long-range space flights. This requires multistage engine installations⁹ and the selection of economical trajectories along which flight can take an extremely long period of time. These trajectories can also be complicated in form with various supplementary phases, for example, with initial insertion into earth orbit of the AES and subsequent additional acceleration to attain the required velocity. /304

2. The nature of the flight trajectory. Its longest individual phases are (in the first, Keplerian approximation) segments of hyperbolas or ellipses with eccentricity close to unity. They are extremely sensitive to motion errors, which increase for motion through the attractive field of any gravitational body, (for example, in flying past the moon). This fact imposes high requirements on the accuracy of the navigation system¹⁰. /305

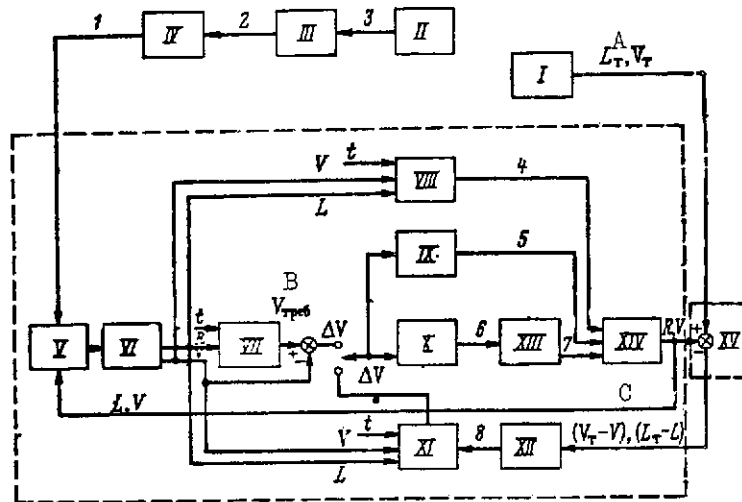


Fig.5.25. Block diagram of the automatic approach control system of spacecraft:

- 1 -- Guidance parameters
- 2 -- Target ephemerides
- 3 -- Target data
- 4 -- Commands for engine firing
- 5 -- Commands for engine cutoff
- 6 -- Commands for the angular velocity of the spacecraft
- 7 -- Angular velocity of spacecraft
- 8 -- Data on the relative position of the spacecraft
- I -- Target
- II -- Ground tracking station
- III -- Computer of target ephemerides
- IV -- Prelaunch computer
- V -- Sensitive elements of inertial system
- VI -- Calculation of position and velocity
- VII -- Calculation of ballistic trajectory phase
- VIII -- Calculation of engine firing instant
- IX -- Calculation of engine cutoff instant
- X -- Calculation of control command
- XI -- Cessation of final correction
- XII -- Relative position instrumentation elements
- XIII -- Autopilot
- XIV -- Dynamics of spacecraft
- XV -- Communications equation
- KEY: A -- $L_t, V_t \sqrt{t}$ = target
- B -- $V_{req} \sqrt{req}$ = required

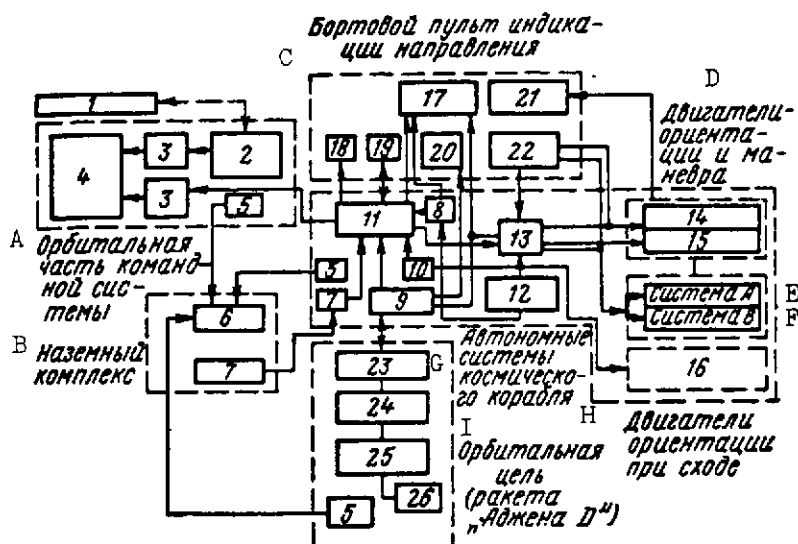


Fig. 5.26. Functional diagram of the control system of the Gemini spacecraft

- 1 -- Ground command navigation radio complex
- 2 -- Ground navigation system
- 3 -- Autopilot
- 4 -- Engine drive
- 5 -- Telemetry sensor
- 6 -- Indicator
- 7 -- Digital command-computer complex
- 8 -- Inertial data (instrumentation) block
- 9 -- Radar
- 10 -- Synchronization system
- 11 -- Onboard digital computer (ODC)
- 12 -- IR /infrared/ horizon sensors
- 13 -- Computer of control system
- 14 -- Maneuvering control engines
- 15 -- Orientation control engines
- 16 -- Retro-engines
- 17 -- Spacecraft position indicator
- 18 -- Velocity change indicator
- 19 -- ODC control panel
- 20 -- Indicator of relative range and velocity
- 21 -- Indicator of fuel level
- 22 -- Manual control of spacecraft
- 23 -- Transceiver
- 24 -- Pulsed light beacon
- 25 -- Docking light beacon
- 26 -- Command instrument

KEY: A -- Orbital part of command system
 B -- Ground complex
 C -- Onboard direction indication panel

Fig. 5.26. Functional diagram of the control system of the Gemini spacecraft /Continued/

- D -- Orientation and maneuver engines
- E -- System A
- F -- System B
- G -- Autonomous spacecraft systems
- H -- Orientation engines for departure
- I -- Orbital target (Agena D rocket)

3. A considerable degrading of the accuracy of trajectory determination using ground instrumentation facilities and an increase in the transit time of the signal at great distances of the spacecraft from the earth. Therefore, in space complexes intended for flight to the moon and especially to the planets, autonomous navigation systems must be assigned an even greater role.

/306

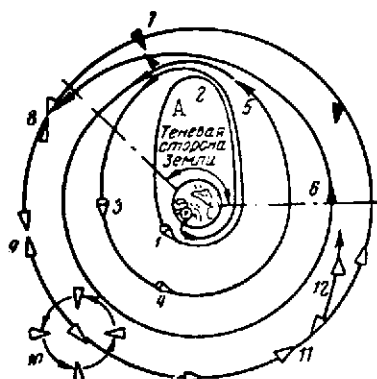


Fig. 5.27. Scheme of maneuvers performed by the spacecraft Gemini VI for encounter with the target Gemini VII:

- 0 -- Launch of the Gemini VI
- 1-6 -- Maneuvers of the Gemini VI (cf Table 5.4)
- 7 -- Approach of the craft toward its target at a distance of 24 km
- 8 -- Last spacecraft maneuver (cf Table 5.4)
- 9 -- Approach with target up to 1 m (group flight)
- 10 -- Fly-by of one craft past another (group flight)
- 11 -- Last stage of group flight
- 12 -- Separation of the two craft and the transfer of the Gemini VI to another orbit

KEY: A -- Dark side of the earth

One of the complicated tasks performed by the Luna 6 space station is the automatic execution of a soft landing on a planet that lacks an atmosphere. Its complexity lies in the fact that this kind of landing can be executed only with retro-engines decreasing the velocity nearly to zero. This necessitates an amount of fuel equal almost to half the weight of the station up to the beginning of deceleration. The flight trajectory¹¹ of the Luna 9 station is shown in Fig. 5.28.

Selection of the optimal flight trajectory to the moon was determined mainly by energy considerations. From this viewpoint, the best trajectory is one with a flight time of 3-4 days, and in its selection the visibility of the moon from certain points of

the Soviet Union during the deceleration of the rocket and immediately after touchdown was taken into account. For payload conditions of photography and to provide the thermal regime, the landing of the station was planned in the region of the morning terminator (a line separating the dark side of the moon from the sunlit side). All this determines the date of the leg to the moon and the launch date. In selecting the control program, analysis of several deceleration variants shows that from the standpoint reliability vertical deceleration was optimum.

TABLE 5.4

/307

Position in Fig. 5.27	Time of Maneuver Execution	Impulse, m/sec	Purpose and Results of Maneuver
1	In the first orbit, at the perigee at $T_0 + 1$ hrs 34 min, 3 sec	+4.3	Achieving calculated apogee altitude. The apogee altitude after the maneuver is 276 km.
2	In the second orbit, at the apogee at $T_0 + 2$ hrs, 18 min	+18.5	Increase in perigee altitude to 224 km in order to reduce the angular approach velocity
3	In the second orbit in the common orbital mode, at $T_0 + 2$ hrs, 42 min, 7 sec	+9.7	0.07° correction of orbital inclination for coinciding of orbital planes
4	In the second orbit, at the perigee, at $T_0 + 3$ hrs, 3 min, 9 sec	+0.24 (engine operating period 0.01 sec)	+0.9 km correction of orbital altitude
5	In the third orbit, at the apogee, at $T_0 + 3$ hrs, 47 min, 37 sec	+12.9	Transfer to circular orbit. At a distance of 435.5 km, the radar of the Gemini VI locked onto the target (Gemini VII), and at a distance of 200 km the crew of the ship first saw the signals of the pulsed beacon on the target.

TABLE 5.4 /Continued/

Position in Fig. 5.27	Time of Maneuver Execution	Impulse, m/sec	Purpose and Results of Maneuver
6	In the fourth orbit, at $T_0 + 5$ hrs, 18 min, 39 sec	+13.5	First maneuver in the terminal approach phase. Relative distance 60 km.
7	In the fourth orbit, at $T_0 + 5$ hrs, 48 min, 40 sec	+12.9	Insertion of craft into orbit of target. Relative distance at end of maneuver is 36 m.

The system of stellar orientation used in correction and deceleration operated with respect to reference celestial bodies: the sun, moon, and earth. The telescopes of the astrosensors were positioned for precalculated instants of time. The final adjustment of the system was executed during the flight based on measurement data. In the correction, the initial automatic orientation toward the sun was carried out in two modes: coarse and precise. After stabilization of one rocket axis toward the sun by turning relative to it, the moon search was carried out. During orientation, the order of the operations was the same as for deceleration; after the moon search, the system began the automatic earth search. /308

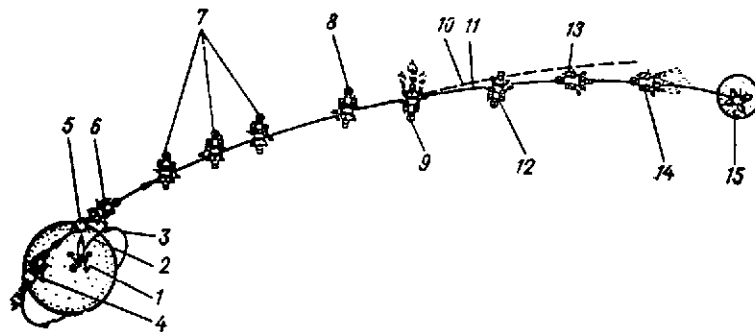


Fig. 5.28. Trajectory and flight stages of the Luna 9 Station

- 1 -- Launch
- 2 -- Powered phase

Fig. 5.28. Trajectory and flight stages of the Luna 9
Station /Continued/

- 3 -- Holding orbit
- 4 -- Final acceleration and insertion into trajectory of flight to the moon
- 5, 6 -- Separation of lunar stage from last missile stage, activation of the time-programing device
- 7 -- Ground sessions of trajectory measurements and reception of telemetry data
- 8 -- Coarse and precise orientation
- 9 -- Trajectory correction and orientation toward the moon
- 10 -- Trajectory without correction
- 11 -- Trajectory after correction
- 12 -- Adjustment of onboard systems for deceleration
- 13 -- Rotation of station and trajectory measurements
- 14 -- Firing of retro-engines
- 15 -- Soft landing on the moon

Preliminary calculations showed that if in deceleration the engine axis was oriented according to the calculated trajectory, the lateral component of velocity at the end of deceleration was approximately proportional to the deviation of the actual point of impact on the moon from the calculated point. Here a deviation of 100 km corresponds to a lateral velocity about 40 m/sec and the requirements on the precision with which the post-correction trajectory was known rose markedly. Therefore the retro-engine, beginning at distance of 8285 km from the lunar center, was oriented along the lunar vertical. After covering this distance, orientation was executed by tracking of optical sensors only aimed at the earth and the sun.

An exact measurement of altitude was made with a radio altimeter, and its antenna axis was oriented parallel to the axis of the engine installation. The beginning of the deceleration cycle was dictated by arriving at an altitude 75 km over the landing point.

The launch of the automatic space station Zond 5 flying past the moon also took place from an intermediate orbit. The minimum distance to the surface of the moon, 1950 km, was reached on 18 September 1968. During the flight terminating in the splash-down in the Indian Ocean, two corrections were executed: the first -- before the fly-by past the moon at a geocentric distance of about 325,000 km, and the second -- after the fly-by, at a distance of about 143,000 km. The flight trajectory of the manned Apollo spacecraft intended to transport astronauts to the moon, land them on the surface, and then to return them to the earth, includes two intermediate orbits: one -- the booster orbit around the earth, and the second -- the holding orbit at the moon (Fig. 5.29 /159, 170/).

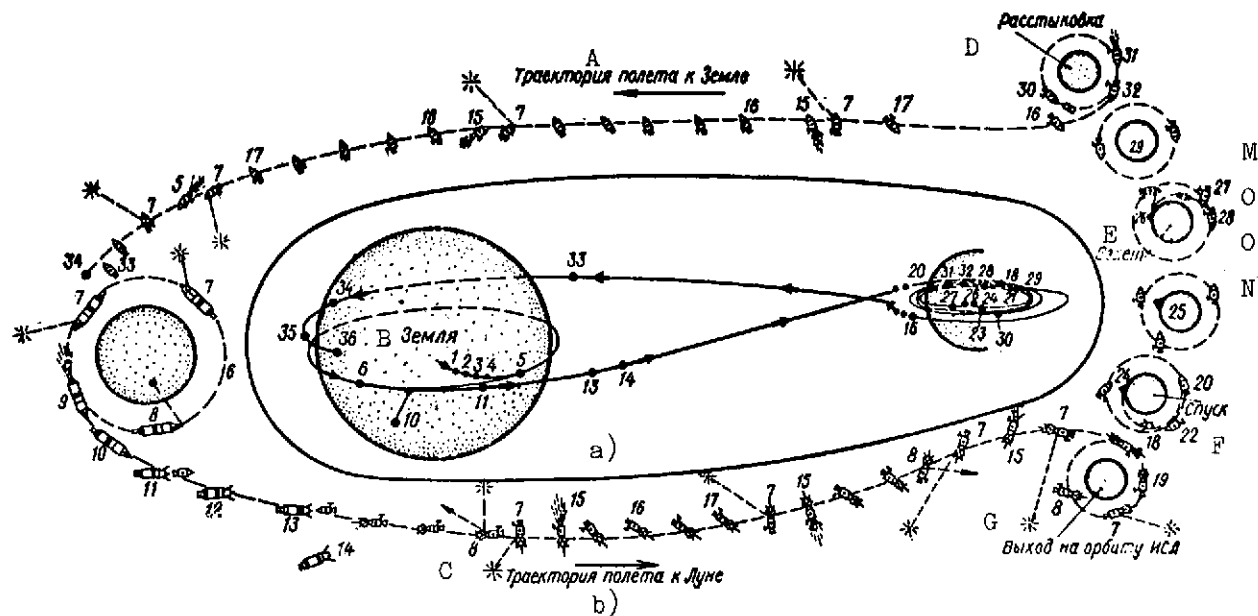


Fig. 5.29. Trajectory and stages of the flight of the Apollo spacecraft [159, 170]

a -- Trajectory

b -- Flight stages

KEY: A -- Trajectory of flight to earth

B -- Earth

C -- Trajectory of flight to moon

D -- Undocking

E -- Liftoff

F -- Descent

G -- Insertion into orbit of artificial moon satellite

The flight of the Apollo XV consisted of the following main stages.

1. Launch of a Saturn V launch vehicle (T + 0).
2. Cutoff of the first-stage engines (T + 159 sec) and separation of the first stage. The maximum g-load at the instant of engine cutoff is 4.5 g. Firing of the second-stage engines.
3. Separation of the emergency rescue system (after insertion into the regime of the second-stage engines and rocket stabilization).
4. Cutoff of the second-stage engines and separation of the second stage. Firing of the third-stage engines.
5. Insertion of the spacecraft and the third stage with partially consumed fuel into a holding earth orbit with altitude of 185 km (T + 0.2 hour). Over all phases of powered flight, except for the first, the astronauts can, in the event that the launch vehicle navigation system malfunctions, take command for themselves by using the navigation system of the Apollo craft.
6. Revolution in an earth orbit (1-3 revolutions). Check-out of equipment and crew status.
7. Erection of the inertial data instrumentation block.
8. Navigation measurements.
9. Firing of the third-stage engine and final acceleration of the spacecraft.
10. Insertion into a sustainer flight trajectory to the moon (T + 2.8 hours). Separation of aerodynamic fairings of the adapter. Orientation for motion in the sustainer trajectory and redocking of modules. /311
11. Separation of the main module (command and auxiliary bays) of the Apollo craft.
12. 180° turn of the main module.
13. Docking of the main module with its forward part (with a hatch for crew exit) onto the lunar module (T + 3.3 hours). During this operation in the position of the last stage of the launch vehicle with the lunar module is fixed by a stabilization system.
14. Separation of the third stage of the launch vehicle (T + 3.5 hours).
15. Correction of the trajectory with the sustainer engine.

16, 17. Beginning and end of the twisting of the spacecraft at the speed of 2 rev/hr.

18. Beginning of transfer to the selenocentric orbit ($T + 78.5$ hours). When this maneuver is not performed (nonfiring of the engine), on flying past the moon, the craft must again return to the earth and land.

19. Passive flight in selenocentric orbit. Transfer of two astronauts through hatch into lunar module.

Final check-out of lunar module. Input of required data from main module system into the navigation system of the lunar module.

20. Separation of the lunar module from the main module and orientation of the former ($\sim T + 100.25$ hours), and firing of the landing-stage engine (104.5 hours).

21. Transfer of the lunar orbiter into an elliptical orbit with altitude of apolune and perilune of 110 and 15 km, respectively.

22. The main module with a single astronaut in the selenocentric orbit monitors the guided motion of the lunar module to the moon by radar. Its trajectory is revised for an hour up to the instant of arrival of the lunar module at the perilune. This is carried out by the ground instrumentation complex and by the astronauts in the main module and the lunar module, using a sextant and radar. If a decision to land the lunar module is not taken, then the lunar module approaches the apolune with the main module, into which the entire crew is again gathered after docking.

23. Deceleration of the lunar module at an altitude of about 15 km from the lunar surface; the distance to the selected landing region is about 300 km. The altitude after deceleration is 2.6 km. 312

24. Landing on the lunar surface ($\sim T + 104.5$ hours). The landing is executed by the astronauts using a manual control system.

25. Time spent by the astronauts on the moon (67 hours). They exit onto the moon's surface three times (total duration ~ 20 hours), making trips on the moon traveler.

26. Firing of engines and launch from the lunar surface ($\sim T + 171.5$ hours). The landing stage of the lunar module remains on the moon.

27. Motion of the lunar module in a Hohmann ellipse to the selenocentric holding orbit of the main module. Trajectory correction.

28. Transfer of the lunar module to a circular orbit.

29. Encounter and docking of the main module with the command compartment ($\sim T + 173.5$ hours). Transfer of two astronauts to the main module and the removal of scientific material thereto. When the lunar module is malfunctioning after its liftoff, all approach maneuvers are performed by the main module.

30. Separation of lunar module (it remains in the selenocentric orbit; $\sim T + 177.3$ hours). Equipment check-out. Orientation of the main module for transfer to the trajectory of motion to the earth.

31. Firing of the booster engine.

32. Transfer to a trajectory of motion to the earth ($\sim T + 223.7$ hours).

33. Separation of the auxiliary bay of the main module.

34. Entry of the command module into the earth atmosphere. Aerodynamic correction of the trajectory.

35. Jettisoning of the heat shield (at an altitude of about 15 km), and deploying of drogue and main parachutes ($\sim T + 294.7$ hours).

36. Separation of parachutes and splashdown of command compartment with crew ($\sim T + 292.2$ hours).

The lunar module consists of two parts, which execute the lunar landing in the docked mode. The landing stage remains on the lunar surface, but the liftoff stage is launched and docks with the command module in the selenocentric holding orbit.

Fig. 5.30 /1567 gives the values of the required increments of velocity V and fuel consumption G_{fu} required to realize the flight trajectory of the Apollo craft. /313

The atmospheric re-entry is one of the most crucial and complex (in the sense of the accuracy required) flight stages. The re-entry trajectory must be made within the limits of a very narrow corridor (Fig. 5.31). If it is made higher, the craft can ricochet from the upper atmospheric layers and move away from the earth, but if it is made lower -- then the craft experiences such heating and g-loads which can lead to the death of the crew or the failure of the structure. Therefore the atmospheric re-entry angle required for a favorable landing must be $(-6.4 + 10^\circ)$ at a flight velocity of about 11.2 km/sec /1557. The calculated external surface temperature of the heat shield will be 3040°C in this case, and about 50°C on the inner surface of the module walls.

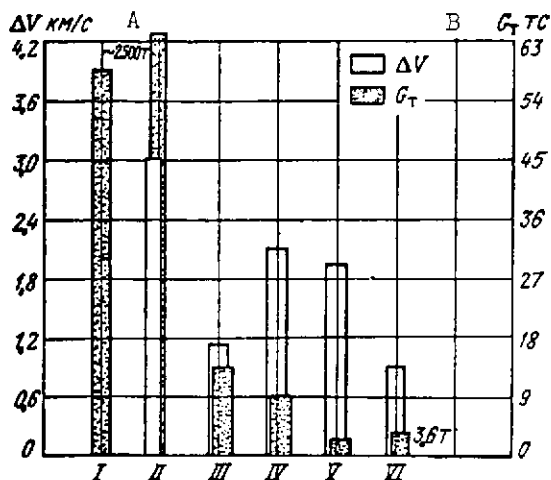


Fig. 5.30. Required increments in velocity ΔV and fuel consumption G_{fu} in flight stages

of the Saturn V launch vehicle and the Apollo spacecraft:

- I -- Insertion of last stage of launch vehicle with spacecraft into intermediate geocentric orbit
- II -- Transfer of craft to lunar flight trajectory
- III -- Transfer of craft to selenocentric orbit
- IV -- Landing of lunar module on the moon
- V -- Launch of liftoff stage of lunar module from the moon
- VI -- Transfer of main module of craft to earth's return trajectory

KEY: A -- ΔV , km/sec
 B -- G_{fu} , tons
 C -- G_{fu}

There is also another scheme of atmospheric re-entry in which 314 the speed of the craft is reduced by means of re-entry with several reflections (Fig. 5.31 b). In the atmospheric trajectory phase of landing, the onboard navigation system of the Apollo craft must provide, by means of bank control, a g-load not exceeding 10 g.

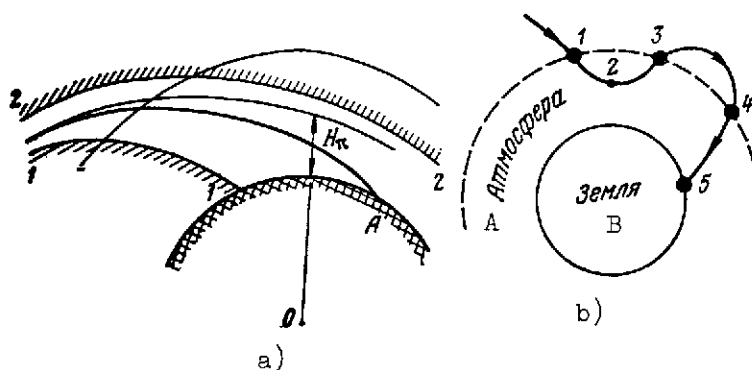


Fig. 5.31. Atmospheric re-entry trajectory of spacecraft:
 a -- Re-entry without immersion:
 1-1 -- Lower bound of acceptable trajectories
 2-2 -- Upper bound

Fig. 5.31. Atmospheric re-entry trajectory of spacecraft:

/Continued/

b -- Re-entry with immersion:

- 1 -- First immersion into the atmosphere at an altitude of about 120 km
- 2 -- Flight in the atmosphere
- 3 -- Departure from the atmosphere and ballistic flight
- 4 -- Second immersion into the atmosphere
- 5 -- Landing point

KEY: A -- Atmosphere

B -- Earth

The navigation system of the Apollo spacecraft consists of two independent systems: the navigation of the main craft module for the sustainer trajectory and the navigation of the module intended to land on the lunar surface. Initially it was assumed that navigation during the flight to the moon and back again would be executed with an autonomous system, and the command system must serve as back-up. Later, NASA decided to switch their roles: the main system would be the command, and the autonomous system would be the back-up system /151/.

Preliminary studies led to a rational degree of automation. Most of the operations in the complex control system are executed both automatically, or manually. An exception is the docking, which is performed by the crew /198/, by controlling the lunar module using two levers. One of them varies the longitudinal position of the craft and operates in two modes: impulse and continuous. /315 The second controls the rotation of the craft around its longitudinal axis, also providing for stopping of rotation at any instant of time /140/.

Fig. 5.32 a shows the block diagram of the navigation system of the main Apollo craft in the sustainer trajectory. Fig. 5.32 b, c gives the block diagram /191/ of the processes of determining the actual flight trajectory and the requisite correcting impulses.

Fig. 5.33 /140/ presents the structural block diagram of the /316 integrated system of the lunar module. The use of given instrumentation, controlled by earth commands, and the autonomous performance of navigation problems are executed by the onboard computer.

Orientation, stabilization, and all maneuvers in the trajectory are executed by means of the forces and the moments developed by liquid-fuel jet engines.

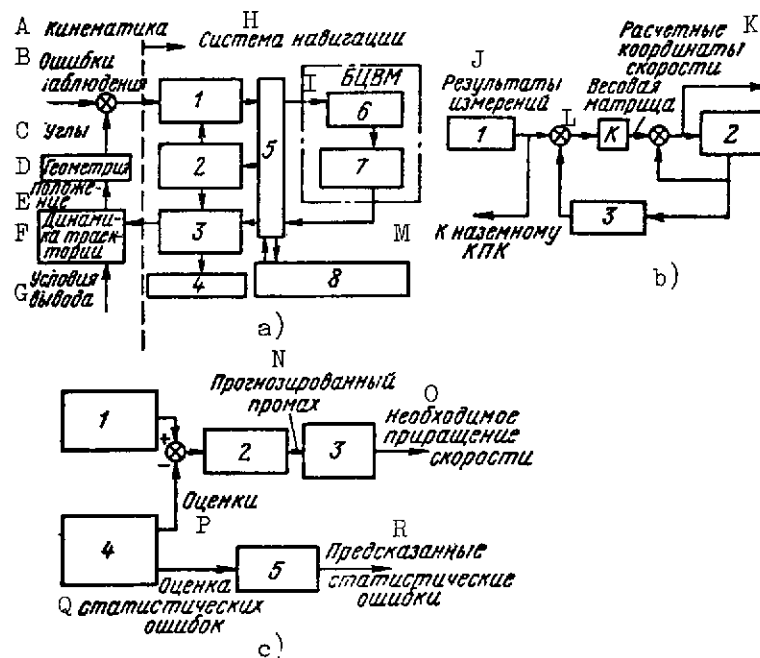


Fig. 5.32. Block diagram of individual control systems of the Apollo spacecraft:

a -- Navigation layout of main Apollo craft:

1 -- Optical sensors

2 -- Orientation devices

3 -- Velocity correction

4 -- Accelerometers

5 -- Crew

6 -- Trajectory determination

7 -- Determination of control law

8 -- Ground computer center

b -- Block diagram of the determination of the actual spacecraft trajectory:

1 -- Optical sensors

2 -- Calculation of trajectory (solving a bounded four-body problem)

3 -- Conversion of coordinates

c -- Block diagram of the determination of the correcting impulses:

1 -- Calculation of reference trajectory

2 -- Deviation prediction matrix

3 -- Control matrix

4 -- Calculation of actual trajectory

5 -- Error prediction matrix

KEY: A -- Kinematics

B -- Observational errors

Fig. 5.32. Block diagram of individual control systems of the Apollo spacecraft [Continued]:

- C -- Angles
- D -- Geometry
- E -- Position
- F -- Trajectory dynamics
- G -- Conditions of insertion
- H -- Navigation system
- I -- Onboard computer
- J -- Results of measurements
- K -- Calculated velocity coordinates
- L -- Weighting matrix
- M -- To ground spacecraft control center
- N -- Predicted miss
- O -- Necessary velocity increment
- P -- Estimates
- Q -- Estimate of statistical errors
- R -- Predicted statistical errors

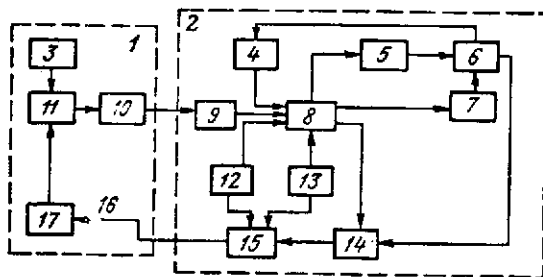


Fig. 5.33. Block diagram of the control system of the lunar module of the Apollo craft:

- 1 -- Ground facilities
- 2 -- Onboard equipment
- 3 -- Operator
- 4 -- Inertial platform
- 5 -- Orientation control system
- 6 -- Craft dynamics
- 7 -- Engines
- 8 -- Onboard computer
- 9 -- Command decoder

- 10 -- Encoder
- 11 -- Display and control panel
- 12 -- Radio altimeter
- 13 -- Lateral velocity meter
- 14 -- Telemetry system
- 15 -- Encoder and transmitter
- 16 -- Telemetry data (trajectory parameters)
- 17 -- Data decoding and processing

5.4. Ground and Onboard Devices of Spacecraft

The selection of the makeup and characteristics of ground and onboard spacecraft facilities fundamentally affects the tasks that the spacecraft must perform. Considering, however, the broad makeup of the control equipment of the space complex (ground and onboard radars, ground and onboard digital computers, gyroscopic instruments, radio altimeters, radio and laser rangefinders, and so on), in this section the reader's attention will be directed only to the basic equipment: radar (ground and onboard), gyroscopic instruments, onboard computers, and optical sighting devices.

Ground equipment for trajectory measurements of the spacecraft, using a radar transponder, consists of the interrogation radar and the reply signal receiver. The transponder onboard the spacecraft, on being excited by the ground radar signal, beams reply signals coherent in frequency and phase with the adopted values. This permits isolating the Doppler frequency and measuring the range to the space object with high precision.

The main elements of the radio beacon are a sensitive super-heterodyne receiver, a powerful transmitter for sending code pulse reply signals, and a pulse decoder. The output pulse power of the radio beacon intended for operation at moderate distances from the earth is about 1 kw at a mean power not exceeding 30 watts. Telemetry data can also be sent via a special channel using the same beacon.

Use of a beacon with a continuously beamed signal permits determining the range to satellites in low orbits with high precision, based on the Doppler frequency shift. These telemetry facilities are used in systems whose characteristics depend heavily on the accuracy of orbital determination (for example, in space communication systems).

The advantages of narrow-band systems with continuous signals compared to pulse systems lie in the smaller output power of the onboard transponder, and therefore, in its lesser weight, and also in the greater signal-noise ratio.

Fig. 5.34 shows the block diagram of a Doppler receiving set that is capable of detecting, tracking, and recording trajectories of both one AES, as well as several (when selective receivers are used) in different orbits. The reference standard for all heterodynes and reference frequency generators in the synthesizing unit is an ultrastable reference generator; precise time signals are used to synchronize this system and to correct for the slow drift of the reference generator frequency.

It is also possible to track AES by the Doppler frequency shift. In this case there is no need for a stable onboard radio beacon, but the power of the ground transmitter located -- in order to ensure the reception only of reflected signals -- at some distance from the receiver must be very much larger. The use of modern techniques of encoding the transmitted data and the requirement of precise time synchronization make it necessary not only to generate oscillations that are stable in frequency, but also to precisely determine the time and frequency. The latter is due, in particular, to the necessity of providing high precision in tracking this space object for its navigation and control. /319

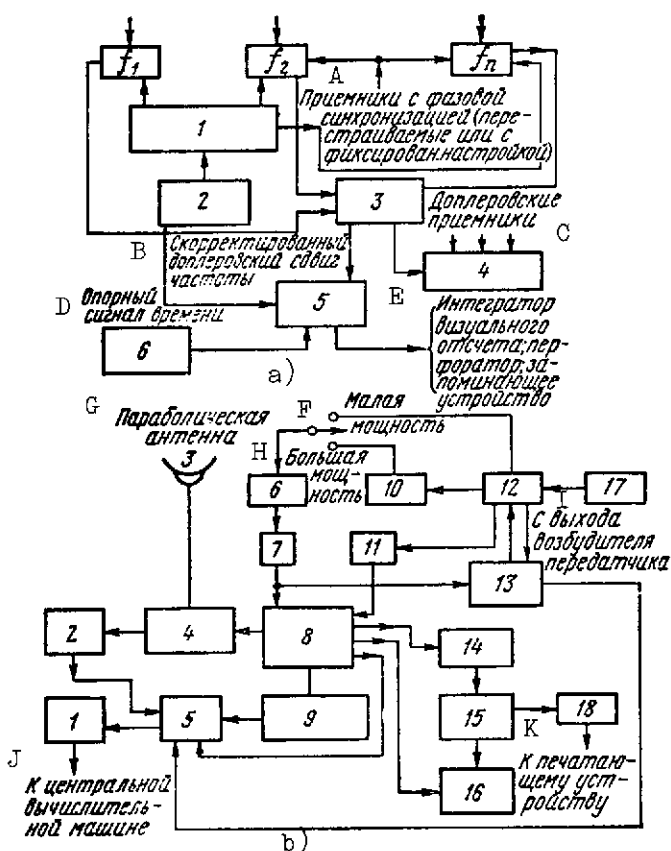


Fig. 5.34. Block diagram /318 of ground Doppler stations:

- a -- For the determination of AES trajectories:
- 1 -- Frequency-synthesizing unit
 - 2 -- Reference generator
 - 3 -- Equipment correcting errors due to refraction
 - 4 -- Memory
 - 5 -- Data monitoring and processing unit
 - 6 -- Precise time signal receivers
- b -- For determination of long-range spacecraft trajectories (a DSIF /deep space instrumentation facility/ unit):
- 1 -- Telegraph
 - 2 -- Angular data encoder
 - 3 -- Parabolic antenna
 - 4 -- Tracking antenna drive
 - 5 -- Data processing unit
 - 6 -- Duplexer
 - 7 -- KPU /spacecraft intercommunication unit/
 - 8 -- Tracking receiver
 - 9 -- Precision Doppler frequency shift meter

- 10 -- Power amplifier
- 11 -- Frequency monitor
- 12 -- Transmitter
- 13 -- Range measurement subsystem
- 14 -- Telemetry receiver
- 15 -- Carrier frequency discriminator
- 16 -- Data recorder
- 17 -- Command generator and encoder
- 18 -- Decoder

- KEY:
- A -- Receivers with phase synchronization (adjustable or with fixed adjustments)
 - B -- Corrected Doppler frequency shift
 - C -- Doppler receivers
 - D -- Reference time signal
 - E -- Integrator of visual readout; perforator; memory
 - F -- Low power
 - G -- Parabolic antenna
 - H -- High power
 - I -- From output of transmitter exciter
 - J -- To central computer
 - K -- To printer

Errors in time and frequency measurements are interdependent. Error in the time determination, for example, of 10 msec, with an orbital velocity of the object of 7.5 km/sec, leads to a 75 m error in the position determination. Therefore stations at a long distance from each other must be synchronized for a long time with a precision of several microseconds [59, 104].

Precise frequency reference standards are based on the use of atomic resonance phenomena in vapor containing atoms of cesium or rubidium, or ammonium molecules. Reference standards using rubidium and cesium can provide long-term frequency stability and an accuracy of the order of 10^{-10} . Short-term stability can be increased by more than one order of magnitude.

As an example of tracking stations used in command systems and intended for navigation in deep space, we can consider the DSIF /Deep Space Instrumentation Facility/ system [59]. It consists of three tracking stations separated by longitude-intervals of about 120° .

The stations are mounted in mobile installations and can be used for tracking, communication, reception of telemetry data, and the transmission of control commands soon after the launch of the spacecraft intended to study the moon or the planets.

A block diagram of a DSIF system facility is shown in Fig. 5.34 b. Its makeup includes an automatic angular tracking unit and a 26-m diameter parabolic reflector. Tracking data, which consist of [320] two angular coordinates and the radial velocity, are fed into a computer. The range measurement system is included in the auxiliary facility equipment. From published data, this system provides an accuracy for angles, range, and velocity of 0.01° , 15 m, and 0.1 m/sec, respectively.

Another command-instrumentation complex of the Apollo system, the MSFN /Manned Space Flight Navigation/, consists of a coordinating-computer center and radar tracking stations located on the earth, ships, and aircraft. In the stage of the Apollo craft insertion into orbit with a launch vehicle, radar stations located along the track of the orbital insertion were used. The coordination-computer center, CCC [147, 203], includes two control posts equipped with several displays, television image systems, a medical-biological monitoring post, a communications center, and a computer center equipped with four IBM-360 computers and three UNIVAC-490 computers for preliminary real-time processing of data coming from the tracking stations at a rate of 2400 bits/sec.

The MSFN system stations must track the Saturn V launch vehicle and the spacecraft in its different flight stages and maintain communication with it, and retransmit the data to the CCC. Characteristics of the main antennas with which the ground and ship stations are equipped are given in Table 5.5.

TABLE 5.5

Kind of station	Reflector diameter, m	Width of radiation pattern, deg	Gain factor, db	Transmitter power, km
Ground	26	0.35	51	2×10
Stations w/ Cassegrain system ant.	9	1	44	10
Shipboard	3.7*	—	—	—

* These antennas were installed in two of the five ships equipped with radar.

Besides the main antennas, the stations also have auxiliary antennas for primary capture of the spacecraft with a 1-m diameter reflector and a 10° -wide radiation pattern; additionally, they are equipped with uncooled parametric amplifiers. The radar operates on one of these following five fixed frequencies: /321

2106.4 MHz -- for transmission to the main module of Apollo spacecraft;

2101.8 MHz -- for transmission to the lunar module of the Apollo spacecraft;

2287.5 MHz -- for receiving from the main module;

2272.5 MHz -- for receiving from the auxiliary main module transmitter; and

2882.5 MHz -- for receiving from the lunar module.

Each ground station is equipped with two UNIVAC 1230 computers. One of these is intended for the preliminary processing of data coming from the spacecraft. The second is intended for the processing, check-out, and storage commands before transmitting to the craft.

Ocean-going vessels intended for tracking the Apollo spacecraft are equipped with UNIVAC-CP 642V computers and navigation systems (including, the Loran C navigation system).

The use of aircraft tracking stations intended for tracking communications with the Apollo spacecraft when it is beyond the visibility zone of ground and ship radar made it possible to avoid building 20-30 additional ground stations /147/. The aircraft tracking antenna, 2.1 m in diameter and 320 kg in weight, housed in the forward part of the fuselage, is intended to operate in the centimeter (for communications with the spacecraft) and the meter (for communications with ground stations) ranges. It can rotate by $+80^\circ$ with respect to azimuth and (-30°) to $(+80^\circ)$ as to the angle of elevation.

The system for communications with the Apollo craft must have high carrying capacity, approximately 2400 bits/sec. The onboard control systems of the Gemini and Apollo spacecraft include radar approach stations.

The approach radar of the Gemini 152, 155, 163, in addition to the inertial block and the computer, forms a system performing the navigation rendezvous task. In addition, a command link for 322 motion control of the spacecraft-target during docking with it is formed with the onboard radar. An interferometer type radar provides information on the attitude of the target, relative range, and its derivative.

The radar set consists of a transmitter of interrogating pulses, an antenna complex, and a reply pulse receiver. A transceiver located on the target consists of an antenna complex, receiver, and transponder. The radar gives information in digital form to the onboard computer at relative distances of from 460 km to 150 m, and in the analog form to the relative range and velocity indicator, which has a velocity scale with ranges (-30.5 to +152.5) m/sec and (-1.5 to +1.5) m/sec, and a range scale with the range 0 - 92 km.

Main Characteristics of the Gemini Onboard Radar:

Mean radiation power	2 w
Wavelength	30 - 32 cm
Maximum target lock-on range	460 km
Error of range measurement	less than 1 percent to a range of 400 m
Weight	20 kg
Volume occupied	0.05 m ³

The equipment of the lunar module of the Apollo system includes two radars. One of them (built by Ryan) is designed to provide for landing on the lunar surface. It determines the relative flight velocity by measuring the Doppler frequency shift in the continuous-wave mode, and the altitude by operating in the radar altimeter mode. This radar is built with a four-beam antenna. Three beams are used to measure velocity, and the fourth -- to measure altitude.

Data arriving from it are fed into the onboard computer; beginning at an altitude of 12 km, it is additionally displayed on the astronaut panel. The second radar, built by RCA, is an automatic tracking radar. It provides for rendezvous in the lunar module orbit with the main module and determines the range, angles, and their derivatives. Its Cassegrain type antenna has a 51-cm diameter prime reflector and a 10.2 cm diameter secondary reflector.

Characteristics of the Lunar Module Onboard Radar

Angles of view	225 x 140°
Power,	
required design, in w	110
maximum, in w	145
radiated, in w	0.3 - 0.5
Signal/noise ratio	10 db
Working range	
for range	25 m to 740 km
for relative velocity	±1.5 km/sec

The maximum allowable errors in radar measurements are given in Table 5.6 [147, 197, 203]. It can operate both by onboard computer command in the automatic mode, as well as by astronaut command. Depending on the working distance, it can function with or without a transceiver. It can also operate by a radio beacon in landing on the lunar surface.

TABLE 5.6
MAXIMUM ALLOWABLE ERRORS IN MEASUREMENTS BY THE LUNAR MODULE
ONBOARD RADAR

Parameter measured	Range of measurements	Absolute error	Relative error
Range	180 m — 9.3 km	1.8—93 m	1%
	9.3 km — 740 km	23—1850 m	0.25%
Radial velocity	180 m — 9.3 km	1.8—93 m	1%
	9.3 km — 740 km	23—1850 m	0.25%
Angles	At a range of 370 km	2 mrad	—
	At a range of 555 km	3 mrad	—
Angular velocity	At a range of 185 km	±0.2 mrad/sec	—
	At a range of 740 km	±0.4 mrad/sec	—

The tracking and determination of space object coordinates is possible also with optical devices. Optical radars using lasers can provide a resolution of up to 1" and 20-30 m for angles and range, respectively [59, 165].

With optical ranging, not only can the illuminating beam of a ground pulse laser amplified by the onboard optical reflector be used, but also the reflected sunlight on an onboard light source.

Precise optical tracking was accomplished with the American Baker-Nunn cameras and precise time standards [165]. Processing of results obtained with these cameras made it possible to determine the position of an object in a trajectory with an accuracy of one angular minute. Electro-optical systems with tracking telescopes and photographic cameras provided for recording the position of an object fixated in time with an accuracy up to fractions of a millisecond [59]. Unfavorable meteorological conditions and the optical visibility of the objects are factors limiting the use of optical devices.

Onboard optical facilities of the Apollo system are the sextant and telescope. Both of these instruments are part of the navigation system of the spacecraft. The main characteristics of the sextant and telescope are given in Table 5.7.

The telescope is used for scanning and searching the navigation reference point. The sextant is used to measure its position. Either instrument has eyepieces which permit positioning the eye at a distance up to 5 cm, i.e., to bring the observation into the space helmet. After the images of two reference points obtained in the sextant have been brought into correspondence, the astronaut -- by pressing a button -- feeds into the onboard computer data on the time of measurement and the angle between these reference points, which is measured with an accuracy to 10". This error is equivalent to an error in spacecraft position determination in the flight trajectory between the earth and the moon equal to several kilometers. /325

Performance of the navigation tasks of the Apollo craft provides for measuring angles between the bearings to the navigational star and an object on the earth or moon, or else the angle between the bearing to the navigation star and the bearing to the earth or lunar horizon (Fig. 5.35).

TABLE 5.7

Optical instruments	Power	Angle of field of view, deg	Diameter of entr. aperture mm	Error of measurement (max), angular, sec
Sextant	28	1.8	40	10
Telescope	1	60	5.1	30

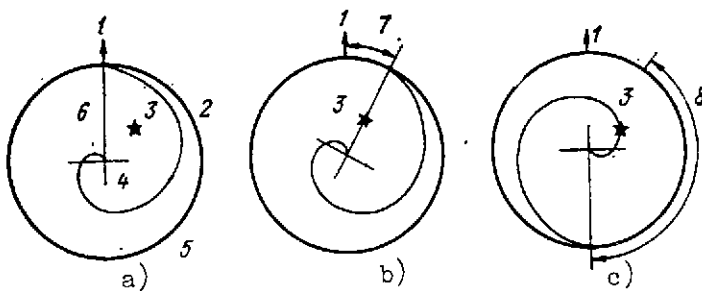


Fig. 5.35. Measurement of bearing to star with a telescope mounted in the lunar module:

- a -- Sighting grid
- b -- First measurement
- c -- Second measurement:
- 1 -- Beginning of orientation angle reading
- 2 -- Spiral for reading between star and center of field of view

- 3 -- Star
- 4 -- Auxiliary line
- 5 -- Field of view ($55 - 60^\circ$)
- 6 -- Orientation line
- 7 -- Orientation angle
- 8 -- Quantity proportional to the angular distance of the star from the center of the field

Gyrostabilized platforms and gyro-sensors of spacecraft control systems

Gyrostabilized platforms are part of the autonomous navigation system of spacecraft. The gyrostabilized platform of the Gemini spacecraft consists of a four-ring gimbal suspension of the platform with three two-degree-of-freedom floated gyroscopes mounted on it, along with three single-integrating accelerometers placed along mutually orthogonal axes [152, 155, 163]. The roll axis of the gyrostabilized platform coincides with the roll axis of the spacecraft, which permits data to be obtained on the position of the craft based on this axis immediately without recalculation. /326

Floated gyroscopes (FG) can operate both in the stabilization mode, as well as in the mode of three-dimensional integration. The frequency of the pulsed output of the accelerometers is proportional to the increment of the orbital velocity ΔV and has a discretization of 0.03050 m/sec. The total weight of the inertial data block (including the output signal conversion electronics, the malfunctioning detection system, and the power block) is 54 kg, with the floated gyroscope going 13.6 kg. The floated gyroscope can be erected manually (which takes about 15 minutes) or automatically (in orbit) using an infrared horizon sensor with an accuracy up to $\pm 5^\circ$.

The horizon sensor consists of an infrared device operating in the wavelength range $\lambda = 15 \pm 1$ microns and scanning with respect to the azimuth. It is intended to construct the local vertical in the mode of automatic stabilization of the craft based on the pitch and bank angles (with the inertial block turned off) and for automatic direction of the gyro-stabilized platform in the stages of encounter and docking. To increase reliability, two independent systems of sensors, which the astronauts switch on manually, are installed on the craft.

The main characteristics of the infrared horizon sensor are as follows /169/:

working altitude	90 - 1700 km
angle of field view of the IR telescope	1°
angle of field of view with respect to the horizon	160°
time of initial horizon lock-on	2 min
time of second horizon lock-on	30 sec
accuracy of constructing the vertical	$\pm 0.1^\circ$
weight	4.5 kg

The gyro-stabilized three-degree-of-freedom platform of the Apollo craft includes three MUT-25 IRIG integrating floated gyroscopes, three pulsed MUT-16PIPA integrating pendulum accelerometers, and three differentiating accelerometers. Spherical floats and magnetic suspensions are used in the integrating gyroscopes. The magnetic suspension reduces the effect of perturbing moments and precludes the harmful effect of impact and vibration.

The most essential parameters of the integrating gyroscopes affecting the accuracy of spacecraft navigation are the gyroscope drifts ϵ_1 , independent of accelerations, the drifts ϵ_K -- proportional to acceleration along the input axis and caused by axial unbalancing, and the drifts ϵ_g , which are a consequence of radial unbalancing and are proportional to acceleration along the axis of inherent rotation. /327

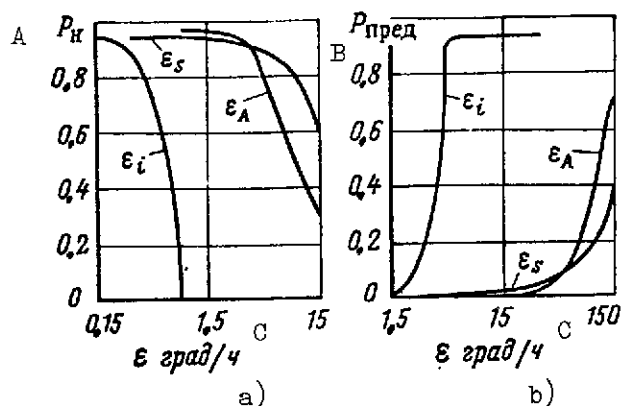


Fig. 5.36. Probability of successful operation of the gyro-platform as a function of drift:

a -- In normal condition
b -- With maximum flight trajectory deviations

KEY: A -- P_n [n = normal]

B -- P_{\max}

C -- ϵ , deg/hr

Fig. 5.36 a [75] shows the probability that the gyroscope drift, not exceeding the values indicated in the graph, does not affect successful gyroscope operation. Here it is assumed that the gyroscope operates successfully if the errors it causes lead to deviations in the position of the geocentric orbital perigee ≤ 3.6 km, an error in the altitude of the selenocentric orbit ≤ 1.8 km, an error in the position of the plane of the selenocentric orbit $\leq 0.05^\circ$, and an error in the first correcting impulse ≤ 2.3 m/sec. Fig. 5.36 b shows the probability of the maximum allowable trajectory deviations caused by these gyroscope drifts. Deviations 10 times greater than the values shown above are taken as maximum allowable values. For greater deviations the flight is unsafe. Thus, the accuracy characteristics of gyroscopes as related to conditions of the exact execution of the flight program must lie to the left of the curves shown in Fig. 5.36 a, and as related to the conditions of flight safety -- to the left of the curves shown in Fig. 5.36 b. /328

At the launch the gyro-platform is erected with respect to the azimuth using a gyro-compass; during the flight this is done with the sextant. To erect the inertial system, the telescope can be placed in three specific positions. It is equipped with a rotating sighting grid shown in Fig. 5.35 a. The reading is taken with the aid of the radial orientation line and spirals imaged on it. In the first measurement (cf Fig. 5.35 b), the astronaut aligns the orientation line with the reference star, and in the second measurement -- he aligns the spiral with the star. The value of the angle after each measurement is fed into the onboard computer.

These measurements must be performed with at least two stars, and then the onboard computer determines the requisite orientation of the inertial system and erects it [197, 203]. The equipment of the spacecraft control system also includes rate gyros consisting of two blocks with three two-degree-of-freedom gyroscopes in each [cf Chapter Three].

TABLE 5.8
MAIN CHARACTERISTICS OF SPACECRAFT ONBOARD COMPUTERS

Characteristics		Gemini $\overline{163}$, $\overline{163,190}$	Apollo $\overline{19,203}$
Number of digits in memory cell		39	16
Duration of memory cycle, in μsec			11,7
Memory capacity in bits: permanent operational		117 000 4096	36 864 2048
Total nr. of instructions			44
One-operation time, in μsec	Addition	140	23,4
	Addition w/ doubled accuracy	None	35,1
	Multiplication	420	46,8
	Division	840	
	Multiplication w/ doubled accuracy		57,5
Principle of design execution		Micromodular, semiconductor elements, and ferrite cores	Two parallel-action computers, ferrite cores
Power required, w			100
Weight of computer devices alone, kg		26,8	26,3
Volume occupied by computer devices alone, decimeter ³		38	28,3

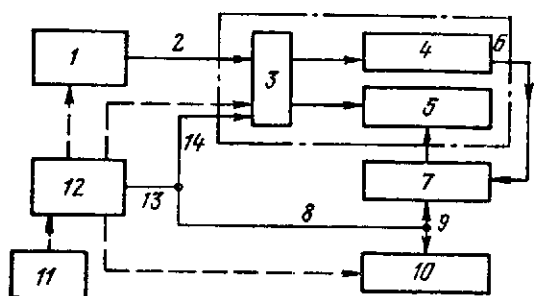
Onboard digital computers of spacecraft control systems

Onboard digital computers used to perform tasks of navigation during flight are installed on the Gemini and Apollo spacecraft. Onboard digital computers of these spacecraft are of the universal, sequential-action type, with fixed decimal point.

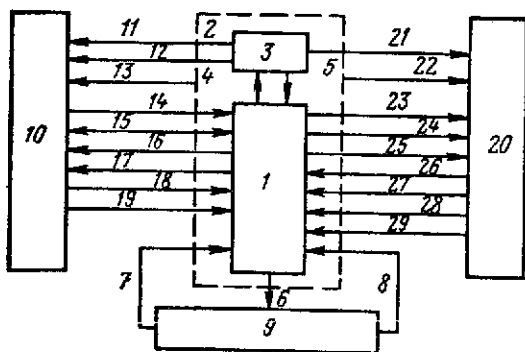
The main characteristics of the onboard digital computers are shown in Table 5.8. Fig. 5.37 a shows the block diagram of an onboard digital computer; Fig. 5.37 b shows its connections with onboard systems [19, 203].

Computation is controlled with the aid of pushbuttons of a panel feeding data into the onboard computer and interrogating it. When the computer performs operations on astronaut interrogation, other operations are interrupted.

The information arriving from accelerometers and range and velocity-measuring radars is fed directly into the onboard computer, while data coming from the remaining information units (optical, radar, and the angular quantities picked off the inertial block) are fed via data-matching blocks (five blocks), which are analog-to-digital converters.



a)



b)

Fig. 5.37. Layout of the Apollo-330 onboard digital computer and its connections with the control system:

a -- Block diagram

Control channel

----- Data transmission channels

1 -- Instruction counter

2 -- Instruction address

3 -- Selector

4 -- Permanent memory

5 -- Operational memory

6 -- Memory

7 -- Buffer memory

8 -- Instructions

9 -- Digits

10 -- Arithmetic unit

11 -- Synchronizing circuit

12 -- Sequencer generator

13 -- Operational code

14 -- Data address

b -- Layout of connections of onboard computer with navigation and control system:

Fig. 5.37. Layout of the Apollo craft onboard computer and its connections with the control system Continued:

- 1 -- Onboard computer of the Apollo craft navigation system
- 2 -- Computer subsystem
- 3 -- Display and control panels
- 4 -- Display and signaling data
- 5 -- Astronaut instruction
- 6 -- Control signal for scanning telescope and sextant
- 7 -- Operating mode indicator
- 8 -- Telescope and sextant sighting angles
- 9 -- Optical subsystem
- 10 -- Spacecraft
- 11 -- Telemetry data
- 12 -- Earth-onboard communications channel
- 13 -- Emergency signaling
- 14 -- Engine control
- 15 -- Craft control
- 16 -- Code of onboard-earth communications channel
- 17 -- Synchronization channel
- 18 -- Synchronization signals of onboard-earth channel
- 19 -- Code of earth-onboard communications channel
- 20 -- Inertial subsystem
- 21 -- Switching of operating mode
- 22 -- Emergency instructions
- 23 -- Signals of platform suspension drive
- 24 -- Synchronization signals
- 25 -- Gyrostabilization instructions
- 26 -- Emergency condition signals
- 27 -- Operating mode indicator
- 28 -- Velocity change
- 29 -- Gyro-platform position

FOOTNOTES

¹ The point of vernal equinox is the point on the celestial sphere at which the sun is located on the day of vernal equinox.

² [85] is one of the main works on this subject.

³ The lifetime of an AES in orbit must be distinguished from its active lifetime, defined as the duration of the operation of onboard equipment.

⁴ In this case we are not speaking of the stabilization of AES relative to the mass center, but about the stabilization of their position in orbit one with respect to the other.

The curves in Fig. 5.10 require, generally speaking, corrections that allow for the probability of malfunction of equipment due to radiation exposure at altitudes below 18,000 km.

⁵ Inzhenernyy spravochnik po kosmicheskoy tekhnike (Engineering Handbook on Space Technology), edited by A. V. Solodov, Voenizdat, 1969.

⁶ Cf. footnote 5.

⁷ Cf. footnote 5.

⁸ That is, the time by which firing of the engine of the maneuvering spacecraft is deliberately delayed in order to obtain boundary conditions that are more favorable from the standpoint of the trajectory being formed.

⁹ The possibility of using promising, but as yet not actually used engines of the plasma, ionic, and other types is not discussed here.

¹⁰ The first and fundamental investigation of flight trajectories to the moon was given in the work [37].

¹¹ Desyat' let kosmicheskikh issledovaniy v SSSR (Ten Years of Space Research in the USSR), Moscow, "Nauka" Publishing House, 1967.

GENERAL PRINCIPLES OF DESIGNING FLIGHT COMPLEXES AND
THEIR CONTROL SYSTEMS

Modern aircraft and missile complexes are complicated interconnected dynamic systems with regular and stochastic parameters. Each of these complexes is intended to perform several wholly specific operations. For example, aircraft attack complexes are designed to strike ground targets; aircraft and missile defense complexes are designed to intercept and attack air targets, and so on.

The use of active defense facilities by an enemy markedly affects the control systems of flight craft. The performance of antiaircraft maneuvers by an enemy's airplanes requires either an increase in the number of antiaircraft missiles launched, or else allowance for the maneuver in the missile control law. When radio countermeasure equipment is used on aircraft attacking ground targets the AAD facilities (fighter-interceptors and antiaircraft missiles) must also be increased, or else control systems must be constructed on which jamming does not have a marked effect.

In performing operations of attack or defense, the tactics of employing active countermeasures can be varied. The use of different kinds of traps by the attacking side varies in relation to the enemy's capabilities. If the number of interception facilities that an enemy has is large, the use of traps is most expedient. As the number of interceptors is reduced, the number of traps must be decreased. As we can see, this solution varies during the conduct of a military operation, which complicates the appraisal of the effectiveness of defense or attack facilities. /332

Requirements of interrelatedness of group operations also strongly affect control systems. For example, fighter-reconnaissance craft transmit data on detected targets to attacking airplanes, which then strike these targets. Without mutual communication and cooperation in the actions of the reconnaissance airplanes and bombers, success in performance of a given operation is markedly reduced. When there is a breakthrough in a front line, fighter-interceptors give cover to multimission attack fighters, and when the actions of these groups of aircraft are brought into accord, the success of the given operation becomes greater. Aircraft control systems must be provided with technical devices facilitating group actions. For example, inter-aircraft navigation equipment, group displays, and so on. Actions

of antiaircraft missiles and fighter-interceptors in AAD systems executed in an agreed upon plan are vital. All this indicates that in designing control systems, complicated dynamic models of defense and attack must be used. These models permit not only setting up effectiveness criteria in evaluating means of attack or defense, but also designing control systems on a sound foundation. Monetary outlays for manufacture and operation of complexes, and the costs of attack and defense facilities must also be allowed for in models.

Modeling analog or analog-digital computers become the principal tool of the designer when operation models are used. However, the need for a preliminary selection of the parameters of a flightcraft or control system equipment requires simplified general designing methods. This chapter deals with general methods of designing control systems based upon the use of effectiveness and cost criteria. Additionally, methods of synthesizing control systems by using mathematical modeling are discussed.

6.1 Effectiveness of Complexes

/333

The effectiveness of complexes is evaluated by using effectiveness criteria, which in general form consist of a function or a functional

$$E = E(x_1, \dots, x_n; y_1, \dots, y_n), \quad (6.1)$$

where x_i are the controlling parameters, and y_i are external actions on the controlling functions.

These criteria can be represented as deterministic or stochastic functionals. The time to perform an operation, the amount of fuel (energy) consumed, cost, and so on can be classified as deterministic functionals. The following are used as stochastic functionals: the probability of entering a zone (region) of attack, the probability of performing an operation, the mathematical expectation of damage inflicted on the enemy or prevented, and so on.

The existence of several effectiveness criteria leads to the problem of selecting a generalized criterion E_a [24]. The generalized criterion E_a is a function of the partial effectiveness criteria

$$E_a = E(E_1, E_2, \dots, E_n). \quad (6.2)$$

As we know [24], the generalized effectiveness criterion E_a is expressed in terms of partial criteria by means of a finite number of several elementary operations.

These elementary operations are as follows:
 summation with weighting λ_i

$$E_a = \sum_{i=1}^n \lambda_i E_i; \quad (6.3)$$

alternative transition

$$\left. \begin{array}{l} E_i = 1, \quad E_i \geq E_i^0 = \text{const}; \\ E_i = 0, \quad E_i < E_i^0, \end{array} \right\} \quad (6.4)$$

negation

$$E_i = 1 - \bar{E}_i, \quad (6.5)$$

expressing a target opposite to the given \bar{E}_i :

/334

conjunction

$$E_a = E_i \& E_{i+1} = \prod E_i; \quad (6.6)$$

disjunction

$$E_a = E_i \vee E_{i+1} = 1 - \prod_i (1 - E_i), \quad (6.7)$$

expressing the satisfaction of all E_i criteria, or at least one of them, respectively.

The last three operations are used directly in calculating the reliability of systems consisting of n elements, or their different combinations and various standby methods. In the form written here, these operations are applicable only for criteria taking on the value of 0 or 1. When any criteria are used, they

can be represented in a more general form, namely:

$$\left. \begin{aligned} \neg E_i &= -\tilde{E}_i; \\ E_a &= \min_i \lambda_i E_i; \\ E_a &= \max_i E_i \lambda_i; \quad \lambda_i \geq 0. \end{aligned} \right\} \quad (6.8)$$

The summation operation with weights is written as follows

$$E_a = \int E(n) \lambda(n) dn. \quad (6.9)$$

for continuous functions. The similarity of the operations of the union of criteria with the operations of mathematical logic can permit the construction of a final algorithm to obtain the generalized criterion.

One of the most important results obtained thus far is that the generalized criterion $E_a = F(E_1, \dots, E_n)$, that is continuous in a bounded range of values of the variables E_i , can with any prespecified accuracy be represented as the result of a minimax operation performed on some linear form of these variables [24]. In other words, for specified conditions for any $\epsilon > 0$, we can find 335 a finite number of constants a_{1ki} or C_{1k} such that the inequality

$$\left| E_a - \min_{1 \leq i \leq l_0} \max_{1 \leq k \leq k_0} \left(\sum_{i=1}^n a_{1ki} E_i + C_{1k} \right) \right| \leq \epsilon. \quad (6.10)$$

is satisfied. However, even this theorem does not indicate the method of selecting coefficients appearing in expression (6.10).

In the general case, the synthesis of a system satisfying several imposed criteria, of which one can be selected as the effectiveness criteria, reduces to solving a problem in linear or nonlinear programming (depending upon the nature of the system), with allowance for the constraints dictated by the remaining requirements. This formulation of the problem is adequate for the synthesis of a system satisfying the generalized criterion constructed by means of the above-indicated elementary operations. Its solution is made difficult by the awkwardness of the problem and the mathematical complexity of attaining the absolute

extremum, especially when there are nonlinear constraints and criteria, and also when the controlling parameters are nonmonotonic and discrete. One very common practical procedure consists of, if the synthesized system must satisfy two criteria: deterministic and stochastic, ordinarily calculating a system by satisfying initially only the first criterion, and then testing the value of the second, or correcting some parameters on the condition that it has been satisfied. This method implicitly assumes the smallness of the change in the deterministic criterion when the parameters are varied to satisfy the stochastic criterion. The use in engineering practice of two stages of the calculation -- optimization of the system based on the deterministic, and then based on the statistical criterion -- is illustrated by the following example.

Let us assume that the capture complex representing a deterministic system (stochastic external actions, all kinds of errors and noise are absent), has been synthesized, on the condition that the deterministic criterion admitting of only two outcomes (the interception has taken place or the interception has not taken place), and several constraints, for example, with respect to the maximum cost, maximum power-to-weight ratio of the flight craft, maximum interception time, and so on, have been satisfied. /336

Now suppose that this same complex operates in stochastically varying external conditions and flight craft parameters; also suppose that all the elements of the complex deviate randomly from their nominal values. If the interception act is repeated several times in this situation, then in some cases it will take place (the earlier-adopted effectiveness criterion will be equal to unity), while in others it will not (the criterion will be equal to zero).

Assuming the massive use of this complex, in this situation it is natural to assume that the stochastic effectiveness criterion refers to the probability of the performance of the combat mission whose solution is provided for by the synthesis based on the deterministic criterion². It is precisely this approach that is taken in most practical cases: a functional expressing the probability of the performance of a combat mission serves as the stochastic effectiveness criterion of the complex E_a , and its numerical value for given values of the random functions serves as the measure of effectiveness. Thus, we can write

$$E_a = \int_{\substack{x_i \in X \\ 1 \leq i \leq n}} p(x_1, \dots, x_n) dx_1 \dots dx_n, \quad (6.11)$$

where ρ is the function of the probability density of the performance of the combat mission by the complex, and

X is the range of the arguments x_i ($1 \leq i \leq n$).

The performance of a combat mission consists in the realization of m successive stages, at each of which a particular task is executed. Therefore

$$\rho(x_1, \dots, x_n) = \prod_{j=1}^m \rho_{j|j-1}(x_1, \dots, x_n), \quad (6.12)$$

where $\rho_{j|j-1}$ ($1 \leq j \leq m$) are the functions of the densities of the conditional probabilities that the specific tasks will be performed at each stage. /337

Here it is indicated that each of the $\rho_{j|j-1}$ depends on the entire set of n variables x_i . Actually, in each of these functions certain x_i can be identically equal to zero. When their poor correlation exists, which as a rule is almost always the case, the range of X can be divided into a sum of nonoverlapping regions, such that

$$x_i \in X_i; \quad \sum_i X_i = X. \quad (6.13)$$

with reference to the foregoing, expression (6.11) can be written as

$$\begin{aligned} E_k &= \int_{x_1 \in X} \int_{x_2 \in X_2} \dots \int_{x_n \in X_n} \rho_1(x_1, \dots, x_n) \cdot \rho_{2|1}(x_1, \dots, x_n) \dots \\ &\quad \dots \rho_{m|m-1}(x_1, \dots, x_n) dx_1 dx_2 \dots dx_n = \\ &= W_1 W_{2|1} \dots W_{m|m-1}, \end{aligned} \quad (6.13a)$$

$$\begin{aligned} W_{j|j-1} &= \int_{x_1 \in X} \int_{x_2 \in X_2} \dots \int_{x_n \in X_n} \rho_{j|j-1}(x_1, x_2, \dots, x_n) \times \\ &\quad \times dx_1, dx_2 \dots dx_n. \end{aligned}$$

$$(6.14)$$

which are conditional probabilities of the realization by the complex of successive stages in the performance of the combat mission.

Since these complexes are a totality of assemblies and technical devices, the performance of a combat mission by a flight craft is possible only when they operate error-free, which is characterized by operating reliability, that is, by one of the properties of a technical device to perform the functions assigned it.

Error-free operation is possible if the values of the equipment parameters do not depart beyond certain set bounds. The failure of a technical device is that a random event, as a rule is subject to Poisson's distribution law.

Besides the probability of failure or the probability of error-free operation (these two events constitute a complete system of events), there are also other characteristics of reliability. For example, the intensity of failures $\lambda(t)$ refers to the ratio of the number of failed articles per unit time $n(t)$ to the mean number of properly operating articles $N(t)$ in a given time interval Δt , that is, /338

$$\lambda(t) = \frac{n(t)}{N(t) \Delta t}; \quad (6.15)$$

or any i -th system element for any statistical law of distribution of failures, the probability of error-free operation P_i is associated with the function $\lambda_i(t)$ by the function

$$P_i = \exp \left[- \int_0^t \lambda_i(t) dt \right] \quad (6.16)$$

The general reliability of a system consisting of series- or parallel-connected elements is determined, as already stated, by the formulas of the superpositioning of criteria analogous to the concepts of conjunction (the system operates with the error-free performance of all its elements) and disjunction (the system operates with the error-free performance of even one element). Table 6.1 gives the mean values of the rate of failures [68, 109, 117, 179] of equipment elements and the corrective coefficients of the Hughes Company that allow for equipment operating conditions [87] (in laboratory conditions, on the ground, and on aircraft and missiles in the air). The failure rate is determined by the following function, with reference to the corrective coefficients: /339

$$\bar{\lambda}_i = K_i \lambda_i, \quad (6.17)$$

where λ_i is the failure rate (neglecting the equipment operating features), and

k_i is the Hughes Company corrective coefficient.

Fig. 6.1 presents the function of the failure rate of typical devices of electronic equipment consisting of 1,000 parts. As we can see from this figure, replacement of electronic vacuum devices with transistors led to an appreciable rise in the operating economy of electronic equipment. Electronic equipment has even higher reliability indicators after transistorized instruments are replaced with solid state devices.

The overall reliability of a system P_{sys} increases with a decrease in its complexity, in particular, in the number of its parts included in a circuit N , and their reliability P_i . In

Fig. 6.2a the operating reliability of an electronic system is given as a function of the number of series-connected parts and their reliability. In the combined calculations of the graphs it was assumed that all parts have the same operating reliability.



Fig. 6.1. Rate of failures of typical electronic devices consisting of 1,000 parts

KEY: A -- T_{av} , hrs

- B -- years
- C -- year
- D -- month
- E -- week
- F -- time, years
- G -- microelectronic elements
- H -- transistors
- I -- vacuum electronic devices

An increase in the reliability of systems is attained by providing standby status, that is, the parallel connection of redundant elements and blocks (separate standby status) or of entire systems (general standby status). The number of parallel-connected redundant branches of the same types determines the standby multiplicity k . The probability of error-free operation in general standby status is found by the formula

$$P_{tot} = 1 - \left(1 - \prod_{i=1}^n P_i\right)^k, \quad (6.18)$$

TABLE 6.1 RATES OF FAILURES λ_i AND CORRECTIVE COEFFICIENTS k_i OF EQUIPMENT ELEMENTS

/340

Name of element	$\lambda \cdot 10^3 \text{ hr}^{-1}$	Corrective coefficients, K_1			
		in laboratory cond.	in ground conditions	in air	
				air-craft	missile
Capacitors:					
paper	0.01	0.92	1.0	2.0	5.0
ceramic	0.10	0.92	1.0	2.0	5.0
porcelain	0.09	0.92	1.0	2.0	5.0
tantalum	0.60	0.85	1.0	4.0	25.0
foil	0.10	0.85	1.0	4.0	25.0
variable	0.16	0.83	1.0	5.0	42.0
Diodes					
general type	0.20	0.95	1.0	1.5	2.6
"Fenera"	0.15	0.95	1.0	1.5	2.6
heavy-duty	0.20	0.80	1.0	4.0	25.0
Transistors:					
general type	0.50	0.90	1.0	2.5	8.5
switching	0.40	0.90	1.0	2.5	8.5
Electrovacuum devices					
receiving-amplifying	1.5-3.0	0.81	1.0	6.5	80.0
oscillators	30.0	0.71-0.65	1.0	20-40	1000.0
Resistors:					
composition-carbon	0.043	0.92	1.0	2.0	5.0
film-carbon	0.03	0.92	1.0	2.0	5.0
precision	0.125	0.92	1.0	2.0	5.0
potentiometric	0.10	0.85	1.0	4.0	25.0
Induction coils:					
low-frequency	0.01	0.82	1.0	6.0	70.0
high-frequency	0.01	0.82	1.0	6.0	7.0

TABLE 6.1 RATES OF FAILURES λ_i AND CORRECTIVE COEFFICIENTS k_i OF EQUIPMENT ELEMENTS

/341

[Conclusion]

Name of element	$\lambda \cdot 10^3 \text{ hr}^{-1}$	Corrective coefficients, K_i			
		in laboratory cond.	in ground conditions	in air	
				air-craft	mis-sile
Transformers:					
incandescent	0.2	0.82	1.0	6.0	70.0
heavy-duty	0.2	0.82	1.0	6.0	70.0
pulsed	0.15	0.82	1.0	6.0	70.0
Microelectronic equip.					
computers	0.06	0.90	1.0	2.5	8.5
regular	0.1	0.90	1.0	2.5	8.5
Safety fuses	0.5	0.83	1.0	5.0	42.0
Switches:					
tumblers	0.05	0.83	1.0	5.0	42.0
pushbutton	0.06	0.83	1.0	5.0	42.0
rotary	0.17	0.83	1.0	5.0	42.0
Relays:					
general type	0.25	0.71	1.0	20.0	1000.0
miniaturized	0.25	0.74	1.0	12.0	340.0
heavy-duty	0.30	0.73	1.0	15.0	550.0
Outlet connections:					
soldering	0.004	0.76	1.0	10.0	220.0
twisting	0.02	0.71	1.0	20.0	1000.0
welding	0.9	0.65	1.0	40.0	5500.0
Electromech. parts:					
general type	0.5	0.73	1.0	15.0	550.0
counters	1.4	0.71	1.0	20.0	1000.0
motors	1.25	0.73	1.0	15.0	550.0
Mechanical parts:					
gyroscopes	10.0	0.76	1.0	10.0	220.0
selsyns	5.5	0.76	1.0	10.0	220.0
followup system motors	12.5	0.71	1.0	20.0	1000.0
geared & other transm.	8.2	0.76	1.0	10.0	220.0
	15.5	0.67		30	2800.0
10-pin plug connectors	1.2	0.71	1.0	20.0	1000.0

and for its separate standby status -- by the formula

$$P_{ind} = \prod_{i=1}^n [1 - (1 - P_i)^k]. \quad (6.19)$$

/342

Fig. 6.2 b [68] gives as an example the probability of error-free operation as a function of the number N of elements in a system, various standby methods and multiplicity k . As we can see, as a system becomes more complex, separate standby provision becomes more rational.

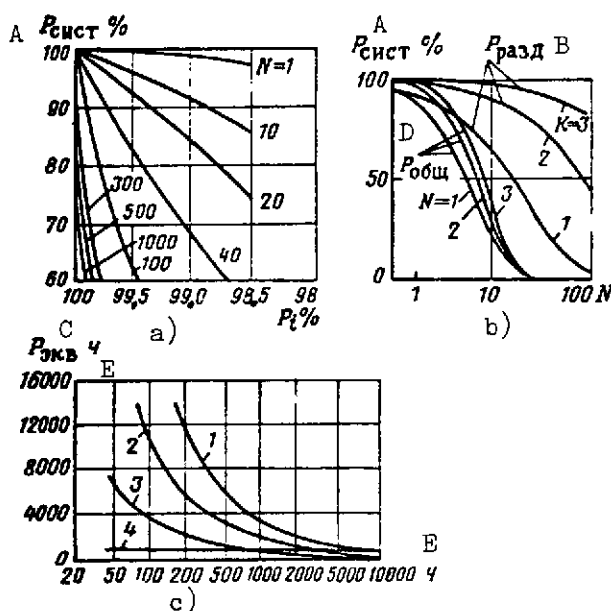


Fig. 6.2. Probability of error-free operation of electronic systems as a function of the following:

- a -- Operating reliability of parts when they are series-connected (N is the number of parts)
- b -- Number of parts (N), and standby methods (general or separate) and multiplicity (k)
- c -- Operating time of the space system and the type of standby:

1 -- system with a single operating channel and other standby channels identical to the operating channel, which must be connected manually by the astronaut after he has detected a malfunctioning of the first channel

2 -- system with two parallel-operating channels, in each of which there is a control device for determining malfunctions and subsequent switching off of the channel

3 -- system with three parallel-operating channels, in which two control devices are continually selected for control of only two channels

4 -- single-channel system, whose operating reliability is characterized by one partial failure for a standard of 1,000 hours (a reliability equivalent unit)

KEY: A -- P_{sys}

B -- P_{sep}

Fig. 6.2 (Cont.)

C -- P_{gen}
 D -- P_{equiv}
 E -- hours

The effect of the duration of system operation on operating reliability is illustrated in Fig. 6.2 c, where four space systems with different types of standby and operating reliability are compared [196]. /343

A comparison of the curves shows that as the flight becomes longer (especially after 1,000 hours) the effectiveness of the auxiliary channels for higher reliability diminishes markedly. Here the concept of reliability equivalent P_{equiv} is applied to systems with auxiliary channels in order to compare with the reliability equivalent a single-channel system with which it can perform the assigned task for a given flight duration.

From Fig. 6.2 c it is clear that a standby-operating system provides greatest reliability for any flight duration if the astronaut has enough time to discover a malfunction and to switch off a channel.

Now returning to expressions (6.11) and (6.12) and assuming that the reliability of a system participating in the realization of the j -th stage of the performance of a combat mission, and the probability of the realization of this stage with an error-free system are statistically independent, we represent each $\rho_{j/j-1}$ as the product of specifically this density of conditional probability by the probability density function of error-free operation of the system in this same stage $r_j(x_1, \dots, x_n)$. This notation assumes the statistical independence of the r_j functions at each stage and the dependence of each of them on the same set of arguments as for $\rho_{j/j-1}$. The latter does not lead to any restriction, for the set $\{x_i\}$ can always be expanded as needed given the condition that certain x_i are identical to zero for certain functions $\rho_{j/j-1}$ and r_j .

Thus, we can write instead of (6.12)

$$\rho(x_1, \dots, x_n) = \prod_{j=1}^m \rho_{j/j-1}(x_1, \dots, x_n) r_j(x_1, \dots, x_n). \quad (6.20)$$

If it is assumed that no general provision is made in the control system for duplication of systems carrying out individual stages of the performance of a mission (the standby is exercised only within limits of each of the system $j (1 \leq j \leq m)$), instead of expressions (6.13 a) and (6.14), we get /344

$$E_a = \prod_{j=1}^m W_{j/j-1} P_j, \quad (6.21)$$

where

$$P_j = \int_{x_1 \in X} \int_{x_2 \in X} \dots \int_{x_n \in X} r_j(x_1, x_2, \dots, x_n) \times \\ \times dx_1 dx_2 \dots dx_n. \quad (6.22)$$

For an assigned effectiveness E_a , the domain of integration of (6.13) is a set of admissible values of the variables $\{x_i\}$ which provide for the execution of the combat mission with assigned effectiveness. When applied to interception complexes, this domain is called the interception region with probability of performance of the combat mission not below the assigned level. To each point in this region a specific value of the complex effectiveness E_a can be brought into correspondence.

A different meaning can be invested in the indicator of system effectiveness E_a , depending on the target mission it performs: the probability of interception or, when applied to a group of interception facilities, the probability of beating off an enemy raid. For attack facilities this can be the probability of inflicting assigned damage in a bombing or missile attack against ground targets, and so on.

Let us consider the method of determining the effectiveness criterion E_a and its constituent elements, which are generally identical for all complexes, with the example of the interception of air targets.

When targets are intercepted, from expression (6.21) we get

$$E_a = \prod_{j=1}^m W_{j/j-1} P_j = W_{gu} W_{cap} W_{hom} W_{str} \times \\ \times P_{gu} P_{cap} P_{hom} P_{str} \quad (6.23)$$

where W_{gu} is the probability of realizing long-range guidance of the flight craft;
 W_{cap} is the probability of target interception by the on-board equipment of the aircraft or missile;
 W_{hom} is the probability that by homing the flight craft enters the firing zone of cannon-gun armament (CGA) or the missile launch zone; /345
 W_{str} is the probability of the target being struck by the CGA or a missile;
 P_{gu} is the probability of the reliable operation of the interceptor's long-range guidance system;
 P_{cap} is the probability of the operating reliability of the onboard capture equipment;
 P_{hom} is the probability of the operating reliability of the homing system; and
 P_{str} is the probability of the operating reliability of the missile, fuse, or CGA installation.

If according to the mission conditions a more detailed analysis of systems is required, these stages can be divided into smaller ones. For example, processes of target detection, capture, and tracking by ground radar can be singled out from the process of flight craft guidance; when using a remote fuse, from W_{str} we can separate out W_{miss} -- the probability of the miss distance, i.e., the probability that the fuse will be activated at a distance from the target not exceeding the maximum distance dictated by the mean force of fragments.

The remaining cofactors of the formula written can be similarly represented.

When considering flight craft of different types, individual cofactors of this product can also be assumed equal to unity if the corresponding stage in the execution of the target mission is not realized in the given flight complex.

The probability of guidance W_{gu} is determined by the probability of the interceptor entering some acceptable region of phase space associated with the target in which its detection, lock-on, and tracking by the homing head or onboard radar are carried out. This determination is valid regardless of whether we are discussing a fighter airplane armed with cannon-gun armament (CGA), a mother aircraft equipped with air-to-air missiles, or an anti-aircraft guided missile. If homing is the last stage, the size and shape of this region, as shown in Chapter Four depends on the type and characteristics of the interceptor detection system, target characteristics (its contrast with the background and jamming used), and of the mutual position and relative motion of /346

interceptor and target (cf. Fig. 4.15). Thus, the probability of interceptor guidance is the probability of its entering the sector AOB and is determined by the accuracy of implementation of the guidance law by the control system. In view of the complexity of the guidance process, W_{gu} , with the exception of several simplest cases, can be determined only by mathematical modeling with analog or digital computers.

This modeling mathematically describes the motion of the interceptor and the target, operation of the guidance and control system of the interceptor, and the operating conditions of the onboard detection equipment.

If the overall guidance errors (the errors of entering the sector AOB) are subject to the normal law of distribution, W_{gu} can be found from the relationship

$$W_{gu} = \frac{1}{2} \left[\hat{\Phi} \left(\frac{h_1 - h_{gu}}{\sigma_h \sqrt{2}} \right) - \hat{\Phi} \left(\frac{h_2 - h_{gu}}{\sigma_h \sqrt{2}} \right) \right], \quad (6.24)$$

where h_{gu} is the mathematical expectation of guidance error;
 σ_h is the mean-square guidance error; and
 $\hat{\Phi}$ is the reduced Laplace function (cf. [21] or [103]), whose values are determined from tables.

The probability of capture W_{cap} characterizes the random event that the onboard homing equipment not only detects the target, but also "locks" onto it, that is, maintains it within its field of view. Usually this does not occur at once after detection, therefore the "lock-on" rate is $R_{cap} < R_{det}$. W_{cap} depends entirely on the external characteristics of the target and the characteristics of the interceptor's onboard equipment; the latter, however, do not remain constant for different cases of relative motion.

The probability of homing W_{hom} characterizes the incursion of the interceptor or the missile into some zone also associated with the target in which the use of the CGA or the activation of the missile's aerial-burst fuse becomes possible. W_{hom} depends on the maneuverability of the target and the interceptor or the missile, and also on the homing range: the same long-range guidance error of a more maneuverable interceptor is capable

/347

of being corrected in a shorter time, that is, for a shorter initial separation from the target.

The probability of a strike W_{str} is determined in different ways, depending on whether the strike is made against a target from CGA, missiles with proximity fuses, or missiles with aerial-burst fuses [22].

For firing from CGA and for missiles with proximity fuses, we introduce the concepts of the strike and vulnerability regions.

Let us assume that the target is some region lying in the plane perpendicular to the firing trajectory. This region is replaced by some circle whose center coincides with the geometrical center of the target, called the strike region. Let us further assume that the target will be struck if one or several missiles (fragments) enters the strike region.

The graph shown in Fig. 6.3 a [158] gives us some idea of the number of incursions of burst shells ensuring the striking of aircrafts of different types.

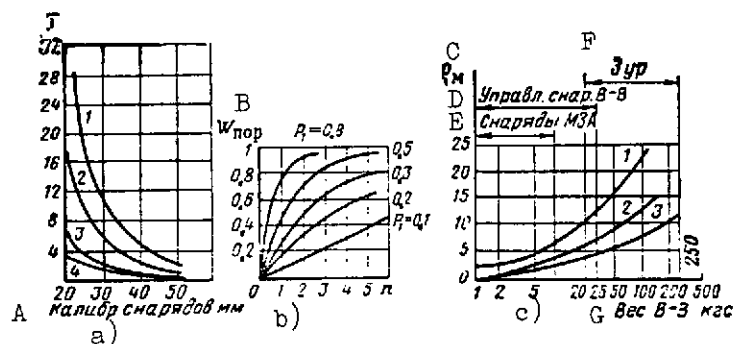


Fig. 6.3. Functions characterizing air target strikes:

a) number of incursions of n shells required to hit airplanes; 1 -- bomber weighing > 40 tons; 2 -- bomber weighing about 20 tons; 3 -- fighter weighing > 2 tons; 4 -- fighter weighing about 8 tons

b) dependence of W_{str} on the number of shells fired

c) distance from epicenter of burst leading to an aircraft hit; 1 -- light fighter weighing about 8 tons; 2 -- fighter > 8 tons; 3 -- bomber > 40 tons

KEY: A -- Shell size, mm

B -- W_{str}

C -- R_{miss}

D -- Air-to-air guided missiles

E -- Small-caliber antiaircraft artillery shells

F -- Antiaircraft guided missiles

G -- Weight of explosive, kg

The vulnerability region refers to the planar region consisting of the projections of all target elements having different vulnerabilities onto a plane perpendicular to the relative shell flight velocity. This means that a target strike begins for different numbers of shells entering each of these elements.

Using the concept of the strike region, let us denote by p_1 the probability of the target being struck by a single shell, that is, the probability of the shell entering the strike zone. Then the strike possibility W_{str} for n fired shells and the absence of the accumulation of damage is

$$W_{str} = 1 - (1 - p_1)^n. \quad (6.25)$$

Fig. 6.3 b shows the dependence W_{str} on the number n and p_1 .

If the target elements have different vulnerabilities ω_i (that is, a different number of shells putting the target out of action by entering each element is needed), W_{str} is defined by the formula

$$W_{str} = 1 - \sum_{i=1}^k \left(1 - \frac{p_{1i}}{\omega_i}\right)^{n_i}. \quad (6.26)$$

Aerial-burst fuses of shells use information from various sensors (radars, Doppler units, infrared or optical coordinators, and so on), with which the relative position of the shell and the target is determined. In all cases the radiation patterns of the sensors must be coordinated with the scattering pattern of the warhead fragments, whose statistical law is close to Poisson's law [22]. Therefore the probability of even one fragment entering the i -th element of an aircraft is

$$p_{1i} = 1 - e^{-\lambda S_i}, \quad (6.27)$$

where S_i is the projection of the area of the i -th element onto the plane perpendicular to the direction of the stream of fragments,

$$k = \frac{N}{S_i} \quad (\text{here } N \text{ is the total number of fragments}).$$

Assuming that all fragments have the same energy and are distributed statistically independently in the scattering region, we can calculate W_{str} by formula (6.26), using expression (6.27), and multiplying the result by W_{str} .

The graphs in Fig. 6.3 c [158] show at which distances ρ from the burst epicenter different air targets can be struck by shells of different force.

Let us consider, finally, a number of numerical examples illustrating the dependence of the effectiveness on the main complex parameters. For greater clarity of the solution, several simplifying assumptions were made in setting up the problem.

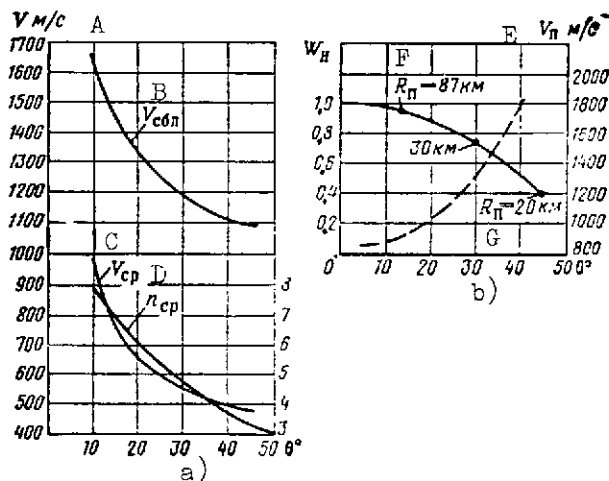


Fig. 6.4 Function characterizing the conditions of missile guidance onto a target

KEY: A -- m/sec
 B -- V_{ap}
 C -- V_{av}
 D -- n_{av}
 E -- $V_{\text{in}}, m/\text{sec}$
 F -- $R_{\text{in}} = 87 \text{ km}$
 G -- $R_{\text{in}} = 20 \text{ km}$

Example 6.1. Determine the capture effectiveness for an air target flying at the altitude

$H = 15 \text{ km}$ and a velocity of $M 2.5$; for zero parallax, and with an antiaircraft missile with a combined guidance system (command guidance from the ground is executed over the initial flight phase of the missile, followed by a conversion to homing). We will assume that the information on the target and interceptor positions arrives at the missile's command guidance system at the rate $\tau = 5 \text{ seconds}$. The accuracy of determining the coordinates of the target and the interceptor will be taken as $\sigma_{\text{co}} = 500 \text{ km}$.

Let us represent by the graph shown in Fig. 6.4 a the law of variation of the mean interceptor velocity V_{av} as a function of the angle of inclination of the interception trajectory to the earth's surface θ . In the same figure is shown the variation of the mean g-load n_{av} and the mean approach velocity of interceptor and target V_{ap} as a function of angle θ .

The capture range of the homing head $R_{cap} = 30$ km, and the accuracy of the determination of the angular velocity of the sighting line $\sigma_v = 0.1$ deg/sec. In addition, we will assume that the time constant of the homing loop $T = 0.1$ and the allowable miss value $h_{miss} = 5$ m.

/350

Let us determine the probability of long-range guidance, taking as h -- the allowable missile miss for the capture range of the homing head. Then by formula (6.24) we will get (Fig. 6.4 b):

$$W_{gu} = \Phi\left(\frac{h}{\sigma_h}\right), \quad (6.28)$$

where σ_h is the mean-square error of long-range guidance for $r = R_{cap}$.

In determining σ_h we will assume that the missile generates long-range guidance commands without any delay. Moreover, the time the missile travels along the line to the lead point is equal to the time the target flies from the instant of missile launch to the point of impact. In this case the flight leg of the missile to the target is

$$h = \frac{r^2 \Omega}{V_{ap}}, \quad (6.29)$$

where Ω is the angular velocity of the sighting line;
 V_{av} is the approach velocity; and
 R is the range to target.

The angular velocity of the sighting line can be represented without difficulty in the form (Fig. 6.5)

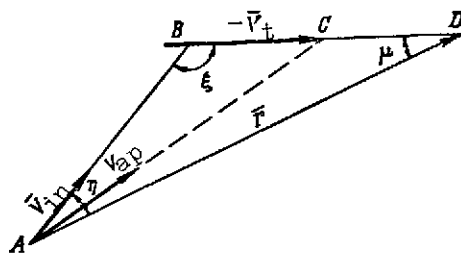
$$\Omega = \frac{V_{ta} \sin \eta - V_t \sin \mu}{r}. \quad (6.30)$$

The error of measurement of the angular velocity of the sighting line will be

$$\delta\Omega = \frac{\delta V_{in} \sin \eta + \delta V_{in} \cos \eta - \delta V_t \sin \mu - \delta V_t \cos \mu}{r} \quad (6.31)$$

Then the mean-square deviation of the angular velocity will be determined as

$$\sigma_\Omega^2 = \frac{1}{r^2} (\sigma_{V_{in}}^2 \sin^2 \eta + \sigma_{V_{in}}^2 \cos^2 \eta + \quad (6.32) \quad \underline{351}$$



$$+ 2R_{V_{in}} V_{in} \sin \eta \cos \eta + \sigma_{V_t}^2 \sin^2 \mu + \sigma_{V_t}^2 \cos^2 \mu + 2R_{V_t} V_t \sin \mu \cos \mu).$$

Fig. 6.5. Relative position of vectors in missile homing

Hence it is clear that the mean-square error of the leg can be written as

$$\sigma_h = \frac{r}{V_{ap}} \sqrt{\sigma_{V_{in}}^2 \sin^2 \eta + \sigma_{V_{in}}^2 \cos^2 \eta + 2R_{V_{in}} V_{in} \sin \eta \cos \eta + \sigma_{V_t}^2 \sin^2 \mu + \sigma_{V_t}^2 \cos^2 \mu + 2R_{V_t} V_t \sin \mu \cos \mu} \rightarrow \quad (6.33)$$

Let us express the sighting error η and the angle determining the attack rate is μ by ξ , using the expression

$$\cot \mu = \frac{\frac{V_t}{V_{in}} - \cos \xi}{\sin \xi}; \cot \eta = \frac{\frac{V_{in}}{V_t} - \cos \xi}{\sin \xi} \quad (6.34)$$

The mean-square error in the determination of the velocities, heading angles of the target and interceptor flight, and also their interrelationship can be expressed by the following functions:

$$\left. \begin{aligned} \sigma_{V_{in}} &= \frac{\sigma_c \sqrt{2}}{v}; & \sigma_{\gamma} &= \frac{\sigma_s \sqrt{2}}{V_{in}}; \\ R_{V_{in}} &= \frac{2\sigma_c^2}{V_{in}^2}; & \sigma_{V_t} &= \frac{\sigma_c \sqrt{2}}{v}; \\ \sigma_{\mu} &= \frac{\sigma_c \sqrt{2}}{V_t}; & R_{V_t} &= \frac{2\sigma_c^2}{V_t^2}. \end{aligned} \right\} \quad (6.35)$$

Usually, the largest number of measurements of the parameters of target and interceptor motion is "remembered" in guided systems in order to reduce the dynamic error associated with target maneuvering. Therefore, let us limit ourselves to the case when the estimate of these quantities can be obtained on the basis of two successive measurements. Bearing this in mind and substituting expressions (6.34) and (6.35) in formula (6.33), we get

$$\sigma_h = \frac{\sigma_c \sqrt{2}}{V_{ap}} \times \sqrt{2(1+a^2)(1-\cos \xi \sin \xi) - 4a(\cos \xi - \sin \xi)}, \quad (6.36)$$

where $a = V_t/V_{in}$.

To calculate the capture probability by formula (6.28), we must determine the allowable value of the missile fly-by past the target after the target has been captured by the homing head. In this case we can use the well-known expression for the equi-accelerated motion of a missile with mean g-load n_{av} :

$$h = \frac{n_{av}}{2} \left(\frac{R_{cap}}{V_{ap}} \right)^2. \quad (6.37)$$

In the derivation of formula (6.37) it was also assumed that acceleration acts perpendicularly to the sighting line. Using the above given data and the expressions (6.36) and (6.37), W_{gu} (by formula (6.28)) was calculated as a function of angle θ . The corresponding construction is shown in Fig. 6.4 b with a solid line.

On inspecting this figure, it is clear that for the interception scheme we have chosen the probability of guidance decreases as the line of interception approaches the launch point.

The probability of capture in this scheme can be enhanced by introducing an extrapolator serving to smooth over the measurements. We will assume that in our case $W_{gu} = 0.9$.

To estimate the probability of guidance, let us use formula (6.22), then we get

$$W_{hom} = \Phi \left(\frac{h_{miss}}{\sqrt{2}\sigma_{h_{miss}}} \right). \quad (6.38)$$

where h_{miss} is the allowable missile miss affording a strike by the warhead on the target; and $\sigma_{h_{miss}}$ is the mean-square value of the miss caused by blinding of the homing head.

The quantity h_{miss} depends on the characteristics of the warhead and determines the allowable missile fly-by past the target for which a strike can be made on the target with given probability.

The value of $\sigma_{h_{miss}}$ is calculated by the formula

$$\sigma_{h_{miss}} = \frac{R_{b,r}^2}{V_{rel}} \sigma_{\Omega}, \quad (6.39)$$

where $R_{b,r}$ is the blinding range of the homing head; and

σ_{Ω} is the mean-square value of the determination of the angular velocity by the radar homing head. In estimational calculations, we can assume that

$$R_{b,r} = 37V_{rel}. \quad (6.40)$$

Substituting expression (6.40) into formula (6.39), we get

$$\sigma_{h_{miss}} = 972V_{rel} \sigma_{\Omega}. \quad (6.41)$$

For the parameters we have adopted, we get

$$a_{\text{miss}} = 9 \cdot 0.12 \cdot 400 \cdot 0.1 = 3.6 \text{ m},$$

then, by formula (6.38) we obtain

353

$$W_{\text{hom}} = 0.85.$$

The maximum miss value is

$$h_{\text{max}} = 3 \cdot 3.6 + 5 = 15.8 \text{ m}.$$

From Fig. 6.3 it is clear that for this value $h_{\text{max}} = \rho$ -- the probability of a fighter strike, $W_{\text{str}} \approx 1.0$ will hold for the weight of the warhead explosive $G_{\text{exp}} = 50$ kg. If we assume the missile $G_{\text{exp}} = 60$ kg, then $W \approx 1.0$ even more so. We will additionally assume that $W_{\text{cap}} = 0.95$. Then to determine the effectiveness of the combat use of the interception complex without allowing for the operating reliability of the equipment, we get (cf. formula (6.23))

$$E_a = W_{\text{gu}} W_{\text{cap}} W_{\text{hom}} W_{\text{str}} = 0.9 \cdot 0.95 \cdot 0.85 \cdot 1.0 = 0.73.$$

Let us estimate the effectiveness of a given interception complex with reference to the operating reliability of the equipment. To do this, let us determine the overall failure rate of the homing equipment and determine P_{hom} by formula (6.16).

We will arbitrarily assume that the homing equipment of the hypothetical missile consists of several thousand parts connected in series. The number and types of the parts are given in Table 6.2. Also in this table are the values of the corrective coefficients that allow for the operating conditions of the missile homing equipment (from the data in Table 6.1).

In ground conditions the mean elapsed operating time to failure is $T_{\text{av}} = 1897.9$ hours, but in flight conditions (with allowance for the corrective coefficients), T_{av} drops off to 11.98 hours, which permits a more exact prediction of the reliability of the missile's onboard equipment.

For the case we are examining, $\lambda_{\text{tot}} = 83,468.32 \cdot 10^{-6} \text{ hr}^{-1}$, that is, $P_{\text{hom}} = 0.96$. By a similar method we can determine the operating reliability of the equipment of the ground guidance facilities P_{gu} , the equipment providing for target lock-on T_{cap} , and the equipment of the radio fuse and the detonator mechanism P_{str} .

We will assume that $P_{\text{gu}} = 0.95$, $P_{\text{cap}} = 0.98$, and $P_{\text{str}} = 1.0$, and then by formula (6.23) we calculate the effectiveness of the interception complex with reference to the operating reliability of the equipment:

$$E_a = 0.9 \cdot 0.95 \cdot 0.85 \cdot 1.0 \cdot 0.95 \cdot 0.98 \cdot 0.96 \cdot 1.0 = 0.65,$$

that is, 11 percent lower than the value earlier obtained.

. In more complicated interception complexes, the amount of equipment is considerably greater and the loss in the effectiveness of the combat application due to the operating reliability becomes even larger.

Let us evaluate the effect of several additional factors serving to lower the probability of the combat effectiveness of the interception complex.

Example 6.2. Let us leave the conditions of the previous example unchanged, assuming here that the enemy is using false targets to lower the effectiveness of lock-on of the true target by the homing head. With five false targets lying within the field of view of the head, we have

$$W_{\text{cap}} = \frac{1}{5} 0.95 = 0.19.$$

Due to this, the overall effectiveness of the combat use of the interception complex is considerably reduced and becomes equal to

$$E_a = 0.9 \cdot 0.19 \cdot 0.85 \cdot 1.0 \cdot 0.95 \cdot 0.98 \cdot 0.96 \cdot 1.0 \approx 0.13.$$

To raise the effectiveness of the complex, false-target selecting blocks must be installed in the radar homing head, complicating the head design and adding to its weight.

Now let us examine the effect of active enemy countermeasures on the effectiveness of the interception complex.

TABLE 6.2 FAILURE RATES λ_i AND CORRECTIVE COEFFICIENTS K_i FOR THE HOMING OF A HYPOTHETICAL MISSILE /354

Type of parts	Number	$\lambda_i \cdot 10^6$, on earth		K_i	$\lambda_i \cdot 10^6$ in air for all parts
		for part	for all parts		
Resistors:					
composition-carbon	1420	0,043	61,1	5,0	305,5
film-carbon	120	0,03	3,6	5,0	18
variable	80	0,06	4,8	25,0	120
Capacitors:					
paper	430	0,01	4,3	5,0	20,5
tantalum	140	0,09	12,6	25,0	315,0
variable	25	0,16	4,0	42,0	168,0
potentiometric	65	0,10	6,5	25,0	162,5
Electrovacuum receiving-amp. devices	15	2,0	30,0	80,0	2400,0
Transistors:					
general type	100	0,5	50,0	8,5	425,0
switching	16	0,4	64,0	8,5	54,4
General-type diodes	850	0,2	170	2,6	422
Transformers:					
incandescent	6	0,2	1,2	70	84
heavy-duty	12	0,9	10,8	70	756
pulsed	25	0,15	3,75	70	262,5
High-frequency chokes	12	0,1	1,2	70	84,0
Relays:					
general type	2	0,25	6	1000	500,0
miniaturized	10	0,25	2,5	340	850,0
Switches:					
tumblers	10	0,05	0,5	42,0	21
pushbutton	6	0,17	1,02	42,0	42,84
10-pin connecting plugs	12	1,2	14,4	1000	14400

TABLE 6.2 FAILURE RATES λ_i AND CORRECTIVE COEFFICIENTS K_i FOR /35/
THE HOMING OF A HYPOTHETICAL MISSILE
[Conclusion]

Type of part	Number	$\lambda_i \cdot 10^6$, on earth		K_i	$\lambda_i \cdot 10^6$ in air for all parts
		for part	for all parts		
Electrotechnical parts:					
general type	10	0.5	5.0	550	2750.0
motor	4	1.25	5.0	550	2750.0
Mechanical parts:					
gyroscopes	3	10	30	220	6600.0
selsyns	4	5.5	22	220	4640.0
Followup system motors	2	12.5	25	1000	25000.0
gear transmissions	4	12.5	50	400	20000.0
Outlet connections and soldering	420	0.004	1.68	220	370.0
total	3811	$\lambda_i = 49,077 \times 10^{-6}$	$\lambda_i = 526,89 \times 10^{-6}$	$\lambda_i = 83468,32 \cdot 10^{-6}$	
Mean operating time elapsed to failure					
		$T = \frac{1}{\lambda_i} = 1897,6 \text{ hr}$ $T = \frac{1}{\lambda_i} = 11,98 \text{ hr}$			

Example 6.3. Let us estimate that the effectiveness of air target capture (example 6.1) when there are active enemy countermeasures. The antiaircraft guided missile is detected by the radars of enemy aircraft and can be hit by their onboard armament.

Let us assume that the probability of destroying the anti-aircraft missile with the aircraft's armament is $P_{\text{des}} = 0.2$. Then the effectiveness of the target interception complex can be determined by the formula

$$E_a = E_{\text{gu}} W_{\text{cap}} W_{\text{hom}} W_{\text{str}} (1 - P_{\text{des}}) P_{\text{gu}} P_{\text{cap}} P_{\text{hom}} P_{\text{str}}, \quad (6.42)$$

which after insertion of the corresponding numerical values becomes

/330

$$E = 0,9 \cdot 0,95 \cdot 0,85 \cdot 1,0 (1 - 0,2) \cdot 0,95 \cdot 0,98 \cdot 0,95 \cdot 1,0 = 0,52.$$

Thus, in this case as well the effectiveness of the combat use of a complex is reduced. Therefore when estimating the effectiveness of aircraft and missile interception and strike complexes, we must allow for the effect of enemy countermeasures (passive and active). The effects of different kinds of jamming and active countermeasures is considered in greater detail in Sections 6.3-6.5.

6.2. Costs of Complexes, and the Period and Stages of Their Designing

In evaluating interception or attack complexes it is not enough to know the values of their combat effectiveness under different conditions. Their cost is a very important indicator in the evaluation of complexes. This indicator is particularly important when examining groups of complexes (cf. Section 6.5) whose costs are exceptionally high. Therefore, of late economic characteristics, including the costs of prevented damage, have begun to be considered as an indicator of a complex's effectiveness; this quantity characterizes the effectiveness of anti-aircraft defense facilities beating off attacks by strike or reconnaissance enemy flight craft, where the results of their action can be expressed in the form of the material damage inflicted to the defending side. The effectiveness of attack facilities can be similarly evaluated, by using here the cost of the damage inflicted (cf. for example [67]).

If in the general case, the cost of a group of complexes C_{com} can be represented as the function

$$C_{\text{com}} = F(x_1, x_2, \dots, x_n),$$

where x_1, x_2, \dots, x_n refer to parameters characterizing the appearance of the flight complex and the conditions of its use in the group. Actually, C_{com} is a certain sum

$$C_{\text{com}} = N \left(\sum_{i=1}^n C_i + C_{\text{l.p.}} \right) + C_{\text{sup}}. \quad (6.43)$$

The terms in this sum are as follows:

C_i are the costs of individual elements of the complex;
 N is the number of complexes in the group;
 $C_{1.p}$ is the cost of launch positions and airfields; and
 C_{sup} is the cost of support facilities.

/357

Costs of individual complex elements C_i can be subdivided into groups; they are functions of independent parameters, which may be the coordinates of the launch positions or airfields, coordinates of interception regions when interception complexes are under consideration, and so on.

The cost of a group of facilities includes outlays for capital construction and operation of the airfields, launch positions, centers of radar and radio facilities, communications, and access routes, and also outlays for building and operating other ground structures and facilities ensuring the functioning of flight craft.

Additionally, the cost function C_{com} includes outlays for the development and building of flight craft and their equipment, training of personnel, and so on.

In the synthesis of a system, one must be able to evaluate these costs even at the stage of preliminary project-planning when the facilities themselves have not yet been built. Functions agreeing closely enough with actual outlays are available now for this kind of estimate.

These functions are based on known functional relationships between certain system parameters and the costs of elements in a complex. Actual experience in calculations conducted by foreign specialists shows that satisfactory enough results are obtained if the dependence of the cost of missiles and aircraft on their weight is approximated with a linear function. Fig. 6.6 shows a function of this kind (C_{af} is the cost of the airframe; C_{en} is the engine cost; C_{eq} is the equipment cost; and C_{arm} is the armament cost), constructed on the basis of the treatment of weights and costs of various prototypes of American military equipment [130, 131, 136-138, 151, 152, 155, 167]. Since in synthesis the investigation is usually conducted within the limits of a relatively narrow range of initial parameters, this approximation is wholly justified, as can be seen from Fig. 6.6.

In approximate terms, the linear dependence of the cost of launch positions on the weight of flight craft launched from them can also be extended to launch positions and airfields. This is so because larger structures are needed with heavier flight craft in order to provide for their safe and reliable functioning. /358

When this kind of estimate is used, each time numerical characteristics of prorated costs must be refined (the cost per kg of weight), since each newly built system can require during construction the development of new technological processes, the use of new material, and so on. As shown by experience, in building complexes that do not greatly surpass similar existing complexes as to their characteristics, the prorated [specific] costs vary only slightly. Therefore prorated cost characteristics needed for the preliminary project-planning can be obtained by a statistical treatment of earlier built systems and prototypes. We must also bear in mind that the costs of flight craft and other elements in a complex depend heavily on mass production status. Fig. 6.7 shows the dependence of the relative costs of a flight craft on the number of units built in a series (the graph is constructed on the basis of a treatment of foreign data).

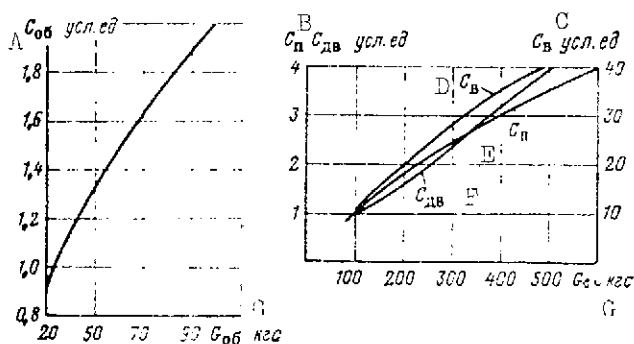


Fig. 6.6 Costs of various elements in U.S. military complexes as a function of their weight.

KEY: A -- C_{eq} , relative units
 B -- C_{af} , C_{en} relative units
 C -- C_{arm} , relative units
 D -- C_{arm}
 E -- C_{af}
 F -- C_{en}
 G -- G_{eq} , kg

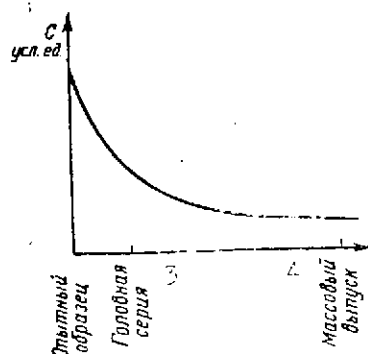


Fig. 6.7 Costs of flight craft as a function of its mass production status.

KEY: 1 -- C , relative units
 2 -- Experimental model
 3 -- Leading series
 4 -- Mass production

A formal expression of the costs of a complex group is as follows:

/359

$$C_{\text{com}} = N \left\{ \left(G_{\text{fu.a}}^K + \sum_{i=1}^m G_{\text{en.c.eq}_1} \right) (1 + \bar{G}_s) \times \right. \\ \times \left[\sum_{i=1}^{\xi} \bar{G}_{1.v_i} C_i + C_{1.p} \left(1 + \sum_{i=1}^{\xi} \bar{G}_{1.v_i} \right) \right] + G_{\text{fu.a}} C_{\text{fu.a}}^K + \\ \left. + \sum_{i=1}^m G_{\text{en.c.eq}_1} C_i + (G_{\text{fu.a}}^K + \sum_{i=1}^m G_{\text{en.c.eq}_1}) \bar{G}_s C_s \right\} + C_o, \quad (6.49)$$

where $G_{\text{fu.arm}}$ is the weight of fuel and armaments of the flight craft;
 $G_{\text{en.c.eq}_1}$ is the weight of engine installations, crew, and equipment;
 \bar{G}_s is the relative weight of the flight craft structure;
 $\bar{G}_{1.v_i}$ is the relative weight of the launch stages per kg of flight craft;
 C_i is the cost of 1 kg of launch stage and elements of flight craft equipment;
 $C_{1.p}$ is the cost of the launch position per kg of flight craft takeoff weight;
 K is the number of power plants on the flight craft;
 $C_{\text{fu.a}}$ is the cost of 1 kg of fuel and armament of the flight craft;
 C_s is the cost of 1 kg of flight craft structure;
 N is the number of complexes in the group; and
 m is the number of elements by which the overall weights of engines and electronic equipment are to be divided.

For a better representation of the factors affecting the costs of complexes, we present in Figs. 6.8 and 6.9³ individual components affecting the costs of a launch site and a missile launch vehicle based on (U.S. data).

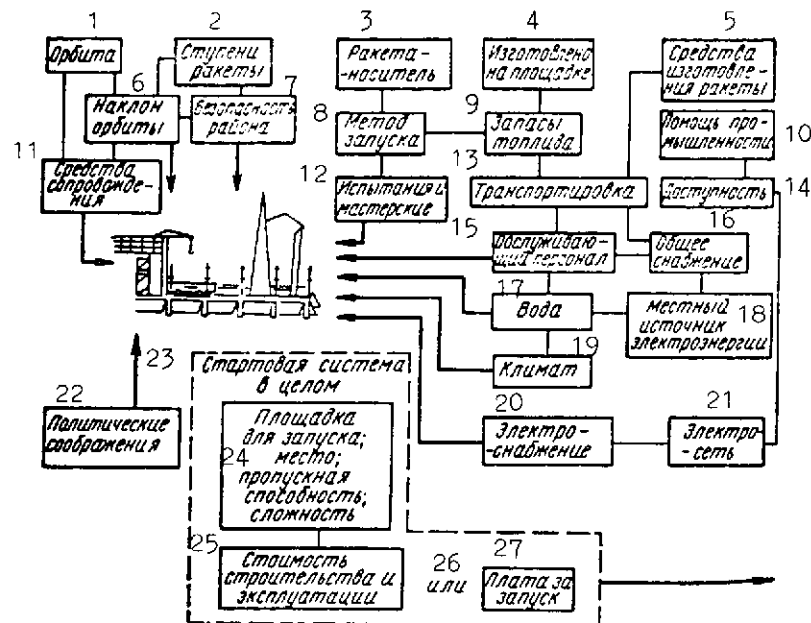


Fig. 6.8. Factors affecting the cost of a structure and the makeup of a launch position for artificial earth satellites (for the example of the Blue Steel missile launch vehicle; Woomera Proving Grounds)

- KEY:
- | | |
|---------------------------------------|--|
| 1 -- Orbit | 15 -- Service personnel |
| 2 -- Missile stages | 16 -- General supply |
| 3 -- Missile launch vehicles | 17 -- Water |
| 4 -- Manufactured on the ground | 18 -- Local power source |
| 5 -- Missile manufacturing facilities | 19 -- Climate |
| 6 -- Orbit inclination | 20 -- Electric power |
| 7 -- Region safety | 21 -- Electric power network |
| 8 -- Launch method | 22 -- Political considerations |
| 9 -- Fuel reserves | 23 -- Launch system as a whole |
| 10 -- Industry assistance | 24 -- Ground for launch; site; handling capacity; complexity |
| 11 -- Tracking facilities | 25 -- Cost of construction and operation |
| 12 -- Tests and workshops | 26 -- Or |
| 13 -- Transportation | 27 -- Payments for launch |
| 14 -- Access | |

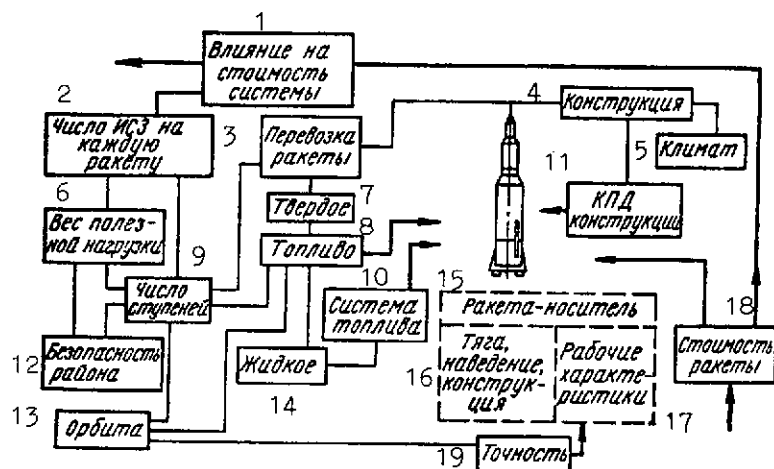


Fig. 6.9. Effect of missile type on total missile costs.

- KEY:
- 1 -- Effect on system costs
 - 2 -- Number of artificial earth satellites per launch vehicle
 - 3 -- Transportation of missile
 - 4 -- Design
 - 5 -- Climate
 - 6 -- Payload weight
 - 7 -- Solids
 - 8 -- Fuel
 - 9 -- Number of stages
 - 10 -- Fuel system
 - 11 -- Efficiency of design
 - 12 -- Region safety
 - 13 -- Orbit
 - 14 -- Liquid
 - 15 -- Missile launch vehicle
 - 16 -- Thrust, guidance, structure
 - 17 -- Working characteristics
 - 18 -- Missile costs
 - 19 -- Accuracy

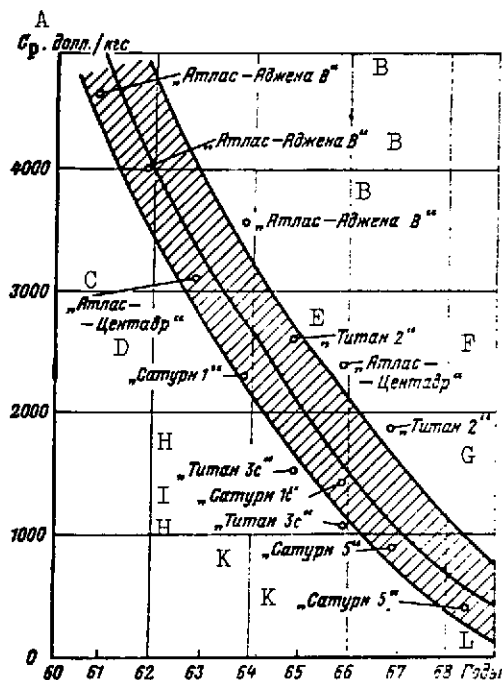


Fig. 6.10. Prorated costs of missile launch vehicles as a function of year of their construction

KEY: A -- C_m , dollars/kg

- ```

B -- Atlas-Agena B
C -- Atlas-Centaur D
D -- Saturn 1
E -- Titan 2
F -- Atlas-Centaur
G -- Titan 2
H -- Titan 3 C
I -- Saturn 1 C
J -- Titan 3 C
K -- Saturn 5
L -- Years

```

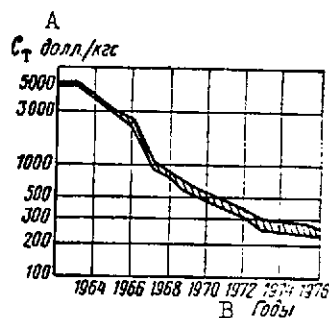


Fig. 6.11. Expected changes in the costs of orbiting 1 kg of an orbital payload.

KEY: A --  $C_{fu}$ , dollars/kg

B -- Years

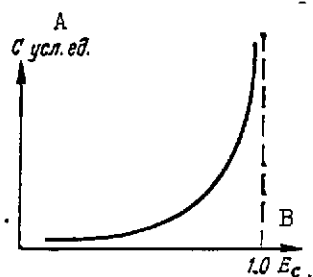


Fig. 6.12. Costs of a group of complexes as a function of its effectiveness  $E_a$  (each of the complexes has an assigned probability of executing the combat mission,  $W_{int}$  [int = interception])

KEY: A -- C, relative units

B - E<sub>2</sub>

Fig. 6.10 shows the prorated costs of U.S. missile launch vehicles as a function of the year they were developed. The value of  $C_m$  can be predicted with this graph. A graph of expected changes in the cost of orbiting 1 kg of orbital payload (Fig. 6.11, based on the data in [181]) is presented for this same purpose.

A set of graphs, shown in Fig. 6.6, is necessary for calculations based on formula (6.44). As an example, in Table 6.3 are given the costs of the missile launch vehicles, and in Table 6.4, the costs of a space communications system.

A comparative analysis of various systems using economic estimates can afford very important results. For example, in Fig. 6.12 is given the dependence of the costs of a group of complexes on the effectiveness of the grouping  $E_a$ ; each of the complexes here ensures an assigned probability of performing a military mission (interception --  $W_{int}$ ).

TABLE 6.3. COSTS AND RELIABILITY OF MISSILE LAUNCH VEHICLES

| Launch vehicle | Orbit                  | Pay-load, kg | Cost, millions of dollars | Launch reliability*    |
|----------------|------------------------|--------------|---------------------------|------------------------|
| Atlas-Centaur  | Synchronous            | 270-         | 9.0, 1965-66              | 0.6, 1966              |
|                | equatorial             | 450          | 6.0, 1975                 | 0.8, 1970              |
| Titan II       | Synchronous equatorial | 295          | 5.0                       | 0.7, 1969<br>0.9, 1975 |

---

\* Launch reliability refers to both launch at intermediate as well as the final orbit of the assigned number of AES [artificial earth satellites].

From the figure it is clear that efforts to increase the effectiveness of each complex can lead to very high cost outlays in building the group.

In turn, this indicates that in some cases efforts toward an appreciable increase in reliability, strike probability, guidance probability, and other statistical characteristics are not always economically advantageous. This example shows the effect of precisely this statistical parameter on the costs of the group.

TABLE 6.4. COSTS OF A PERMANENT SYSTEM OF SPACE COMMUNICATION  
[104]

/363

| Name of operation<br>or process                | Use of equa-<br>torial orbits |                                  | Use of polar<br>orbits |                                  |
|------------------------------------------------|-------------------------------|----------------------------------|------------------------|----------------------------------|
|                                                | num-<br>ber                   | cost,<br>million<br>pd.<br>ster. | num-<br>ber            | cost,<br>million<br>pd.<br>ster. |
| Developing communi-<br>cation satellites       | 1                             | 6,5                              | 1                      | 6,5                              |
| Developing launch<br>facility equipment        | 9                             | 13,5                             | 9                      | 13,5                             |
| Building launch<br>facilities*                 | 1                             | 20,0                             | —                      | —                                |
| Tracking stations                              | 3                             | 4,5                              | 3                      | 4,5                              |
| Relay stations                                 | 16                            | 24,0                             | 16                     | 24,0                             |
| Making communica-<br>tions satellites          | 21                            | 4,5                              | 40                     | 8,0                              |
| Cost of launch veh-<br>icle, incl. launch cost | 21                            | 31,5                             | 40                     | 60,0                             |

\* In the launch of satellites in polar orbit, it is assumed possible to use already existing proving grounds, for example, the Woomera Proving Grounds.

No less typical is an example showing the dependence of the costs of covering the defense belt on the distance between the lines of interception and warning. As follows from Section 6.5, the belt covered by a single aircraft interception complex is the wider, the farther the interception line extends deep into the territory defended. The maximum width of the covered belt is bounded by the tactical radius of interception. The relation between the costs of a group built on the basis of aircraft facilities and the distance between the lines of interception and warning is similar to that shown in Fig. 6.12. This is because for short warning lines interception with surface to air missiles (due to their high speed) is carried out at a greater distance from the launch point than interception using aircraft. From this example it is clear that for range values  $R < R^*$  it is more advantageous to use missiles, but for the distances  $R > R^*$ , fighter-interceptors are better. Even in spite of the fact that the missile is cheaper than an aircraft by almost one order of magnitude, it is more advantageous to use aircraft and not missiles in groups, as we have seen, given certain conditions.

/364

That is why the synthesis of the system must be conducted by estimating the cost of a group of facilities, and not of each individual facility.

From expression (6.44) it follows that the  $C_k$  function minimum is determined, in particular, for missile complexes mainly by the minimum weight of the flight craft and by  $C_0$ . This follows from the fact that the remaining quantities, for an assigned scheme of performance of the mission and for a given equipment composition, vary relatively little. Equipment parameters can be varied within the range of allowable values, but prorated costs  $C_i$  remain nearly unchanged.

$\bar{G}_{H_i}$  is determined with reference to the optimal subdivision of the total weight of the missile stages or of the aircraft into the weights of individual elements and remains practically unchanged in the process. Also changing little in the minimization of costs is the  $C_k$  function.

Let us consider as an example how an air target can be hit with antiaircraft missiles at minimum cost [148]. We will assume that the effectiveness of the antiaircraft complex is estimated by the probability of hitting the target  $E_c$  and can be provided by way of three outlays: in development of the antiaircraft missile, in implementation of the program of increasing its reliability, and in the manufacture and launch of several antiaircraft missiles.

To determine the minimum total cost, we must find each of these three components. Here it must be considered that the number of antiaircraft missiles for hitting a target depends on their reliability and is defined by the outlays in increasing reliability.

Example 6.4. It is required to determine the number of antiaircraft missiles of an AAD [antiaircraft defense] complex destroying an air target with probability  $P_k = 0.5$  with minimum monetary outlays. The missile control system consists of three subsystems: a ground guidance subsystem 1; an onboard guidance subsystem 2; and the launch position equipment 3. For greater reliability of the control system, certain monetary funds are spent in increasing the reliability of its individual subsystems. Let us use for this purpose a study by N. Cox and W. Harter [148], giving a graph of the costs of increasing the reliability of missile control systems (Fig. 6.13). This graph shows what monetary outlays  $C$  provide for the reliability of error-free operation  $P_k$  of a complex control system. Approximating the dashed curve with a straight line, we obtain a function written

/365

in terms of the function of a multiple logarithm in the form

$$C = \mu_{re} \lg \lg \frac{1}{P_{com}} - C_{re_0} \quad , \quad (6.45)$$

where  $\mu_{re}$  is the slope of the characteristics, and

$P_{re_0}$  is the cost of the system providing a certain initial reliability  $P_{com_0}$ .

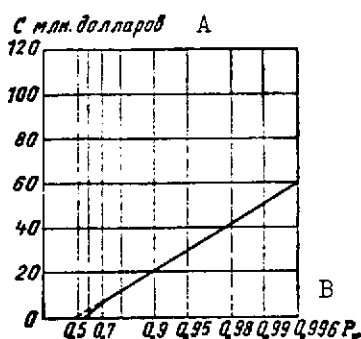


Fig. 6.13. Graph characterizing the cost of increasing the reliability of missile subsystems (the entire control system of the missile is considered as a complex system)

KEY: A -- C, millions of dollars

B --  $P_{com}$

The cost for striking the air target with antiaircraft missiles is determined by the formula

$$C = n(C_m + C_1) + C_0 + C_{re_0} \quad , \quad (6.46)$$

where  $C_m$  is the cost of building the missile;

$C_1$  is the cost of launching the missile;

$C_0$  is the unchanged cost of developing the design and ground equipment; and

$C_{re}$  is the cost to increase the reliability of the control systems.

The cost of a missile without providing for standby system equipment can be defined as

$$C = n \left( \mu_m \sum_{i=1}^N S_i + \mu_{in} \sum_{i=1}^{N'} S'_i \right) + \mu_{re} \sum_{i=1}^N S_i \lg \lg \frac{1}{P_{com.i}} - C_{re_0} + C_0. \quad (6.47)$$

where  $\mu_m$  and  $\mu_{in}$  are the slopes of the cost characteristics;

$S_i$  and  $S_i'$  are the complexity factors of the missile subsystems and the launch facilities<sup>4</sup>;

$i$  is the number of the missile subsystems and launch facilities; and

$N$ ,  $N'$  is the number of series-connected subsystems in missile and launch facilities.

The reliability of the  $i$ -th subsystem is determined by the formula /366

$$P_i = P_i^{S_i k_i t_i}, \quad (6.48)$$

where  $k_i$  is the coefficient allowing for environmental effects on the operation of the subsystem, and

$c_i$  is the system operating period.

Referring to formula (6.48), let us determine the reliability of the entire missile as

$$P_m = P_{bo} \prod_i P_i^{S_i k_i t_i}, \quad (6.49)$$

where  $P_{bo}$  is the probability of the error-free operation of the booster.

The number of missiles launched to achieve the desired target strike probability is obtained by using the following expression:

$$n = \frac{\lg(1 - P_{com})}{\lg(1 - P_m)}, \quad (6.50)$$

where  $P_m$  is the probability of error-free operation of the missile.

Let us use the method of indeterminate Lagrange multipliers to determine the optimal number of missiles launched, on the condition of minimum cost as a function of reliability.

To do this, let us set up the auxiliary operation of the form

$$\begin{aligned} \Phi(P_i, \lambda) = & \sum_{i=1}^N S_i \left( c_{re} \lg \frac{1}{P_i} - c_{re} \right) + \\ & + \lambda \left( \prod_i P_i^{S_i k_i t_i} - \frac{P_m}{P_{bo}} \right), \end{aligned} \quad (6.51)$$



where  $\lambda$  is an indeterminate Lagrange multiplier, based on equations (6.47) and (6.49).

Equation (6.51) is valid when

$$\prod_i \left( P_i^{S_i k_i t_i} - \frac{P_m}{P_{bo}} \right) > 0.$$

using the expressions

$$\frac{\partial \Phi_i}{\partial P_i} = 0 \quad \text{and} \quad \frac{\partial \Phi_i}{\partial \lambda} = 0$$

we find

$$\left. \begin{aligned} \frac{S_i \mu_{re}}{P_i \lg P_i} + \lambda S_i k_i t_i P_i^{S_i k_i t_i - 1} \prod_{j \neq i} P_j^{S_j k_j t_j} &= 0, \\ \prod_i P_i^{S_i k_i t_i} - \frac{P_m}{P_{bo}} &= 0. \end{aligned} \right\} \quad (6.52)$$

Let us substitute the second equation of system (6.52) into the first, and then we get /367

$$\frac{\mu_{re}}{\lg P_i} = -\lambda k_i t_i \frac{P_m}{P_{bo}}. \quad (6.53)$$

by equation (6.53), we have the following for the first subsystem:

$$\frac{\mu_{re}}{\lg P_1} = -\lambda k_1 t_1 \frac{P_m}{P_{bo}}. \quad (6.54)$$

Dividing equation (6.54) by equation (6.53), we get

$$P_i = P_1^{\frac{k_1 t_1}{k_i t_i}} \quad \text{for } i \neq 1. \quad (6.55)$$

then from the equation

$$\frac{P_m}{P_{bo}} = \prod_i P_i^{S_i k_i t_i}, \quad (6.56)$$

we obtain

$$\frac{P_m}{P_{bo}} = P_1^{S_1 k_1 t_1} \prod_{i \neq 1} P_i^{\left(\frac{k_i t_i}{k_1 t_1}\right) S_i k_i t_i} = P_1^{S_1 k_1 t_1}. \quad (6.57)$$

on the condition (6.55). Let us rewrite expression (6.50), using the formulas (6.49) and (6.57), as

$$n = \frac{\lg(1 - P_{com})}{\lg(1 - P_{bo} P_1^{S_1 k_1 t_1})}. \quad (6.58)$$

To determine the minimum cost, let us review the formula

$$C = n(\mu_m S_2 + \rho + \mu_{in} S_3) + \mu_{re} P_{in}^{\frac{k_i t_i}{k_1 t_1}} - C_{re_0} + C_0. \quad (6.59)$$

The values of the coefficients  $\mu_m$ ,  $\mu_{in}$ , and  $\rho^5$  are taken from cost graphs similar to Fig. 6.6.

The costs of a missile and its launch are determined by the formulas (6.46) and (6.59), that is

$$\left. \begin{aligned} C_m &= \mu_m S_2, \\ C_{in} &= \mu_{in} S_3 + \rho. \end{aligned} \right\} \quad (6.60)$$

The anticipated reliability of each subsystem is

$$P'_{in} = P_{in}^{S_i k_i t_i}, \quad (6.61)$$

and the optimal number of missiles launched (cf. formula (6.58)) is /368

$$n = \frac{\lg(1 - P_{\text{com}})}{\lg(1 - P_{\text{bo}}^{S_i, k_i, t_i})} \cdot \quad (6.62)$$

Let us construct, with formulas (6.60)-(6.62), the graphs of the total cost of performing the combat mission with  $P_k = 0.95$ .

The complexity factors of the three subsystems will be  $S_1 = 1.0$ ,  $S_2 = 0.2$ , and  $S_3 = 0.5$ ; their operating time will be  $t_1 = 60$  hours,  $t_2 = 60$  hours, and  $t_3 = 1$  hour; the operating conditions will be  $k_1 = k_2 = k_3 = 1.0$ . We will assume that the operating reliability of each of the subsystems is identical, that is,  $P_{10} = P_{20} = P_{30} \cong P_{\text{bo}} \cong 1.0$ .

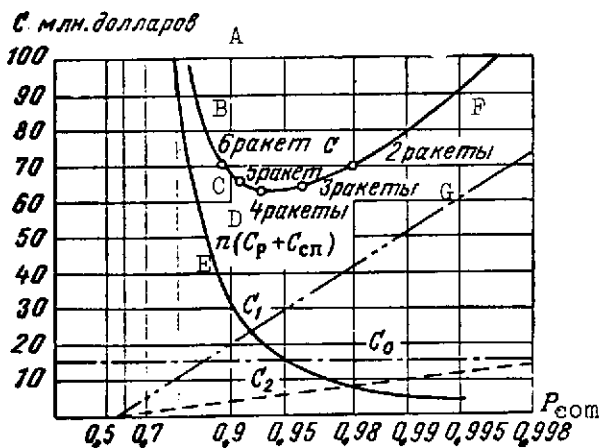


Fig. 6.14. Dependence of cost components and total cost on subsystem reliability

KEY: A -- C, millions of dollars  
 B -- 6 missiles, C  
 C -- 5 missiles  
 D -- 4 missiles  
 E --  $n(C_m + C_1)$   
 F -- 2 missiles  
 G -- 3 missiles

We will take the cost factors to be as follows:  $\mu_m = 0.2 \cdot 10^6$  dollars;  $\mu_{1n} = 2 \cdot 10^6$  dollars;  $\rho = 1 \cdot 10^5$  dollars;  $C_0 = 15 \cdot 10^6$  dollars; and  $C_{re_0} = 0$ .

These curves are plotted in Fig. 6.14. From the plots it is clear that the minimum cost  $C_{\text{min}} = 63 \cdot 10^6$  dollars is attained for four missiles ( $n = 4$ ). The cost components corresponding to this case are given in Table 6.5.

From the data in Table 6.5 and Fig. 6.14, it is clear that outlays to increase reliability for a minimum-cost program can exceed the costs of developing the design (15 million dollars).

Now let us consider an example when standby subsystems are employed in control systems.

Example 6.5. It is required to determine the number of antiaircraft missiles striking an air target with  $P_k = 0.95$  or with minimum monetary outlays. The control system  $k$  consists of five subsystems with different degrees of standby provision.

TABLE 6.5

/369

| Cost component                                  | Cost, millions of dollars    |
|-------------------------------------------------|------------------------------|
| Cost of developing missile and ground equipment | $C_0=15$                     |
| Cost of building and launching 4 missiles       | $n(C_m + C_1) = 16$          |
| Cost of increasing reliability of 1st subsystem | $C_{10}=27$                  |
| of 2nd subsystem                                | $C_{20}=5$                   |
| of 3rd subsystem                                | $C_{30}=0$                   |
| Total                                           | $C_{min}=63$ million dollars |

Let us denote the standby degree by  $m_{ik}$ , then formulas (6.48) and (6.49) must be written as

$$P_i' = 1 - (1 - P_i^{S_i k_i t_i})^{m_{ik}}; \quad (6.63)$$

$$P_{\Sigma} = P_{bo} \prod_i [1 - (1 - P_i^{S_i k_i t_i})^{m_{ik}}], \quad (6.64)$$

where  $m_{ik} = 1$  for  $i = 1, 2, \dots, N'$ , and

$N'$  is the number of subsystems in which standby is impossible.

As in example 6.4, let us set up an auxiliary equation

$$\begin{aligned} \Phi_i(P_i, \lambda) = & \sum_{i=1}^N S_i \left( \frac{1}{P_i \lg P_i} - C_{re} \right) + \\ & + \lambda \left\{ \prod_i [1 - (1 - P_i^{S_i k_i t_i})^{m_{ik}}] - \frac{P_m}{P_{bo}} \right\}. \end{aligned} \quad (6.65)$$

Then by calculating the derivatives of the function  $\Phi_i$  and equating them to zero, we get

/370

$$\left. \begin{aligned} & \frac{S_i \mu_{re}}{P_i \lg P_i} + \lambda \left\{ S_i k_i t_i m_{ik} P_i^{S_i k_i t_i - 1} \times \right. \\ & \times (1 - P_i^{S_i k_i t_i})^{m_{ik} - 1} \prod_{i \neq 1} [1 - (1 - P_i^{S_i k_i t_i})^{m_{ik}}] \Big\} = 0; \\ & \prod_i [1 - (1 - P_i^{S_i k_i t_i})^{m_{ik}}] - \frac{P_m}{P_{bo}} = 0. \end{aligned} \right\} \quad (6.66)$$

Multiply the first equation in system (6.66) by the expression

$$\frac{1 - (1 - P_i^{S_i k_i t_i})^{m_{ik}}}{m_{ik} P_i^{S_i k_i t_i} (1 - P_i^{S_i k_i t_i})^{m_{ik} - 1}},$$

then we get

$$\frac{\mu_{\text{reg}} [1 - (1 - P_i^{S_i k_i t_i})^{m_{ik}}] S_i}{m_{ik} (1 - P_i^{S_i k_i t_i})^{m_{ik}-1} P_i^{S_i k_i t_i} \lg P_i^{S_i k_i t_i}} + \\ + \lambda \prod_i [1 - (1 - P_i^{S_i k_i t_i})^{m_{ik}}] = 0. \quad (6.67)$$

Let us introduce the auxiliary function

$$y(P_i, m_{ik}) = \frac{1 - (1 - P_i^{S_i k_i t_i})^{m_{ik}}}{m_{ik} (1 - P_i^{S_i k_i t_i})^{m_{ik}-1} P_i^{S_i k_i t_i} \lg P_i^{S_i k_i t_i}} \quad (6.68)$$

into equation (6.67), and let us use the second equation of system (6.66), then we get

$$S_i y(P_i, m_{ik}) + \frac{\lambda P_{\text{in}}}{\mu_{\text{in}} P_{\text{bo}}} = 0. \quad (6.69)$$

For actual calculations, let us represent the function (6.68) as

$$y(P, m) = \frac{1 - (1 - P)^m}{m (1 - P)^{m-1} P \lg P}. \quad (6.70)$$

Its graph is plotted in Fig. 6.15.

Using equation (6.69), let us find

$$y(P_i, m_{ik}) = \frac{S_i}{S_l} y(P_l, m_{ik}). \quad (6.71)$$

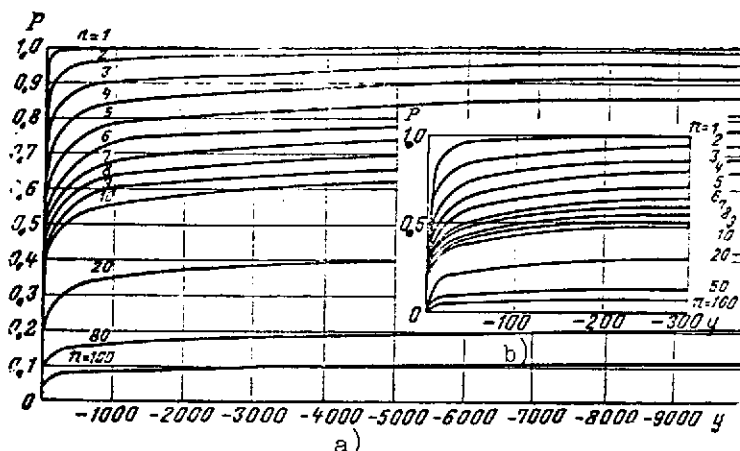


Fig. 6.15. Determining the standby extent of a system for minimum outlays; reliability  $P$  as a function of the auxiliary quantity  $y$ :

a -- For large  $y$  values

b -- for small  $y$  values

$n$  is the number of missiles striking the target with specified probability

From formula (6.71) it is clear that the more complicated a subsystem, the lower lies the family of characteristics  $y(P_i, m_{ik})$  in the graph. Therefore to obtain the same reliability, we must increase the extent of standby  $m_{ik}$ . Though this principle is obvious, the quantitative determination of the required standby is possible only by using formula (6.70).

To determine the minimum cost and the minimum number of missiles when standby of subsystems is provided, we must use the following formula:

$$C = n \left( \mu_m \sum_{i=1}^N m_i S_i + \rho + \mu_{re} \sum_{i=1}^N m_i S_i \right) + \mu_{re} P_i^{S_i k_i l_i} - C_{re0} + C_{sup}, \quad (6.72)$$

where  $P_i$  is determined from Fig. 6.15.

$$n = \frac{\lg(1 - P_{com})}{\lg \left\{ 1 - P_{00} \prod_i \left[ 1 - (1 - P_i^{S_i k_i l_i})^{m_{ik}} \right] \right\}}. \quad (6.73)$$

Using formulas (6.71) - (6.73), let us determine the cost plots as functions of the reliability of the standby provisions of four controlled subsystems with  $W_K = 0.95$  and  $k_1 = k_2 = k_3 = k_4 = 1.0$ ;  $S_1 = 0.4$ ,  $S_2 = 0.2$ ,  $S_3 = 0.5$ ,  $S_4 = 0.6$ ,  $t_1 = 60$  hours,  $t_2 = 60$  hours,  $t_3 = 1$  hour,  $t_4 = 60$  hours;  $P_{10} = P_{20} = P_{30} = P_{40} = P_{b0} = 1.0$ ;  $\mu_m = 0.2 \cdot 10^6$  dollars;  $C_1 = (0.1 \cdot 10^6 + 2 \cdot 10^6 \sum m_i S_i)$  dollars,  $C_0 = 15 \cdot 10^6$  dollars,  $C_{re.0} = 0$ ;  $m_1 = 1.0$  (the subsystem has no standby),  $m_2, m_3$ , and  $m_4$  vary from 1 to 3.

From the graphs plotted on the basis of the data (Fig. 6.16) it is clear that applying standby provisions permits cutting the costs of hitting an air target. Table 6.6 gives the data on the costs of individual components when two or three missiles are launched with different degrees of standby (in the first column,  $m_i = (1, 2, 1, 2)$ ; in the second column,  $m = (1, 3, 1, 2)$ ).

1372

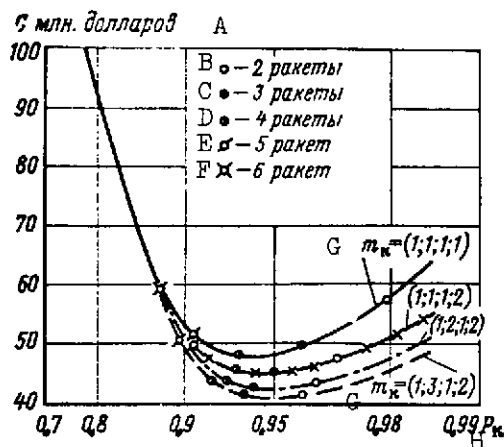


Fig. 6.16. Total cost as functions of reliability for different degrees of standby

KEY: A -- C, millions of dollars

B -- Two missiles

C -- Three missiles

D -- Four missiles

E -- Five missiles

F -- Six missiles

G --  $m_{com}$  H --  $P_{com}$

From the data in Table 6.6 it is clear that employing more far-reaching standby for a missile control system  $m_{13} = 3$  compared with  $m_{12} = 2$ , even though the number of missiles required to hit the target is reduced from three to two, still the total cost

is changed but little. Accordingly, there is a redistribution of monetary outlays. The cost of launching the missiles is reduced, but the cost of the nonstandby missile control subsystem rises owing to the use of more expensive (reliably operating) parts to 7.8 million dollars, and the complexity of the standby subsystem (owing to an increase in the extent of standby) -- to 15.0 million dollars.

The examples 6.4 and 6.5 that we have been considering demonstrate that the application of technical facilities (standby status) for greater reliability of control systems leads to a reduction in monetary outlays and in the number of missiles needed



to hit targets with assigned probability. Therefore at the outset of designing control systems calculations must be made to estimate the costs of control systems and to select the required degree of standby with respect to the minimum monetary outlays.

TABLE 6.6

/373

| Cost components                                 | Cost, millions of dollars |                   |
|-------------------------------------------------|---------------------------|-------------------|
|                                                 | $n=3$                     | $n=2$             |
| Cost of developing missile and ground equipment | $C_0=15$                  | $C_0=15$          |
| Cost of building and launching missiles         | $n(C_m+C_1)=15.7$         | $n(C_m+C_1)=11.6$ |
| Cost of increasing reliability                  |                           |                   |
| of 1st subsystem                                | $C_{10}=12.6$             | $C_{10}=17.8$     |
| of 2nd subsystem                                | $C_{20}=12.6$             | $C_{20}=15.0$     |
| of 3rd subsystem                                | $C_{30}=3.0$              | $C_{30}=2.3$      |
| of 4th subsystem                                | $C_{40}=0$                | $C_{40}=0$        |
| Total                                           | 58.9                      | 58.7              |

Another important characteristic, in addition to cost, is the time expended in the development, building, and commissioning of flight complexes. When this time is too great, the complex (or its control system) will become obsolescent by the time it is commissioned. If the available time is short, the design complex can have characteristics that are not high enough, which leads to its rapid qualitative aging.

The determination of time outlays presents considerable difficulties and is carried out, as a rule, by predicting statistically treated data characterizing previous developments. Here the total time is composed of the time expended in each of the stages of design and production of the flight complex.

These stages are as follows.

Presentation of the technical assignment when the ordering organization, based on preliminary scientific studies and experimental developments of individual complex and system elements, determines their layout, main characteristics, and parameters (the time outlay denoted by  $T_{as}$ ).

Development of the advanced plans of the complex when the leading industrial organization, based on the technical assignment

/374

TABLE 6.7

| Type of<br>missile or AES \ Years | 1951 | 1952 | 1953 | 1954 | 1955 | 1956 | 1957 | 1958 | 1959 | 1960 | 1961 | 1962 | 1963 | 1964 | 1965 |
|-----------------------------------|------|------|------|------|------|------|------|------|------|------|------|------|------|------|------|
| Atlas D                           |      |      |      |      |      |      |      |      |      |      |      |      |      |      |      |
| Titan I                           |      |      |      |      |      |      |      |      |      |      |      |      |      |      |      |
| Titan II                          |      |      |      |      |      |      |      |      |      |      |      |      |      |      |      |
| Minuteman                         |      |      |      |      |      |      |      |      |      |      |      |      |      |      |      |
| Polaris A1                        |      |      |      |      |      |      |      |      |      |      |      |      |      |      |      |
| Samos                             |      |      |      |      |      |      |      |      |      |      |      |      |      |      |      |
| Midas                             |      |      |      |      |      |      |      |      |      |      |      |      |      |      |      |
| Transit                           |      |      |      |      |      |      |      |      |      |      |      |      |      |      |      |
| Nike-Zeus                         |      |      |      |      |      |      |      |      |      |      |      |      |      |      |      |

received, works out approaches toward building the assigned complex and determines, jointly with the ordering organization, the requisite tactical-technical requirements imposed on it (the time outlay is denoted by  $T_{a.d}$ ).

Development of preliminary and technical plans sometimes can be divided into two stages, and in several cases these stages are united into one in order to shorten time in development. Here the technical solution adopted in the advanced design is worked out in detail. The preliminary or technical plan of the system is completed by the development of technical documentation, building of mockups, and prototypes of its individual elements.

This stage is characterized by the time which is denoted by  $T_{p.t}$ .

Industrial manufacture and check-out tests of prototype and the system as a whole. This stage is characterized by the actual production process in building the developed complex, and also by its laboratory and full-scale tests to obtain the specified characteristics. The length of this stage depends on the level of the production and experimental base and the state of the art. The duration of this stage is denoted by  $T_{in}$ .

The stage of the release tests is characterized by the customer, based on appropriate statistical experiments, declaring whether the proffered model of the system measures up to specified characteristics throughout the entire range of proposed operating conditions.

The duration of this stage can be shortened by using mathematical and physical modeling of the control processes. When the prototype measures up to the imposed requirements, after release tests, it is taken up for series production. The time required for the stage of release tests is denoted by  $T_{re}$ .

The stage of series production and introduction of the prototype. On the completion of the release tests, the industrial enterprises for series production are determined, to which the leading industrial organizations turn over the necessary technical documentation. This stage terminates in the introduction of the prototype. By introduction we mean the commissioning, mastery, and operation of the number of the models which can afford attaining the required level of mission performance. /376

We will let  $T_{int}$  stand for the time of the stage of series-production and introduction.

Thus, the total time required to develop and build systems is defined as the sum

$$T = T_{as} + T_{a.d} + T_{p.t} + T_{in} + T_{re} + T_{int} \quad (6.74)$$

Table 6.7 gives some idea of the duration of individual stages of development, building, and introduction of flight craft complexes.

As we can see from the table, these schedules are extremely stable, for example, 3-4 years for spacecraft and 5-6 years for long-range ballistic missiles and launch vehicles.

### 6.3. Effect of Natural and Artificial Interference on the Effectiveness of Performing an Assigned Mission

All the kinds of interference acting on radar sets, homing heads, heat direction finders, infrared heads, radio altimeters, and laser and radio rangefinders can be divided into natural and artificial. Natural and especially artificial interference has a considerable effect on the effectiveness of the combat use of defense and offense complexes, and therefore must be taken into account in designing control systems.

Natural interference is commonly held to include the following: atmospheric, ionospheric, industrial, and interference induced by the effect of the earth or ocean waves. Atmospheric interference (rain and fog) reduces the coverage of ground and on-board radar complexes (cf. Fig. 3.4). Ionospheric interference also reduces radar coverage and sometimes can lead to the appearance of interference hampering the radar tracking of objects.

Artificial interference is commonly held to refer to means of radio and infrared countermeasures. Means of radio countermeasures (RCM) can be divided into active and passive. A classification of RCM is shown in Fig. 6.17. The effectiveness of interference [jamming] depends on the power of the interference and the signal, that is, /377

$$K = \left( \frac{P_j}{P_{si}} \right)_{inp} \geq K_j \quad (6.75)$$

where  $K_j$  is the coefficient of suppression of the radar or the RHH [radar homing head] by the given kind of jamming, and

$K$  is the ratio of the jamming power  $P_j$  to signal power  $P_{si}$  at the radio receiver input [20].

The jamming power is determined from the formula

$$P_{re\ 1} = P_j' A_j F^2(\phi_{hor}, \phi_h) \gamma_j, \quad (6.76)$$

where  $P_j'$  is the flux density of the jamming power at the input of the antenna of the suppressed radar;

$\phi_{hor}$  and  $\phi_h$  are the azimuth and elevation angles of the jamming supplier;

$F$  is a function describing the radiation pattern of the suppressed radar with respect to the field; and

$A_j$  is the equivalent absorption surface of the antenna of the suppressed radar and determined by the formula

$$A_j = \frac{G_a \lambda^2}{4\pi}. \quad (6.77)$$

Here  $G_a$  is the maximum coefficient of the directivity of the antenna of the suppressed radar, and  $\lambda$  is the jamming wavelength. /378

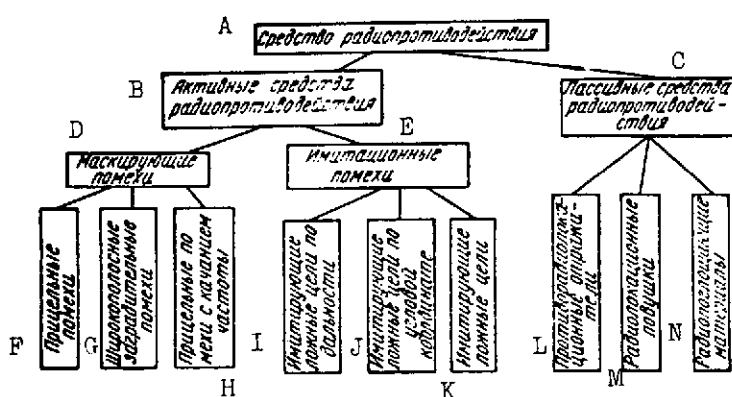


Fig. 6.17. Classification of means of RCM

KEY: A -- Means of radio countermeasures  
 B -- Active means of countermeasures  
 C -- Passive means of countermeasures  
 D -- Camouflaging jamming  
 E -- Simulation jamming  
 F -- Sighting jamming  
 G -- Wideband barrage jamming

H -- Sighting jamming with wobbling  
 I -- Simulating false targets as to range  
 J -- Simulating false targets as to angular coordinate  
 K -- Simulating false targets  
 L -- Counter radar reflectors  
 M -- Radar traps  
 N -- Radio-absorbing materials

The density of the jamming signal is

$$P_j' = \frac{P_j G_j}{4\pi R_j^2} \cdot 10^{-0.1 \alpha R_j}, \quad (6.78)$$

where  $G_j$  is the maximum coefficient of the directivity of the jamming transmitter antenna;  
 $\alpha$  is the coefficient that allows for the attenuation of the signal in the atmosphere, in db/km; and  
 $R_j$  is the range to the jammer (Fig. 6.18 a).

Considering that only part of the jamming power reaches the receiver determined by the ratio of the width of the spectrum of the jamming signal  $\Delta F_j$  to the passband of the receiver of the suppressed radar  $\Delta F_{re}$ , the jamming power is

$$P_{re.inp} = \frac{P_j G_j A_j \Delta F_{re}}{4\pi R_j^2 \Delta F_j} F^2(\phi_{hor}, \phi_h) \cdot 10^{-0.1\alpha R_j} \quad (6.79)$$

The power of the useful signal at the receiver input of the suppressed radar is determined by the formula

$$P_{si.inp} = \frac{P_{si} G_{si} A_t A_j}{4\pi^2 R_{si}^2} \cdot 10^{-0.2\alpha R_{si}} \quad (6.80)$$

where  $R_a$  is the range to the covered aircraft.

Substituting formulas (6.79) and (6.80) into equation (6.75), we find

$$K = \frac{4\pi R_j G_j \Delta F_{re}}{R_{si} G_{si} A_t \Delta F_j} \left( \frac{R_{si}}{R_j} \right)^4 F^2(\phi_{hor}, \phi_h) \cdot 10^{0.1\alpha(2R_{si} - R_j)} \quad (6.81)$$

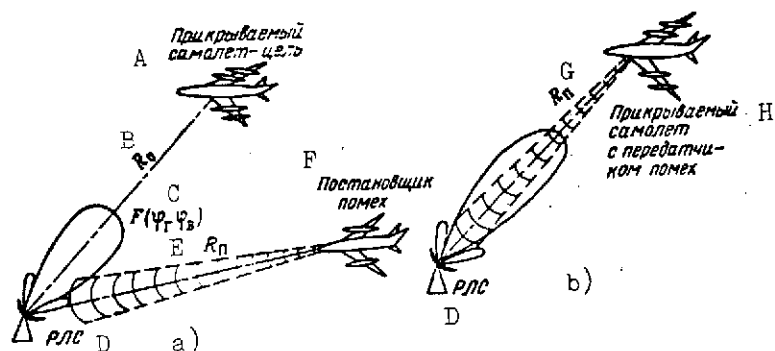


Fig. 6.18. Scheme for producing active jamming:  
a -- When a jammer is present  
b -- When the jammer coincides with the covered aircraft  
(cont. on next page)

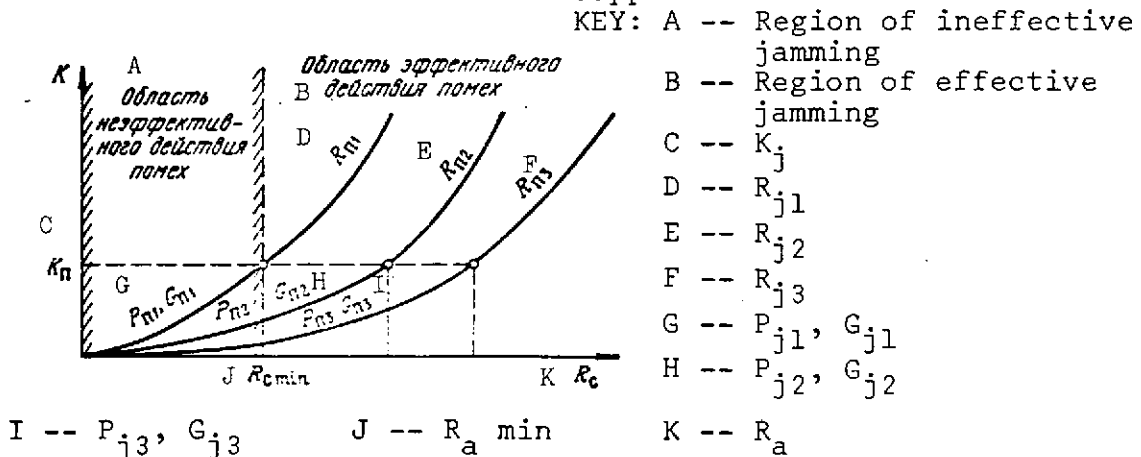
KEY: A -- Covered aircraft-target  
 B --  $R_j$   
 C --  $F(\phi_{hor}, \phi_h)$   
 D -- Radar  
 E --  $R_j$   
 F -- Jammer  
 G --  $R_j$   
 H -- Covered aircraft with jammer device

The function (6.81) is the fundamental formula for radio countermeasures for active jamming.

Fig. 6.19 presents the variation of the coefficient  $K$  as functions of  $R_a$  and  $P_j$ ,  $G_j$ , and  $R_j$  as parameters. When  $K = K_j$ , the jamming becomes ineffective; the region in which jamming is effective is usually called the suppression zone.  $K > K_j$  in the suppression zone. The formula (6.81) changes when the covered aircraft itself carries the jamming device. Then we get

$$K = \frac{4\pi R_j G_j \Delta f_{re}}{P_{si} G_{si} A_t \Delta F_j} R_j^2 \cdot 10^{0.1 \alpha R_j} \quad (6.82)$$

Fig. 6.19. Determining the radar suppression zone



In correcting the absorption of radiowaves in the atmosphere, let us find the formulas for the determination of the minimum suppression range. Based on the function (6.81), we have

$$R_{j \min} = 2R \sqrt{\frac{\pi K_j P_j G_j F^2 (\phi_{hor}, \phi_h) \Delta f_{re} \gamma_j}{P_{s1} G_{s1} A_t \Delta F_j}} \quad (6.83)$$

and from formula (6.82)

380

$$R_{j \min} = \frac{1}{2} \sqrt{\frac{K_j P_{s1} G_{s1} A_t \Delta F_j}{\pi P_j G_j \gamma_j \Delta f_{re}}} \quad (6.84)$$

From these formulas it is clear that as the jammer approaches the radar, the jamming effectiveness drops off. This is attributable to the fact that in the approach of the aircraft with the jamming device to the radar, the power of the signal reflected from the aircraft increases more rapidly (since it is proportional to  $R_j^4$ ) than the power of the jamming at the radar receiver input (since it is proportional to  $R_j^2$ ) [20].

From formula (6.81) it also follows that if the jammer acts with respect to the main lobe of the radiation pattern, the suppression zone will be broader than for suppression of a side lobe.

We will estimate the effectiveness of jamming by the coverage of target detection  $R_{re \min}$ . The smaller the range, the more effective the radio countermeasures:

$$W_j = \frac{R_{det} - R_{j \min}}{R_{det}} \quad (6.85)$$

Table 6.8 gives data on the effect of different types of jamming [20].

TABLE 6.8 ESTIMATE OF THE EFFECTIVENESS OF JAMMING,  $P_j = 1000$  w/MHz;  $R_{det} = 50$  km (WITHOUT JAMMING)

| Type of jamming                        | $R_{j \min}$<br>km | $W_j$ |
|----------------------------------------|--------------------|-------|
| Camouflaging:                          |                    |       |
| noise                                  | 48                 | 0.04  |
| sighting in the side-lobe of the radar | 37                 | 0.26  |
| sighting in the main-lobe zone         | 9                  | 0.82  |
| Simulating false-target position       | 5                  | 0.90  |



Simulation jamming is jamming in the form of the signals of false targets, diverting the radar from the true target. The method of producing simulation jamming consists in the reception of the radar signal, and its amplification and re-beaming with a time delay. As a result of this delay, the signal picked up by the radar yields false information on the range and azimuth. The simulation jamming device can also pick up and amplify pulses of the side lobes, then several false targets will reach the radar. The reception and rebeaming of pulses reflected from ground objects is also possible. Passive radio countermeasures can be implemented by ejecting large numbers of dipole reflectors (passive jamming), the launch of missile-traps, or the ejection of corner reflectors. In addition, different kinds of coatings producing the effective reflective surface of flightcraft are also possible as passive measures.

Passive jamming (Fig. 6.20). The aircraft-target is not detected in the dipole jamming when the power of the signals reflected from the dipoles exceeds the power of the useful signal by several times, that is,

$$K = \left( \frac{P_j}{P_{\text{signal}}} \right) = \frac{\bar{V}_d}{\bar{V}_t}, \quad (6.96)$$

where  $\bar{V}_d$  is the mean effective surface for reflection from the dipoles, and  $\bar{V}_t$  is the mean effective reflecting surface of the target.

$\bar{V}_d$  can be represented as

$$\bar{V}_d = N \bar{\sigma}_d, \quad (6.97)$$

where  $N$  is the number of dipoles, and  $\bar{\sigma}_d$  is the mean effective scattering surface of a single dipole.

In practical calculations, of  $\bar{\sigma}_d$ , the following formula is usually employed

$$\bar{\sigma}_D = 0.17 \pi^2 h_d^2 N \eta, \quad (6.98)$$

where  $h_d$  is the height of a half-wave dipole ( $h_d = \lambda/\pi$ );  $\eta$  is the coefficient of the effective number of dipoles;

and  $\bar{V}_t$  is taken as  $20 \text{ m}^2$  (cf. Chapter Three) and by formula (6.98), we find for 1000 dipoles

$$\bar{\sigma}_d = 85 \text{ m}^2; \quad K = 85/20 = 4.25,$$

indicating the adequate effectiveness of dipole reflectors.

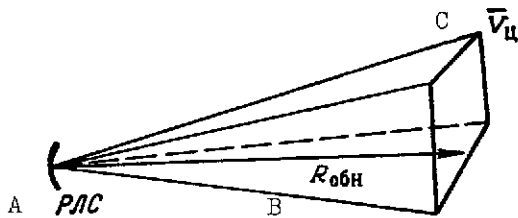


Fig. 6.20 Pulse volume of radar  
KEY: A -- Radar  
B --  $R_{det}$   
C --  $V_t$

Radar traps cause a disruption in guidance by diverting the attacking flight craft from the plane or missile being attacked, by the radar (Fig. 6.21).

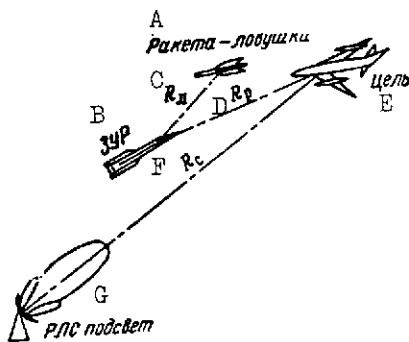


Fig. 6.21 Use of missile traps  
for breakdown of antiaircraft  
missile homing

KEY: A -- Missile-traps  
B -- Guided missile  
C --  $R_{tr}$   
D --  $R_m$   
E -- Target  
F --  $R_a$   
G -- Coverage radar

Let us write out the equation of radio countermeasures in the form

$$K = \left( \frac{P_j}{P_{si}} \right)_{\text{inp}} = \frac{4\pi P_j G_j R_{si}^2 R_j^2 \gamma_j \Delta f_{re}}{P_{si} G_{si} A_{tr} R_{tr}^2 \Delta F_j} \quad (6.99)$$

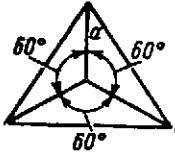
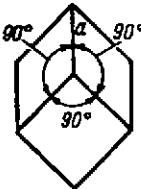
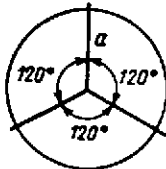
and with  $K = K_j$  and  $R_a = R_j$ , we find that the jamming power is

$$P_j = \frac{P_{s1} G_{s1} A_{tKj}}{4 \pi R_{s1}^2 G_j} \quad (6.100)$$

From formula (6.100) it is clear that a reflected signal simulating a false target must exceed in power the real reflected signal by several times.

Ejected traps in the form of corner reflectors have maximum effective reflecting areas amounting to several thousands of square meters. Working formulas for calculating the maximum effectiveness strike areas of different kinds of corner reflectors are given in Table 6.9.

TABLE 6.9 MAXIMUM EFFECTIVE REFLECTION AREAS OF CORNER REFLECTORS

| Name of corner reflector | Kind of corner reflector                                                            | $A_{\text{eff max}}$                    |
|--------------------------|-------------------------------------------------------------------------------------|-----------------------------------------|
| Triangular               |    | $\frac{4}{3} \pi \frac{a^2}{\lambda^2}$ |
| Rectangular              |  | $12\pi \frac{a^4}{\lambda^2}$           |
| Circular                 |  | $2\pi \frac{a^4}{\lambda^2}$            |

Radar coatings lead to an appreciable reduction in the effective reflecting surface of a flight craft which makes it less "visible" to the radar. These coatings are made in the form of horns, which lowers the intensity of reflection by ninety percent in the wavelength range 1-12 cm. Their weight is quite high (1 m<sup>2</sup> weighs 2 kg or more). Coatings of foamed glass fiber 12.7 mm thick are lighter in weight (0.91 kg). Here the intensity of reflection is reduced by ninety-nine percent in the wavelength range 0.9-77 cm [117].

The rational use of radio countermeasures can appreciably increase the effectiveness of an aircraft or missile complex. Fig. 6.22a shows the variation in the probability of striking  $W_{str}$  a bomber with a certain hypothetical defense system as a function of the weight of the jamming equipment (which can characterize the effectiveness of the radio countermeasures)  $G_j$  installed on board it [117]. Since the payload of each aircraft is limited to some maximum value, there arises the problem of its rational distribution: for a bomber, for example, between the bomb load and the radio jamming equipment. On the one hand, it is important to inflict the greatest damage on the enemy, that is, to increase the bomb load, and on the other, to deliver this load to the target with the highest probability.

This optimal relationship can be characterized by a certain parameter  $Q$ :

$$Q = (1 - W_{str})D. \quad (6.101)$$

here  $D$  is the percentage of the total possible destruction (uniquely related to the weight of the bomb load) inflicted by the bomber.

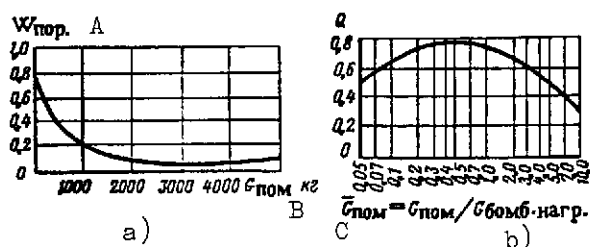


Fig. 6.22 Effect of weight of radio countermeasure equipment and bomb load:

- a -- Strike probability of a bomber as a function of the weight of the radio countermeasure equipment installed on it  
b -- Coefficient  $Q$  as a function of relative weight  $\bar{G}_j$

KEY: A --  $W_{str}$   
B --  $G_j$ , kg

C --  $\bar{G}_j = G_j / G_{bomb-ld}$  [bomb-ld = bomb payload]

A graph (cf. Fig. 6.22 b) plotted for the same hypothetical defense system as the graph in Fig. 6.22 a shows the dependence of the coefficient Q on the relative weight

$$\bar{G}_j = \frac{G_j}{G_{\text{bomb-ld}}} ,$$

$G_{\text{bomb-ld}}$  is the weight of the bomb load.

The calculation was made for a maximum payload of 4500 kg.

#### 6.4 Effect of Active Enemy Countermeasures on the Effectiveness of Performing an Assigned Mission

Active countermeasures or active defense is one of the main factors strongly influencing the effectiveness of carrying out a combat mission by an attacker. This factor can alter the make-up of the control system of a complex and its characteristics<sup>6</sup>. We will illustrate the effect of active countermeasures on the cost of a group attack by flight complexes using the following model [67].

A certain target (or a complex of targets) defended by interceptors is subjected to an attack by enemy aircraft or his tactical missiles, or long-range ballistic missiles. The quality of performance of the military mission by the attacker is evaluated by the function f, which is the cost of the attack. Here it is assumed that the military flight craft not hit by means of active defense reduces, with a certain probability the usefulness of the ground target attack by some constant quantity, or puts out of commission, with some other probability, one of the guidance centers of the interceptors. The effects of the combat facility (the missile warhead) can vary. According to the above-adopted model [67], each of the attacking flight craft can be struck, with different probabilities, by the means of active defense by interceptors both before the attack on the ground target, as well as after it. When tactical or long-range missiles are used, it is assumed that they are destroyed at the moment the warheads are delivered onto the target.

/386

The costs of the means of attack and defense are different; they depend on the type of the flight complex, on the above-indicated probabilities of carrying out the combat mission, and on the size of the warhead carried.

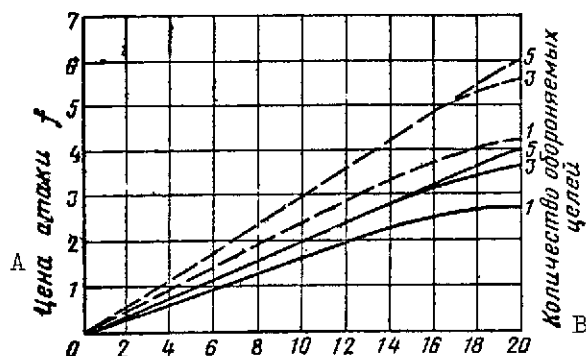


Fig. 6.23 Effect of the intensities of active defense on the cost of an attack  $f$  by bombers [141]

- - - low-altitude defense  
— high-altitude defense

KEY: A -- Cost of attack,  $f$   
B -- Number of targets defended

Thus, the "quality" of performance of a combat mission by the attacker is the higher, the smaller the  $f$  -- the cost of the attack ( $f = 0$  if all ground targets have been destroyed). The function  $f = 0$  also obtains when all interceptors or all guidance centers have been destroyed. That is, there is no active defense. When missiles are used in this case, the function  $f \neq 0$ , but it reaches some minimum value. Actions of the active defense raise the value of  $f$ , degrading the performance of the combat mission by the attacker.

The dependence of the cost  $f$  in an attack by bombers on the intensity of the active defense is shown in Fig. 6.23 for the model described. Since the probability of destroying the ground target depends on the bomber altitude and since, under otherwise equal conditions, the probability of the bomber being struck by an interceptor depends on this same factor, which varies as a function of the type of the active defense (low- or high-altitude defense), then in the situation described the variants listed in Table 6.10 are possible (the numerical values of the parameters in this example have been taken from [67]).

/387

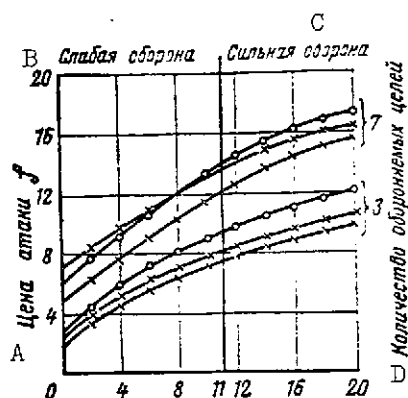


Fig. 6.24 Effect of intensity of active defense on the cost of attack  $f$  by tactical ballistic missiles [141]:

-0-0- -- missiles with heavy warheads  
-x-x- -- missiles with small warheads  
-|-|- -- optimal combination of different kinds of missiles

KEY: A -- Cost of attack,  $f$   
B -- Weak defense  
C -- Strong defense  
D -- Number of targets defended

From Fig. 6.24 and Table 6.11, the effect of the intensity of the active defense on an expedient missile warhead size is clearly seen. When missiles of different types are optimally combined, some improvement in the attack results is achieved.

Fig. 6.25 shows the effect of the probability of a long-range ballistic missile being struck by one interceptor on the cost of an attack by long-range ballistic missiles. The calculations were made for two different numbers of interceptors simultaneously guided by each guidance center, and for two different values of the total reserve of interceptors. Here it was assumed that each warhead carries 19 traps, all these 20 elements are of equal value from the standpoint of defense, and the interceptors are distributed evenly between them in accordance with an optimal strategy.

TABLE 6.10      PROBABILITIES OF A GROUND TARGET BEING HIT BY BOMBS AND PROBABILITIES OF BOMBERS BEING DESTROYED IN AN ACTIVE DEFENSE [67] /388

| Type of bomber                  |    | Probability of ground target strike | Probability of bomber being struck by one interceptor |                   |
|---------------------------------|----|-------------------------------------|-------------------------------------------------------|-------------------|
|                                 |    |                                     | low-alt. defense                                      | high-alt. defense |
| High-altitude attack by bombers | I  | 0,9                                 | 0,3                                                   | 0,4               |
|                                 | II | 0,3                                 | 0,4                                                   | 0,5               |
| Low-altitude attack by bombers  | I  | 0,3                                 | 0,2                                                   | 0,1               |
|                                 | II | 0,1                                 | 0,3                                                   | 0,2               |

As we can see, an increase in the number of simultaneously guided interceptors becomes less advantageous with an increase in the probability of long-range ballistic missiles being struck by each individual interceptor.

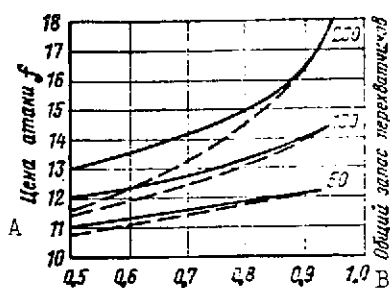


Fig. 6.25 Effect of the probability of a long-range ballistic missile being struck by a single interceptor on the cost of an attack [67]:

--- simultaneous guidance of 20 interceptors  
 --- simultaneous guidance of 40 interceptors  
 KEY: A -- Cost of attack, f  
 B -- Total reserve of interceptors

Now let us consider two specific examples of the effect of active countermeasures on how well a combat mission is performed.

In Table 6.10, two types of bombers have been assumed:

I is a model with high flight data and conditional costs  $a_1 = 2.5$ , and  
 II is a model with low flight data and conditional costs  $a_2 = 1.0$ .

Fig. 6.24 shows the effect of an active defense on the cost of an attack  $f$  by tactical ballistic missiles for values of the initial parameters listed in Table 6.11.

/389

TABLE 6.11 EFFECT OF ACTIVE DEFENSE ON THE COST OF AN ATTACK BY TACTICAL MISSILES [67]

| Resolving power of missile warhead | Missile cost | Prob. of ground target strike | Probability of missile being hit by 1 intercep. |
|------------------------------------|--------------|-------------------------------|-------------------------------------------------|
| I                                  | 1.0          | 0.90                          | 0.5                                             |
| II                                 | 1.5          | 0.95                          | 0.5                                             |

Example 6.6. Let us determine the probability of the performance of a combat mission by a multimission fighter against an operating ground target in conditions of countermeasures by the enemy AAD. We will assume that the enemy AAD consists of six 20-mm rapid-firing, small-caliber cannon, and two batteries of missiles (each of the batteries can launch only one missile at the target). Additionally, the multimission fighter can on its tracking to the target be attacked by two fighter-interceptors armed with missiles and cannon. The effectiveness criterion



in this case is defined as

$$E_a = W_{AAD} W_{det} W_{str} P_{AAD} P_{det} P_{str}, \quad (6.102)$$

where  $W_{AAD}$  is the probability of the multimission fighter penetrating the AAD facility;  
 $W_{det}$  is the probability of detection of the ground target;  
 $W_{str}$  is the probability of the ground target being struck with bombs;  
 $P_{AAD}$  is the operating reliability of the AAD system;  
 $P_{det}$  is the operating reliability of the onboard equipment detecting the ground target; and  
 $P_{str}$  is the reliability of the ground-to-air missile.

A multimission fighter penetrates AAD facilities if the aircraft is not struck by the small-caliber antiaircraft artillery, the antiaircraft missiles, and the fighter-interceptors;

$$W_{AAD} = (1 - W_{s.a.a})(1 - W_{a.g.m})(1 - W_{f-i}), \quad (6.103)$$

where  $W_{s.a.a}$  is the probability of the multimission fighter being hit by small-caliber antiaircraft artillery;  
 $W_{a.g.m}$  is the probability of the multimission fighter being hit by antiaircraft guided missiles; and  
 $W_{f-i}$  is the probability of the multimission fighter being struck by fighter-interceptors.

Probabilities of hitting an aircraft attacking ground targets are defined as:

$$\left. \begin{aligned} W_{s.a.a} &= 1 - (1 - W_{s.a.al})^{n_{s.a.a}}; \\ W_{a.g.m} &= 1 - (1 - W_{a.g.ml})^{n_{a.g.m}}; \\ W_{f-i} &= 1 - (1 - W_{f-il})^{n_{f-i}}, \end{aligned} \right\} \quad (6.104) \quad \underline{/390}$$

where  $W_{s.a.al}$  is the probability of a multimission fighter being struck by a single battery of small-caliber antiaircraft artillery;  
 $W_{a.g.ml}$  is the probability of the multimission fighter being struck by a single antiaircraft missile;

$W_{f-i}$  is the probability of the multimission fighter being struck by a single fighter-interceptor; and  $n_{s.a.a}$ ,  $n_{a.g.m}$ , and  $n_{f-i}$  are the number of batteries, small-caliber antiaircraft artillery, anti-aircraft missiles, and fighter-interceptors, respectively.

The probability of an aircraft being struck by antiaircraft missiles (or by AAD interceptor-fighters) was considered in example 6.1. Let us define by formulas (6.104)  $W_{s.a.a}$ ,  $W_{a.g.m}$ , and  $W_{f-i}$ , considering  $W_{s.a.a1} = 0.05$ ,  $W_{a.g.m1} = 0.3$ , and  $W_{f-i1} = 0.15$ .

$$W_{s.a.a} = 1 - (1 - 0.05)^6 = 0.27;$$

$$W_{a.g.m} = 1 - (1 - 0.3)^2 = 0.51;$$

$$W_{f-i} = 1 - (1 - 0.15)^2 = 0.28.$$

Hence the probability of penetrating AAD facilities will be  $W_{AAD} = 0.26$ , by formula (6.103). We will determine the effectiveness of the performance of the combat mission by a multimission fighter, given the condition  $W_{det} = 0.95$ ,  $W_{str} = 0.9$ ,  $P_{AAD} = 0.99$ ,  $P_{det} = 0.95$ , and  $P_{scr} = 0.98$ . Then

$$E_a = 0.26 \cdot 0.95 \cdot 0.9 \cdot 0.99 \cdot 0.95 \cdot 0.98 = 0.2 \quad .$$

From this example it is clear that the probability of the successful performance of a combat mission by a multimission fighter is low. Let us consider this very same problem when there is a partial suppression of the AAD defense by the armament of the multimission fighter. We will assume that two air-to-surface missiles ( $W_{a.g.m} = 0$ ), then  $W_{AAD} = 0.73 \cdot 0.72 = 0.52$  and  $E_a = 0.41$ . In this case  $E_a$  is approximately twice as high as in the first case, however the use of a multimission fighter is, as before, unwarranted, since  $E_a < 0.5$ .

Example 6.7. Let us determine the effectiveness of the actions of a multimission fighter against a ground target in the situation of AAD when RCM radio countermeasure equipment is

used on the multimission fighter. In this case, we will assume that  $W_{s.a.al} = 0.01$ ,  $W_{a.g.m} = 0.05$ , and  $W_{f-1} = 0.02$ , then  $W_{AAD} = 0.82$  and  $E_a = 0.65$ .

When the radar of the antiaircraft missile installation is hit,  $E_a$  becomes 0.72. Thus, the RCM equipment and the partial suppression of the AAD facilities permit a marked rise in the effectiveness of the combat application of multimission fighters in striking ground targets.

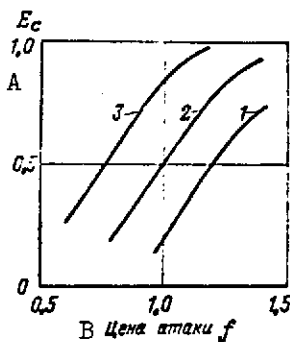


Fig. 6.26. Cost of an attack on a ground target by a single aircraft (1), acting in a group of two (2) and three (3) aircraft  
KEY: A --  $E_a$   
B -- Cost of attack,  $f$

Using these data for  $E_a$ , let us determine in Examples 6.6 and 6.7 the dependence of the cost of an attack on a standard ground target on the probability of its being hit. The

corresponding numerical values are given in Table 6.12.

The data in Table 6.12 were used in indicating in Fig. 6.26 (curve 1) the cost of an attack on a standard ground target made by a single aircraft; here also is given for sake of comparison a plot of the cost of an attack by one aircraft (curve 2) acting in a group of two aircraft. Here one of the airplanes strikes the ground target, and the second aircraft of the group suppresses the AAD facilities. Curve 3 corresponds to the cost of an attack by one aircraft acting in a group of three airplanes.

## 6.5. Groups of Complexes

The effectiveness of a system, as already indicated, is determined by the probability of the successful performance of a combat mission under specific conditions of the use of the system. In complex conditions of the use of complexes, the effectiveness of a system can take on any of a set of different values. The effectiveness is strongly affected by the layout of ground facilities of the system, active and passive countermeasures of the enemy, the possibility of performing combat operations by groups of flight craft, and so on. Ground facilities of the system are connected with each other into a unified cell or group. This refers both to AAD facilities and offense facilities. Groups always have a higher effectiveness of action, especially in conditions of active or passive enemy countermeasures. The

TABLE 6.12 COST OF AN ATTACK AGAINST CONVENTIONAL  
GROUND TARGETS BY A MULTIMISSION FIGHTER WITH  
DIFFERENT KINDS OF ONBOARD ARMAMENT (BASED  
ON FOREIGN DATA)

| Armament version                             | Prob. of penetrating AAD & performing combat mission |       | Cost of attack in rel. units (neglecting operating reliability of the air-to-ground missile and active jamming equipment) |
|----------------------------------------------|------------------------------------------------------|-------|---------------------------------------------------------------------------------------------------------------------------|
|                                              | $W_{AAD}$                                            | $E_a$ |                                                                                                                           |
| Bombs                                        | 0.26                                                 | 0.2   | 1.00                                                                                                                      |
| Bombs and two air-to-ground missiles         | 0.32                                                 | 0.41  | 1.15                                                                                                                      |
| Bombs & jamming                              | 0.82                                                 | 0.65  | 1.25                                                                                                                      |
| Bombs, 2 air-to-ground missiles, and jamming | 0.90                                                 | 0.72  | 1.40                                                                                                                      |

malfunctioning of individual subsystems in a group, even though reducing the effectiveness of use of the group, still in a rational communications arrangement does afford a high enough combat capability.

As an example, let us look at a standard group of AAD system facilities (Fig. 6.27). The width of the defense belt Z is chosen in accordance with the tactical-operational situation. Within this belt at a distance from the frontier lie the ground radar stations affording the simultaneous determination of the parameters of air targets and their transmission to the command post (CP) where a decision is made on the use of interception facilities (missiles or fighter-interceptors) based on conditions of the possible position of the interception lines with respect to the width of the belt B. Obviously, the number of interception groups in the belt Z must be equal to the number of the belts with width B. This precludes the possibility of the unimpeded penetration of an enemy deep into the defended territory.

The number of AAD facilities for interception and striking of air targets is selected so that for different methods of enemy raids, an assigned effectiveness of striking the targets  $E_a$  is provided.

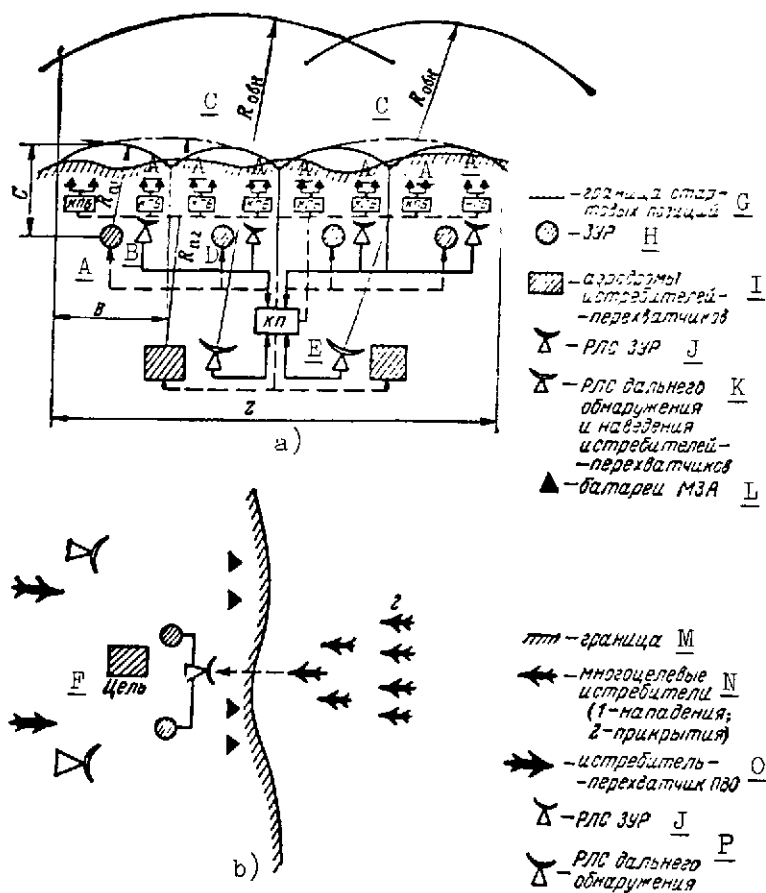


Fig. 6.27. Investigating groups of complexes

KEY: A -- Battalion command post

B -- R<sub>j1</sub>

C -- R<sub>det</sub>

D -- R<sub>j2</sub>

E -- Command post

F -- Target

G -- boundary of launch positions

H -- Antiaircraft guided missiles

I -- airfields of fighter-interceptors

J -- radar of antiaircraft guided missiles

K -- long-range detection and guidance

radar of fighter-interceptors

L -- batteries of small-caliber antiaircraft artillery

M -- boundary

[Caption continued on following page]

Fig. 6.27. Investigating groups of complexes /continued/

KEY: N -- multimission fighters (1 -- offense  
2 -- cover)  
O -- AAD fighter-interceptors  
P -- long-range detection radar

A large number of interception facilities in the belt Z /394 requires that a certain level of their combat readiness  $W_{c.r}$  be assured, and also that assigned effectiveness levels of individual complexes  $W_a$  be maintained. In addition, the effect on  $W_a$  of facilities of active and passive enemy protection and natural external conditions (weather, visibility, and so on) must be taken into account.

Thus, the effectiveness of a group  $E_{a.com}$  is defined as

$$E_{a.com} = W_{c.r} W_a . \quad (6.105)$$

The combat readiness of interception facilities can be determined by the following formula:

$$W_{c.r} = \frac{T_{c.r}}{\bar{T}_{c.r} + \bar{T}_{nc.r}} , \quad (6.106)$$

where  $\bar{T}_{c.r}$  is the mean time that all AAD facilities are in a combat-ready condition; and  
 $\bar{T}_{nc.r}$  is the mean time that all AAD facilities are in a non-combat-ready condition.

To determine  $\bar{T}_{c.r}$  and  $\bar{T}_{nc.r}$ , let us use the method suggested in the work [67], according to which

$$\bar{T}_{c.r} = \left( 1 - e^{-\left(\frac{T_{s.m}}{T_{f-f}}\right)} \right) T_{f-f} , \quad (6.107)$$

where  $T_{s.m}$  is the scheduled maintenance period; and

$T_{f-f}$  is the failure-free operating period of all facilities.

The mean time that all facilities are in a noncombat-ready condition depends on the waiting time of spare parts  $T_{s.p}$ ; the scheduled maintenance time  $T_{s.m.t}$ ; the time spent in detecting a failure  $T_{f.d}$ ; the repair waiting time  $T_{wa}$ ; and the time spent in making repairs  $T_{rep}$ :

$$\begin{aligned} \bar{T}_{nc.r} = & (T_{s.m.t} + P_{s.p}T_{s.p})e^{-\frac{T_{s.m}}{T_{f-f}}} + \\ & + \left(1 - e^{-\frac{T_{s.m}}{T_{f-f}}}\right) (P_{f.d}T_{f.d} + P_{wa}T_{wa} - T_{rep}), \end{aligned} \quad (6.108)$$

where  $P_{s.p}$  is the probability of waiting for spare parts to be obtained;

$P_{f-f}$  is the probability of an undetected failure coming to light; and

$P_{wa}$  is the probability of the onset of repair work.

It must be noted that in complex control systems of aircraft and missile AAD complexes the time  $\bar{T}_{nc.r}$  is quite large owing to significant values of  $T_{s.m.t}$  and especially  $T_{rep}$ , requiring the arrangements of additional AAD facilities in the defense belt to achieve assigned  $E_{a.com}$  values [215].

Example 6.8. Let us determine the probability of an anti-aircraft AAD complex being in a combat-ready condition and the effectiveness of air targets being hit by missiles of this complex (cf. Fig. 6.27 a) given the condition that  $T_{s.m.t} = 0.5$  hr;  $T_{s.p} = 1.0$  hr;  $T_{f-f} = 1.0$  hr;  $T_{wa} = 1.0$  hr;  $T_{rep} = 10.0$  hr;  $T_{s.m} = 100.0$  hr;  $T_{f-f} = 500$  hr;  $P_{s.p} = 0.7$ ;  $P_{f-f} = 0.6$ ; and  $P_{wa} = 0.9$ . For the adopted values we find  $\bar{T}_{nc.r} = 12.62$  hr and  $T_{c.r} = 200$  hr, whence  $W_{c.r} = 0.94$ . With these data, let us assume that -- with reference to the radio countermeasures of the enemy --  $W_a = 0.77$ ; then  $E_{a.com} = 0.725$ .

Example 6.9. Let us determine the effectiveness of a ground target being hit by a group of attack aircraft (Fig. 6.27 b), here using the first scheme of combat operations. The probability of a fighter-interceptor being shot down by the fire of a cover aircraft is determined by the formula

$$W_{f-1}^{sd} = W_{1sa_{cov}} + (1 - W_{1sa_{cov}})(1 - W_{1sa_{f-1}})W_{2sa_{cov}}, \quad (6.109)$$

where  $W_{1sa_{cov}}$  and  $W_{2sa_{cov}}$  are the probabilities of a fighter-interceptor being struck by the first and second salvos of a cover aircraft, respectively;  
 $W_{sa_{f-1}}$  is the probability of the striking aircraft being hit by the reply salvo of the fighter-interceptor.

The probability of the fighter-interceptor not being downed by the cover aircraft will be

$$W_{nsd_{f-i}} = 1 - W_{sd_{f-i}} =$$

$$= (1 - W_{lsa_{cov}}) [1 - (1 - W_{lsa_{f-i}}) W_{2sa_{cov}}]. \quad (6.110)$$

If it is assumed that the probability of being shot down by a salvo of two missiles is 0.5 for each of the salvos (of the fighter-interceptor and the cover aircraft), then

$$W_{nsd_{cov}} = 0.375.$$

This is the probability that the fighter-interceptor can strike the cover aircraft with the remaining half of its ammunition load.

Now let us determine the probability of an attack aircraft penetrating to a target after breaking through the AAD, based on formula (6.103), considering here that

$$W_{f-i} = W_{nsd_{f-i}} W_{int_{f-i}}.$$

Here  $W_{int_{f-i}}$  is the probability of interception by a fighter-interceptor of an attack aircraft with the expenditure of the remaining half of his ammunition load. Referring to these functions, let us find the probability of the attack aircraft performing their combat mission /396

$$E_{a.com} = W_{c.r} W_{AAD} W_{det}, \quad (6.111)$$

where  $W_{det}$  is the probability of detection of a target by an attack aircraft when only one aircraft out of a group attacks a target.

The probability of detecting a ground target by an attack aircraft using optical, radar, and infrared means can be represented as

$$W_{det} = 1 - (1 - W_{opt})(1 - W_{rad})(1 - W_{ir}), \quad (6.112)$$

where  $W_{opt}$ ,  $W_{rad}$ , and  $W_{ir}$  are the probabilities of target detection with optical, radar, and infrared units of the attack craft.



To determine the numerical value of  $E_{a.com}$ , let us assume that the AAD system includes the following: 10 20-mm small-caliber rapid-firing cannon, 10 batteries of missiles (each of the batteries can launch only one missile at the target), and four fighter-interceptors. Part of the AAD facilities is suppressed by the attack aircraft; then there remains  $n_{s.a.a} = 6$ ,  $n_{a.g.m} = 2$ . By formulas (6.104) let us find  $W_{s.a.a} = 0.02$  and  $W_{a.g.m} = 0.15$  and  $W_{AAD} = 0.32$  (for  $W_{str_{f-i}} = 0.5$ ). We will assume that  $W_{opt} = 0.6$ ,  $W_{rad} = 0.6$ , and  $W_{ir} = 0.6$ . In this case,  $W_{det} = 0.94$ . The probability of performing the combat mission can be determined with formula (6.111), that is,

$$E_{a.com} = 0.9 \cdot 0.32 \cdot 0.94 = 0.27.$$

Here it was assumed that the combat readiness of all AAD facilities (s.a.a, antiaircraft missiles, and fighter-interceptors) is  $W_{c.r} = 0.94$ .

In the last two examples the operating reliability of the onboard equipment of the missiles and aircraft was left out of consideration. When this is taken into account, the values found,  $E_{a.com} = 0.725$  (Example 6.6) and  $E_{a.com} = 0.28$  (Example 6.9), will be somewhat less; however, the ratio between the effectiveness of the group operations of AAD facilities and attack facilities will be retained. The resulting probability of performing the combat mission by one attack aircraft,  $E_{a.com} = 0.28$ , will be increased with the operations of two aircraft against the same target (cf. Fig. 6.26). These examples show how group operations of AAD facilities or air attack facilities influence the effectiveness of combat mission performance.

## 6.6. Synthesis of Control Systems of Flight Craft Complexes

Approximate characteristics of control systems and parameters of flight craft can be determined with methods of analysis based on statistical data and mathematical functions given in Chapters Two to Four. This method of preliminary project-planning requires constructing quite a large number of graphs with which the most optimal system parameters can be found<sup>7</sup>. This approach <sup>/397</sup> involves large time outlays. It is best to use methods of synthesis to reduce the time outlays at the initial stages of project-planning.

One of the possible formulations of problems in synthesis is to select the values of the most important system and system-element parameters, given the condition that the complex performs its combat mission with assigned effectiveness at minimum cost.

The interrelationship of system parameters and the complexity of the equations describing system functioning, and sometimes even the impossibility of a mathematical description of several processes rule out the possibility of a successive application of analytical methods of synthesis. Therefore, in project-planning complex systems often one is compelled to resort to a combination of heuristic methods of determining values of individual parameters with methods of mathematical modeling to select the remaining parameters<sup>8</sup>.

The synthesis of control systems embraces the following stages.

The first stage (setting up the block diagram of the system) makes it possible to establish functional relationships between the main subsystems. Here the a priori information on the conditions of the combat use of the system is taken into account (the parameters of the targets struck, probabilities of performing a combat mission with reference to enemy counteraction, possible variants of the layout of system facilities, and so on). Then the makeup of the facilities of the entire system and the structure of the block diagram are refined.

The second stage is the determination of the cost of the subsystems and of the system as a whole, with reference to outlays for increasing operating reliability for an assigned effectiveness of performing a combat mission. At this stage, usually the complexity of individual subsystems is established and the system cost functional is set up. By minimizing it, one determines the minimum cost of the system and the requisite depth of standby status of individual subsystems, as a function of their complexity and operating reliability. Statistical data on early-completed developments are used in determining the dependence of cost on various parameters. /399

The third stage is the selection of the main parameters of the subsystems and of the entire system as a whole. After determining the extent of standby status of the subsystems, the block diagram of the control system is again refined, and on the basis of this refinement working algorithms and system modeling schemes are set up to select the system's main parameters. Modeling is carried out with digital or analog-digital computers. From the parameters found, the effectiveness of use of the system in various application conditions is determined and its cost is found again (the cost of the development and manufacture with reference to the series status of its production, use, and so on).

The fourth stage is the construction of a CPM graph and the determination of the time required to develop and build the system. The stages of system development and building that are the most heavily loaded as to time are determined on the basis

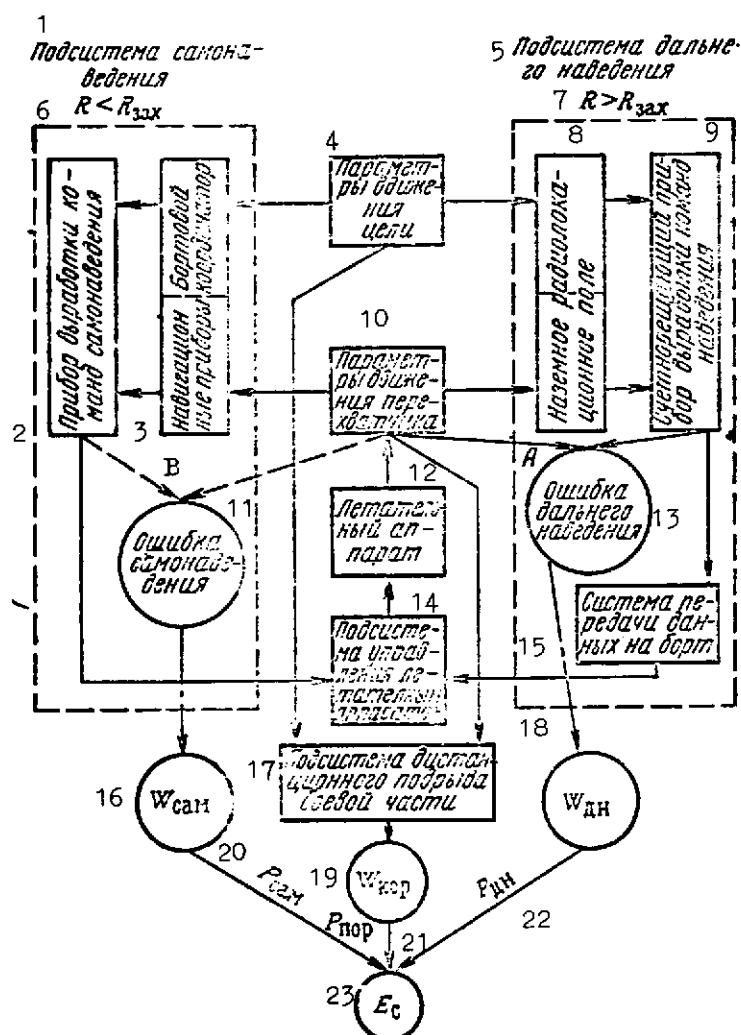


Fig. 6.28. Block diagram of an air target-interception system

- KEY:
- 1 -- Homing subsystem
  - 2 -- Homing command generating instrument
  - 3 -- Navigation instruments / Onboard coordinator
  - 4 -- Target motion parameters
  - 5 -- Long-range guidance subsystem
  - 6 --  $R < R_{зах}$
  - 7 --  $R > R_{зах}$
  - 8 -- Ground radar field
  - 9 -- Homing command-generating computing instrument
- [Caption continued on next page]

Fig. 6.28. Block diagram of an air target-interception system

Continued

- KEY: 10 -- Interceptor motion parameters  
 11 -- Homing error  
 12 -- Flight craft  
 13 -- Long-range guidance error  
 14 -- Flight craft control subsystem.  
 15 -- System for transmitting data on board  
 16 --  $W_{\text{hom}}$   
 17 -- Warhead aerial-burst fuse subsystem  
 18 --  $W_{1-r \text{ gu}}$  1-r gu = long-range guidance  
 19 --  $W_{\text{cor}}$  cor = correction  
 20 --  $P_{\text{hom}}$   
 21 --  $P_{\text{str}}$   
 22 --  $P_{1-r \text{ gu}}$   
 23 --  $E_a$

of the CPM graph, and the technical measures to correct these stages are projected. Then the cost of the development and manufacture is against refined.

The fifth stage involves working out the possible group operations of complexes with the projected control systems in defense or offense. At this stage various tactical-operational schemes of combat operations are examined; optimal compositions of groups and their rational connections with other complexes are established.

Difficulties in synthesizing a system lie, first of all, in the time connection of quantities differing in their physical nature that characterize the complex and its functioning (costs, effectiveness of combat mission performance, target detection probabilities, and parameters of flight craft and their onboard equipment), the need to use various a priori information (about the target, the layout of means of offense or defense, and so on), and also the necessity of using heuristic methods of selecting individual parameters. Let us consider by way of example a scheme for the synthesis of the control system of a one-time interception complex.

Example 6.10. The block diagram of air target interception by a flight craft is shown in Fig. 6.28. Each of these subsystems (denoted by rectangles in the figure) must be chosen on the conditions of its technical feasibility. Selection of the main subsystem parameters is presented in Chapters Two to Four and their dynamic characteristics are given in several books of the present series.

400

We will assume that an air target flying at altitude  $H_t$  and velocity  $V_t$  is detected by a ground radar at the range  $R_{det}$  with probability  $W$ . Based on this information we will formulate variants of the interception schemes that would ensure, with assigned effectiveness  $E_a$ , interception and striking of the air target in defense belt  $Z$  at a penetration depth  $l$  (cf. Fig. 6.27 a). The interceptor must execute interception of the target with assigned probability along the interception line  $R_{in}$ . Depending on the parameters of the interceptor, the interception line can be  $R_{in1} < R_{in2} < R_{in3}$ .

With the adopted radar arrangement scheme, the required mean interceptor velocity  $V_{av}$  will depend on  $R_{det}$  and  $R_{in}$ . The smaller  $R_{det}$  is for an assigned depth of launch position location  $C$ , the greater will be  $V_{av}$  and the speed of encounter with the target at the instant of its being struck.

Locating launch points closer to the boundary  $\angle \text{frontier}$  for some  $R_{det}$  leads to a decrease in  $C$  and for equal  $V_{av1} = V_{av2} = V_{av3}$  of the interceptors -- to a narrowing of the belt  $B$ . In this case a larger number of launch points for the interceptors is needed in the cover belt. An increase in  $V_{av}$  for fixed  $R_{det}$  and  $C$  leads to an enlargement of the belt  $B$ .

The number of launch points and interceptors affects the cost of the control system and the interception complex. Therefore, the required system (complex) parameters must be determined with reference to their operating reliability and the use of standby provisions, for a minimum cost of destroying the target.

During the planning of the control system, certain other parameters of the block diagram are also refined. From Fig. 6.28 it is clear that the parameters of target and interceptor motion during long-range guidance ( $R > R_{cap}$ ) are determined by the ground field for the target and for the interceptor. These parameters are fed into a digital computer to generate guidance commands, which are then sent via the data transmission subsystem to the flight craft control subsystem. The control system processes these commands and moves the actuators of the flight craft. When the flight craft reaches the range  $R_{cap}$ , equal to the capture range for the onboard target homing coordinator, the homing command generating instrument is triggered. These commands are sent to a subsystem controlling the motion of the flight craft. At a certain distance to the target, depending on the relative motion parameters of the flight craft and the target, the aerial-burst fuse subsystem of the warhead is triggered, destroying the target.

A system with the block diagram considered above functions with random deviations of its parameters (owing to the influence of random perturbations acting along the detection and control channels, passive and active jamming, and target maneuvering). Therefore in the control system arise errors in the execution of the stages of long-range guidance (A) (cf. Fig. 6.28) and homing (B), influencing the probability of the performance of these stages  $W_{1-r\text{ gu}}$  and  $W_{\text{hom}}$ . The probability  $W_{1-r\text{ gu}}$  is strongly affected by the radar field parameters. But the effectiveness of interception performance is evaluated by formula (6.23).

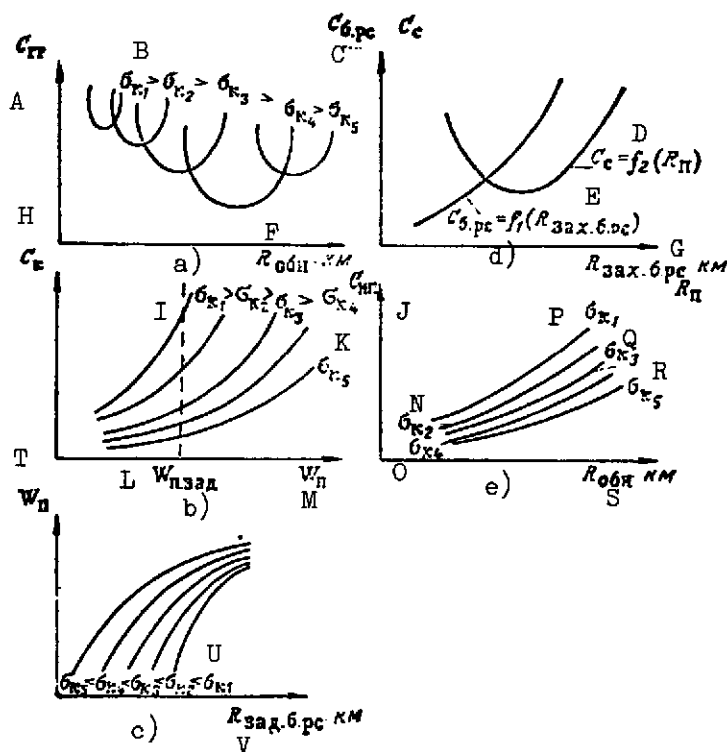


Fig. 6.29. Dependence of the costs of a group of interception complexes on the errors of the radar field

KEY: A --  $C_{gr}$  [gr = group]

B --  $\sigma_{\text{com}_1} > \sigma_{\text{com}_2} > \sigma_{\text{com}_3} > \sigma_{\text{com}_4} > \sigma_{\text{com}_5}$

C --  $C_{\text{onb-r}}$  [onb-r = onboard radar],  $C_a$

D --  $C_a = f_2(R_{\text{in}})$

E --  $C_{\text{onb-r}} = f_1(R_{\text{cap.onb-r}})$  [cap.onb-r = onboard radar, capture]

[Caption continued on following page]

Fig. 6.29. Dependence of the costs of a group of interception complexes on the errors of the radar field

KEY: F --  $R_{\text{det}}$ , km  
 G --  $R_{\text{cap.onb-r}}$ , km;  $R_j$   
 H --  $C_{\text{com}}$   
 I --  $\sigma_{\text{com}_1} > \sigma_{\text{com}_2} > \sigma_{\text{com}_3} > \sigma_{\text{com}_4}$   
 J --  $C_{\text{gr.f}}$   $\angle \text{gr.f} = \text{ground radar field}$   
 K --  $\text{com}_5$   
 L --  $W_{\text{in.rear}}$   $\angle \text{in.rear} = \text{rear hemisphere of interception}$   
 M --  $W_{\text{in}}$   $\angle \text{in} = \text{interception}$   
 N --  $\sigma_{\text{com}_2}$   
 O --  $\sigma_{\text{com}_4}$   
 P --  $\sigma_{\text{com}_1}$   
 Q --  $\sigma_{\text{com}_3}$   
 R --  $\sigma_{\text{com}_5}$   
 S --  $R_{\text{det}}$   
 T --  $W_{\text{in}}$   
 U --  $\sigma_{\text{com}_5} < \sigma_{\text{com}_4} < \sigma_{\text{com}_3} < \sigma_{\text{com}_2} < \sigma_{\text{com}_1}$   
 V --  $R_{\text{rear onb-r}}$   $\angle \text{rear hemisphere of onboard radar}$

Let us determine the dependence of the cost of a group of interception complexes on the errors of a field of radar stations  $\sigma_{\text{com}}$ . It is clear from Fig. 6.29 a that for each  $\sigma_{\text{com}}$  there exists a minimum cost  $C_{\text{gr}}$   $\angle \text{gr} = \text{group}$ . This is explained by the fact that the cost of the radar field increases with decrease in the detection range owing to an increase in the number of stations. The cost of a field also increases with rise in the radar coverage owing to the necessity of preserving the assigned accuracy  $\sigma_{\text{com}_1}$ , which can be achieved only by greater complexity of the station or the computer processing the target information. /401

A reduction in the minimum cost  $C_{gr}$  in the interval  $[\sigma_{com_4}, \sigma_{com_1}]$  occurs through a decrease in the monetary outlays for the active facilities; a further increase in  $C_{gr}$  (for  $\sigma_{com_4} > \sigma_{com_5}$ ) is attributable to an increase in the cost of the radar of the ground field, exhibiting increased accuracy.

To determine the cost of a group  $C_{gr}$ , we must know the dependence of the cost of one interception complex  $C_{com}$  on the probability of striking the target and the size of the error  $\sigma_{com}$ . From Fig. 6.29 b it is clear that as  $W_{in}$  is increased, the cost of one interception complex goes up. This is due to an increase in the required target capture range by the onboard homing coordinator to ensure high capture probabilities (Fig. 6.29 c), and thus, by an increase in the cost of the coordinator itself (cf. Fig. 6.29 d). At the same time, with a rise in the accuracy of the radar field  $\sigma_{com}$ , the cost of the complex becomes lower. /402

Thus, to obtain the graphs (Fig. 6.29 a), we must first construct the graphs Fig. 6.29 b,c,d and, in addition, obtain the dependence of the cost of the ground field on the range of the ground radars and their accuracy (Fig. 6.29 e).

In this example we have examined the method of determining the parameters of a ground radar field for fixed parameters of the flight craft during the synthesis of the complex. During a synthesis, we also could have found the optimal parameters of the flight craft for fixed values of the ground field. The function given in Fig. 6.29 d shows that for small interception ranges the cost of a group rises, owing to an increase in the number of the complexes. A further rise in cost is related to an increase in the speed of interception.

This synthetic pathway considered is not the sole one. One can conceive of a good many other schemes permitting the selection of the control system parameters (or the parameters of complexes). They all, however, in general outline will follow the scheme described in this section.

---

#### FOOTNOTES

<sup>1</sup>While this principle is valid for linear and relatively uncomplicated systems whose functioning is described by ordinary differential equations, this acceptability is, strictly speaking, not obvious in the construction of complex systems represented by the superpositioning of nonlinear operators.



# FOOTNOTES [Continued]

<sup>2</sup>The general principle of this transition from a quantitative to a qualitative criterion when the stochastic nature of external parameters  $y_1$  appears is given, in particular, in the work [24].

<sup>3</sup>Pardow, J., "Communication Satellites," in: Sistemy Svyazis Ispol'zovaniyem ISZ (Communications Systems Using Artificial Earth Satellites), (translated from the English), Moscow, "Mir" Publishing House, 1964.

<sup>4</sup>The complexity factor characterizes the complexity of a subsystem. We will assume that  $S_1 = 1.0$  is the "ordinary complexity" factor. By "ordinary complexity" we mean the complexity of a subsystem equivalent to 10,000 series-connected resistors (cf. Table 6.1).

<sup>5</sup> $\rho$  is the constant cost component paid in the form of a tax in buying or renting land for launch points; it is typical of the United States and other capitalist countries.

<sup>6</sup>Of course, on the nature and degree of active countermeasures depend the tactics of using combat facilities, which in some cases can be employed only against means of defense. A discussion of these problems is -- however -- beyond the scope of the present volume.

<sup>7</sup>Cf. also books in this present series dealing with methods of project-planning various kinds of control systems and their equipment. For example, Krinetskiy, Ye. I., Sistemy Samonavedeniya (Homing Systems), Moscow, "Mashinostroyeniye" Publishing House, 1970.

<sup>8</sup>When control systems are modernized, physical modeling incorporating actual equipment is possible.

<sup>9</sup>The values of  $\sigma_{com}$  and the subsequent characteristics of the system for long-range guidance and homing are determined by modeling.

1. E. L. Akim and T. M. Eneyev, "Determination of Motion Parameters of a Spacecraft Based on Data of Trajectory Measurements," Kosm. Issled., 1, No. 1 (1963).
2. Ye. P. Aksenov, Ye. A. Grebennikov, and V. G. Dyomin, "General Solution of the Problem of the Motion of an Artificial Satellite in the Earth's Normal Gravitational Field," in: "Iskusstvennyye Sputniki Zemli" (Artificial Earth Satellites), Moscow, USSR Academy of Sciences Publishing House, 1961, No. 8.
3. K. B. Alekseyev and G. G. Bebenin, "Upravleniye Kosmicheskimi Letatel'nyimi Apparataimi" (Control of Spacecraft), Moscow, "Mashinostroyeniye" Publishing House, 1964.
4. M. N. Aleshkov and I. I. Zhukov, "Fizicheskiye Osnovy Raketnogo Oruzhiya" (Physical Essentials of Missile Weaponry), Moscow, Voenizdat, 1965.
5. N. I. Andreyev, "Korrelyatsionnaya Teoriya Statisticheskikh Optimal'nykh Sistem" (Correlation Theory of Statistically Optimal Systems), Moscow, "Nauka" Publishing House, 1966.
6. R. F. Appazov, S. S. Lavrov, and V. P. Mishin, "Ballistika Upravlyayemykh Raket Dal'nego Deystviya" (Ballistics of Long-Range Guided Missiles), Moscow, "Nauka" Publishing House, 1966.
7. A. A. Afanas'yev and V. A. Gorbunov, "Effektivnost' Obnaruzheniya Tseley Radiotekhnicheskimi Sredstvami Nablyudeniya" (Effectiveness of the Detection of Targets With Radio Observational Facilities), Moscow, Voenizdat, 1964.
8. A. M. Afonin, N. S. Golubev, N. I. Kolotkov, et al., "Bespilotnyye Letatel'nyye Apparaty" (Unmanned Flight Craft), Moscow, "Mashinostroyeniye" Publishing House, 1967.
9. M. Barrer, A. Zhomott, B. F. Vebek, and Zh. Vandenkerkhove, "Raketnyye Dvigateli" (Rocket Engines), (translated from the English), Moscow, Oborongiz, 1962.
10. R. Bellman, "Dinamicheskoye Programirovaniye" (Dynamic Programming), Moscow, For. Lit. Pub. House, 1960.
11. K. U. Besserer, "Inzhenernyy Spravochnik po Upravlyayemykh Snaryadam, Seriya 'Osnovy Proyektirovaniya Upravlyayemykh Snaryadov'" (Engineering Handbook on Guided Missiles, Series -- Essentials of Designing Guided Missiles), edited by G. Merrill, (translated from the English), Moscow, Voenizdat, 1962.

12. B. Billik and K. Prays, "Preferential Schemes of Multiple Interorbital Transfers," Raketnaya Tekhnika i Kosmonavtika, No. 8 (1963).
13. V. F. Bolkhovitinov, "Puti Razvitiya Letatel'nykh Apparatov" (Approaches in the Development of Flight Craft), Moscow, Oborongiz, 1962.
14. I. K. Bazhinov and V. N. Pochukayev, "Optimal Distribution of Navigation Measurements," Kosm. Issled., 9, No. 2 (1971).
15. E. A. Bonin, M. D. Zukrou, and K. U. Besserer, "Aerodinamika. Silovyye Ustanovki. Konstruktsiya i Praktika Proyektirovaniya. Seriya 'Osnovy Proyektirovaniya Upravlyayemykh Snaryadov'" (Aerodynamics, Power Plants, Airframe and Design Practice, Series -- Essentials of Designing Guided Missiles), edited by G. Merrill, Moscow, Voenizdat, 1959. /404
16. Dzh. G. Bleyklok, "Avtomaticheskoye Upravleniye Samoletami i Raketami" (Automatic Control of Aircraft and Missiles), (translated from the English), Moscow, "Mashinostroyeniye" Publishing House, 1969.
17. E. Burgess, "Upravlyayemoye Reaktivnoye Oruzhiye" (Guided Jet Weaponry), (translated from the English), Moscow, For. Lit. Pub. House, 1958.
18. R. Bettin, "Navedeniye v Kosmose" (Guidance in Space), Moscow, "Mashinostroyeniye" Publishing House, 1966.
19. R. Bettin and F. Maktin, "Computer in the Flight Control System of the Apollo Spacecraft," Voprosy Raketnoy Tekhniki, No. 8 (1968).
20. S. A. Vakin and L. N. Shustov, "Osnovy Radioprotivodeystviya i Radiotekhnicheskoy Razvedki" (Essentials of Radio Countermeasures and Radiofrequency Reconnaissance), Moscow, "Sovetskoye Radio" Publishing House, 1968.
21. Ye. S. Venttsel', "Teoriya Veroyatnostey" (Probability Theory), Moscow, Fizmatgiz, 1962.
22. Ye. S. Venttsel', "Vvedeniye v Issledovaniye Operatsiy" (Introduction to Operations Research), Moscow, "Sovetskoye Radio" Publishing House, 1964.
23. Ye. S. Venttsel', "Elementy Dinamicheskogo Programirovaniya" (Elements of Dynamic Programming), Moscow, "Nauka" Publishing House, 1972.

24. Yu. G. Germeyer, "Metodologicheskiye i Matematicheskiye Osnovy Issledovaniya Operatsiy i Teorii Igr (tekst lektsey)" (Methodological and Mathematical Essentials of Operations Research and Game Theory (Text of Lectures)), Nos. 1 and 2, Department of Computer Mathematics of Moscow State University imeni M. V. Lomonosov, Computer Center of the USSR Academy of Sciences, 1967.
25. A. I. Gordeyev, "Avtonomnyye Sistemy Upravleniya Ballisticheskikh Raket" (Autonomous Control Systems of Ballistic Missiles), Moscow, Voenizdat, 1964.
26. B. T. Goroshenko, "Raschet Maksimal'noy Skorosti Poleta" (Calculating Maximum Flight Velocity), Moscow, Oborongiz, 1944.
27. B. T. Goroshchenko, "Dinamika Poleta Samoleta" (Aircraft Flight Dynamics), Moscow, Oborongiz, 1954.
28. V. Grin and R. Kross, "Reaktivnyye Samolety Mira" (Jet Aircraft of the World), Moscow, For. Lit. Pub. House, 1957.
29. V. G. Grigor'yants, "Tekhnicheskiye Pokazateli Radiolokatsionnykh Stantsiy" (Technical Indicators of Radar Stations), Moscow, Voenizdat, 1963.
30. V. G. Denisov, "Navigatsionnoye Oborudovaniye Letatel'nykh Apparatov" (Navigation Equipment of Flight Craft), Moscow, Oborongiz, 1963.
31. V. G. Demin, "Dvizheniye Iskusstvennogo Sputnika v Netsentral'nom Pole Tyagoteniya" (Motion of an Artificial Satellite in a Noncentral Gravitational Field), Moscow, "Nauka" Publishing House, 1968.
32. A. F. Donovan and G. R. Lourens, "Aerodinamika Chastey Samoleta pri Bol'shikh Skorostyakh" (Aerodynamics of Aircraft Parts at High Speeds), Moscow, For. Lit. Pub. House, 1959.
33. G. N. Duboshin and D. Ye. Okhotsimskiy, "Certain Problems of Aerodynamics and Celestial Mechanics," Kosm. Issled., Moscow, USSR Academy of Sciences Pub. House, 1, No. 2 (1963).
34. Yu. G. Yevtushenko, I. A. Krylov, R. F. Merzhanova, and G. V. Samoylovich, "Dvizheniye Iskusstvennykh Sputnikov v Gravitatsionnom Pole Zemli" (Motion of Artificial Satellites in the Earth's Gravitational Field), USSR Academy of Sciences Pub. House, 1967.

35. S. M. Yeger, "Proyektirovaniye Passazhirskikh Reaktivnykh Samoletov" (Designing Passenger Jet Aircraft), Moscow, "Mashinostroyeniye" Pub. House, 1964.
36. S. Yeger and A. Shteyngardt, "One More TU," Grazhdanskaya Aviats., No. 6 (1968).
37. V. A. Yegorov, "Prostranstvennaya Zadacha Dostizheniya Luny" (Three-Dimensional Problem of Reaching the Moon), Moscow, "Nauka" Pub. House, 1965.
38. G. I. Yermolayev, A. G. Gamulin, I. L. Prager, and Ye. V. Sofronov, "Osnovy Radiolokatsii i Radiolokatsionnoye Obo-  
rudovaniye Letatel'nykh Apparatov" (Essentials of Radar and Radar Equipment of Flight Craft), Moscow, "Mashino-  
stroyeniye" Pub. House, 1967.
39. A. M. Zhakov and F. A. Pigulevskiy, "Upravleniye Ballisti- /405  
chestkimi Raketami" (Control of Ballistic Missiles),  
Moscow, Voenizdat, 1965.
40. I. D. Zhongolovich, "Earth Satellites and Geodesy," Astron.  
Zh., 41, No. 1 (1964).
41. Ya. B. Zel'dovich, M. A. Rivin, and D. A. Frank-Kamenetskiy,  
"Impul's Reaktivnoy Sily Porokhovykh Raket" (Momentum of  
of the Jet Force of Powder Missiles), Moscow, Oborongiz,  
1962.
42. N. I. Zolotukhina and D. Ye. Okhotsimskiy, "Investigation  
of the Motion of Spacecraft in the Atmosphere," Kosm. Is-  
sled., 3, No. 4 (1965).
43. "Inertsial'nyye Sistemy Upravleniya" (Inertial Guidance Sys-  
tems), edited by D. Pittman, (translated from the English),  
Moscow, Voenizdat, 1964.
44. N. V. Inozemtsev, "Aviatsionnyye Gazoturbinnyye Dvigateli"  
(Gas Turbine Aircraft Engines), Moscow, Oborongiz, 1955.
45. S. Karlin, "Matematicheskiye Metody v Teorii Igr, Programmi-  
rovani, Ekonomike" (Mathematical Methods in Game Theory,  
Programming, and Economics), Moscow, "Mir" Pub. House,  
1964.
46. V. M. Kaula, "Kosmicheskaya Geodeziya" (Space Geodesy),  
(translated from the English), Moscow, "Nedra" Pub. House,  
1966.
47. M. S. Katsenbogen, "Kharakteristiki Obnaruzheniya" (Charac-  
teristics of Detection), Moscow, "Sovetskoye Radio" Pub.  
House, 1965.

48. A. S. Kel'zon, "Dinamicheskiye Zadachi Kibernetiki" (Dynamic Problems in Cybernetics), Leningrad, Sudpromgiz, 1959.
49. D. King-Khili, "Teoriya Orbit Iskusstvennykh Sputnikov Zemli" (Theory of the Orbits of Artificial Earth Satellites), (translated from the English), Moscow, "Nauka" Pub. House, 1965.
50. Kislik, M. D., "Motion of an Artificial Satellite in the Earth's Normal Gravitational Field," in: "Iskusstvennyye Sputniki Zemli" (Artificial Earth Satellites), Moscow, USSR Academy of Sciences Pub. House, No. 4, 1960.
51. M. D. Kislik, "Analysis of Integrals of the Equations of the Motion of an Artificial Satellite in the Earth's Normal Gravitational Field," in: "Iskusstvennyye Sputniki Zemli," Moscow, USSR Academy of Sciences Pub. House, No. 13, 1962.
52. "Kosmicheskiye Radiotekhnicheskiye Kompleksy" (Radiofrequency Space Complexes), general editor: S. I. Bychkov, Moscow, "Sovetskoye Radio" Pub. House, 1967.
53. S. Ye. Konikov, "Determination of Actual Transit Orbits and the Regions of Their Existence in Studies of Orbital Maneuvers of AES /Artificial Earth Satellites/," Kosm. Issled., 5, No. 6 (1967).
54. "Konstruirovaniye Upravlyayemykh Snaryadov" (Designing Guided Missiles), edited by A. Ye. Paket and S. Ramo, (translated from the English), Moscow, Voenizdat, 1963.
55. "Kosmicheskaya Tekhnika" (Space Equipment), edited by G. Seyfert, (translated from the English), "Nauka" Pub. House, 1964.
56. L. Z. Kriksunov and I. F. Usol'tsev, "Infrakrasnyye Sistemy Obnaruzheniya, Pelengatsii i Avtomaticheskogo Soprovozhdeniya Dvizhushchikhsya Ob'yektov" (Infrared Systems of Detecting, Ranging, and Automatic Tracking of Moving Objects), Moscow, "Sovetskoye Radio" Pub. House, 1968.
57. "Kosmonavtika. Malen'kaya Entsiklopediya" (Cosmonautics, a Brief Encyclopedia), Moscow, "Sov. Entsiklopediya" Pub. House, 1968.
58. V. T. Kochetkov, A. M. Polovko, and V. M. Ponomarev, "Teoriya Sistem Teleupravleniya i Samonavedeniya Raket" (Theory of Systems of Remote Control and Homing of Missiles), Moscow, "Nauka" Pub. House, 1964.

59. G. N. Kressner and Dzh. V. Mikhayels, "Vvedeniye v Sistemy Kosmicheskoy Svyazi" (Introduction to Space Communication Systems), Moscow, "Svyaz' " Pub. House, 1967.
60. G. D. Krysenko, "Sovremennyye Sistemy PVO" (Modern Antiaircraft Defense Systems), Moscow, Voenizdat, 1966.
61. V. I. Kurotkin and V. L. Sterligov, "Samonavedeniye Raket" (Homing of Missiles), Moscow, Voenizdat, 1963.
62. Larson, "Inertial Guidance System of the Titan III Launch Vehicle," (translated from the English), Voprosy Raketnoy Tekhniki, No. 6 (1966). /406
63. A. A. Lebedev and L. S. Chernobrovskin, "Dinamika Poleta Bespilotnykh Letatel'nykh Apparatov" (Dynamics of the Flight of Unmanned Flight Craft), Moscow, Oborongiz, 1962.
64. A. A. Lebedev and V. A. Karabanov, "Dinamika Sistem Upravleniya Bespilotnymi Letatel'nyimi Apparatami" (Dynamics of the Control Systems of Unmanned Flight Craft), Moscow, "Mashinostroyeniye" Pub. House, 1965.
65. Lidov, M. L., "Determination of Atmospheric Density Based on the Observed Deceleration of the First Artificial Earth Satellites," in: "Iskusstvennyye Sputniki Zemli" (Artificial Earth Satellites), Moscow, USSR Academy of Sciences Pub. House, No. 1, 1958.
66. A. S. Lokk, "Upravleniye Snaryadami. Seriya 'Osnovy Proyektirovaniya Upravlyayemykh Snaryadov' " (Control of Missiles, Series -- Essentials of Designing Guided Missiles), edited by G. Merrill, (translated from the English), Moscow, Gostekhteorizdat, Moscow, 1957.
67. Makkraken, "Model of the Effectiveness of a Weapons System," Voprosy Raketnoy Tekhniki, No. 7 (1968).
68. I. M. Malikov, A. M. Polovko, N. A. Romanov, and P. A. Chukreyev, "Osnovy Teorii i Rascheta Nadezhnosti" (Essentials of Reliability Theory and Calculation), Leningrad, Sudpromgiz, 1960.
69. V. I. Marisov and K. I. Kucherov, "Upravlyayemye Snaryady" (Guided Missiles), Moscow, Voenizdat, 1959.
70. D. T. Martin, A. M. O'Brayen, A. F. Rays, and R. F. Silvers, "Control, Navigation, and Sighting of the Saturn V Launch Vehicle," Voprosy Raketnoy Tekhniki, No. 9, 10 (1957).
71. A. K. Martynov, "Eksperimental'naya Aerodinamika" (Experimental Aerodynamics), Moscow, Oborongiz, 1958.

72. G. Merrill, G. Gol'dberg, and R. Gel'mgol'ts, "Issledovaniye Operatsiy. Boyevyye Chasti. Pusk Snaryadov. Seriya 'Osnovy Proyektirovaniya Upravlyayemykh Snaryadov'" (Operations Research, Warheads, and Launch of Missiles, Series -- Essentials of Designing Guided Missiles), edited by G. Merrill, Moscow, For. Lit. Pub. House, 1959.
73. "Metody Optimizatsii s Prilozheniyami k Mekhanike Kosmicheskogo Poleta" (Methods of Optimization With Applications to Space Flight Mechanics), edited by D. Leytman, (translated from the English), Moscow, "Nauka" Pub. House, 1965.
74. "Microelectronics and Large Systems," "Trudy Simpoziuma v SShA" (Proceedings of a Symposium in the United States), Moscow, "Mir" Pub. House, 1967.
75. D. Miller and D. Fel'dman, "Reliability of Gyroscopes in the Guidance System of the Apollo Spacecraft," Voprosy Raketnoy Tekhniki, No. 8 (1968).
76. Mur and Uayt, "Use of Standby Provision in the Guidance and Control Systems of the Saturn V Rocket," Voprosy Raketnoy Tekhniki, No. 7 (1968).
77. Ye. A. Nikitin and A. A. Balashova, "Proyektirovaniye Differentsiruyushchikh i Integriruyushchikh Giroskopov i Akselerometrov" (Designing Differentiating and Integrating Gyroscopes and Accelerometers), Moscow, "Mashinostroyeniye" Pub. House, 1968.
78. "Innovations in Rocket Technology (A Review)," Voprosy Raketnoy Tekhniki, No. 8 (1968).
79. B. Olezayna and Ye. Stayer, "Computing Cost in the Designing of the Structures of Space Rocket Systems," Voprosy Raketnoy Tekhniki, No. 7 (1968).
80. B. V. Orlov and G. Yu., "Termodinamicheskiye i Ballisticheskiye Osnovy Proyektirovaniya Raketnykh Dvigatelay na Tverdom Toplivo" (Thermodynamic and Ballistic Essentials of Designing Solid-Fuel Rocket Engines), Moscow, "Mashinostroyeniye" Pub. House, 1964.
81. B. V. Orlov, G. Yu. Mazing, A. L. Reydel', M. N. Stepanov, and Yu. I. Topcheyev, "Osnovy Proyektirovaniya Raketno-Pryamotochnykh Dvigatelay" (Essentials of Designing Ramjet Rocket Engines), Moscow, "Mashinostroyeniye" Pub. House, 1967.



82. I. V. Ostoslavskiy and N. V. Strazheva, "O Formirovani Kontura Upravleniya Samoletom" (Forming an Aircraft Control Loop), Moscow, Oborongiz, 1960. /407
83. I. V. Ostoslavskiy and N. V. Strazheva, "Dinamika Poleta. Trayektorii Letatel'nykh Apparatov" (Flight Dynamics, Trajectories of Flight Craft), Moscow, "Mashinostro-yeniye" Pub. House, 1969.
84. D. Ye. Okhotsimskiy, V. A. Rysin, and N. N. Chentsov, "Optimal Strategy in Designing," DAN SSSR, 175 (1967).
85. D. Ye. Okhotsimskiy and T. M. Eneyev, "Certain Variational Problems Associated With the Launch of an Artificial Earth Satellite," Usp. Fiz. Nauk, 63, No. 1a (1957).
86. D. Ye., Okhotsimskiy, T. M. Eneyev, G. P. Taratynova, "Determining the Lifetime of an Artificial Earth Satellite and Investigating Secular Perturbations of Its Orbit," Usp. Fiz. Nauk, 63, No. 1a (1957).
87. A. I. Paliy, "Radiovoyna" (Radio War), Moscow, Voenizdat, 1963.
88. S. A. Peresada, "Zenitnyye Upravlyayemye Rakety" (Antiaircraft Guided Missiles), Moscow, Voenizdat, 1961.
89. V. P. Petrov and A. A. Sochivko, "Upravleniye Raketami" (Control of Missiles), Moscow, Voenizdat, 1963.
90. A. K. Platonov, "Investigation of the Properties of Corrective Maneuvers in Interplanetary Flights," Kosm. Issled., 4, No. 5 (1966).
91. A. M. Polovko, "Osnovy Teorii Nadezhnosti" (Essentials of Reliability Theory), Moscow, "Nauka" Publishing House, 1964.
92. L. F. Porfir'yev and V. V. Smirnov, "Analytical Estimates of the Accuracy of Determining Coordinates and Velocity of an Artificial Earth Satellite Based on the Results of Statistical Treatment of Astronomical Observations," Kosm. Issled., 6, No. 3 (1968).
93. V. S. Pugachev, "General Condition for the Minimum Mean-Square Error of a Dynamic System," Avtomat. Telemekh., 14, No. 4 (1956).
94. V. S. Pugachev, "Teoriya Sluchaynykh Funktsiy i Yeye Primeniye k Zadacham Avtomaticheskogo Upravleniya" (Theory of Random Functions and Its Application to Automatic Control Problems), Moscow, Fizmatgiz, 1963.

95. V. S. Pyshnov, "Aerodinamika Samoleta" (Aerodynamics of Aircraft), Moscow, Oborongiz, 1943.
96. "Raketnoye Oruzhiye Kapitalisticheskikh Stran. Obzor 1960-1962 gg." (Missile Weaponry of the Capitalist Countries, A 1960-1962 Review), compilers: I. I. Popad'ko and R. A. Uryupin, Moscow, Voenizdat, 1962.
97. B. A. Rezinkov, "Parametric Observability of Spacecraft," Kosm. Issled., 6, No. 3 (1968).
98. G. V. Samoylovich, "System of Parameters for a Description of Spacecraft Orbits," in: "Iskusstvennyye Sputniki Zemli" (Artificial Earth Satellites), Moscow, USSR Academy of Sciences Pub. House, No. 16, 1963.
99. G. V. Samoylovich, "Motion of an Artificial Satellite of a Nonspherical Earth," in: "Iskusstvennyye Sputniki Zemli," Moscow, USSR Academy of Sciences Pub. House, No. 16, 1963.
100. G. V. Samoylovich, "Rendezvous of Spacecraft With a Constant Direction of the Relative Range Vector," Kosm. Issled., 6, No. 6 (1968).
101. A. P. Sivers, N. A. Suslov, and V. I. Metel'skiy, "Osnovy Radiolokatsii" (Essentials of Radar), Leningrad, Sudpromgiz, 1959.
102. "Control System of the Minuteman Missile (A Review)," Voprosy Raketnoy Tekhniki, No. 5 (1966).
103. N. V. Smirnov and I. V. Dunin-Barkovskiy, "Kratkiy Kurs Matematicheskoy Statistiki dlya Tekhnicheskikh Prilozheniy" (Short Course in Mathematical Statistics for Technical Applications), Moscow, "Nauka" Pub. House, 1965.
104. "Sputniki Svyazi" (Communications Satellites), edited by K. Getlend (translated from the English), Moscow, Voenizdat, 1966.
105. E. Stirns, "Kosmicheskaya Navigatsiya" (Space Navigation), (translated from the English), Moscow, Voenizdat, 1966.
106. G. P. Taratynova, "Motion of an Artificial Satellite in the Central Attractive Field of the Earth in the Presence of Atmospheric Drag," Usp. Fiz. Nauk, 63, No. 1a (1957).
107. A. Tatarchenko, "Ballisticheskiye Rakety" (Ballistic Missiles), Moscow, Voenizdat, 1961.

108. S. S. Tokmalayeva, "Calculation of Transits in the Field of One Attractive Center," in: "Iskusstvennyye Sputniki Zemli," Moscow, USSR Academy of Sciences Pub. House, No. 16, 1963.
109. "Trudy 5-go Natsional'nogo Simpoziuma po Nadezhnosti i Kontrolyu Kachestva Radioelektronnoy Apparatury (Yanvar', 1958, SShA)" (Proceedings of the Fifth National Symposium on Reliability and Monitoring of the Quality of Radioelectronic Equipment (January 1958, USA), Moscow, For. Lit. Pub. House, 1958.
110. "Upravleniye Kosmicheskimi Letatel'nymi Apparatami" (Control of Spacecraft), edited by K. T. Leondes, (translated from the English), Moscow, "Mashinostroyeniye" Pub. House, 1967.
111. V. I. Feodos'yev and G. B. Sinyarev, "Vvedeniye v Raketnuyu Tekhniku" (Introduction to Missile Technology), Moscow, Oborongiz, 1961.
112. M. Khobbs, "Tekhnika Upravleniya Raketami" (Missile Control Equipment), (translated from the English), Moscow, Voenizdat, 1963.
113. D. Chandler and I. Smit., "Iterative Guidance of Missiles," Voprosy Raketnoy Tekhniki, No. 12 (1967).
114. O. A. Chembrovskiy, "Problems of Antispace Defense and Approaches to Their Solution," Vest. Protivovozdushnoy Oborony, No. 3 (1965).
115. Ya. M. Shapiro, G. Yu. Mazing, and I. Ye. Prudnikov, "Teoriya Raketnogo Dvigatelya na Tverdom Toplive" (Theory of the Solid-Fuel Rocket Engine), Moscow, Voenizdat, 1966.
116. A. F. Shibayev, "Bor'ba s Raketami" (Missile Combat), Moscow, Voenizdat, 1965.
117. R. Dzh. Shleyzinger, "Radioelektronnaya Voyna" (Radioelectronic War), (translated from the English), Moscow, Voenizdat, 1963.
118. R. B. Shroyer, "Control System of the Titan III Launch Vehicle," Voprosy Raketnoy Tekhniki, No. 7 (1967).
119. Shuneyko, I. I., "Winged Spacecraft," "Itogi Nauki i Tekhniki. Seriya 'Mashinostroyeniye' i Raketostroyeniye' 1963-1965 (Advances in Science and Technology, Series -- Machinebuilding and Rocket Building, 1963-1965), USSR Academy of Sciences, VINITI, 1966.

120. P. Ye. El'yasberg, "Vvedeniye v Teoriyu Poleta Iskusstvennykh Sputnikov Zemli" (Introduction to Flight Theory of Artificial Earth Satellites), Moscow, "Nauka" Pub. House, 1965.
121. P. Ye. El'yasberg, "Approximate Formulas for the Determination of the Lifetime of Artificial Earth Satellites," Kosm. Issled., 11, No. 2 (1964).
122. K. Erike, "Kosmicheskiy Polet. Seriya 'Osnovy Proyektirovaniya Upravlyayemykh Snaryadov' " (Space Flight, Series -- Essentials of Designing Guided Missiles), Vol. 1, edited by G. Merrill, Moscow, Fizmatgiz, 1963.
123. V. V. Yagodkin and G. A. Khlebnikov, "Giroskopicheskiye Priборы Ballisticheskikh Raket" (Gyroscopic Instruments in Ballistic Missiles), Moscow, Voenizdat, 1967.
124. A. Adler, "An Analytic Determination of the Maximum Range of a Ballistic Missile from Launch to Target," ARS Paper, Easton (Pa.), 1959, VI, No. 868159, p. 31.
125. A. Aepli, "The SM-80 Minuteman American Ballistic Weapons System," Flugwehr und Technik, Frauenfeld, 25, No. 2, 49-50 (1963).
126. Aero Dig., N.Y., 10, No. 5, 300-309 (1955).
127. Technique et Science Aeronautiques, Paris, No. 2 (1966). /409
128. Aeroplane, London, Nos. 2440, 2572, 2595, 2617; Nos. 2678, 2731, 2735, 2853, 2863, 2864, 2865, 2866, 2873.
129. Aerosp. Eng., N.Y., 23, No. 4 (1964); 26, No. 5 (1967).
130. Aircraft, Toronto, No. 1 (1960); No. 2 (1964); Nos. 3, 7 (1966).
131. Air Force and Space Digest International, Washington, 2, No. 6 (1966).
132. Aeroplane, London, Nos. 2353, 2357.
133. E. Andreosky, "Functional Design of the Minuteman Flight Control System," SAE/NASA Aerospace Vehicle Flight Control Conference, July 13-15, 1965, pp. 335-344.
134. Armed Forces Management, Rockford, 9, 83 (1966); 14, No. 10 (1968).
135. Astronaut. Aeronaut., N.Y., 3, No. 12 (1965); 4, No. 9 (1966).

136. Aviat. Age, N.Y., 1, No. 6, 108-111 (1957).
137. Aviat. Week Space Technol., N.Y., Nos. 4, 6, 25, 26 (1959); No. 21 (1960); No. 7 (1961); Nos. 5, 6, 7, 8, 9 (1962); Nos. 4, 10, 14, 17, 18 (1963); No. 25 (1964); Nos. 19, 20 (1966); No. 19 (1966); No. 4 (1967).
138. Aviat. Week Space Technol., N.Y., Nos. 3, 9, 13 (1967); Nos. 1, 6, 11, 25 (1968); Nos. 13, 24 (1969).
139. W. R. Boehm, "Microelectronics -- Its Impact on Naval Ships," Nav. Eng. J., Washington, 76, No. 3 (1964).
140. R. F. Brissenden, "LEM Docking in Lunar Orbit," Astronaut. Aeronaut., 3, No. 4, 30-31 (1965).
141. C. Brownlow, "Problems Cloud Future of V/STOL Fighter," Aviat. Week, N.Y., 86, No. 24 (1967).
142. I. S. Butz, "Aviation's Widening Horizon," Air Force and Space Digest International, Washington, 47, No. 8, 29-33 (1964).
143. I. S. Butz, "Needed: New Ways to Push," Air Force and Space Digest International, Washington, 47, No. 4, 64-51 (1964).
144. Canadian Aviation, Toronto, 39, No. 11, 15-17 (1966).
145. R. Cockburn, "A New Phase in Aviation?" Aeronautical J. of the Royal Aeronautical Society, London, No. 687 (1968).
146. H. I. Coleman, "Rolls Explores Third-Generation Lift Jets," Aviat. Week, N.Y., 84, No. 19 (1966).
147. G. R. Chilton, "Apollo Spacecraft Control Systems," Pre-print IFAC Symposium on Automatic Control in Peaceful Uses of Space, Stavanger, 1965, Cambridge, Mass., Mass. Inst. of Technol., 1965
148. N. E. Cox and W. W. Harter, "One-Shot Mission Success of Minimum Cost," Aerosp. Eng., N.Y., 20, No. 11 (1961).
149. D. O. Davies, "Development of the RB-162," Flight International, London, 89, No. 2979 (1966).
150. E. Ehrlich, "Navigation by Satellite," Space World, Amherst (Wisc.), E, No. 3 (1968).
151. Electronics News, N.Y., 9, No. 456, 19 (1964); 10, No. 521, 6 (1965); 12, No. 580, 22, 23 (1967), No. 586, 5 (1967).

152. Electronics, N.Y., 32, No. 9, 94-95 (1959); 33, No. 18 (1960); 38, No. 7, 40-112 (1965); 40, No. 1, 109-118 (1967); 41, No. 24, 18 (1967); 41, No. 11 (1968).
153. K. Elbel, "Design Characteristics of the New Supersonic Passenger Airliner," Luftfahrttechnik, Dusseldorf, 13, No. 9 (1967).
154. D. Fink, "U.S.-German Fighter System Reviewed," Aviat. Week, 410 N.Y., 86, No. 26 (1967).
155. Flight International, London, Nos. 2629, 2650, 2667, 2678, 2731, 2734, 2745, 2868, 2874, 2882, 2884, 2885, 2886, 2990, 2901, 2903, 2913, 2956, 3036, 3038, 3059, 3065.
156. "Flight Electronics for Saturn and Apollo," Interavia, 21, No. 5, 1761-1766 (1966).
157. Flight International, London, 92, No. 3061, 758-771 (1967).
158. Flugwehr und Technik, Frauenfeld, No. 9, 21 (1959).
159. Flug-Revue International, Stuttgart, No. 1, 24-30 (1967).
160. Flying Review International, London, 17, No. 11 (1962).
161. R. L. Foss, W. M. Magruder, I. Sitrownik, and D. R. Wyrick, "Low-Speed Aerodynamic Characteristics of the Double-Delta Supersonic Transport," Journal of Aircraft, Easton (Pa.), 3, No. 6 (1966).
162. E. D. Geissler and W. Halussermann, "Saturn Guidance and Control," Astronautics, Easton (Pa.), 7, No. 2, 44-45, 88-92 (1962).
163. Gemini Midprogram Conference Including Experiments Results, NASA, Feb. 1966, pp. 23-25, Manned Spacecraft Center, Houston, Texas.
164. B. H. Goethert, "Hypersonic Cruise Vehicles in the 'World of Tomorrow'," Astronaut. Aeronaut., N.Y., 4, No. 10 (1966).
165. J. J. Grady, "The Operational Capacity of Some Optical Systems for Tracking Satellites and Space Probes," IRE Transactions, Proc. Fifth Natl. Symp. Space Electron. Telemetry, Sep. 1960.
166. R. R. Heppe and C. R. Engleby, "Supersonic Transport Design Evolution," Aircraft Engineering, 39, No. 1 (1967).

167. Jane's All the World's Aircraft, London, 1954-1955; 1955-1956; 1956-1957; 1957-1958; 1958-1959; 1963-1964; 1965-1966; 1966-1967; 1967-1968; 1969.
168. ICAS Paper, Tallahassee (Flor.), No. 66-1.
169. IEEE Trans. Rel. Qual. Contr., N.Y. R-14, Oct., No. 2, 120-136 (1965).
170. Interavia, Geneva, 21, Nos. 9, 10, 11, 12 (1966); 23, No. 5 (1968).
171. Interavia Air Letter, Geneva, Nos. 3589, 4857, 5078, 5169, 5178, 5181, 5203, 5496, 5500, 5519, 5530, 5445, 5448, 5453, 5455, 5545, 5546, 5585, 5588, 5590, 5602, 5603, 5607, 5649, 5650, 5655, 5930, 6021, 6023, 6035, 6096, 6131, 6140, 6141, 6152, 6162, 6192, 6202, 6211, 6222, 6245, 6260, 6261, 6272, 6303, 6313, 6346.
172. Interavia Air Letter, Geneva, Nos. 6099, 6109, 6162, 6163, 6491.
173. "Interstellar Guidance System of the Titan III and Its Checkout Connections," Space Aeronautics, N.Y., 40, No. 3, 79 (1963).
174. Interavia, Review of World Aviation, Geneva, 15, No. 2, 4, 7 (1960); 16, No. 11 (1961); 18, No. 11 (1963); 21, No. 9, 10, 11 (1966).
175. Journal of the Armed Forces, Washington, 106, No. 29 (1969).
176. J. Aircr., Easton (Pa.), 1, No. 5, 6 (1964); 2, No. 3. /411
177. J. Space Flight, Chicago, 5, No. 5, 1-9 (1953); 6, No. 3, 2-6 (1954).
178. J. Spacecr. Rockets, Easton (Pa.), 4, No. 5, 628 (1967).
179. P. J. Klass, "Avionics Fights Its Own Silent War," Aviat. Week, N.Y., 67, No. 20, 50-58 (1957); No. 21, 102-103.
180. P. J. Klass, "F-111A Flies Land Profile Supersonically," Aviat. Week, N.Y., 86, No. 2 (1967).
181. N. J. Korman and M. Handelsman, "Telecommunication Satellites," N.Y., 1964.
182. Der Luftwaffenring, Bremen, No. 6, 1962.
183. Luftfahrttechnik, Dusseldorf, 12, No. 1 (1966).

184. R. H. Miller, "HST -- Developing the Foundation," Astronaut. Aeronaut., N.Y., 4, No. 10 (1966).
185. Missiles Rockets, Washington, 6, No. 21 (1960); 11, No. 25 (1962); 13, No. 14, 32 (1963), No. 15, 52, 53 (1963); 16, No. 26, 22-24 (1965); 18, No. 4, 18 (1966).
186. Missiles and Space, N.Y., 16, Dec., No. 27 (1965).
187. G. E. Mueller, W. B. Hebenstreit, and E. R. Spengler, "Communications Satellites," London-N.Y., Academic Press, 1962.
188. Navigator, Washington, 16, No. 1, 6 (1968).
189. B. H. Paiewonsky, "Transfer Between Vehicles in Circular Orbits," Jet Propul., Easton (Pa.), 28, No. 7 (1958).
190. Proc. IEEE, N.Y., 55, No. 6, 266 (1967).
191. Raumfahrtforschung, Stuttgart, 1, 34 (1968).
192. L. Rider, "Characteristic Velocity Requirements for Impulsive Thrust Transfer Between Noncoplanar Circular Orbits," ARS J., Easton (Pa.), 31, No. 3, 345-358 (1961).
193. R. R. Rodwell, "Test Flight in the A-4B," Flight International, London, 89, No. 2990 (1966).
194. M. Roessler, "Optimal Aerodynamic-Propulsive Maneuvering for the Orbital Plane Change of a Space Vehicle," J. Spacecr. Rockets, Easton (Pa.), 4, No. 12 (1967).
195. A. M. Schneider, E. Capen, C. M. King, and E. P. Waller, "Navigation for Rendezvous in Space," Navigation, Los Angeles (Calif.), 8, No. 3, 221-248 (1961).
196. Ch. L. Seacord, "Flight Control for Manned Spacecraft," Space Aeronautics, N.Y., 40, No. 6, 72-80 (1963).
197. E. N. Sears, "Technical Development Status of Apollo Guidance and Navigation," Preprint Amer. Astronaut. Soc., Rockville (Md.), No. 17, 1-38 (1964).
198. I. F. Shea, "The Approach to Apollo," Astronaut. Aeronaut., N.Y., 3, No. 4, 26-29 (1965).
199. R. W. Simpson and I. Hursch, "Guiding the Hypersonic Transport," Astronaut. Aeronaut., N.Y., 4, No. 10 (1966).
200. Space Aeronautics, N.Y., 45, No. 3, 4, 6 (1966); 46, No. 10, 12 (1966); 47, No. 6 (1967).



201. G. L. Smith and I. D. McLean, "Midcourse Navigation for the Apollo Mission," Paper to be Presented at the IAE National Aeronautic Meeting, 3-6 April 1962, N.Y., National Aeronautics and Space Administration, Ames Research Center, Moffett Field, Calif.
202. Technol. Week, Washington, 19, No. 2, 21 (1966). /412
203. M. B. Trageser and D. G. Hoag, "Apollo Spacecraft Guidance System," Preprint, IFAC Symposium on Automatic Control in Peaceful Uses of Space, Stavanger, 1965, Cambridge, Mass. Inst. Technol. 1965.
204. B. K. Thomas, "New Wing Promises Design Breakthrough," Aviat. Week, N.Y., 87, No. 3 (1967).
205. U.S. News and World Report, N.Y., 3 Sep 1963.
206. D. A. Wall, "A Study of Hypersonic Aircraft," Journal of Aerospace Transport Division, 90, No. 2, 9-24 (1964).
207. Westinghouse Engineering, Pittsburg, January 1964, pp. 19-23.
208. A. D. Wheelon, "Free Flight of a Ballistic Missile," ARS J., Easton (Pa.), 29, No. 12 (1959).
209. A. L. Wilde and I. F. Coplin, "Lift Turbo-Fans," Journal of the Royal Aeronautical Society, London, 69, No. 565 (1965).
210. M. Wilson, "The British Phantom," Flight International, London, 89, No. 2990 (1966).
211. L. A. Zadeh, "What is Optimal!" IRE Trans. Inf. Theory, N.Y., 1T-4, No. 1 (1958).
212. Zeitschrift fuer Flugwissenschaften, Braunschweig, No. 9. (1965).
213. W. Zuerl, "With Notebook and Camera Through the United States," Der Flieger, Muenchen, No. 4 (1967).
214. I. I. Anureyev, "Oruzhiye Protivoraketnoy i Protivokosmicheskoy Oborony" (Weaponry in Antimissile and Antispace Defense), Moscow, Voenizdat, 1971.
215. V. R. Durov, "Boyevoye Primeneniye i Boyevaya Effektivnost' Istrebiteley-Perekhvatchikov" (Combat Application and Combat Effectiveness of Fighter-Interceptors), Moscow, Voenizdat, 1972.